

**Developing Ion Mobility-Mass Spectrometry for
Measurements of Solution-Relevant Protein Structures**

by

Linjie Han

**A dissertation submitted in partial fulfillment
of the requirements for the degree of
Doctor of Philosophy
(Chemistry)
in the University of Michigan
2014**

Doctoral Committee

**Assistant Professor Brandon T. Ruotolo, Chair
Professor Kristina L. Håkansson
Associate Professor Mi Hee Lim
Professor Philip C. Andrews**

© Linjie Han

All Rights Reserved

2014

Acknowledgements

First of all, I would like to express my special appreciation and thanks to my advisor Professor Brandon Ruotolo, who has been a tremendous mentor for me. During the past years, he's been not only teaching me the related knowledge and skills, but also showcasing me by himself how to be a successful scientist with great passion and patience, critical thinking, attention to details and persistence to never give up. I would like to thank him for unlimitedly encouraging my research and allowing me to explore new experimental findings. Without his careful guidance and insightful inspirations, I would not have achieved so many accomplishments.

I would also like to express my gratitude to my committee members, Professor Philip Andrews, Professor Kristina Håkansson and Professor Mi Hee Lim for serving as my committee members and providing me so many valuable questions and advices in the candidacy exam, data meeting and oral defense, which helped to increase my understanding of my research, improve my experimental design and feasibility, and add significant values to my final thesis. Specially, I would like to thank Professor Kristina Håkansson for introducing me into the mass spectrometry field through terrific lectures and rotation project during my first year, Professor Philip Andrews for instilling new ideas and thoughts into my research, and Professor Mi Hee Lim for inspiring me from the perspective of Chemical Biology and Bioinorganic Chemistry.

It is also a great privilege and pleasure working with a group of talented and friendly people in the Ruotolo lab in the past years. Specifically, I would like to acknowledge Dr. Suk-joon Hyung, who is like my ‘sub-advisor’ affording me all the instrumental trainings and bringing me into my first Ph.D. project. Dr. Yueyang Zhong and I have been involved in multiple collaborative projects, in which I learned from her lots of skills and tricks in operating the instruments. In addition, I want to deliver my heartfelt appreciation to Dr. Billy Samulak for teaching me dialysis and bottom-up MS analysis, Russ Bornschein for sharing research experience and scheduling the group meeting, Shuai Niu and Molly Soper for instructing me to use computational calculation, Jessica Rabuck for sample ordering, python calculation and sharing literatures, Joe Eschweiler for showing me how to use the LC-MS instrument, and Dr. Richard Kerr, our new postdoc, for his thoughtfulness and eagerness to always help others.

In addition to my lab colleagues, I am very thankful to my collaborators, Professor Charles Brooks and his student Evan Arthur from Biophysics Department for building computational models to support my experimental data, Professor Robert Hausinger and his student Mark Farrugia from Michigan State University for broadening my knowledge in urease activation, and Andrew Chang from the Gafni lab for instructing me DSC analysis. I would also like to say thank you to Dr. Hangtian Song, Ning Wang and Wendi Hale in the Hakansson lab. As the mentor for my rotation project, Dr. Hangtian Song showed me how to use the FTICR MS instrumentations and imparted me the experience to manage time effectively. Besides, Ning Wang and Wendi Hale did me a huge favor to collect the LC-MS data for my protein digest.

A special thanks to my family and friends. Words cannot express how grateful I am to my parents for unconditionally supporting my academic pursuit and aspiration. I feel so guilty that I could not take care of them by their side in the past years, and knowing that they have been keeping themselves healthy all the time is the biggest 'placebo' that allows me to concentrate on my Ph.D. study. Finally, I would like to thank all of my friends, Xiaoguang Hao, Junsi Gu, Si Yang, Ning Wang, Ying Zhou, Bei Ding, Yunlong Zhang for their great help and support. They have made my Ph.D. life full of joy and happiness.

Table of Contents

Acknowledgements.....	ii
List of Figures.....	xii
List of Tables.....	xvi
List of Abbreviations.....	xvii
List of Appendices.....	xx
Abstract.....	xxi
Chapter 1. Introduction.....	1
1.1 Approaches for Protein Structure Characterization.....	1
1.1.1 Non-Mass Spectrometry Related Technologies.....	1
1.1.2 Mass Spectrometry Related Technologies.....	6
1.2 Ion Mobility-Mass Spectrometry for Protein Structure Characterization.....	10
1.2.1 Protein Ion Generation.....	11
1.2.2 High-Mass Protein Ions Transmission and Detection.....	13
1.2.3 Tandem MS Measurement.....	15
1.2.4 IM Separation.....	17
1.3 Challenges in Applying MS to Protein Structure: Structural Alterations in the Gas Phase.....	19
1.3.1 Side Chain Collapse.....	20
1.3.2 Unfolding.....	21
1.3.3 Spontaneous Compaction.....	23

1.3.4 Collapse in Response of Activation	24
1.3.5 Dissociation.....	25
1.3.6 Nonspecific Protein-Protein Interactions in Mass Spectrometry	25
1.4 Strategies to Stabilize Proteins and Protein Complexes in the Absence of Bulk Solvent ..	26
1.4.1 Side Chain Micro-solvation	27
1.4.2 Charge Manipulation	28
1.4.3 Evaporative Cooling	29
1.4.4 Hofmeister-type Salts.....	30
1.5 Strategies to Differentiate Specific versus Nonspecific Interaction	33
1.5.1 Non-binding Reference	34
1.5.2 Reporter Molecule	35
1.5.3 HDX.....	36
1.5.4 Monte Carlo Simulation.....	37
1.6 Summary	37
1.7 References.....	40
Chapter 2. Bound Anions Differentially Stabilize Multiprotein Complexes in the Absence of Bulk Solvent.....	48
2.1 Abstract.....	48
2.2 Introduction.....	49
2.3 Experimental.....	53
2.3.1 Materials	53
2.3.2 IM-MS.....	54
2.3.3 Data analysis	54
2.4 Results and Discussion	55
2.4.1 Measuring the stability of protein complexes via collision induced unfolding and dissociation	55

2.4.2 Ion-Mobility MS reveals differential stability of protein complexes in gas-phase.....	59
2.4.3 Classifying and ranking the effect of anions on protein stability	63
2.4.4 Towards a mechanistic understanding of gas-phase protein stabilization through bound anions	65
2.5 Conclusions.....	71
2.6 References.....	74
Chapter 3. Bound Cations Significantly Stabilize the Structure of Multiprotein Complexes in the Gas-phase.....	77
3.1 Abstract.....	77
3.2 Introduction.....	78
3.3 Experimental.....	80
3.3.1 Materials	80
3.3.2 IM-MS and CIU/CID analysis.....	80
3.3.3 Data analysis	81
3.4 Results and Discussion	82
3.4.1 Measuring the stability of cation-bound protein complexes via collision induced unfolding and dissociation	82
3.4.2 Classifying and ranking the influence of cations on protein stability.....	85
3.4.3 Towards a mechanistic understanding of gas-phase protein stabilization through bound cations	87
3.5 Conclusions.....	88
3.6 References.....	89
Chapter 4. Dramatically Stabilizing Multiprotein Complex Structure in the Absence of Bulk Water using Tuned Hofmeister Salt Pairs.....	91
4.1 Abstract.....	91
4.2 Introduction.....	92

4.3 Experimental.....	95
4.3.1 Materials	95
4.3.2 IM-MS.....	96
4.3.3 CIU and CID	96
4.3.4 Data Analysis	97
4.4 Results and Discussin	98
4.4.1 Gas-phase proteins and their complexes are stabilized by cationic and anionic additives through different mechanisms and to different extents	98
4.4.2 Drastic differences of protein stabilization by cationic/anionic Hofmeister series in solution and in the gas phase	102
4.4.3 Tailored anion/cation combinations to enhance the stability of gas-phase proteins and multiprotein complexes.....	106
4.4.4 The influence of tuned salt additives on protein tetramer dissociation in the gas phase	111
4.4.5 CIU unfolding ‘fingerprints’ reveal mechanistic insights in cation-bound protein stabilization.....	114
4.5 Conclusions.....	118
4.6 References.....	120
Chapter 5. Charge Mobility as a Driving Force in the Collision Induced Collapse of Multiprotein Complex Ions	124
5.1 Abstract.....	124
5.2 Introduction.....	125
5.3 Experimental.....	128
5.3.1 Materials	128
5.3.2 IM-MS.....	129
5.3.3 Computational Cation Docking	130

5.3.4 Determination of CCS.....	131
5.4 Results and Discussion	131
5.4.1 Assessing the effect of bound Hofmeister-type cations on lower-charged SAP/CRP ions	131
5.4.2 Probing the origin of CCS increase upon cation binding.....	135
5.4.3 Assessing the effect of bound Hofmeister-type cations on higher-charged SAP ions.....	138
5.5 Conclusions.....	141
5.6 References.....	142
Chapter 6. Hofmeister Salts Recover a Misfolded Multiprotein Complex for Subsequent Structural Measurements in the Gas Phase.....	146
6.1 Abstract.....	146
6.2 Introduction.....	147
6.3 Experimental.....	148
6.3.1 Materials	148
6.3.2 IM-MS.....	149
6.3.3 CIU and CID	150
6.3.4 CD	150
6.3.5 DSC.....	151
6.4 Results and Discussion	151
6.4.1 Capturing misfolded form of ConA by IM-MS.....	151
6.4.2 Gas-phase structures reflecting those in solution.....	154
6.4.3 Hofmeister anions/cations recovering misfolded ConA	156
6.4.4 Monitoring the recovery of ConA' to ConA by salts in solution through CD and DSC	157
6.4.5 Possible mechanisms driving the CCS change in ConA tetramer, dimer and monomer	160

6.4.6 Comparison of ConA salt stabilization to Literature Hofmeister effects.....	163
6.5 Conclusions.....	165
6.6 References.....	166
Chapter 7. Ion Mobility Mass Spectrometry Differentiates Multiprotein Complex Structures formed in Solution and in Electrospray Droplets	168
7.1 Abstract.....	168
7.2 Introduction.....	168
7.3 Experimental.....	170
7.3.1 Materials	170
7.3.2 IM-MS.....	170
7.3.3 CID.....	171
7.3.4 Ligand binding and CRP interaction.....	171
7.3.5 Data analysis	172
7.3.6 Protein-protein docking	172
7.3.7 Theoretical CCS determination.....	173
7.4 Results and Discussion	173
7.4.1 IM-MS reveals biomodal dodecamer conformations for bovGDH	173
7.4.2 Larger dodecameric bovGDH follows an atypical CID pathway	176
7.4.3 IM-MS reveals biomodal decamer conformations for SAP	179
7.4.4 Ligand binding experiments drive the formation of a specific SAP decamer	180
7.5 Conclusions.....	182
7.6 References.....	184
Chapter 8. Conclusions and Future Directions	187
8.1 Conclusions.....	187
8.2 Further directions	189

8.2.1 Develop specific small molecule strategies for stabilizing the native-like structure of gas phase proteins	189
8.2.2 Develop IM-MS for differentiating disulfide-mediated structural isoforms in monoclonal antibodies	191
8.2.3 Develop IM-MS for distinguishing various topologies in antibody dimerization.....	193
8.3 References.....	195
Appendices.....	197

List of Figures

Figure 1-1. CD spectra of poly-L-lysine in three different secondary structures.	5
Figure 1-2. Schematic representation of DSC.	5
Figure 1-3. Schematic depiction of novel chemical probes and analytical techniques coupled to MS.....	7
Figure 1-4. A Schematic diagram of the Synapt G2, quadrupole-ion mobility-time-of-flight mass spectrometry instrument used in these studies.....	10
Figure 1-5. Schematic depiction of the positive ion mode nESI process.	13
Figure 1-6. Ion Mobility-Mass Spectrometry Data Acquisition and Basic Principles.	18
Figure 1-7. Types of structural rearrangement of proteins and protein complexes when transmitted into the gas phase.	20
Figure 1-8. Strategies for stabilizing gas-phase proteins and protein complexes from structural rearrangement at different levels.	27
Figure 1-9. Hofmeister series.....	31
Figure 2-1. Addition of anions in solution alters the dissociation and unfolding profiles of a protein assembly.	57
Figure 2-2. The mass spectra of TTR incubated with a range of anions reveal different extents of dissociation.	60
Figure 2-3. Elucidating the extent of unfolding and dissociation of the four protein complexes in the presence of different anions from IM-MS.	62
Figure 2-4. A plot of collision energy (eV*) averaged over the four protein complexes indicates differential stabilizing effect of the anions.	64
Figure 2-5. IM-MS reveals a mechanism of protein complex stabilization through anion attachment.	67
Figure 3-1. Elucidating the extent of unfolding and dissociation of the five protein complexes in the presence of different cations from IM-MS.	83

Figure 3-2. Ion mobility-mass spectrometry reveals protein complex stabilization achieved through cation attachment.....	86
Figure 3-3. A mechanistic diagram of protein structure stabilization through bound cations that summarizes our current data set.....	88
Figure 4-1. Comparison of anion and cation-mediated stabilization afforded to gas-phase protein ions.....	101
Figure 4-2. Correlations between our gas-phase data and protein-salt interactions in solution.	105
Figure 4-3. nESI mass spectra of the four protein complexes obtained from different solution conditions.....	108
Figure 4-4. Elucidating the extent of unfolding and dissociation of the four protein complexes as a function of buffer composition from IM-MS.....	110
Figure 4-5. Elucidating the influence of tuned salt additives on protein tetramer dissociation in the gas phase.	113
Figure 4-6. CIU fingerprint contour plots reveal combined salt effect and additional mechanistic details in cation-mediated stabilization.....	118
Figure 5-1. Charge reduction of SAP and CRP ions by TEA.....	133
Figure 5-2. Assessing the effect of bound Hofmeister-type cations on lower-charged SAP/CRP ions.....	134
Figure 5-3. CCS increase of SAP and CRP upon cation binding.	136
Figure 5-4. CCS difference calculated for SAP model structures with and without Gdm ⁺ ions.	138
Figure 5-5. Assessing the effect of bound Hofmeister-type cations on higher-charged SAP ions.	140
Figure 6-1. Capturing misfolded form of ConA by IM-MS.	152
Figure 6-2. Effect of disrupting agents on ConA structure and stability in bulk solution.....	155
Figure 6-3. Hofmeister anions/cations recovering misfolded ConA.	157
Figure 6-4. Recovery of the ConA' structure upon addition of specific salts in bulk solution. .	158
Figure 6-5. A schematic diagram showing three possible mechanisms that describe the formation of ConA' from ConA.....	161
Figure 7-1. IM-MS reveals bimodal dodecamer conformations for bovGDH. IM-MS data for bovGDH.....	174
Figure 7-2. Larger dodecameric bovGDH follows an atypical CID pathway.	177

Figure 7-3. IM-MS reveals biomodal decamer conformations for SAP. IM-MS data for SAP.	180
Figure 7-4. Ligand binding experiments drive the formation of a specific SAP decamer.	182
Figure 8-1. Develop specific small molecule strategies for stabilizing the native-like structure of gas phase proteins.	190
Figure 8-2. Open and closed structures of DnaX (τ/γ) trimer.	191
Figure 8-3. CIU ‘fingerprints’ reveal disulfide pattern differences in IgG subclasses.	192
Figure 8-4. Schematic representations of the three proposed dimer conformations and their ability to bind antigen.	194
Figure I-1. Stabilization of avidin tetramer by salt additives is dependent on additive concentration.	198
Figure I-2. Anion additives stabilize BLA, a dimeric protein.	199
Figure I-3. A plot of the gas-phase acidity against pKa reveals a positive correlation between them.	200
Figure I-4. CIU data reveal subtle differences in the partially unfolded intermediates.	202
Figure I-5. Adducts removal upon activation.	204
Figure II-1. One example showing peaks with and without cationization.	207
Figure II-2. Workflow chart of measuring the stability of cation-bound TTR by IM-MS.	208
Figure II-3. Detailed data regarding ADH dissociation.	209
Figure II-4. Further observations revealing the potential difference in stabilization mechanism provided by cationic and anionic additives.	211
Figure II-5. Charge-per-unit-area as an important factor for different mode of stabilization. ...	213
Figure III-1. SAP compaction upon collisional activation.	215
Figure III-2. Hofmeister-type anions cannot bind charge-reduced SAP ions.	216
Figure IV-1. Comparison of ConA and ConA’ MS data.	217
Figure IV-2. Generation of misfolded ConA by acid and MeOH.	219
Figure IV-3. Generation of misfolded ConA by MeOH.	220
Figure IV-4. DMSO fails to produce misfolded ConA.	221
Figure IV-5. Confirmation of the ConA’ assignment as a misfolded form of ConA through collisional activation.	223
Figure IV-6. Cation concentration-dependent recovery of ConA’.	224
Figure IV-7. Collisional activation of ConA' and ConA incubated with added Mg^{2+}	226

Figure IV-8. Calcium nonspecifically binding to ConA'	227
Figure V-1. Mass spectrum of denatured bovGDH hexamer.	231
Figure V-2. bovGDH and SAP concentration-dependent analysis.	232

List of Tables

Table I-1. Physical constants of selected Hofmeister anions including pKa, gas-phase acidity and ionic radii.	205
Table I-2. Physical property of proteins studied herein represents a broad range of thermodynamic stabilities and sizes.....	205
Table I-3. Triplicate measurements of CIU and CID avidin tetramer and example standard deviation calculation.	206
Table II-1. Physical constants of selected Hofmeister cations and anions including charge, ionic radii and charge-per-unit-area.....	213
Table V-1. Experimental and theoretical CCS for bovGDH and bacGDH dodecamers	229
Table V-2. Experimental and theoretical CCS for SAP and CRP decamers	230
Table V-3. Structural similarity analysis between bovGDH and bacGDH hexamers, and between SAP and CRP pentamers using TM-align	231

List of Abbreviations

3D	three-dimensional
ADH	alcohol dehydrogenase
AP	affinity purification
ATD	arrival time distribution
bacGDH	bacterial glutamate dehydrogenase
BLA	β -lactoglobulin A
bovGDH	bovine glutamate dehydrogenase
CCMV	cowpea chlorotic mottle virus
CCS	collision cross-section
CD	circular dichroism
CE	crown ether
CID	collision induced dissociation
CIU	collision induced unfolding
ConA	concanavalin A
CRM	charge residue model
CRP	C-reactive protein
cryo-EM	cryo-electron microscopy
CXL	crosslinking
CYC	cytochrome c
dAMP	deoxyadenosine monophosphate
DBN	1,5-diazabicyclo[4.3.0]non-5-ene
DBU	1,8-diazabicyclo[5.4.0]undec-7-ene
DDM	dodecylmaltoside
DMA	differential mobility analyzer
DMSO	dimethyl sulfoxide

DSC	differential scanning calorimetry
DT	drift tube
<i>E. Coli</i>	<i>Escherichia coli</i>
ECD	electron capture dissociation
EHSS	exact hard-sphere scattering
EM	electron microscopy
ESI	electrospray ionization
ETD	electron transfer dissociation
GDH	glutamate dehydrogenase
Gdm ⁺	guanidinium
GEMMA	gas-phase electrophoretic mobility molecular analysis
HAc	acetic acid
HBV	hepatitis B virus
HDX	hydrogen-deuterium exchange
IEM	ion evaporation model
IgG	immunoglobulin G
IM	ion mobility
IM-MS	ion mobility-mass spectrometry
ITC	isothermal titration calorimetry
MALDI	matrix-assisted laser desorption/ionization
MD	molecular dynamics
MeOH	methanol
MS	mass spectrometry
NAD(H)	nicotinamide adenine dinucleotide
NADP(H)	nicotinamide adenine dinucleotide phosphate
nESI	nanoelectrospray ionization
NMR	nuclear magnetic resonance
OFP	oxidative footprinting
PA	projection approximation
PDB	protein data bank
PK	pyruvate kinase

SAP	serum amyloid P component
SAXS	small-angle X-ray scattering
SEC	size-exclusion chromatography
SID	surface-induced dissociation
SP-1	stable protein 1
TEA	triethylamine
TIM	triosephosphate isomerase
TM	trajectory method
TMA	tetramethylammonium
ToF	time-of-flight
TRAP	tryptophan RNA-binding attenuator protein
Tris	2-Amino-2-hydroxymethyl-propane-1,3-diol
TTR	transthyretin
T-wave	traveling wave
UV-Vis	ultraviolet-visible
XRD	X-ray diffraction

List of Appendices

Appendix I. Chapter 2 Supporting Information.....	197
Appendix II. Chapter 3 Supporting Information.....	207
Appendix III. Chapter 5 Supporting Information	215
Appendix IV. Chapter 6 Supporting Information.....	217
Appendix V. Chapter 7 Supporting Information	229

Abstract

Ion mobility-mass spectrometry (IM-MS) has emerged as a robust tool in structural proteomics. However, native solution protein structure must be retained in the gas phase for accurate models to be determined by IM-MS.

To meet this challenge, we screen a broad set of anions and cations separately for their ability to stabilize protein structure in the absence of bulk solvent in Chapter 2 and 3, respectively, and find different mechanisms of stabilization. Cations tend to tightly bind protein complexes and act to reduce Coulombic unfolding. By contrast, anion-protein complexes exhibit a ‘dissociative cooling’ type mechanism. These differences prompt us to study the combined effects of tuned salt-pairs in Chapter 4, where we further reveal cation stabilization mediated by tethering the regions of protein structure. In Chapter 5, we use cation charge carriers to demonstrate that reduced charge mobility is a key parameter in altering the energetic thresholds associated with the gas-phase compaction for ring-like multiprotein complexes.

In addition to the challenges delineated above, many proteins exist in a range of conformational states in solution that subtly depend upon the local environment. In chapter 6, we report on the ability of a lectin tetramer, concanavalin A, to misfold in solution by exposure to denaturants, such as acid and organic solvents, or by multiple freeze-thaw cycles. We then demonstrate that this misfolded tetramer can be recovered to a more native-like state by adding specific Hofmeister-type salts in solution, and that these transitions can be followed using electrospray ionization coupled to IM-MS.

Moreover, a significant challenge in using MS to define the stoichiometry of unknown protein complexes involves the formation of non-specific protein-protein interactions during protein ionization/desolvation. In Chapter 7, we highlight the capacity of IM-MS to distinguish specific *versus* nonspecific quaternary structures in the case of bovine glutamate dehydrogenase and serum amyloid P component, by identifying those conformers with a clear concentration dependence.

Future endeavors will be made to develop new general strategies to stabilize proteins in the gas phase, and further explore IM-MS to distinguish monoclonal antibody disulfide variants and dimerized assemblies, critical in the process and formulation development of biotherapeutics.

Chapter 1. Introduction

The analysis of protein complexes and protein interaction networks is a critical endeavor, as almost all biological processes involve regulated cooperation between multiple protein subunits in both time and space¹. Equally important interactions with other biomolecules, such as DNA, cofactors and messenger molecules, also contribute to the complexity of regulation². Identification of the interacting components, followed by the structural and functional characterization of the intact macromolecular machines involved, is clearly required in order to understand many biological processes at the molecular level. Proteins possess a hierarchy of structural features including: primary, secondary, tertiary, and higher-order levels of structure. Furthermore, deviation at any level within this hierarchy can cause malfunctions that lead to severe diseases³. As such, it is of great necessity to develop technologies capable of determining the complete structural architecture of large protein complexes.

1.1 Approaches for Protein Structure Characterization

1.1.1 Non-Mass Spectrometry Related Technologies

There are myriads of well-established technologies capable of characterizing biomolecular structures over many different levels of structural resolution⁴. At the lowest level of resolution, the configuration of the components specifies the relative positions and interactions of the macromolecules. At higher-resolution values, models generated depict more of the details of molecular architecture, including the relative orientations of the interacting components. The

highest level of resolution achievable is one where the atomic structure of the biomolecule is revealed in detail, showing the absolute positions of the atomic constituents of the structure, with precisions on the Angstrom scale.

XRD and NMR, undoubtedly, are the two most mature technologies available for high-resolution protein structure characterization. Since the first XRD structures of proteins were revealed the 1950s⁵, remarkable accomplishments have pushed the technology forward dramatically, including: cloning and expression technology, more powerful computational methods, novel phasing approaches, synchrotron-based beam-lines, and the Protein Data Bank (PDB)⁶. Using this method, the amplitudes, and sometimes the phases, of structure factors within a crystal sample are measured. Together with a molecular-mechanics force field, this information is used in an optimization process that can result in an atomic structure of the biological units that comprise the crystal lattice. Among the large and complex assemblies currently defined by XRD include intact ribosomes^{7,8}, RNA polymerases⁹, RNA exosomes¹⁰ and the signal-recognition-particle complex¹¹. Despite these successes, lingering question still exists surrounding the challenges of relating structures captured in a solid crystalline environment to those that are physiologically relevant. NMR can claim a closer relationship to the 'native state' of proteins, as it allows for the determination of atomic structures of proteins and small complexes in solution in a solvated environment at native pH values. NMR works by aligning nuclei in a strong external magnetic field, and then uses an orthogonal pulsed magnetic field to measure the magnitude of nuclear magnetic moments of the aligned nuclei as they are selectively excited, using defects in the observed frequencies of their nuclear spins to deduce atomic geometries¹². NMR techniques are used frequently used to determine the structures and dynamics of proteins

in solution, in contrast to X-ray analyses, which are typically comprised of static structures¹³. Nevertheless, NMR also remains a technology with many challenges when applied to the structural characterization of protein complexes. Chief amongst these are its rather restrictive size limit (50-100 kDa, generally) for molecules to be amenable to complete analysis while a 900 kDa GroEL-GroES complex has been probed by NMR analysis¹⁴. In addition, there are some common limitations for XRD and NMR. Although the detection limits for both technologies continue to improve, relatively large amounts of protein are still required to acquire usable data. Furthermore, since neither technology seeks to separate components during analysis, both require highly purified samples.

While atomic structures of components and their interactions can be determined by XRD and NMR, lower resolution structural information, such as the shape of the assembly, can be revealed by cryo-EM and SAXS. Cryo-EM analysis of large proteins and complexes can generate structure information that is almost at the level of refinement achievable by NMR and XRD (~10 Å)¹⁵. This allows shape and topology definition to be obtained for large complexes in a native-like state, along with information on protein secondary and tertiary structure. In a cryo-EM experiment, a beam of electrons is aimed towards a flash-frozen sample in vitreous ice. Electrons diffracted by protein samples in this manner can be converted into a two-dimensional image. Single-particle picking combined with class-average structural analysis, as well as electron tomography with multiple tilted views of the same object, can reveal the three-dimensional shape and symmetry of an assembly¹⁶. Another method that enables lower resolution structures to be determined in solution is SAXS. SAXS collects the average signal over all protein conformations and orientations for molecules in solution, which results in protein structure data¹⁷. SAXS is

suitable for assemblies of 50-250 kDa, and can be applied to relatively small amounts of protein, conditions that often exclude cryo-EM, NMR and XRD analysis¹⁸.

In addition to these classical structural biology tools, optical biophysical techniques can be used to derive protein structure information. Spectroscopic methods are widely employed due to their high sensitivity and ease of use, which include UV-Vis absorption spectroscopy, CD and fluorescence spectroscopy. Among them, CD provides direct elucidation of protein local-level structure, which will be utilized as an orthogonal technique in Chapter 6. CD utilizes the fact that chiral molecules absorb left and right circular polarized light differently, and different protein secondary structures give rise to distinct CD signals in the far-UV (190-250 nm) region¹⁹ (Figure 1-1). Tertiary structure can also be estimated by near UV CD measurements in the range of 250-350 nm²⁰. In this wavelength region protein absorption spectra are dominated by side chains of aromatic residues (Phe, Tyr and Trp). On the global level, calorimetric methods, such as DSC and ITC, are often used to measure the fundamental thermodynamic driving forces behind the processes of protein stability and binding interactions, respectively²¹. Note that DSC, which measures the heat capacity of states and the excess heat associated with transitions that can be induced by temperature change (Figure 1-2), is exploited in Chapter 6 to correlate the thermal stability to gas-phase conformational states to those observed in solution.

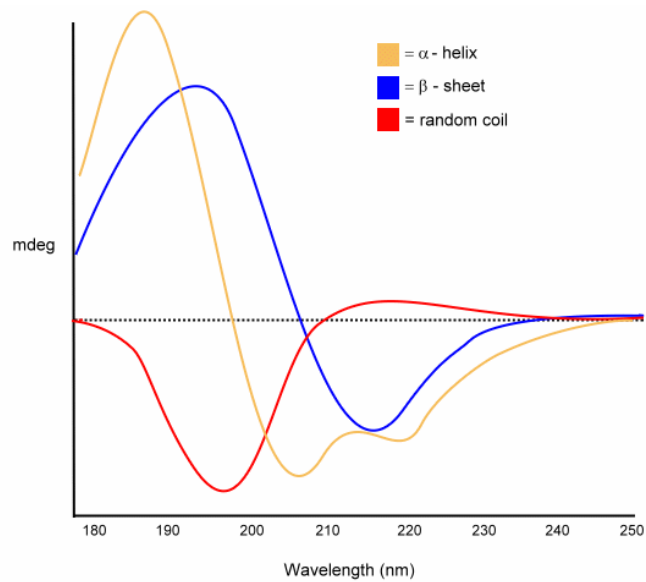


Figure 1-1. CD spectra of poly-L-lysine in three different secondary structures. α -helix, β -sheet and random coil structures each give rise to a characteristic shape and magnitude of CD spectrum. The spectrum for an all α -helix protein has two negative bands of similar magnitude at 222 and 208 nm, and a positive band at \sim 190 nm. The spectrum for an all β -sheet protein has in general a negative band between 210-220 nm and a positive band between 195-200 nm. The spectrum for a disorderly protein has a negative band of great magnitude at around 200 nm.

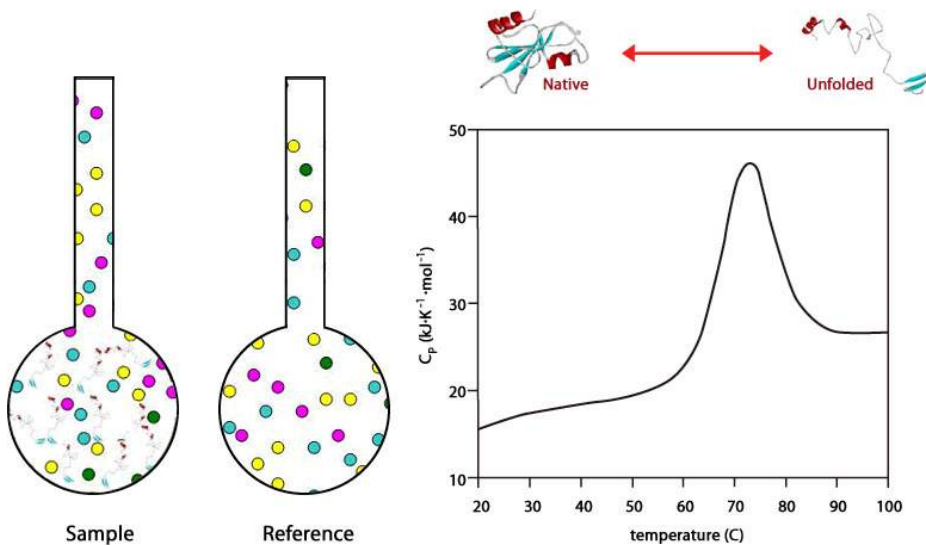


Figure 1-2. Schematic representation of DSC. In DSC, the heat supplied to a sample protein and solvent in an open or covered pan at a given temperature is measured and compared to that of a reference of solvent only at the same temperature (left). A schematic DSC curve plots temperature against excess heat capacity of protein, which can track thermal-induced protein unfolding and measure the thermal transition midpoint (right).

1.1.2 Mass Spectrometry Related Technologies

While the above-mentioned technologies, particularly XRD and NMR, have been highly successful for a large number of protein complexes and networks, the vast majority of multiprotein systems provide significant challenges for those approaches. For example, although the detection limits for both XRD and NMR technologies continue to improve, relatively large amounts of protein are still required to acquire usable data. In addition, as the complexity of the protein network under investigation increases, so do many parameters that complicate NMR and XRD analysis, such as the increased presence of protein flexibility, heterogeneity and polydispersity²². Furthermore, since neither technology seeks to separate components during analysis, both require highly purified samples. These and other challenges highlight the need to develop new approaches aimed at high-throughput multiprotein structure determination⁴.

Recent improvements in resolution, sensitivity, speed, and accuracy have established MS as a key technology within the field of structural biology. MS is capable of probing the structure and dynamics of multiprotein complexes present at physiologically relevant concentrations over a wide range of solution conditions²³. Moreover, the integration of novel chemical probes and analytical techniques has strengthened the capacity of MS to characterize heterogeneous samples and retrieve structural information, especially higher order protein structures²⁴. Techniques like HDX^{25,26}, OFP^{27,28}, CXL^{29,30} and IM separation^{31,32} have been coupled with MS as powerful tools for the determination of protein structure and have established themselves as crucial tandem technologies for revealing the structure of multiprotein complexes at various levels of structural resolution (Figure 1-3). Many of the contributions of MS-based structural analysis have included models of the eukaryotic exosome³³, ribosomal initiation factor^{34,35}, signalosome³⁶, replisome^{37,38}, chaperone³⁹⁻⁴³, ATPase⁴⁴, and transcriptional regulation complexes⁴⁵.

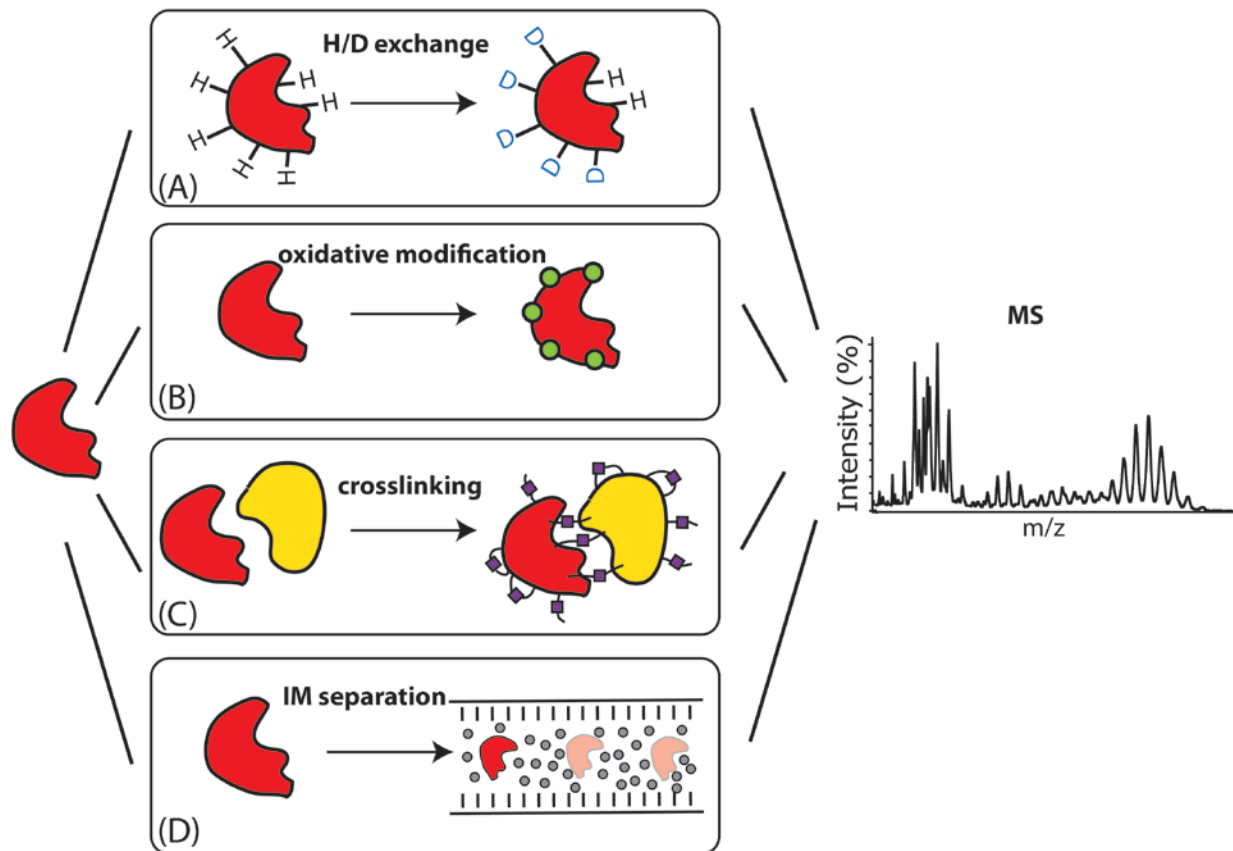


Figure 1-3. Schematic depiction of novel chemical probes and analytical techniques coupled to MS. Four representative methods, HDX (A), OFP (B), CXL (C) and IM separation (D), will be discussed in detail in the text.

HDX-MS can effectively measure solvent accessibility of a protein structure, and this information can be further used to annotate regions of a protein according to its apparent flexibility and stability. In a typical HDX-MS experiment, the protein sample is diluted in a deuterated buffer and all amide-exchangeable protons become replaced with deuterium (Figure 1-3A) and the exchange rate is a function of protein structure and dynamics²⁶. Recently, significant improvements in the spatial resolution of HDX-MS information, extending to the single amino acid residue level, have been attained through both the optimization of digestion and exchange conditions and also by employing gas-phase fragmentation methods that suppress the scrambling of protons, such as ETD⁴⁶ or ECD⁴⁷.

OFP-MS probes the conformational states of protein complexes by covalently modifying surface-accessible amino acid residues through chemical oxidation (Figure 1-3B). The extent of labeling depends on the protein surface area exposed to the solvent and the reactivity of exposed amino acid residues. Thus, analyzing proteolytic peptide fragments of an oxidatively-labeled protein can reveal the structures and dynamics of proteins in solution, similar to other methods such as HDX-MS²⁸. While OFP experiments can provide information similar to HDX-MS, amino acid modifications generated in OFP differ in that they are typically irreversible. Some OFP chemistries can be relatively selective for specific functional groups within proteins⁴⁸. Thus, selecting the appropriate oxidation chemistry for the protein sequence under investigation is a crucial starting point for maximizing the information content of OFP-MS data sets. Very recently, OFP-MS has played a crucial role in identifying and characterizing key amino acid residues involved in subunit folding and interfacial regions that result in multiprotein complex formation⁴⁹.

CXL-MS measurements can capture interactions between flexible regions of proteins in solution by covalently linking functional groups of amino acid side chains (Figure 1-3C). The covalent bonds may be formed by reaction between different components of protein complexes (intermolecular), or amino acid residues belonging to the same polypeptide (intramolecular). Identifying the cross-linked sites by MS analysis reveals proximal amino acid residues²⁹. The length of the cross-linker serves to constrain pair-wise interaction sites in the protein sequence and imposes spatial constraints in order to eliminate candidate structural models, and subsequently provides information on both the identity of the interacting partners involved in

protein-protein interfaces⁵⁰. Such an approach has been demonstrated as an effective means of generating accurate backbone structures for small monomeric systems⁵¹.

Recently, the utility of coupling MS to IM separation has generated considerable excitement. IM separates ions based on their ability to traverse a chamber filled with inert neutrals under the influence of a relatively weak electric field (Figure 1-3D). Ion size in the form of an orientationally-averaged CCS is the primary information content of IM separation and established computational approaches can be used in conjunction with this information to assign the structure of analytes⁵². The past several years have witnessed numerous applications of IM-MS to multiprotein complexes in an effort to determine their structures. Early work on the TRAP⁵³ and A β amyloid aggregates⁵⁴ illustrated the power of the IM-MS approach. Recent examples of IM-MS technology used in the structural determination of multiprotein complex architecture typically fall into three main categories. First, IM-MS has been used extensively to refine protein contact maps derived from MS measurements. Recent experiments of the DNA clamp loader assembly⁵⁵, the eukaryotic translation factor eIF3³⁴ and RNA polymerase I and II complexes⁵⁶ have all utilized topologically informative IM data in addition to MS resulting in well-defined topological models. Secondly, IM-MS has been used to monitor the assembly of viral capsid proteins and assess the structure of assembly intermediates⁵⁷. A final area of much research centers on the analysis of small oligomers involved in multiple amyloid-type diseases. Several IM-MS studies have determined topologies and stoichiometries for peptides and protein oligomer populations involved in Alzheimer's disease⁵⁸, type II diabetes⁵⁹, and dialysis-related amyloidosis⁶⁰.

1.2 Ion Mobility-Mass Spectrometry for Protein Structure Characterization

Though the start of the analytical technique termed ‘ion mobility spectrometry’ can be traced back to the beginnings of the 20th century, it is in recent years that IM-MS coupled with the soft ionization techniques ESI and MALDI has gained importance as a tool for the analysis of bio-macromolecules. By using IM-MS to determine changes in mobility and thus conformation and CCS of biomolecules in the gas phase, properties, such as conformational dynamics⁶¹, folding and unfolding intermediates⁶², ligand-induced conformational changes⁶³, aggregation intermediates and quaternary structures (topology)⁵³ can be determined. It should be noted that the measurements described in the thesis were all carried out on a Synapt G2 HDMS (Waters, Milford, MA) platform. The instrument is equipped with a nanoelectrospray ionization (nESI) source, a quadrupole mass analyzer, a T-wave ion mobility separator (IMS), and a time-of-flight (ToF) mass analyzer arranged in tandem, shown in Figure 1-4.

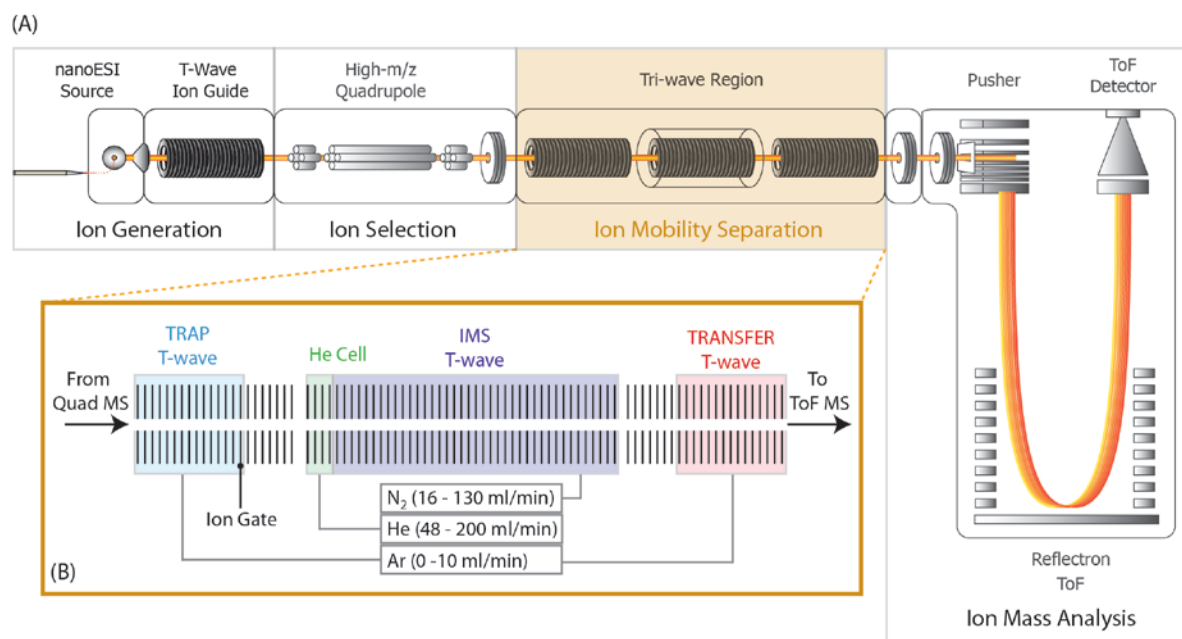


Figure 1-4. A Schematic diagram of the Synapt G2, quadrupole-ion mobility-time-of-flight mass spectrometry instrument used in these studies. (A) A general schematic of the complete

instrument indicating the four main regions of instrument operation: ion generation (using a nESI ion source), ion selection (using a modified quadrupole mass analyzer capable of selecting ions up to 32,000 m/z), ion mobility separation (carried out in the tri-wave region described in detail in B), and ion mass analysis (using a time-of-flight mass analyzer capable of $\sim 40,000$ mass resolving power). (B) Detail is shown for the ion mobility separation, or tri-wave, region of the instrument. Three major T-wave ion guides dominate this section of the instrument, and include the ion trap (blue), ion mobility (purple), and the transfer (light red) regions. A fourth pressurized region is shown as the He cell (green), which facilitates the injections of ions across the pressure gradient that exists between the ion trap and the ion mobility regions with minimal ion activation. Typical mass flow controller values are also shown for the gas flow (in ml/min) into each enclosed region of the instrument.

1.2.1 Protein Ion Generation

The first step in any MS experiment is to generate ions from a sample of interest. ESI and MALDI are routinely used for bio-macromolecule experiments as they have been proven to generate gas-phase ions for large, labile target molecules of high molecular mass. Of the two technologies, applications of ESI to the study of the structure and stability of intact protein complexes far outweigh applications of MALDI. This is primarily because the sample preparation requirements for MALDI typically involve evaporation of solvent from an aqueous analyte solution that contains a 10 to 10,000-fold excess of a UV-absorbent organic acid. Such highly acidic conditions will undoubtedly perturb protein-protein interactions present in solution and will most likely denature the protein. In addition, MALDI mass spectra often yield intense signals for protein aggregates that are thought to be artifacts of the laser desorption/ionization process⁶⁴. By contrast, ESI generates protein ions directly from solution. In addition, ESI typically generates ions having multiple charge states, which give rise to a succession of peaks known as a charge-state distribution. The formation of highly charged species allows the detection of high mass complexes at relatively low mass-to-charge ratios (m/z). Most importantly, because ESI is an extremely soft ionization technique, noncovalent interactions between molecules can be preserved in most cases⁶⁵.

ESI generates gas-phase ions by applying high electrostatic charging to the tip of a capillary (1-4 kV)⁶⁶. For protein-containing solutions, a positive voltage is typically applied, making the liquid at the capillary tip enriched with positive ions, for example $[M+nH]^{n+}$. The high field causes the exposed liquid surface to form an extended structure, known as a Taylor cone, from which droplets are emitted. Aided by both parallel and then counter-directional flows of nebulizing gas, solvent evaporation from the nascent droplets results in a reduction in droplet diameter. This reduction in droplet size continues until the Coulombic repulsion between the increasingly crowded charges becomes strong enough to overcome the surface tension holding the droplet together. At this point, termed the “Rayleigh limit”, droplet fission occurs. This process continues until a point at which essentially desolvated multiply charged protein ions are formed. To enhance ionization and solvent evaporation, nESI, a miniaturized version of ESI, has created opportunities for significant progress^{67,68}. The lowering of the flow rate from microliter per minute to nanoliter per minute and the resulting droplets of reduced size compared with conventional ESI greatly facilitate the desolvation process (Figure 1-5). The overall efficiency is 2000 times higher with nESI source compared with conventional ESI.

Two principal models have been proposed to account for ion formation. CRM, conceived by Dole *et al.* postulates that evaporation and Coulombic fission occur until a droplet containing a single residual analyte ion remains. Complete evaporation of the solvent comprising this droplet eventually yields a “naked” analyte ion, the charged residue^{67,69,70} (Figure 1-5). A second mechanism for gas-phase ion production, based on the work of Iribarne and Thomson, is termed IEM⁷¹. In this model, it is argued that, prior to complete desolvation of the droplet, the repulsion between the charged analyte ion and the other charges in the droplet becomes strong enough to

overcome solvation forces, and the ion is ejected from the droplet surface into the gas phase. For the case of proteins of mass >6000 Da, there is considerable evidence that Dole's CRM is the dominant mechanism of ion formation during ESI. Moreover, researchers have also shown that the extent of charging of species from near-native conditions relates to the surface areas of proteins and macromolecular complexes⁶⁹.

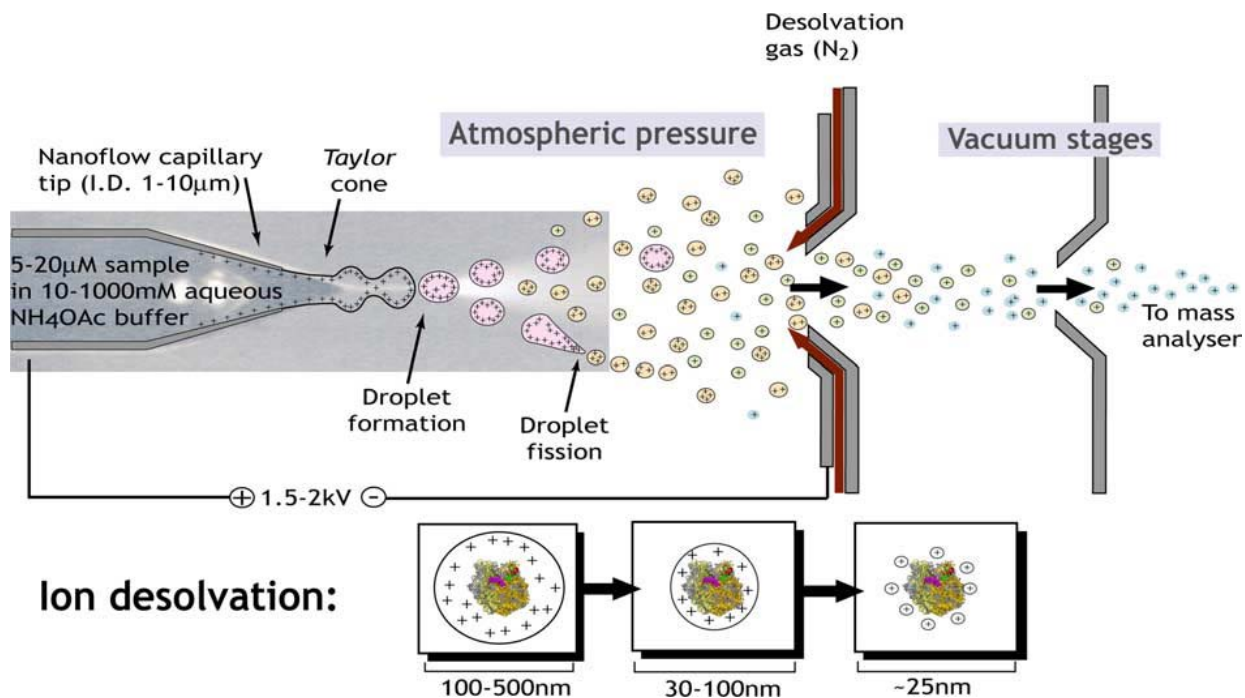


Figure 1-5. Schematic depiction of the positive ion mode nESI process.

1.2.2 High-Mass Protein Ions Transmission and Detection

The study of intact macromolecular complexes is largely the domain of hybrid mass spectrometers, which combine a quadrupole mass filter with an orthogonal ToF analyzer. The operating principle of a ToF analyzer is very straightforward: it is a pulsed analyzer, and separates ions based on their velocity differences in a field-free drift tube after being given a fixed amount of kinetic energy⁷². The ToF flight tube operates under vacuum, free of electrical fields, which is important, as any aberrant differences in flight time detected will lead to a loss in

mass resolving power. In order to limit the influence of any previous velocity profile, many ToF analyzers are arranged such that the direction of flight for ions post acceleration is orthogonal to the original travel axis for the ion population sampled⁷³.

A different type of analyzer that is often combined with ToF in native MS is the quadrupole. Quadrupoles can operate in two mass analysis modes. The first is a scanning mode where they let ions of all m/z pass through, and the second is a selective mode where a certain m/z region can be selected and only ions of that specific m/z will be able to pass through the quadrupole⁷⁴.

There are several methods for improving the transmission of large ions through a mass analyzer. The strategy most often employed is to manipulate the pressure gradients within the mass spectrometer by either introducing collision gas or reducing pumping at various stages along the flight path of the ions⁷⁵. It is also possible to increase the pressure locally in the first ion guide using a flow restricting sleeve⁷⁶. Both approaches provide excess neutral gas molecules that act to damp the radial velocity profile of large ions, and thus 'collisionally cool' their trajectories and focus them through to the detector. This method has the advantage of enhancing the transmission of macromolecular complex ions without noticeably suppressing low mass ions. Standard quadrupole mass filters are only able to transmit ions up to 16000 m/z . For this reason, it is important to substitute a low-frequency quadrupole to facilitate the transmission of high-molecular-mass species, as well as for mass selection⁷⁵.

1.2.3 Tandem MS Measurement

An essential tool in the analysis of multiprotein complexes by MS is tandem MS (MS/MS), where ions are interrogated by ion selection in a quadrupole mass analyzer, followed by activation via energetic collisions with neutral gas (*e.g.* Ar), and dissociation to generate product ions that inform on the composition and stoichiometry of the ionized intact protein complex. There are several crucial mechanistic aspects of gas-phase protein complex dissociation that have been established^{77,78}. For example, the predominant fragmentation pathway for most protein complexes involves expulsion of monomeric proteins from a larger assembly in a sequential fashion to give both highly charged subunits and low charged, multiply ‘stripped’ complex product ion populations^{79,80}. In general, CID has been established as an indispensable analytical tool in assigning protein stoichiometry and composition of multiprotein complexes within heterogeneous samples⁸¹.

Despite the relatively established nature of the above mechanism for most protein complexes, the combination of charge manipulation and CID has provided evidence that the dissociation mechanism can be drastically influenced by precursor charge state. For example, charge-reduced complexes subjected to CID can produce compact and presumably folded product ions⁸². In rare cases, charge amplification has also been observed to enhance the folded character of product ions produced by multiprotein CID⁸³. Either extensive charge reduction or amplification, followed by higher energy CID, can result in the dissociation of covalent bonds within the complex to produce sequence-informative peptide ions from protein termini^{84,85}. This last observation suggests the exciting possibility of ‘top-down’-type protein identification

experiments performed from multiprotein precursor ions, and has recently been duplicated using electron-mediated fragmentation approaches⁸⁶.

While CID methodologies are among the most pervasive for the disruption and dissociation of multiprotein complexes in the gas-phase, alternative techniques, such as ECD, ETD and SID, are emerging that promise to provide enhanced structural information for such assemblies. ECD/ETD, while used widely for obtaining sequence and identity information on proteins and peptides, has also seen use as a tool to assess the structure of some monomeric proteins^{87,88}. In these experiments, backbone cleavages are taken as evidence of the level of intra-molecular interaction surrounding the cleaved region of the sequence, and cleavage frequency can be used to map relatively flexible regions of protein secondary and tertiary structures. In addition to electron-mediated fragmentation, SID experiments often lead to large protein subcomplexes, presumably still in a folded configuration, to be ejected from the assembly, different from those generated by CID⁸⁹. The reason behind such remarkable differences in product ion populations relates clearly to the timescale of the energy deposition in the SID experiment when compared to CID, enabling SID activated protein complexes to follow a shattering-type mechanism. Multiple examples of SID data for multiprotein complexes are available in the literature, encompassing many large homo-oligomers where vast numbers of subcomplexes are observed as fragment ions^{90,91}. Recently, SID data for heterocomplexes have also been reported and further demonstrate the exciting potential of this technology for quickly mapping protein complex connectivity⁹². It should be noted that CID, ECD and SID have all been implemented on versions of the Waters Synapt G2 IM-MS platform.

1.2.4 IM Separation

IM separation, when coupled to MS, enables to collection of protein complex size information, and when this is combined with the connectivity information described above, coarse-grained or atomic models of the assemblies can be constructed⁹³. IM separates protein ions based on their ability to traverse a chamber filled with inert neutrals under the influence of an electric field. Larger protein ions undergo a greater number of collisions with the inert neutrals filling the chamber, and therefore have a larger CCS than more compact protein ions of similar mass (Figure 1-6)⁹⁴. While this description holds for most contemporary IM separations described currently in the literature, modern IM technology expands this basic principle into a variety of instrument platforms available for IM-MS experiments. Such instrumentation, as applied to multiprotein complexes, takes three basic forms: DT-type, DMA-type, and T-wave-type instruments. All of these technologies have both strengths and weaknesses for the analysis of multiprotein assemblies^{95,96}.

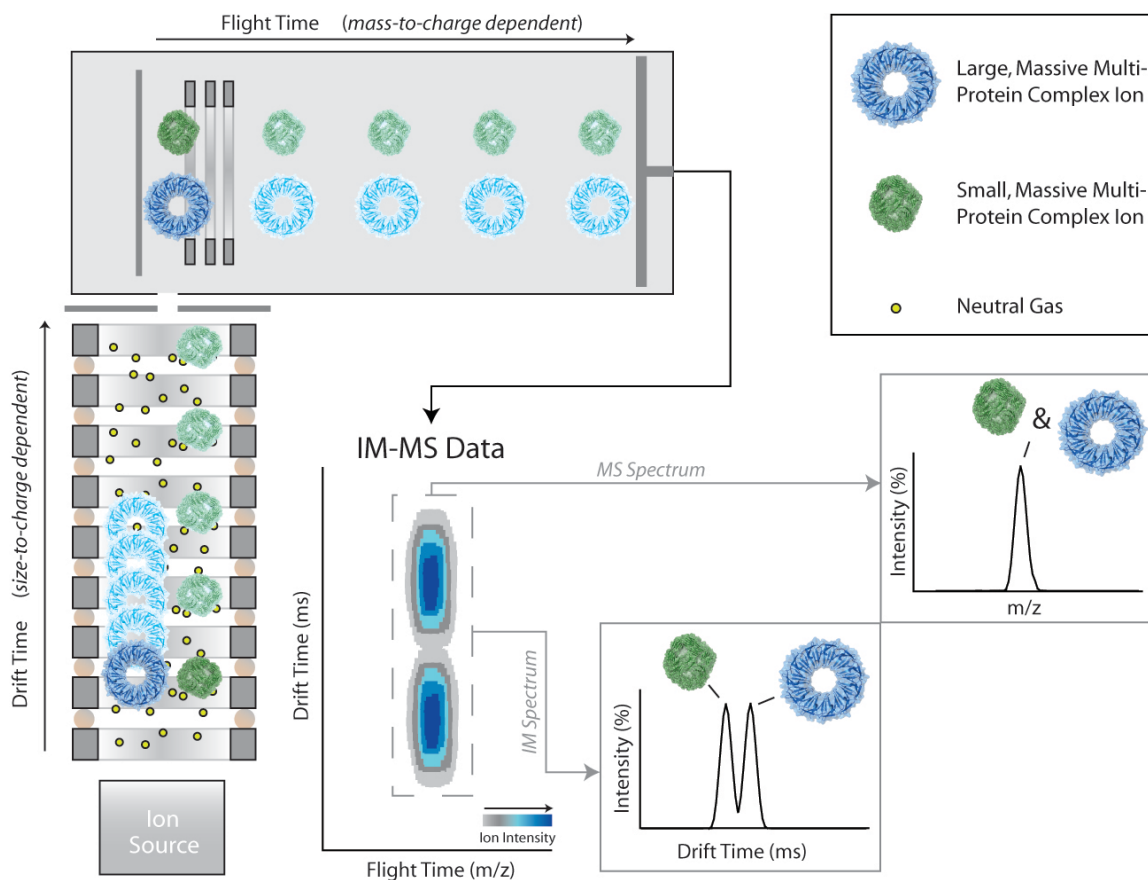


Figure 1-6. Ion mobility-mass spectrometry data acquisition and basic principles. Ions are generated at the ion source (lower left), and are allowed to drift in an ion guide filled with neutral gas molecules under the influence of an electric field. The ions migrate through this region according to their size-to-charge ratio. They are then injected into a time-of-flight (ToF) mass analyzer under vacuum for mass-to-charge (m/z) analysis. The resulting data is 3-dimensional, containing ion intensity, size, and mass information. The various dimensions of the data can be shown as a contour plot (middle, bottom), or 2D selections in drift time or m/z (lower right). A key for the diagram is shown, upper right.

The majority of IM-MS datasets for multiprotein complexes have been generated on IM-MS instruments using T-wave IM analyzers. T-wave IM analyzers are similar in basic construction to DT-type IM devices, but differ significantly in their operation. Rather than a linear field gradient, ions are propelled through the analyzer using a series of low-voltage waves^{97,98}. Ions are carried by the waves relatively briefly before being subsumed by the wave front in a manner depending on the CCS of the ions being separated, generating a time-domain IM separation similar to DT-

IM devices⁹⁹. An important feature of this process is that, due to the nature of the separation mechanism employed, T-wave drift times are most often calibrated using standard CCS values for protein complexes rather than calculated directly from drift time measurements¹⁰⁰. Apart from being the only IM analyzer currently incorporated into commercially available, high-sensitivity IM-MS instrumentation for ion size measurement in wide distribution, T-wave analyzers offer some modest advantages in terms of separation resolution¹⁰¹⁻¹⁰³.

Often defined in terms of the centroid arrival time of the IM peak normalized to the IM peak width ($t/\Delta t$), drift time resolutions for DT analyzers range from 30-150 for research-grade instruments, with those at the high end of the range produced using instruments with very long flight tubes (>1 m) and high separation voltages (multiple kV)¹⁰⁴⁻¹⁰⁶. Because of the physical principles involved in T-wave IM separation, drift time is correlated to CCS through an exponential relationship¹⁰⁰, which results in a T-wave drift time axis that is effectively ‘stretched’ relative to those achieved on DT analyzers. This relationship enables T-wave separators to achieve 40-60 CCS resolution ($CCS/\Delta CCS$) using comparatively shorter devices, operating at lower fields and pressures, than DT devices of equivalent dimensions^{102,103,107}.

1.3 Challenges in Applying MS to Protein Structure: Structural Alterations in the Gas Phase

Although mass spectrometry has become a powerful tool for structural biology, however, an integral part of this technique is the ionization of intact proteins and their removal from bulk solvent. This process, while likely preserving a substantial portion of protein structure and organization, imposes a foreign environment on proteins that may cause structural

rearrangements to occur. As a result, the gas phase conformation may lose its fidelity to the native structure at different levels (Figure 1-7).

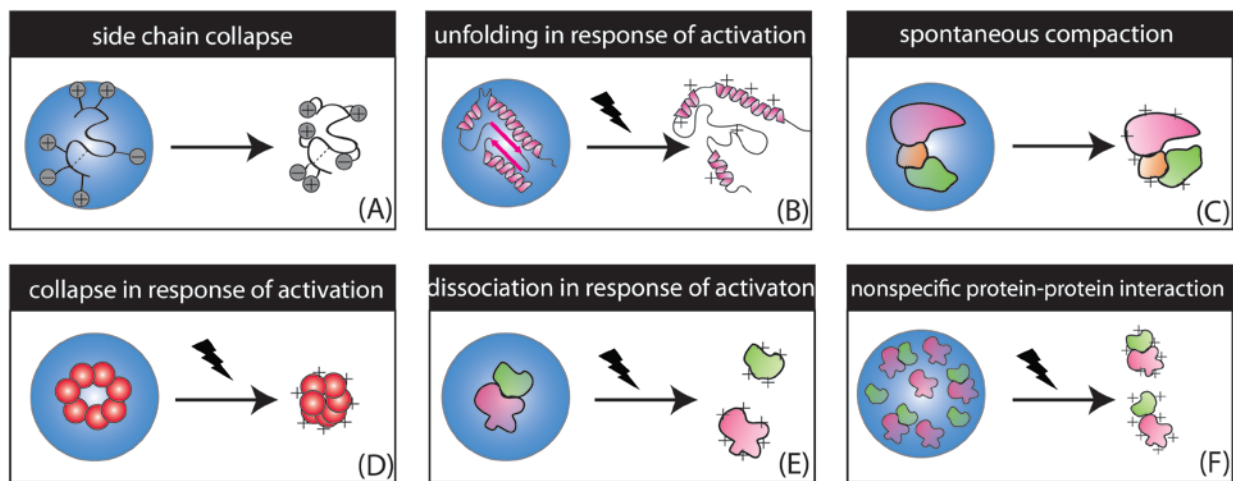


Figure 1-7. Types of structural rearrangement of proteins and protein complexes when transmitted into the gas phase. For details, see the following text.

1.3.1 Side Chain Collapse

The MD simulations reported by Breuker and McLafferty revealed that the very first structural changes after desolvation of native cytochrome c generally involve charged side chains¹⁰⁸. Most of these were found to rapidly collapse onto the protein surface, as illustrated for protonated K79 forming an ionic hydrogen bond with the amide oxygen of Y48. In principle, all proteins or protein complexes might undergo such compaction when transferred into a solvent-free environment. This collapse is characterized by minor rearrangements of the charged residues at the protein exterior, which fold back to the protein surface within picoseconds to form strong electrostatic interactions upon removal of water (Figure 1-7A).

1.3.2 Unfolding

In spite of the ‘ubiquitous’ collapse of charged side chains following desolvation, the backbone fold of most proteins remains essentially the same as that in solution and is deemed as ‘native-like’ structure. Heating the ion beyond the energy required for complete desolvation can then induce unfolding on the millisecond timescale (the timescale of most IM-MS experiments), during which there is a loss of hydrophobic interactions and a subsequent dissociation of electrostatic bonds (Figure 1-7B). Such ‘heating’-initiated unfolding of protein ions in the gas phase was first observed in small monomeric proteins by means of collisional^{109,110} or thermal¹¹¹ activation. Although minimizing the internal energy of protein ions is important for retaining native-like structure in the gas phase, the greatest resolution, mass accuracy and signal intensity can be achieved by using increased source temperature and high levels of ion activation, which will likely induce protein unfolding in most systems.

Multiprotein complexes have also been observed to unfold following activation in the absence of bulk solvent, and recent work has revealed the structural transitions during such unfolding processes¹¹². Following on from pioneering work that provided the first entropy estimates for the transition states associated with protein complex dissociation⁷⁹, and chemical cross-linking experiments that linked directly the charge asymmetry found in the product ions produced by CID to protein unfolding⁷⁸, discrete unfolded forms of multiprotein complex ions were captured using IM-MS measurements following collisional activation. Our current pool of evidence points to a collisional unfolding mechanism for multi-chain protein complexes that leads to asymmetric structures where a single chain unfolds to a much greater extent than all others within the complex. This asymmetric unfolding of a single protein chain amongst many is most-likely

driven by mobile protons, on the surface of the protein, that migrate towards areas of the gas-phase protein structure that have undergone thermal unfolding following energetic collisions with neutral gas molecules. As dictated by this mechanism, the general asymmetry of the unfolded multi-chain structure produced following collisional activation depends strongly upon the charge state of the ion selected and the time-scale over which ion activation occurs.

In addition to collisional unfolding, protein ions in some cases adopt both compact and unfolded conformations in the absence of bulk solvent, which is assumed to be attributed to Coulombic unfolding. These transitions were first recorded in a manner correlated with protein charge state, which is in turn correlated with protein surface area in solution^{109,110,113,114}. For proteins prepared under denaturing solution conditions, and subsequently ionized using ESI, the resulting ions adopt conformers that while compact for low charge states, grow increasingly extended as their overall charge is increased. Such experiments revealed, for the first time, a range of Coulombically-unfolded protein conformational families, and such data have now been reported for several monomeric protein systems, some of which have led to more extensive studies. For example, IM measurement of ubiquitin ions created from acidified, methanol-containing solutions are consistent with the known ‘A state’ of the protein, a less compact partially folded form observed in solution under such conditions^{62,115,116}. Further, IM measurements have identified two distinct families of structures for the intrinsically disordered protein α -Synuclein, a key biomolecule implicated in the etiology of Parkinson’s disease¹¹⁷.

1.3.3 Spontaneous Compaction

More pronounced reorganizations have been reported in which complexes undergo spontaneous compaction when transferred into the gas phase (Figure 1-7C) or collapse in response to collisional activation (Figure 1-7D). In both scenarios, the extent of collapse is related to the topology of the complex and the major difference between the two was shown to be the charge state dependence. For instance, the Robinson lab reported on the structural collapse observed for p53 ions in the gas phase, a protein with folded domains connected by disordered regions¹¹⁸. IM-MS and MD simulation suggested that structural changes in the disordered regions while in the gas phase were primarily responsible for the size reduction of the protein ions. For the p53 constructs used, no correlation between charge state and collapse was observed implying that compaction occurs spontaneously. Very similarly, decrease of the CCS values of the histone multimers were primarily due to the random behaviors of the disordered tail regions in the gas phase¹¹⁹.

In addition to the above-mentioned structural flexibility that arises from disordered region within proteins, the Loo lab and the Heck lab have detected, respectively, the structural collapse of two different virus capsids, CCMV (180mer intact, 4.6 MDa)¹²⁰ and HBV (hexameric nucleus, 96 kDa)¹²¹ in the gas phase, by using IM-MS and GEMMA. It is evidenced by a measured CCS value (IM-MS) or diameter (GEMMA) smaller than their X-ray crystal structures dimensions, which would be a result of a decreased number of interactions between individual subunits relative to the subunit packing in the native capsid.

1.3.4 Collapse in Response of Activation

In contrast to spontaneous compaction, collapse in response of collisional activation occurs to a finite number of large protein systems that adopt barrel-like or ring-like topologies (Figure 1-7D), including SAP (pentamer, 125 kDa)⁸³, TRAP (undecamer, 91 kD)⁵³, and chaperonin GroEL (tetradecamer, 800 kDa)^{41,122}. The activation-induced compaction of these protein complexes has been observed to be more charge state-dependent than the cases of spontaneous protein complex compaction noted above⁸³.

Earliest observations of this phenomenon were made for TRAP undecamer ions, where higher charge states showed evidence of more-compact structures⁵³. One viable explanation for this observation is that minor fluctuations, caused by Coulombic repulsion, could lead to small, local aberrations in structure that subsequently collapse the native-like ring. The second rational possibility is that complexes with higher charge states (21^+ or 22^+) will be subject to more energetic collisions with neutral gas molecules and will consequently accumulate larger amounts of internal energy, leading to changes in structure.

Recently, charge-reduced SAP pentamer ions were also reported to undergo compaction with unusual degree upon collisional activation⁸³. From MD results, the compaction appears to originate from the collapse of the cavity of the native pentamer ring conformation. The data for precursors at a range of different charge states indicate that this conformational change is highly charge state dependent, and the compaction observed at high charge states is unlikely due to Coulombic repulsion forces alone. Additionally, the de la Mora lab has revealed GroEL tetradecamer collapses in the gas phase at high charge states by mean of tandem differential

mobility analysis-mass spectrometry¹²². A mechanism linking all of these observations together has yet to be proposed, but current data points to a clear role of mobile protons on the surface of the protein complex, and the Coulombic repulsion between these mobile charges, as the driving force for the charge state dependencies observed in most data collected to date.

1.3.5 Dissociation

Although (n)ESI is thought to be a gentle ionization technique, capable of preserving labile non-covalent protein-protein interaction during the transfer into the gas phase, some complexes are stabilized in solution predominantly by weak intermolecular interactions, and thus generally exhibit low gas phase stabilities (Figure 1-7E). It is important to note, however, that the gas-phase stabilities of multiprotein complexes generally do not parallel the solution binding affinities¹²³. Collisional heating of gaseous ions can occur at various stages during the ion sampling process, such as within a heated metal sampling capillary (if used), in the nozzle (or orifice)-skimmer region, and during the accumulation of ions within external rf multipole storage device (*e.g.*, hexapole).

1.3.6 Nonspecific Protein-Protein Interactions in Mass Spectrometry

A significant challenge in using MS to define the stoichiometry of an unknown protein complex involves differentiating specific and non-specific protein-protein interactions observed in the gas-phase ion populations detected (Figure 1-7F). This issue arises primarily from the electrospray process itself, which is widely accepted to generate large, folded protein ions⁸¹. According to CRM, ESI droplets undergo solvent evaporation until they approach the Rayleigh limit, at which point they undergo fission, releasing several small multiply charged nanodroplets

(often referred to as offspring or progeny droplets) containing either: no protein, one or more protein units. The presence of multiple protein species within the final offspring droplets, and the subsequent evaporation of these droplets, potentially results in the production of artifactual assemblies not present in solution prior to ESI.

1.4 Strategies to Stabilize Proteins and Protein Complexes in the Absence of Bulk Solvent

In order to achieve the 100% fidelity between solution and gas phase protein structures, multiple strategies have emerged, which include incubating protein targets specific ligands in solution to provide conformational stability, using solution additives that adhere to the surface of the protein to replace solvent contacts, and performing gas-phase chemistry to manipulate charge states or produce stabilizing effects during ESI (Figure 1-8). Whereas the first method has been extensively studied by the MS community, the latter two methods arguably possess more general utility in pursuit of a universal strategy aimed at protecting the structure of proteins and protein complexes in the absence of bulk solvent.

Instrumental conditions can also be tuned to minimize the extent of collisional heating and concomitant gas-phase dissociation with the judicious choice of source parameters, such as low temperatures (drying gas, sampling capillary) and by using a finely tuned set of acceleration voltages and gas pressures¹²³⁻¹²⁵. However, there are usually trade-offs between the use of so-called “gentle” source conditions and signal intensity. Thus, a balance must be found between minimizing the extent of in-source activation and achieving adequate protein ion signal. In cases

where gentle sampling conditions do not eliminate the occurrence of protein structural rearrangement, the employment of stabilizing additives may prove beneficial.

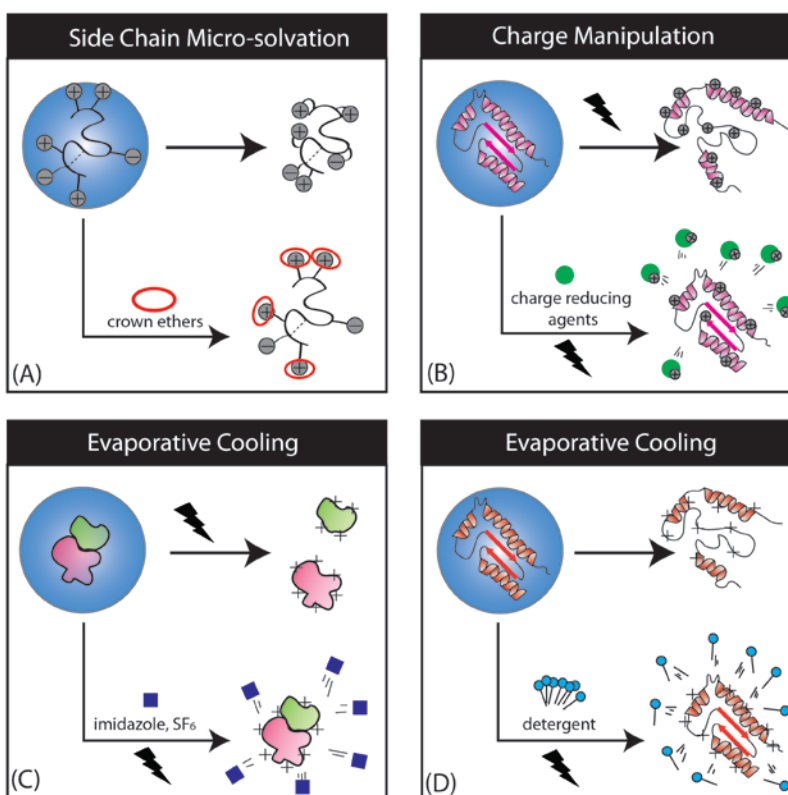


Figure 1-8. Strategies for stabilizing gas-phase proteins and protein complexes from structural rearrangement at different levels. For details, see the following text.

1.4.1 Side Chain Micro-solvation

In order to stabilize the labile orientations of the side chains on the surface of proteins and prevent their collapse, as described in 1.3.1, site specific strategies must be employed that bind protective molecules to those side chains most-likely to adopt ionic charge during ESI. For example, recent data has demonstrated how the attachment of crown ether (CE) compounds to protein ions can stabilize protein structure and prevent, in part, side chain collapse in monomeric protein ions¹²⁶. The CE compounds studied non-covalently bind preferentially to primary amines, e.g. lysine side chains, and serve to solvate the ionic charge present (Figure 1-8A). The IM-MS

data collected showed that 18C6 binding can compensate for rearrangements local to the charge site on the surface of cytochrome c ions in a manner potentially similar to solvent molecules in the condensed phase, thus preserving solution phase structure via pseudo-solvation. The results shown indicate that side-chain microsolvation serves as a good strategy for tuning gas-phase protein structure.

1.4.2 Charge Manipulation

Noted in 1.3.2 and 1.3.4, protein structural rearrangement can be affected by Coulombic repulsion. Therefore, charge manipulation of protein complex ions produced by nESI, especially charge reduction, can be an effective method of protein stabilization in the gas phase. Charge reduction can be achieved by using solution additives or performing gas-phase chemistry (Figure 1-8B). Recent work has indicated that charge reduction approaches that utilize gas-phase chemistries may be the most effective in the universal structural stabilization of multiprotein complexes¹²⁷. In stark contrast to the solution based-additive approach, which requires significant levels of collisional activation to strip off positive ions and generate charge-reduced protein complex ions, thus leading to collisional unfolding, the gas-phase ion-neutral approach universally produces compact ions, because the nebulized base molecules (DBU, DBN and TEA) likely interact with proteins in fewer numbers than the action of the same base molecules in solution. Thus, the complexes created would require less thermal energy to dissociate and generate charge reduced species.

It is important to note that while operative for the base molecules studied here, gas-phase unfolding has not been observed in other cases where small molecules have been added in

solution in order to charge reduce multiprotein complexes. For example, imidazole has been used to reduce the charge state of the GroEL tetradecamer and IM-MS data indicate a compact configuration for the charge reduced species generated¹²⁸. Similarly, crown ether compounds and triethylammonium acetate buffer have recently been used to alter the charge state of transthyretin tetramers in order to study their collision induced dissociation properties⁸². Here again, IM-MS data confirm compact conformations for the charge reduced tetramers prior to activation. Obviously, the lower charge state complex ions may exhibit higher kinetic stabilities and be more resistant to in-source activation.

1.4.3 Evaporative Cooling

Previously, the Klassen lab has published a series of papers describing a general method to stabilize weakly interacting noncovalent biological complexes in nESI-MS. This method involves the use of solution additives. For example, the addition of imidazole to solution, at high concentration (>1 mM), has been shown to prevent gas phase dissociation for a number of different protein-ligand complex ions, including protein-carbohydrate¹²⁵, protein-fatty acid¹²⁹, and protein-small molecule complexes¹²³. The origin of the stabilizing effects of imidazole is believed to be due, at least in part, to enhanced evaporative cooling resulting from the dissociation of imidazole bound nonspecifically to the complex in the ion source¹²³ (Figure 1-8C). The reduction in the average internal energy during the desolvation process can minimize or even eliminate in-source dissociation of the complex. Furthermore, the introduction of imidazole vapor to the ion source also protects complexes against in-source dissociation¹²⁵. It has also been shown that a high partial pressure of SF₆, a gas-phase insulating agent, in the ion source reduces the extent of in-source dissociation for some protein complex ions¹²⁵.

The evaporative cooling effect described above can also be applied to membrane protein ions that are released from detergent micelles in the gas phase, as revealed by the Robinson lab¹³⁰⁻¹³². The small *aquaporin Pagp* from *Escherichia coli* was selected to investigate its mechanism of detachment from DDM micelles¹³³. The IM-MS data indicated that this integral β -barrel protein exists in two conformations in the gas phase: one corresponding to a native-like structure and the other showing partial structural collapse. More surprisingly, the number of bound detergent molecules was found to be inversely proportional to the population of native-like protein remaining. This observation implies that the protein is not protected by the detergent attached but rather by its release, suggesting a mechanism akin to evaporative cooling (Figure 1-8D). Recent evidence implies that the energy required to release membrane proteins from micelles depends both on the detergent and protein or complex.

1.4.4 Hofmeister-type Salts

Proteins are central molecular machines in the critical biological processes necessary for life. In many cases, these essential functions are regulated by structure, dynamics, and stability of proteins¹³⁴. As such, a deep understanding of these properties has been sought by biochemists for well over a century. In that time, we have learned that many of the important biophysical properties of proteins can be influenced dramatically by the presence or absence of salts *in vivo*¹³⁵⁻¹³⁸. Indeed, such disparate biochemical properties as cell growth and protein crystallization have been directly linked to the influences of critical anions and cations^{138,139}. In pioneering work, Hofmeister discovered that such salts can either stabilize or destabilize proteins differentially, and that empirical observations can be used to construct a generally predictive rank order¹⁴⁰. Understanding the basic physical mechanism(s) that underlie the series that now

bears his name (Figure 1-9) has become an active area of research, due to its central importance in our understanding of protein biophysics.

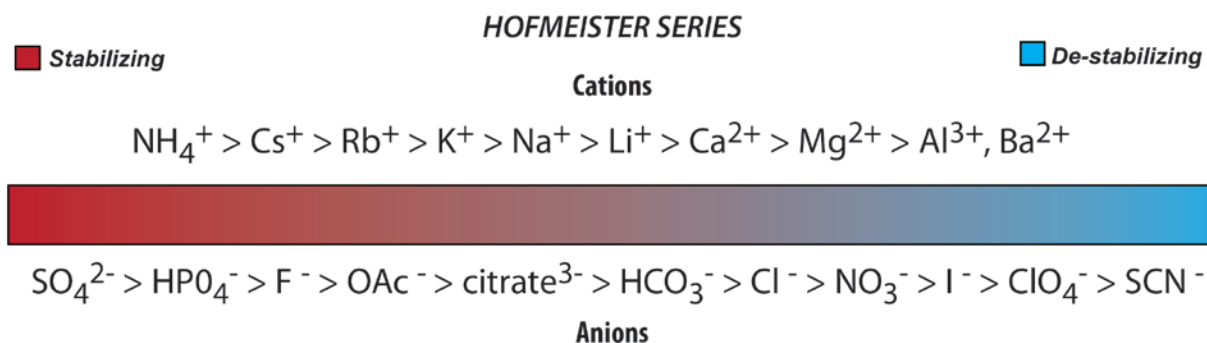


Figure 1-9. Hofmeister series. A rank order for cations and anions to stabilize protein structure in the solution phase

While our knowledge of Hofmeister-type protein-salt interactions is still evolving, several experimental results, some of them fairly recent, have provided tremendous insight into the important aspects of their stabilization mechanism. Originally, the structure of bulk water, and its alteration through specific long range forces generated by anions and cations in solution, was thought to be critical for understanding Hofmeister-type protein stabilization^{141,142}. Anions and cations were classified as either water structure makers (kosmotropes) or breakers (chaotropes), but recent experiments have indicated strongly that such structural effects are minimal at relevant solute concentrations, and have no direct causal relationship to Hofmeister-type protein stabilization¹⁴³⁻¹⁴⁷. Revised theories center on direct anion/cation interactions with proteins in three main ways¹⁴⁸. First, anions and cations may directly interact with the protein backbone and side chains through ion pairing interactions^{149,150}. Anions are known to have high affinity for amino functional groups within proteins¹⁵¹⁻¹⁵⁴, and cations are likely to interact with an array of sites^{155,156}, in many cases involving carboxylate groups^{153,157,158}. Arguably more important, in

light of current data, are the more indirect interactions between Hofmeister ions and the layer of water closely associated with proteins. Anions and cations can alter both the surface tension and hydrogen-bonding network surrounding proteins significantly, such that hydration entropy and protein stability are dramatically affected¹⁵⁹⁻¹⁶². Although canonical Hofmeister series are operative in many cellular processes, reversed Hofmeister series have also been observed, and rationalized through alterations to local water structures and direct protein-ion interactions, as above^{15,30-32}. Thus, while local protein-water interactions have been deemed important in Hofmeister stabilization, the magnitude of their importance is a somewhat malleable concept and subject to change based on the specific process or proteins being studied.

Based on the potential importance of solvent in Hofmeister-type protein stabilization, a number of groups have undertaken experiments carried out in environments of rarefied solvation (e.g., the gas-phase) to study both the local water structure surrounding small ions, and their interactions with proteins. Many of these experiments have been carried out using mass spectrometry (MS), where shifts in ion molecular mass can be interpreted relative to direct protein-counterion binding in solution^{20,21,30-33}. For example, precise measurements of molecular mass allowed Kebarle and co-workers to define the binding mode of many anions and cations to specific proteins¹⁵³. More recently, MS conditions have been identified whereby anion binding observed in the gas-phase can correlate precisely to the number of solvent accessible basic sites on a protein, thus mirroring bound populations in solution¹⁵⁴. Similarly, wavelength-resolved action spectroscopy, using MS detection, has been utilized to deduce the relative population of charge-solvated and zwitterionic structures in a range of amino acid-cation complexes¹⁶³⁻¹⁶⁹. Similar measurements of anions and cations clustered with varying amounts of water have also

been used to deduce ion specific effects on both local and bulk water structure¹⁷⁰⁻¹⁷⁷. While these data have demonstrated significant local water structure effects for specific ions, in some cases extending out to long ranges, they have also shown that bulk water structure is largely unaffected by cations and anions in solution at relevant concentrations.

IM-MS has also been used to study the general dependence of protein structure as a function of bound solvent, revealing both the complexity of protein structural states that exist in the gas-phase and the level of solvation necessary to compact Coulombically unfolded proteins^{41,178,179}. In addition, IM data have been used to deduce the influence of a range of anions and cations on protein stability and structure in the absence of bulk solvent. This data constitutes the majority Chapters 2 through 6 of this thesis. Earlier pioneering work in this area was aimed at adding discrete numbers of solvent molecules to gas-phase peptides and proteins as a means of testing the level of solvation necessary to expand biomolecules to the exact dimensions they possess in solution¹⁸⁰⁻¹⁸³.

1.5 Strategies to Differentiate Specific versus Nonspecific Interaction

MS has emerged as a well-established technology for deciphering function and dysfunction of complicated biological entities. In combination with IM, MS has massively grown its strength in monitoring the assembly of viral capsid proteins¹⁸⁴ and characterizing the structure of assembly intermediates, and more actively, contributed to the determination of topologies and stoichiometries for peptides and protein oligomer populations formed during the early stages of fibrillar aggregates, which give rise to pathological conditions ranging from neurodegenerative

disorders to systemic amyloidosis¹⁸⁵. Most recently, CXL coupled with MS becomes a robust tool to map proteome-wide interaction networks that govern critical cellular processes¹⁸⁶. While MS-based approaches enable the elucidation of protein oligomeric structure and dynamics within polydisperse systems at low concentrations, there remain challenges in using MS data to determine the specificity of interactions detected. Such difficulty arises from the mechanisms described above (section 1.3.6). Therefore, it is critical to discriminate between (n)ESI-induced artefacts and those truly reflective of the solution composition. Multiple strategies have emerged, including those using non-binding reference protein or reporter molecule, employing HDX approach, and via Monte Carlo simulation.

1.5.1 Non-binding Reference

The Klassen lab has developed a ‘reference protein method’ to identify nonspecific protein-ligand interactions in nESI-MS¹⁸⁷. This method involves the addition of a reference protein (P_{ref}), which does not bind specifically to the protein and ligand of interest in solution, to the ESI buffer. The occurrence of nonspecific protein-ligand binding is monitored by the appearance of ions corresponding to nonspecific complexes of P_{ref} and ligand in the mass spectrum. It is worth noting that such method is based on the assumption that nonspecific ligand binding is random, as suggested by the observation that the distribution of nonspecifically bound molecules often resembles that of a stochastic process, and affects equally all protein species present in the ESI droplets. The assumption that the distribution of nonspecifically bound ligand is independent of the nature of the protein in a given ESI-MS experiment has been rigorously tested and shown to be valid for a variety of “ligands”, including neutral and charged carbohydrates, amino acids, peptides, and divalent metal ions. Therefore, while a generally powerful approach in protein-

ligand screening applications, the method is not optimal for monitoring the occurrence of nonspecific interactions formed between two proteins during the ESI process.

1.5.2 Reporter Molecule

An alternative method, called the reporter molecule method, was developed to identify the occurrence of nonspecific protein-protein binding during the ESI process in the Klassen lab¹⁸⁸. Briefly, this method is based on the observation that, on average, specific and nonspecific protein complexes have different droplet histories. While the specific complexes are formed in solution, the nonspecific complexes are produced in the ES process, specifically the evaporating offspring droplets. To distinguish specific from nonspecific protein complexes, a reporter molecule (M_{rep}), which does not interact specifically with the proteins and protein complexes of interest, is added to the ESI buffer. Differences in the distribution of M_{rep} bound nonspecifically to the gaseous ions of the proteins and protein complexes serves to distinguish between protein complexes originating in solution and nonspecific complexes formed during the ESI process. To implement the method, a synthetic trisaccharide was used as the well-suited reporter molecule since it is a neutral molecule and forms relatively strong nonspecific interactions with proteins in the gas phase. A non-interacting small molecule is added to the bovine ubiquitin solution, at elevated concentration. Differences in the distributions of the small molecule bound nonspecifically to the different protein species present (*e.g.*, ubiquitin monomer versus dimer) is used to establish the occurrence of nonspecific protein-protein binding. This method has been demonstrated for cases where the protein complexes originate exclusively from nonspecific binding, exclusively from specific binding in solution, or from both specific and nonspecific binding. However, a weakness

with the reporter molecule methods is that it does not allow ESI mass spectra to be quantitatively corrected for the occurrence of nonspecific binding.

1.5.3 HDX

The Konermann lab recently reported an elegant method to distinguish specific from nonspecific multiprotein complexes detected by ESI-MS¹⁸⁹. This work employs on-line pulsed HDX for probing the origin of various species of hemoglobin. In addition to the canonical hemoglobin tetramer, ESI-MS reveals the presence of monomers, dimers, hexamers, and octamers. Tandem MS is used for extracting HDX levels in a subunit-specific manner. The data showed that dimeric species exhibit exchange levels that are significantly above those of the tetramer. Monomeric hemoglobin subunits are labeled to an even greater extent. This HDX pattern implied that monomers and dimers do not represent dissociation artifacts generated during ESI. Instead, they are derived from preexisting solution-phase structures. In contrast, hexamers and octamers exhibit HDX levels that resemble those of the tetramer, thus identifying these larger species as nonspecific clustering artifacts. Overall, the method combines on-line pulsed hydrogen/deuterium (H/D) exchange and tandem mass spectrometry, and requires many measurements as a function of concentration or under conditions where ESI artifacts are absent. Despite these minor limitations, this approach has demonstrated that the protein complexes formed in the solution (specific) and during the ES process (nonspecific) exhibit different H/D exchange patterns, which were revealed by ESI-MS/MS.

1.5.4 Monte Carlo Simulation

For proteins prone to self-assembly, it is possible to distinguish between specific oligomerization and nonspecific aggregates or artifacts of the measurement based on the statistical properties of the distribution of molecules in the solution. This distribution is influenced by the concentration and the initial droplet size generated at the tip of the needle. If two or more molecules are present in the same droplet, they will form an artificial oligomer ion in the gas phase. To this end, the Robinson lab developed a Monte Carlo approach, in which the concentration-dependent, non-natural oligomerization can be estimated by an algorithm, for assessing the specificity of oligomers of TIM, TTR, PK, ADH and GDH observed in ESI mass spectra¹⁹⁰. The signal above the calculated experimental artifact can then be seen as sample-specific oligomerization. In order for the methodology to work, droplet size must be trained using a dataset using proteins with known self-association properties. Under ideal conditions, such data can be used to accurately estimate final droplet sizes over many discrete protein complex ion populations, but variability in droplet sizes during ESI can potential cloud such estimates of artifact formation.

1.6 Summary

Proteins are critical for cellular function and characterizing their physical organization is the key aim of structural biology. However, applying conventional structural biology approaches is challenging for transient, dynamic, or polydisperse assemblies at low abundance. Therefore, there is a growing demand for hybrid technologies that are able to complement classical structural biology methods. Exciting technological advancements in the field of MS have added a new dimension to the study of protein-protein interactions and protein complex architecture. However, challenges for MS measurements revolve around the ability to either stabilize ‘native’

protein structure in the absence of bulk solvent or to eliminate nonspecific protein-protein complex formation following ionization/desolvation. This thesis is divided into two main parts: the majority (Chapter 2, 3, 4, 5 and 6) deals with developing universal strategies to stabilize proteins and protein complexes in the absence of bulk solvent, and one chapter (Chapter 7) discusses the formation of nonspecific complexes during the (n)ESI process.

In Chapter 2, a universal strategy is developed to stabilize proteins and protein complexes in the gas phase through the addition of Hofmeister-type anions in nESI buffer, and mechanistic insight of gas-phase protein stabilization through bound anions is further provided. **(Published, Han L, Hyung SJ, Mayers JJ, Ruotolo BT, Bound Anions Differentially Stabilize Multiprotein Complexes in the Absence of Bulk Solvent, Journal of the American Chemical Society, 2011, 133, 11358-11367.)**

In Chapter 3, a series of Hofmeister-type cations are screened for their ability to attach to proteins during desolvation and stabilize multiprotein complexes in the absence of bulk solvent, and the possible mechanisms of protein structure stabilization in the gas-phase achieved through nESI cationic additives is elucidated. **(Published, Han L, Hyung SJ, Ruotolo BT, Bound Cations Significantly Stabilize the Structure of Multiprotein Complexes in the Gas Phase, Angewandte Chemie International Edition, 2012, 51, 5692-5695.)**

In Chapter 4, the anion/cation combinations are tailored to significantly enhance the stability of gas-phase proteins and multi-protein complexes, and the additional details in the mechanism associated with stabilizing gas-phase protein ions through cation adduction is revealed.

(Published, Han L, Hyung SJ, Ruotolo BT, Dramatically Stabilizing Multiprotein Complex Structure in the Absence of Bulk Water using Tuned Hofmeister Salts, Faraday Discussion, 2013,160, 371-388. & Han L, Ruotolo BT, Traveling-wave Ion Mobility-Mass Spectrometry Reveals Additional Mechanistic Details in the Stabilization of Protein Complex Ions through Tuned Salt Additives, International Journal for Ion Mobility Spectrometry, 2013, 16, 41-50.)

In Chapter 5, the effect of Hofmeister-type cations for stabilizing the native-like structure of large multi-protein complexes is investigated, and the mechanism of protein cavity collapse upon collisional activation is examined by replacing the mobile protons with tightly-bound cations.

In Chapter 6, a tetrameric protein complex, ConA (103kDa) is reported to misfold in solution by IM-MS, and this misfolded ConA can be recovered by screening a series of Hofmeister-type cations/anions added in nESI buffer prior to ionization/desolvation. **(Published, Han L, Ruotolo BT, Hofmeister Salts Recover a Misfolded Multiprotein Complex for Subsequent Structural Measurements in the Gas Phase, Angewandte Chemie International Edition, 2013, 52, 8329-8332.)**

In Chapter 7, IM-MS is explored to differentiate between multiprotein complex structures formed in solution and in electrospray droplets, in the case of self-dimerization of pentameric SAP and hexameric bovGDH, respectively.

1.7 References

- (1) Alberts, B. *Cell* **1998**, 92, 291.
- (2) Rausell, A.; Juan, D.; Pazos, F.; Valencia, A. *Proc. Natl. Acad. Sci. U. S. A.* **2010**, 107, 1995.
- (3) Lee, D.; Redfern, O.; Orengo, C. *Nat Rev Mol Cell Biol* **2007**, 8, 995.
- (4) Steven, A. C.; Baumeister, W. *Journal of Structural Biology* **2008**, 163, 186.
- (5) Kendrew, J. C.; Parrish, R. G.; Marrack, J. R.; Orland, E. S. *Nature* **1954**, 174, 946.
- (6) Abola, E.; Kuhn, P.; Earnest, T.; Stevens, R. C. *Nat Struct Mol Biol* **2000**, 7, 973.
- (7) Wimberly, B. T.; Brodersen, D. E.; Clemons, W. M.; Morgan-Warren, R. J.; Carter, A. P.; Vonnrhein, C.; Hartsch, T.; Ramakrishnan, V. *Nature* **2000**, 407, 327.
- (8) Ban, N.; Nissen, P.; Hansen, J.; Moore, P. B.; Steitz, T. A. *Science* **2000**, 289, 905.
- (9) Meinhart, A.; Cramer, P. *Nature* **2004**, 430, 223.
- (10) Liu, Q.; Greimann, J. C.; Lima, C. D. *Cell* **2006**, 127, 1223.
- (11) Egea, P. F.; Shan, S.-o.; Napetschnig, J.; Savage, D. F.; Walter, P.; Stroud, R. M. *Nature* **2004**, 427, 215.
- (12) Rabi, I. I.; Zacharias, J. R.; Millman, S.; Kusch, P. *Physical Review* **1938**, 53, 318.
- (13) Palmer, A. G. *Annual Review of Biophysics and Biomolecular Structure* **2001**, 30, 129.
- (14) Fiaux, J.; Bertelsen, E. B.; Horwich, A. L.; Wuthrich, K. *Nature* **2002**, 418, 207.
- (15) Falke, S.; Tama, F.; Brooks Iii, C. L.; Gogol, E. P.; Fisher, M. T. *Journal of Molecular Biology* **2005**, 348, 219.
- (16) van Heel, M.; Gowen, B.; Matadeen, R.; Orlova, E. V.; Finn, R.; Pape, T.; Cohen, D.; Stark, H.; Schmidt, R.; Schatz, M.; Patwardhan, A. *Q. Rev. Biophys.* **2000**, 33, 307.
- (17) Vachette, P.; Koch, M. H. J.; Svergun, D. I. In *Methods in Enzymology*; Charles W. Carter, Jr., Robert, M. S., Eds.; Academic Press: 2003; Vol. Volume 374, p 584.
- (18) Forster, F.; Webb, B.; Krukenberg, K. A.; Tsuruta, H.; Agard, D. A.; Sali, A. *Journal of Molecular Biology* **2008**, 382, 1089.
- (19) Brahm, S.; Brahm, J. *Journal of Molecular Biology* **1980**, 138, 149.
- (20) Kelly, S. M.; Jess, T. J.; Price, N. C. *Biochimica Et Biophysica Acta-Proteins and Proteomics* **2005**, 1751, 119.
- (21) Jelesarov, I.; Bosshard, H. R. *Journal of Molecular Recognition* **1999**, 12, 3.
- (22) Sali, A.; Glaeser, R.; Earnest, T.; Baumeister, W. *Nature* **2003**, 422, 216.
- (23) Benesch, J. L. P.; Ruotolo, B. T. *Current Opinion in Structural Biology* **2011**, 21, 641.
- (24) Hyung, S. J.; Ruotolo, B. T. *Proteomics* **2012**, 12, 1547.
- (25) Konermann, L.; Pan, J. X.; Liu, Y. H. *Chemical Society Reviews* **2011**, 40, 1224.
- (26) Engen, J. R. *Analytical Chemistry* **2009**, 81, 7870.
- (27) Kiselar, J. G.; Chance, M. R. *Journal of Mass Spectrometry* **2010**, 45, 1373.
- (28) Konermann, L.; Stocks, B. B.; Pan, Y.; Tong, X. *Mass Spectrometry Reviews* **2010**, 29, 651.
- (29) Petrotchenko, E. V.; Borchers, C. H. *Mass Spectrometry Reviews* **2010**, 29, 862.
- (30) Jin Lee, Y. *Molecular BioSystems* **2008**, 4, 816.

- (31) Utrecht, C.; Rose, R. J.; van Duijn, E.; Lorenzen, K.; Heck, A. J. R. *Chemical Society Reviews* **2010**, *39*, 1633.
- (32) Bohrer, B. C.; Mererbloom, S. I.; Koeniger, S. L.; Hilderbrand, A. E.; Clemmer, D. E. In *Annual Review of Analytical Chemistry* 2008; Vol. 1, p 293.
- (33) Hernandez, H.; Dziembowski, A.; Taverner, T.; Seraphin, B.; Robinson, C. V. *EMBO Rep.* **2006**, *7*, 605.
- (34) Zhou, M.; Sandercock, A. M.; Fraser, C. S.; Ridlova, G.; Stephens, E.; Schenauer, M. R.; Yokoi-Fong, T.; Barsky, D.; Leary, J. A.; Hershey, J. W.; Doudna, J. A.; Robinson, C. V. *Proceedings of the National Academy of Sciences* **2008**, *105*, 18139.
- (35) Damoc, E.; Fraser, C. S.; Zhou, M.; Videler, H.; Mayeur, G. L.; Hershey, J. W. B.; Doudna, J. A.; Robinson, C. V.; Leary, J. A. *Mol. Cell. Proteomics* **2007**, *6*, 1135.
- (36) Sharon, M.; Mao, H.; Boeri Erba, E.; Stephens, E.; Zheng, N.; Robinson, C. V. *Structure* **2009**, *17*, 31.
- (37) Park, A. Y.; Jergic, S.; Politis, A.; Ruotolo, B. T.; Hirshberg, D.; Jessop, L. L.; Beck, J. L.; Barsky, D.; O'Donnell, M.; Dixon, N. E.; Robinson, C. V. *Structure (London, England : 1993)* **2010**, *18*, 285.
- (38) McInerney, P.; Johnson, A.; Katz, F.; O'Donnell, M. *Molecular cell* **2007**, *27*, 527.
- (39) Rabuck, J. N.; Hyung, S.-J.; Ko, K. S.; Fox, C. C.; Soellner, M. B.; Ruotolo, B. T. *Analytical Chemistry* **2013**, *85*, 6995.
- (40) Han, L.; Ruotolo, B. T. In *International Journal for Ion Mobility Spectrometry* 2013; Vol. 16, p 41.
- (41) Freeke, J.; Robinson, C. V.; Ruotolo, B. T. *International Journal of Mass Spectrometry* **2010**, *298*, 91.
- (42) van Duijn, E.; Heck, A. J. R. *Drug Discovery Today: Technologies* **2006**, *3*, 21.
- (43) van Duijn, E.; Simmons, D. A.; van den Heuvel, R. H. H.; Bakkes, P. J.; van Heerikhuizen, H.; Heeren, R. M. A.; Robinson, C. V.; van der Vies, S. M.; Heck, A. J. R. *Journal of the American Chemical Society* **2006**, *128*, 4694.
- (44) Zhou, M.; Morgner, N.; Barrera, N. P.; Politis, A.; Isaacson, S. C.; Matak-Vinkovic, D.; Murata, T.; Bernal, R. A.; Stock, D.; Robinson, C. V. *Science* **2011**, *334*, 380.
- (45) Jeronimo, C.; Forget, D.; Bouchard, A.; Li, Q.; Chua, G.; Poitras, C.; Thérien, C.; Bergeron, D.; Bourassa, S.; Greenblatt, J.; Chabot, B.; Poirier, G. G.; Hughes, T. R.; Blanchette, M.; Price, D. H.; Coulombe, B. *Molecular cell* **2007**, *27*, 262.
- (46) Rand, K. D.; Zehl, M.; Jensen, O. N.; Jørgensen, T. J. D. *Analytical Chemistry* **2009**, *81*, 5577.
- (47) Pan, J.; Han, J.; Borchers, C. H.; Konermann, L. *Journal of the American Chemical Society* **2009**, *131*, 12801.
- (48) Mendoza, V. L.; Vachet, R. W. *Mass Spectrometry Reviews* **2009**, *28*, 785.
- (49) Angel, T. E.; Gupta, S.; Jastrzebska, B.; Palczewski, K.; Chance, M. R. *Proceedings of the National Academy of Sciences* **2009**, *106*, 14367.
- (50) Lee, Y. J.; Lackner, L. L.; Nunnari, J. M.; Phinney, B. S. *Journal of Proteome Research* **2007**, *6*, 3908.
- (51) Fabris, D.; Yu, E. T. *Journal of Mass Spectrometry* **2010**, *45*, 841.
- (52) Tao, L.; Dahl, D.; Pérez, L.; Russell, D. *Journal of the American Society for Mass Spectrometry* **2009**, *20*, 1593.
- (53) Ruotolo, B. T.; Giles, K.; Campuzano, I.; Sandercock, A. M.; Bateman, R. H.; Robinson, C. V. *Science* **2005**, *310*, 1658.

- (54) Bernstein, S. L.; Wyttenbach, T.; Baumketner, A.; Shea, J.-E.; Bitan, G.; Teplow, D. B.; Bowers, M. T. *Journal of the American Chemical Society* **2005**, *127*, 2075.
- (55) Politis, A.; Park, A. Y.; Hyung, S. J.; Barsky, D.; Ruotolo, B. T.; Robinson, C. V. *Plos One* **2010**, *5*.
- (56) Lane, L. A.; Fernández-Tornero, C.; Zhou, M.; Morgner, N.; Ptchelkine, D.; Steuerwald, U.; Politis, A.; Lindner, D.; Gvozdenovic, J.; Gavin, A.-C.; Müller, C. W.; Robinson, C. V. *Structure* **2011**, *19*, 90.
- (57) Uetrecht, C.; Barbu, I. M.; Shoemaker, G. K.; van Duijn, E.; HeckAlbert, J. R. *Nat Chem* **2011**, *3*, 126.
- (58) Bernstein, S. L.; Dupuis, N. F.; Lazo, N. D.; Wyttenbach, T.; Condrón, M. M.; Bitan, G.; Teplow, D. B.; Shea, J.-E.; Ruotolo, B. T.; Robinson, C. V.; Bowers, M. T. *Nat Chem* **2009**, *1*, 326.
- (59) Dupuis, N. F.; Wu, C.; Shea, J.-E.; Bowers, M. T. *Journal of the American Chemical Society* **2011**, *133*, 7240.
- (60) Smith, D. P.; Radford, S. E.; Ashcroft, A. E. *Proceedings of the National Academy of Sciences* **2010**, *107*, 6794.
- (61) Jenner, M.; Ellis, J.; Huang, W.-C.; Lloyd Raven, E.; Roberts, G. C. K.; Oldham, N. J. *Angewandte Chemie International Edition* **2011**, *50*, 8291.
- (62) Shi, H.; Pierson, N. A.; Valentine, S. J.; Clemmer, D. E. *The Journal of Physical Chemistry B* **2012**, *116*, 3344.
- (63) Hyung, S.-J.; Robinson, C. V.; Ruotolo, B. T. *Chemistry & Biology* **2009**, *16*, 382.
- (64) Song, F. *Journal of the American Society for Mass Spectrometry* **2007**, *18*, 1286.
- (65) Takáts, Z.; Wiseman, J. M.; Gologan, B.; Cooks, R. G. *Analytical Chemistry* **2004**, *76*, 4050.
- (66) Gaskell, S. J. *Journal of Mass Spectrometry* **1997**, *32*, 677.
- (67) Wilm, M. S.; Mann, M. *International Journal of Mass Spectrometry and Ion Processes* **1994**, *136*, 167.
- (68) Wilm, M.; Mann, M. *Analytical Chemistry* **1996**, *68*, 1.
- (69) Fernandez de la Mora, J. *Analytica Chimica Acta* **2000**, *406*, 93.
- (70) Dole, M.; Mack, L. L.; Hines, R. L.; Mobley, R. C.; Ferguson, L. D.; Alice, M. B. *The Journal of Chemical Physics* **1968**, *49*, 2240.
- (71) Iribarne, J. V.; Thomson, B. A. *The Journal of Chemical Physics* **1976**, *64*, 2287.
- (72) Chernushevich, I. V.; Loboda, A. V.; Thomson, B. A. *Journal of Mass Spectrometry* **2001**, *36*, 849.
- (73) Guilhaus, M.; Selby, D.; Mlynski, V. *Mass Spectrometry Reviews* **2000**, *19*, 65.
- (74) March, R. E. *Journal of Mass Spectrometry* **1997**, *32*, 351.
- (75) Sobott, F.; Hernández, H.; McCammon, M. G.; Tito, M. A.; Robinson, C. V. *Analytical Chemistry* **2002**, *74*, 1402.
- (76) Chernushevich, I. V.; Thomson, B. A. *Analytical Chemistry* **2004**, *76*, 1754.
- (77) Jurchen, J. C.; Garcia, D. E.; Williams, E. R. *Journal of the American Society for Mass Spectrometry* **2004**, *15*, 1408.
- (78) Jurchen, J. C.; Williams, E. R. *Journal of the American Chemical Society* **2003**, *125*, 2817.
- (79) Felitsyn, N.; Kitova, E. N.; Klassen, J. S. *Analytical Chemistry* **2001**, *73*, 4647.
- (80) Versluis, C.; Staaij, A.; Stokvis, E.; Heck, A. R.; Craene, B. *Journal of the American Society for Mass Spectrometry* **2001**, *12*, 329.

- (81) Benesch, J. L. P.; Ruotolo, B. T.; Simmons, D. A.; Robinson, C. V. *Chemical Reviews* **2007**, *107*, 3544.
- (82) Pagel, K.; Hyung, S.-J.; Ruotolo, B. T.; Robinson, C. V. *Analytical Chemistry* **2010**, *82*, 5363.
- (83) Hall, Z.; Politis, A.; Bush, M. F.; Smith, L. J.; Robinson, C. V. *Journal of the American Chemical Society* **2012**, *134*, 3429.
- (84) Benesch, J. L. P. *Journal of the American Society for Mass Spectrometry* **2009**, *20*, 341.
- (85) Benesch, J. L. P.; Ruotolo, B. T.; Sobott, F.; Wildgoose, J.; Gilbert, A.; Bateman, R.; Robinson, C. V. *Analytical Chemistry* **2009**, *81*, 1270.
- (86) Zhang, H.; Cui, W. D.; Wen, J. Z.; Blankenship, R. E.; Gross, M. L. *Analytical Chemistry* **2011**, *83*, 5598.
- (87) Breuker, K.; McLafferty, F. W. *Angewandte Chemie International Edition* **2003**, *42*, 4900.
- (88) Breuker, K.; McLafferty, F. W. *Angewandte Chemie International Edition* **2005**, *44*, 4911.
- (89) Wysocki, V. H.; Jones, C. M.; Galhena, A. S.; Blackwell, A. E. *Journal of the American Society for Mass Spectrometry* **2008**, *19*, 903.
- (90) Galhena, A. S.; Dagan, S.; Jones, C. M.; Beardsley, R. L.; Wysocki, V. H. *Analytical Chemistry* **2008**, *80*, 1425.
- (91) Jones, C. M.; Beardsley, R. L.; Galhena, A. S.; Dagan, S.; Cheng, G.; Wysocki, V. H. *Journal of the American Chemical Society* **2006**, *128*, 15044.
- (92) Blackwell, A. E.; Dodds, E. D.; Bandarian, V.; Wysocki, V. H. *Analytical Chemistry* **2011**, *83*, 2862.
- (93) Zhong, Y.; Hyung, S.-J.; Ruotolo, B. T. *Expert Review of Proteomics* **2012**, *9*, 47.
- (94) Mason, E. A.; McDaniel, E. W. *Transport Properties of Ions in Gases*; John Wiley & Sons: New York, 1988.
- (95) Harvey, S. R.; Macphee, C. E.; Barran, P. E. *Methods* **2011**, *54*, 454.
- (96) Kanu, A. B.; Dwivedi, P.; Tam, M.; Matz, L.; Hill, H. H. *Journal of Mass Spectrometry* **2008**, *43*, 1.
- (97) Giles, K.; Pringle, S. D.; Worthington, K. R.; Little, D.; Wildgoose, J. L.; Bateman, R. H. *Rapid Commun Mass Sp* **2004**, *18*, 2401.
- (98) Pringle, S. D.; Giles, K.; Wildgoose, J. L.; Williams, J. P.; Slade, S. E.; Thalassinou, K.; Bateman, R. H.; Bowers, M. T.; Scrivens, J. H. *Int. J. Mass Spectrom.* **2007**, *261*, 1.
- (99) Shvartsburg, A. A.; Smith, R. D. *Analytical Chemistry* **2008**, *80*, 9689.
- (100) Ruotolo, B. T.; Benesch, J. L. P.; Sandercock, A. M.; Hyung, S. J.; Robinson, C. V. *Nature Protocols* **2008**, *3*, 1139.
- (101) Giles, K.; Wildgoose, J. L.; Langridge, D. J.; Campuzano, I. *International Journal of Mass Spectrometry* **2010**, *298*, 10.
- (102) Zhong, Y.; Hyung, S. J.; Ruotolo, B. T. *Analyst* **2011**, *136*, 3534.
- (103) Giles, K.; Williams, J. P.; Campuzano, I. *Rapid Commun. Mass Spectrom.* **2011**, *25*, 1559.
- (104) Dugourd, P.; Hudgins, R. R.; Clemmer, D. E.; Jarrold, M. F. *Review of Scientific Instruments* **1997**, *68*, 1122.

- (105) Kemper, P. R.; Dupuis, N. F.; Bowers, M. T. *International Journal of Mass Spectrometry* **2009**, *287*, 46.
- (106) Merenbloom, S. I.; Glaskin, R. S.; Henson, Z. B.; Clemmer, D. E. *Analytical Chemistry* **2009**, *81*, 1482.
- (107) Roscioli, K. M.; Davis, E.; Siems, W. F.; Mariano, A.; Su, W.; Guharay, S. K.; Hill, H. H. *Analytical Chemistry* **2011**, *83*, 5965.
- (108) Steinberg, M. Z.; Elber, R.; McLafferty, F. W.; Gerber, R. B.; Breuker, K. *Chembiochem* **2008**, *9*, 2417.
- (109) Shelimov, K. B.; Clemmer, D. E.; Hudgins, R. R.; Jarrold, M. F. *Journal of the American Chemical Society* **1997**, *119*, 2240.
- (110) Shelimov, K. B.; Jarrold, M. F. *Journal of the American Chemical Society* **1997**, *119*, 2987.
- (111) Li, J. W.; Taraszka, J. A.; Counterman, A. E.; Clemmer, D. E. *International Journal of Mass Spectrometry* **1999**, *185*, 37.
- (112) Ruotolo, B. T.; Hyung, S. J.; Robinson, P. M.; Giles, K.; Bateman, R. H.; Robinson, C. V. *Angewandte Chemie-International Edition* **2007**, *46*, 8001.
- (113) Shelimov, K. B.; Jarrold, M. F. *Journal of the American Chemical Society* **1996**, *118*, 10313.
- (114) Clemmer, D. E.; Hudgins, R. R.; Jarrold, M. F. *Journal of the American Chemical Society* **1995**, *117*, 10141.
- (115) Segev, E.; Wyttenbach, T.; Bowers, M. T.; Gerber, R. B. *Physical Chemistry Chemical Physics* **2008**, *10*, 3077.
- (116) Wyttenbach, T.; Bowers, M. T. *The Journal of Physical Chemistry B* **2011**, *115*, 12266.
- (117) Bernstein, S. L.; Liu, D. F.; Wyttenbach, T.; Bowers, M. T.; Lee, J. C.; Gray, H. B.; Winkler, J. R. *Journal of the American Society for Mass Spectrometry* **2004**, *15*, 1435.
- (118) Pagel, K.; Natan, E.; Hall, Z.; Fersht, A. R.; Robinson, C. V. *Angewandte Chemie-International Edition* **2013**, *52*, 361.
- (119) Saikusa, K.; Fuchigami, S.; Takahashi, K.; Asano, Y.; Nagadoi, A.; Tachiwana, H.; Kurumizaka, H.; Ikeguchi, M.; Nishimura, Y.; Akashi, S. *Analytical Chemistry* **2013**, *85*, 4165.
- (120) Kaddis, C. S.; Lomeli, S. H.; Yin, S.; Berhane, B.; Apostol, M. I.; Kickhoefer, V. A.; Rome, L. H.; Loo, J. A. *Journal of the American Society for Mass Spectrometry* **2007**, *18*, 1206.
- (121) Uetrecht, C.; Versluis, C.; Watts, N. R.; Wingfield, P. T.; Steven, A. C.; Heck, A. J. R. *Angewandte Chemie-International Edition* **2008**, *47*, 6247.
- (122) Hogan, C. J.; Ruotolo, B. T.; Robinson, C. V.; de la Mora, J. F. *Journal of Physical Chemistry B* **2011**, *115*, 3614.
- (123) Sun, J.; Kitova, E. N.; Klassen, J. S. *Analytical Chemistry* **2006**, *79*, 416.
- (124) Wang, W.; Kitova, E. N.; Klassen, J. S. *Analytical Chemistry* **2003**, *75*, 4945.
- (125) Bagal, D.; Kitova, E. N.; Liu, L.; El-Hawiet, A.; Schnier, P. D.; Klassen, J. S. *Analytical Chemistry* **2009**, *81*, 7801.
- (126) Warnke, S.; von Helden, G.; Pagel, K. *Journal of the American Chemical Society* **2013**, *135*, 1177.
- (127) Bornschein, R. E.; Hyung, S. J.; Ruotolo, B. T. *Journal of the American Society for Mass Spectrometry* **2011**, *22*, 1690.

- (128) Duijn, E. v.; Barendregt, A.; Synowsky, S.; Versluis, C.; Heck, A. J. R. *Journal of the American Chemical Society* **2009**, *131*, 1452.
- (129) Liu, L.; Kitova, E.; Klassen, J. *Journal of the American Society for Mass Spectrometry* **2011**, *22*, 310.
- (130) Rouse, S. L.; Marcoux, J.; Robinson, C. V.; Sansom, M. S. P. *Biophysical Journal* **2013**, *105*, 648.
- (131) Barrera, N. P.; Di Bartolo, N.; Booth, P. J.; Robinson, C. V. *Science* **2008**, *321*, 243.
- (132) Barrera, N. P.; Isaacson, S. C.; Zhou, M.; Bavro, V. N.; Welch, A.; Schaedler, T. A.; Seeger, M. A.; Miguel, R. N.; Korkhov, V. M.; van Veen, H. W.; Venter, H.; Walmsley, A. R.; Tate, C. G.; Robinson, C. V. *Nature Methods* **2009**, *6*, 585.
- (133) Borysik, A. J.; Hewitt, D. J.; Robinson, C. V. *Journal of the American Chemical Society* **2013**, *135*, 6078.
- (134) Benesch, J. L. P.; Ruotolo, B. T.; Simmons, D. A.; Robinson, C. V. *Chemical Reviews* **2007**, *107*, 3544.
- (135) Vrbka, L.; Jungwirth, P.; Bauduin, P.; Touraud, D.; Kunz, W. *Journal of Physical Chemistry B* **2006**, *110*, 7036.
- (136) Zhang, Y. J.; Furyk, S.; Bergbreiter, D. E.; Cremer, P. S. *Journal of the American Chemical Society* **2005**, *127*, 14505.
- (137) Baldwin, R. L. *Biophysical Journal* **1996**, *71*, 2056.
- (138) Kunz, W. *Current Opinion in Colloid & Interface Science* **2010**, *15*, 34.
- (139) Collins, K. D. *Methods* **2004**, *34*, 300.
- (140) Kunz, W.; Henle, J.; Ninham, B. W. *Current Opinion in Colloid & Interface Science* **2004**, *9*, 19.
- (141) Collins, K. D.; Washabaugh, M. W. *Q. Rev. Biophys.* **1985**, *18*, 323.
- (142) Vanzi, F.; Madan, B.; Sharp, K. *Journal of the American Chemical Society* **1998**, *120*, 10748.
- (143) Omta, A. W.; Kropman, M. F.; Woutersen, S.; Bakker, H. J. *Science* **2003**, *301*, 347.
- (144) Kropman, M. F.; Bakker, H. J. *Journal of the American Chemical Society* **2004**, *126*, 9135.
- (145) Batchelor, J. D.; Olteanu, A.; Tripathy, A.; Pielak, G. J. *Journal of the American Chemical Society* **2004**, *126*, 1958.
- (146) Bostrom, M.; Williams, D. R. M.; Ninham, B. W. *Phys. Rev. Lett.* **2001**, *87*.
- (147) Smith, J. D.; Saykally, R. J.; Geissler, P. L. *Journal of the American Chemical Society* **2007**, *129*, 13847.
- (148) Zhang, Y. J.; Cremer, P. S. In *Annual Review of Physical Chemistry, Vol 61*; Leone, S. R., Cremer, P. S., Groves, J. T., Johnson, M. A., Richmond, G., Eds. 2010; Vol. 61, p 63.
- (149) Lund, M.; Vacha, R.; Jungwirth, P. *Langmuir* **2008**, *24*, 3387.
- (150) Lund, M.; Vrbka, L.; Jungwirth, P. *Journal of the American Chemical Society* **2008**, *130*, 11582.
- (151) Prakash, H.; Kansara, B. T.; Mazumdar, S. *International Journal of Mass Spectrometry* **2010**, *289*, 84.
- (152) Stephenson, J. L.; McLuckey, S. A. *Analytical Chemistry* **1997**, *69*, 281.

- (153) Verkerk, U. H.; Kebarle, P. *Journal of the American Society for Mass Spectrometry* **2005**, *16*, 1325.
- (154) Flick, T. G.; Merenbloom, S. I.; Williams, E. R. *Analytical Chemistry* **2011**, *83*, 2210.
- (155) Verkerk, U. H.; Peschke, M.; Kebarle, P. *Journal of Mass Spectrometry* **2003**, *38*, 618.
- (156) Felitsyn, N.; Peschke, M.; Kebarle, P. *International Journal of Mass Spectrometry* **2002**, *219*, 39.
- (157) Timofeev, O.; Zhu, M. M.; Gross, M. L. *International Journal of Mass Spectrometry* **2004**, *231*, 113.
- (158) Kebarle, P.; Verkerk, U. H. *Mass Spectrometry Reviews* **2009**, *28*, 898.
- (159) Pegram, L. M.; Record, M. T. *Journal of Physical Chemistry B* **2007**, *111*, 5411.
- (160) Pegram, L. M.; Record, M. T. *Proc. Natl. Acad. Sci. U. S. A.* **2006**, *103*, 14278.
- (161) Pegram, L. M.; Record, M. T. *Journal of Physical Chemistry B* **2008**, *112*, 9428.
- (162) Pegram, L. M.; Record Jr, M. T. *Chemical Physics Letters* **2008**, *467*, 1.
- (163) Prell, J. S.; Flick, T. G.; Oomens, J.; Berden, G.; Williams, E. R. *Journal of Physical Chemistry A* **2010**, *114*, 854.
- (164) Bush, M. F.; Oomens, J.; Saykally, R. J.; Williams, E. R. *Journal of the American Chemical Society* **2008**, *130*, 6463.
- (165) Dunbar, R. C.; Hopkinson, A. C.; Oomens, J.; Siu, C. K.; Siu, K. W. M.; Steill, J. D.; Verkerk, U. H.; Zhao, J. F. *Journal of Physical Chemistry B* **2009**, *113*, 10403.
- (166) Dunbar, R. C.; Polfer, N. C.; Oomens, J. *Journal of the American Chemical Society* **2007**, *129*, 14562.
- (167) O'Brien, J. T.; Prell, J. S.; Steill, J. D.; Oomens, J.; Williams, E. R. *Journal of Physical Chemistry A* **2008**, *112*, 10823.
- (168) Bush, M. F.; O'Brien, J. T.; Prell, J. S.; Saykally, R. J.; Williams, E. R. *Journal of the American Chemical Society* **2007**, *129*, 1612.
- (169) Armentrout, P. B.; Rodgers, M. T.; Oomens, J.; Steill, J. D. *Journal of Physical Chemistry A* **2008**, *112*, 2248.
- (170) Walters, R. S.; Pillai, E. D.; Duncan, M. A. *Journal of the American Chemical Society* **2005**, *127*, 16599.
- (171) Shin, J. W.; Hammer, N. I.; Diken, E. G.; Johnson, M. A.; Walters, R. S.; Jaeger, T. D.; Duncan, M. A.; Christie, R. A.; Jordan, K. D. *Science* **2004**, *304*, 1137.
- (172) Miller, D. J.; Lisy, J. M. *Journal of Chemical Physics* **2006**, *124*.
- (173) Bush, M. F.; O'Brien, J. T.; Prell, J. S.; Wu, C. C.; Saykally, R. J.; Williams, E. R. *Journal of the American Chemical Society* **2009**, *131*, 13270.
- (174) Iino, T.; Ohashi, K.; Inoue, K.; Judai, K.; Nishi, N.; Sekiya, H. *Journal of Chemical Physics* **2007**, *126*.
- (175) Choi, J. H.; Kuwata, K. T.; Cao, Y. B.; Okumura, M. *The Journal of Physical Chemistry A* **1998**, *102*, 503.
- (176) Robertson, W. H.; Johnson, M. A. *Annual Review of Physical Chemistry* **2003**, *54*, 173.
- (177) Bush, M. F.; Saykally, R. J.; Williams, E. R. *Journal of the American Chemical Society* **2007**, *129*, 2220.
- (178) Merenbloom, S. I.; Flick, T. G.; Daly, M. P.; Williams, E. R. *Journal of the American Society for Mass Spectrometry* **2011**, *1*.

- (179) Freeke, J.; Bush, M. F.; Robinson, C. V.; Ruotolo, B. T. *Chemical Physics Letters* **2012**, 524, 1.
- (180) Woenckhaus, J.; Hudgins, R. R.; Jarrold, M. F. *Journal of the American Chemical Society* **1997**, 119, 9586.
- (181) Fye, J. L.; Woenckhaus, J.; Jarrold, M. F. *Journal of the American Chemical Society* **1998**, 120, 1327.
- (182) Rodriguez-Cruz, S. E.; Klassen, J. S.; Williams, E. R. *Journal of the American Society for Mass Spectrometry* **1999**, 10, 958.
- (183) Wyttenbach, T.; Bowers, M. T. *Chemical Physics Letters* **2009**, 480, 1.
- (184) Knapman, T. W.; Morton, V. L.; Stonehouse, N. J.; Stockley, P. G.; Ashcroft, A. E. *Rapid Communications in Mass Spectrometry* **2010**, 24, 3033.
- (185) Bernstein, S. L.; Wyttenbach, T.; Baumketner, A.; Shea, J. E.; Bitan, G.; Teplow, D. B.; Bowers, M. T. *Journal of the American Chemical Society* **2005**, 127, 2075.
- (186) Herzog, F.; Kahraman, A.; Boehringer, D.; Mak, R.; Bracher, A.; Walzthoeni, T.; Leitner, A.; Beck, M.; Hartl, F. U.; Ban, N.; Malmstrom, L.; Aebersold, R. *Science* **2012**, 337, 1348.
- (187) Sun, J. X.; Kitova, E. N.; Wang, W. J.; Klassen, J. S. *Analytical Chemistry* **2006**, 78, 3010.
- (188) Sun, J.; Kitova, E. N.; Sun, N.; Klassen, J. S. *Analytical Chemistry* **2007**, 79, 8301.
- (189) Hossain, B. M.; Konermann, L. *Analytical Chemistry* **2006**, 78, 1613.
- (190) Lane, L. A.; Ruotolo, B. T.; Robinson, C. V.; Favrin, G.; Benesch, J. L. P. *International Journal of Mass Spectrometry* **2009**, 283, 169.

Chapter 2. Bound Anions Differentially Stabilize Multiprotein Complexes in the Absence of Bulk Solvent

Han L*, Hyung SJ*, Mayers JJ, Ruotolo BT, Bound Anions Differentially Stabilize Multiprotein Complexes in the Absence of Bulk Solvent, *Journal of the American Chemical Society*, 2011, 133, 11358-11367. (*equal contribution)

2.1 Abstract

The combination of IM separation with MS is an emergent and powerful structural biology tool, capable of simultaneously assessing the structure, topology, dynamics and composition of large protein assemblies within complex mixtures. An integral part of the IM-MS measurement is the ionization of intact multiprotein complexes and their removal from bulk solvent. This process, while likely preserving a substantial portion of protein structure and organization, imposes a foreign environment on proteins that may cause structural rearrangements to occur. Thus, a general means must be identified to stabilize protein structures in the absence of bulk solvent. Our approach to this problem involves the partial replacement of contacts between bulk solvent and the protein complex with selected stabilizing counter-ions by carefully controlling buffer conditions prior to protein desolvation. During ESI, large numbers of counter-ions adhere to the surface of the complex during desolvation and can stabilize its structure by forming a protective ‘shell’ around critical flexible regions of the protein. By using IM-MS, we observe both the

dissociation and unfolding transitions for four tetrameric protein complexes bound to populations of twelve different anions using collisional activation. The data presented here quantifies, for the first time, the influence of a large range of counter ions on gas-phase protein structure and allows us to rank and classify counter ions as structure stabilizers in the absence of bulk solvent. The rank order determined by our data is substantially different when compared to the known Hofmeister salt series in solution. While this is an expected outcome of our work, due to the diminished influence of both anion and protein solvation by water, our data provides direct information on protein anion binding in solution and highlights the fact that both hydration layer and anion-protein binding effects are critical for Hofmeister-type stabilization in solution. Finally, we present a complete and detailed mechanism of action for counter-ion stabilization of proteins and their complexes in the gas-phase. Anion-resolved data acquired for smaller protein systems allows us to classify anions into three categories in terms of their relative acidities and proton affinities.

2.2 Introduction

Characterizing the structures and functions of multiprotein complexes on a global level within living organisms is a far-reaching scientific goal for the field of structural genomics¹⁻³. While significant progress has been made in this field over the past few years, it is becoming increasingly apparent that no single analytical tool has the capacity to completely describe the structural complexity of even the simplest proteome. This fact is evident in recent reports where multiple structural datasets have been integrated in order to produce models of large multiprotein systems⁴⁻¹¹. For example, a structural model of the yeast nuclear pore complex was recently determined by integrating the distance constraints derived from multiple datasets, including:

affinity chromatography, SEC, sedimentation coefficients, EM, and chemical CXL-MS⁵. In this and other experiments in integrative structural biology, the orthogonality of the tools employed translates into a structural picture that none of the technologies could produce in isolation.

MS has played a significant role in such integrative structural biology ventures, as MS has the ability to assess the composition, stoichiometry, and dynamics of multiprotein complexes of low in abundance^{6,7,12,13}. These attributes have allowed MS to provide organizational diagrams, or protein-protein contact maps, for a number of assemblies in advance of atomic resolution structures from XRD or NMR datasets¹⁴⁻¹⁸. In some cases, MS data have reported on multiprotein systems that exhibit high degrees of polydispersity and complexity^{19,20}, and are excellent examples of the unique role that MS can play in defining the structure and function of multiprotein complexes. In addition, recent experiments that demonstrate the ability of MS to interrogate the organization of membrane protein systems identifies MS as a technology on the forefront of structural biology research^{21,22}.

Recently, the utility of IM separation in tandem with MS to the analysis of protein complexes has generated considerable interest, because early studies have indicated that the quaternary structure of protein complexes can be retained in the absence of solvent²³⁻²⁶. Originally applied to problems in chemical physics²⁷⁻²⁹, trace detection^{30,31}, and used for the analysis of small biomolecules for well-over a decade³²⁻³⁷, IM separates ions based on their ability to traverse a chamber filled with inert neutrals under the influence of a weak electric field. In a process roughly analogous to gas-phase version of electrophoretic separation in solution, ions that are large undergo a greater number of collisions with neutral molecules and thus take more time to

elute from the chamber than smaller, more compact ions. Ion size in the form of an orientationally-averaged CCS is, therefore, the primary information content of IM separation and established computational approaches can be used in conjunction with this information to assign the structure of small biomolecules to a high degree of precision³⁸.

IM-MS experiments have been used to interrogate the structure of a number of multiprotein systems and have provided information that is able to refine topology maps³⁹⁻⁴¹, establish cavity regions within a protein complex^{25,42}, and identify conformational changes upon ligand binding^{18,43}. In addition, protein complexes have been demonstrated to undergo structural collapse and unfolding upon activation with energetic collisions in the gas phase^{25,44,45}. Current evidence points to a mechanism for collision induced unfolding where a single subunit within the assembly unfolds, inhabiting a number intermediate structures that are relatively stable on the timescale of the IM measurement^{44,46,47}. In parallel with these experiments aimed at the controlled disruption of protein structure in the gas phase, several reports have highlighted the uncontrolled distortion of protein structure in the absence of solvent, including both the general compaction of protein size and structural rearrangements that may occur upon desolvation and transfer to the gas phase^{40,48}. While simple normalization procedures have been used extensively to analyze IM-MS data for protein complexes, and remove the influence of protein compaction in order to construct topology models^{39,40,49}, such rearrangements prompt the development of general strategies aimed at the protection of protein structure, at every level, in the absence of bulk solvent. Such strategies would have far reaching implications in characterizing the structures of gas-phase biomolecules and relating such data to analogues in solution including IM-MS, ion spectroscopy⁵⁰, and gas-phase HDX⁵¹.

In solution, the identity and concentration of salts can drastically influence the structure and stability of proteins and their assemblies. Recognized initially in pioneering work by Hofmeister⁵², a well-known rank-order of the ability of different salts to act as structural stabilizers or denaturants has been developed over decades of biochemical observations^{53,54}. While the mechanistic details that lead to this rank order are currently an active area of research, recent work points to the importance of direct salt-protein interactions and the local water structure that surrounds both interacting partners as the driving forces behind the Hofmeister series⁵⁵. In ESI of large protein complexes, buffer material and charge carriers condense and adhere to the assembly during the final stages of desolvation, and previous data indicates that components added in solution can influence the stability of the ions generated⁵⁶. While the use Hofmeister-type salts is potentially a compelling approach for preventing protein unfolding in the absence of bulk solvent, the quantitative influence and mechanism of such stabilizing counter-ions is largely unknown.

In this chapter, we screen a series of anions for their ability to increase the structural stability of multiprotein complexes in the absence of bulk solvent using IM-MS. Specifically, we use data from four different tetrameric protein complexes, spanning a 100 kDa mass range, where the threshold energies necessary for achieving CID and CIU are measured as a function of specific anions added to ammonium acetate-based buffers in solution. In some cases, the residual counter-ions screened here are found to substantially stabilize protein quaternary structure, in other cases gas-phase protein stability is decreased measurably upon addition of the anions in solution. We use this data to classify anions in terms of their ability to stabilize protein structure in the absence of bulk solvent, and we compare this rank order with known Hofmeister effects in

solution. Finally, we consider the mechanism of protein stabilization in our experiments and demonstrate that our results for protein tetramers can be explained by analyzing smaller monomeric protein systems and analyzing adduct-resolved ion populations in terms of their gas-phase stability. We find that bound counter-ions that act as protein stabilizers tend to bind in high abundance to the protein in solution (or during nESI) and then evaporate from the assembly upon collisional activation, carrying away excess vibrational energy from the protein in the process. In those cases where stability of protein structure is not observed, counter-ions may bind with high-affinity to the protein but not dissociate upon collisional activation. Another class of anions exhibit very little binding affinity for the proteins, and thus shows no significant ability to stabilize protein structure in the absence of bulk solvent. The anion-protein binding affinity we observe in our protein monomer experiments correlates very well with the relative proton affinities of these ions, and corroborates our findings with larger multiprotein complexes.

2.3 Experimental

2.3.1 Materials

The protein complexes, avidin, TTR, ConA and ADH, and salts (ammonium cation with acetate, fluoride, chloride, nitrate, citrate, thiocyanate, bicarbonate, tartrate, iodide, hydrogen phosphate, sulfate and perchlorate counter-anions) were purchased from Sigma (St. Louis, MO, USA). All protein samples were buffer exchanged into 100 mM ammonium acetate at pH 7 using Micro Bio-Spin 6 column (Bio-Rad, Hercules, CA). In order to study the influence of different salts on proteins, the salts were prepared as stock solutions in 100 mM ammonium acetate at a concentration of 20 mM, each of which was then added to the protein solution. The final concentrations of protein and salt were both 5 μ M in avidin and TTR, while both 10 μ M in ConA

and ADH samples. Higher salt additive concentrations were avoided in this work to avoid nESI-based ion suppression effects.

2.3.2 IM-MS

Collisional activation in the ion trap T-wave ion guide prior to the IM separator was used to CIU and CID of protein complexes in order to investigate the gas-phase stability of protein ions in the presence of different salts. This work was all performed in tandem-MS (Quad selection) mode. Ions were selected in the quadrupole mass filter at an m/z corresponding to 16^+ charge state of Avidin, 20^+ of ConA, 14^+ of TTR or 24^+ of ADH tetrameric ions. Charge states were chosen based on their intensity across each solution state interrogated, and control IM arrival time data were screened for evidence of overlapping non-tetrameric ions at the same m/z value. Each of these mass-selected ions was activated by increasing the trap collision voltage (Trap CE, as indicated in the instrument control software) which acts as a bias voltage between the quadrupole and ion trap T-wave ion guide to accelerate ions to increased kinetic energies for CIU and CID experiments. For all protein-salt systems detected here, activation profiles for arrival-time distribution (CIU ‘fingerprints’) were constructed through 5 V step-wise increments. Upper voltage limits were considered to be where no further dissociation was observed.

2.3.3 Data analysis

All mass spectra were calibrated externally using a solution of cesium iodide (100 mg/mL) and were processed with Masslynx 4.1 software (Waters, Milford, MA, USA). Spectra are shown with minimal smoothing and without background subtraction. The relative abundance of mass-selected tetrameric ions (I_{tet}) was calculated as a percentage of the total intensity of the peaks in

the mass spectra assigned to the selected charge state of tetrameric ions and all charge states of monomeric ions. The relative abundance of the compact tetrameric ions separated by IM cell (I_f) was calculated as a percentage of the total intensity of the peaks in the arrival time distribution:

$$I_{\text{tet}} (\%) = \frac{I_{\text{tet}}}{I_{\text{tet}} + I_{\text{mon}}} \times 100$$

$$I_f (\%) = \frac{I_{\text{folded}}}{\sum I_{\text{conformers}}} \times 100$$

The data shown in Figure 2-2, Figure 2-4 and Figure 2-5 include axes labeled in collision energy (units of eV*). The axis are a normalized version of ion kinetic energy, that takes into account both the charge on the ion and reduced mass of the ion-neutral collision complex, for making comparison across great mass ranges. Although the conversion used here is identical to center-of-mass energy conversions used elsewhere in the literature⁵⁶, we do not use this term in this report, as the definition of this quantity has clear implications for ion internal energy and these claims may not extend to the large ions studied here due to the large number of degrees of freedom possessed by protein complex ions. We use the conversion only as a means of normalizing kinetic energies for CIU and CID comparisons across broad mass ranges.

2.4 Results and Discussion

2.4.1 Measuring the stability of protein complexes via collision induced unfolding and dissociation

To investigate the influence of anions on the stability of protein complexes in the absence of bulk solvent, we developed a combined CIU/CID approach that allows us to assess the relative stability by monitoring the unfolding and dissociation profiles of protein complexes. Figure 2-1

illustrates the work-flow using TTR, a 55 kDa tetrameric protein as an example. The mass spectra of TTR in ammonium acetate buffer (100 mM), acquired at trap collision voltage of 35 V (blue) and 70 V (red), shows peaks corresponding to 13⁺, 14⁺, and 15⁺ charge states of tetramer exclusively at 35 V (Figure 2-1A). By contrast, a large fraction of the tetramer ion population dissociates into monomer and trimer at a trap collision voltage of 70 V. The charge state distribution of monomeric TTR spans from 6⁺ to 11⁺, with 8⁺ (1732 m/z) and 7⁺ (1980 m/z) as the two most intense monomer ion signals.

Drift times for the ions were acquired under the same conditions as above and are shown in a plot of drift time versus m/z (Figure 2-1B). At a collision voltage of 35 V (blue), the plot shows a number of peaks resolved in the drift time dimension corresponding to the charge state series for tetrameric TTR, with 3980 m/z assigned to 14⁺ charge state of tetrameric TTR (dashed box). At trap collision voltage of 70 V (red) the majority of the tetrameric ion current is converted into monomer. The peaks corresponding to the tetramer, however, extend to longer drift times, indicating that the remaining tetramers exist in a range of structural states at elevated internal energies. These data are consistent with previous reports where TTR was observed to occupy a number of partially folded intermediate states that are stable on the millisecond timescale^{57,58}. In addition, stability of the tetramer ions produced during its course of unfolding transition can be enhanced through specific binding of small molecule ligands to the protein complex⁵⁹.

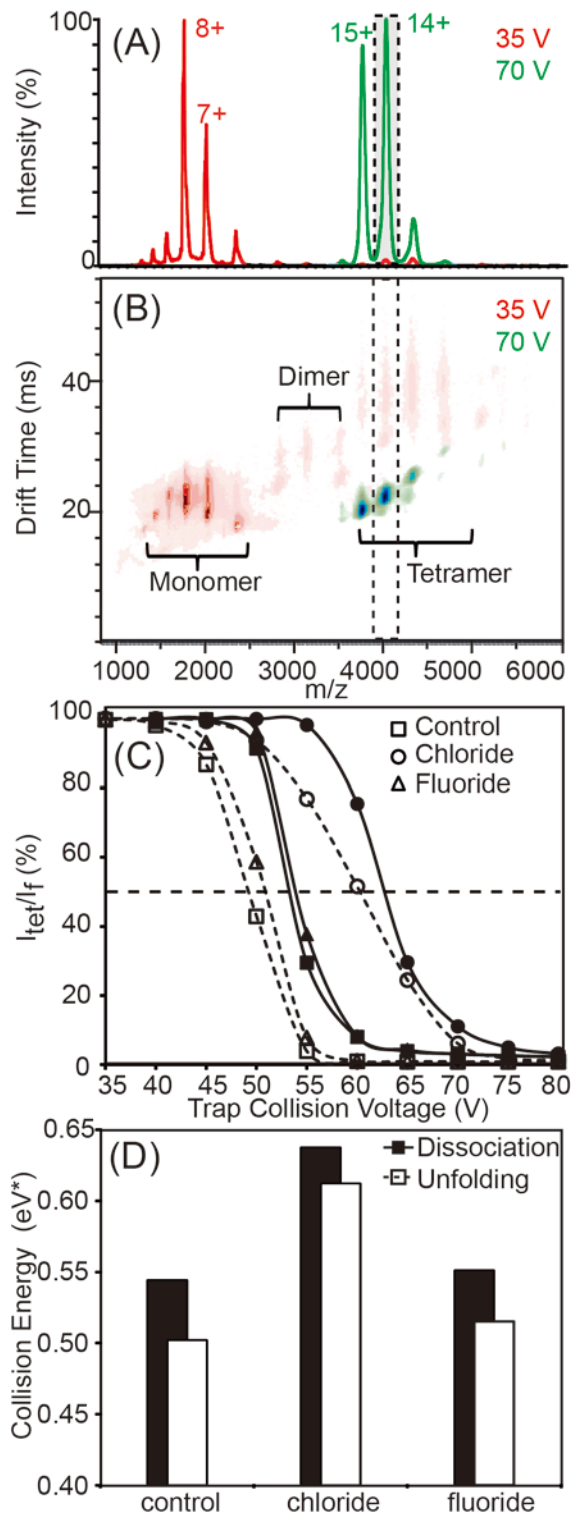


Figure 2-1. Addition of anions in solution alters the dissociation and unfolding profiles of a protein assembly. (A) Mass spectra of TTR acquired at instrument conditions that preserve the tetrameric assembly (trap collision voltage: 35 V, green), or that activate the protein ion (70 V, red). Peaks corresponding to 13–15⁺ charge states of tetramer and 6–10⁺ charge states of monomer are shown. (B) Contour plots of m/z versus drift time acquired at a trap collision voltage of 35 V (green) and 70 V (red). A narrow window that contains the peak corresponding to the 14⁺ ion of tetrameric TTR indicates the populations of compact and extended tetrameric TTR generated under different instrument conditions (dashed box). (C) Plots of the relative intensities of TTR tetramer 14⁺ ions (I_{tet} , solid lines), and the relative intensities of compact TTR tetramer 14⁺ ions (I_f , dashed lines) are shown as a function of trap collision voltage. TTR ion was generated with solutions containing either chloride (circle), fluoride (triangle), or acetate anion (control, square). The energy at which the relative intensity reduces to 50% is marked with a horizontal dashed line. (D) A histogram showing the 50% dissociation yield (black) and unfolding yield (white) for TTR tetramers generated from solutions with various additives is shown.

For quantitative measurement of the stability afforded to TTR tetramer, the trap collision voltage at which ions undergo CIU and CID is monitored, and plots of collision voltage versus the

intensity observed for compact (I_f) and intact (I_{tet}) tetramer ions are shown respectively. Based on these plots, a simplified descriptor of tetramer stability is constructed by plotting the center-of-mass energy (energy) at which the intact/compact tetramers (I_{tet}/I_f respectively) decrease to 50% of their initial values. For example, a plot of I_f and I_{tet} for 14^+ charge state of TTR incubated in three different buffers compositions (control/100% 100 mM ammonium acetate, 100 mM ammonium acetate with 5 mM added ammonium fluoride and 100 mM ammonium acetate with 5 mM added ammonium chloride) as a function of trap collision voltage is shown (Figure 2-1C). Both I_f and I_{tet} are shown to decrease as energy is increased with I_f decreases prior to I_{tet} in all three buffer salts. The results indicate that protein complexes dissociate only after tetramer precursor ions have undergone significant unfolding in the absence of the bulk solvent. Importantly, when comparing a plot of I_{tet} (red, solid) and I_f (blue, dashed), we observe that the addition of ammonium chloride to the sample solution (circles) increases the energy at which I_f and I_{tet} begin to decrease, and that this change in transition energy is significantly greater than that observed for the addition of ammonium fluoride (triangles) to the sample, relative to the measurements made in 100% ammonium acetate based control (squares).

This result is clearly shown through a comparison of energy at which I_{tet} and I_f decrease to 50% of their original intensity (Figure 2-1D). This result implies that the addition of the chloride anions in solution causes the stability of the TTR tetramer to increase relative to control, while such effects are negligible when fluoride anions are added. Thus the collective approach described in Figure 2-1 provides us the basis for quantitatively comparing the stability of protein complexes in terms of both their unfolding (CIU) and dissociation (CID) profiles.

2.4.2 Ion-Mobility MS reveals differential stability of protein complexes in gas-phase

In order to assess the influence of anions to the stability of protein complexes in general, we examined a range of anions whose relative ability to stabilize protein complex in solution is recognized. Figure 2-2 shows a series of tandem mass spectra of the 14^+ charge state of tetrameric TTR acquired at trap collision voltage of 60 V. For each spectrum, all instrument parameters are kept constant and only the composition of buffer additives is altered and their effect on protein complex dissociation (I_{tet}) is monitored. We find that the peaks corresponding to TTR tetramer and monomer are produced at substantially different abundance, clearly demonstrating the influence of the anions on the relative dissociation yields. Of the anions examined here, the addition of tartrate in solution confers the greatest stability to TTR tetramer, as evidenced by a lack of peaks corresponding to TTR monomer at low m/z in the mass spectrum (Figure 2-2). MS spectra reveals the appearance of a minor peak corresponding to 15^+ charge state of TTR tetramer due to the loss of negatively charged counter ions from 14^+ charge state of tetramers⁶⁰, and 13^+ tetramer ion signals corresponding to positive charge stripping⁶¹. Note that such signals are prominent even in the mass spectrum acquired from the control, and are likely enhanced by the long life-times of the tetramer ions in the ion trap region of the IM-MS instrumentation used in our experiments. While the charge state distribution of the monomer ions produced from all TTR tetramer remains relatively constant, we note that a peak corresponding to the 9^+ monomer is observed primarily when relatively destabilizing salts, such as hydrogen phosphate and sulfate, are added. The dissociation yield of TTR tetramer, measured from the data shown in Figure 2-2, increases in the following rank order: tartrate, chloride, nitrate, citrate, thiocyanate, bicarbonate, fluoride, iodide, acetate (control), hydrogen phosphate, sulfate and

finally perchlorate. The difference in the stability conferred to tetrameric protein can be quantified through comparing the signal intensity for TTR monomer ions relative to TTR tetramer, as previously described.

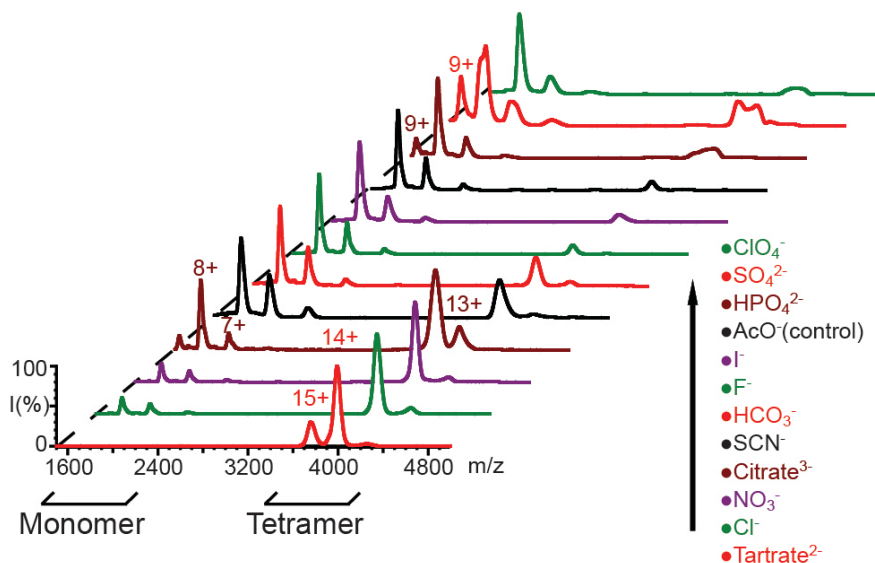


Figure 2-2. The mass spectra of TTR incubated with a range of anions reveal different extents of dissociation. The 14^+ charge state of TTR ions selected by the quadrupole mass filter was subjected to a trap collision voltage of 60 V in the trapping region between the quadrupole mass analyzer and IM separator. Major peaks from the charge state series corresponding to monomeric and tetrameric TTR are labeled. The anions are arranged by their ability to limit dissociation of TTR.

We investigated the stability afforded to three other tetrameric protein complexes (avidin, ConA and ADH) in the gas-phase upon addition of the same 12 anions in solution prior to ion desolvation. Each protein/anion pairing was assessed by examining a single charge state isolated by the quadrupole mass filter, and the same charge state for each complex was assessed across all solution compositions by CIU and CID experiments. Both I_f and I_{tet} followed typical sigmoid-type decay curves as a function of the trap collision voltage for all systems⁵⁹. Figure 2-3A shows a histogram plot of the energy necessary to reduce I_{tet} to 50% of its original value as a function of anion identity for each of the four protein complexes studied here. The plot reveals a

surprisingly wide range of values for the energy necessary to delete tetramer intensity by 50%, and a comparison among the datasets shown here reveals several features of multiprotein stability. We first note that, in general, several anions added in solution have a universally stabilizing influence on I_{tet} . These include tartrate, chloride, nitrate, and thiocyanate. Conversely anions such as perchlorate, sulfate, and iodide have a destabilizing influence on protein complexes relative to control (ammonium acetate) in general. In addition, we note a significant difference in the energy required to dissociate the four different protein complexes studied here. The stability order of protein complexes relative to CID in our dataset indicates that the ADH tetramer is the most stable, followed by avidin, TTR, and finally ConA, (Figure 2-3A). Both previous data and the stability order reversal in our control data for TTR and ConA tetramers leads us to conclude that variations in I_{tet} between protein complexes is a composite of several factors including protein stability (I_f), strength of protein-protein interaction, and protein mass. In a similar manner, Figure 2-3B tracks the changes in I_f through CIU experiments for each of the same 48 ion/protein pairs shown in Figure 2-3A. In contrast to the dissociation data shown in Figure 2-3A, TTR is the most stable relative to unfolding, followed by avidin, ConA, and ADH is again the least stable tetramer by CIU measurements. Similar trends in the influence of protein stability as a function of the anion composition of the buffer can be identified in unfolding data as in dissociation data. The stabilizing anions identified relative to the unfolding transition probed in Figure 2-3B are identical to those identified in Figure 2-3A (e.g. tartrate, chloride and nitrate). Bound anions that act as destabilizing agents for protein structure in the gas-phase are less obvious by CIU measurements than in CID data, with no anions identified in our dataset as noticeably destabilizing the gas-phase unfolding transition.

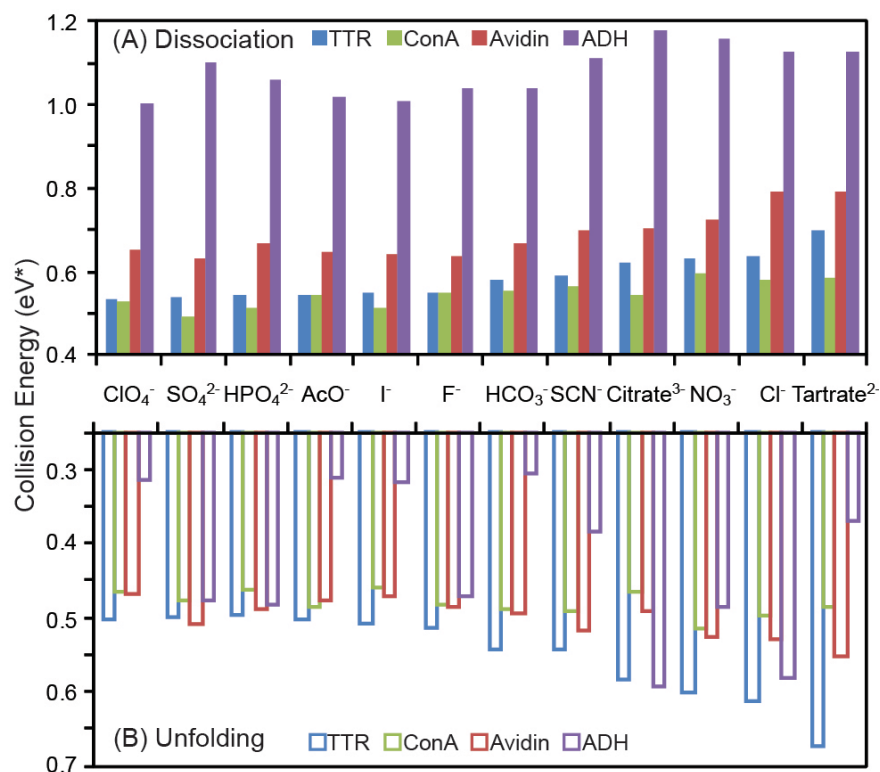


Figure 2-3. Elucidating the extent of unfolding and dissociation of the four protein complexes in the presence of different anions from IM-MS. Histogram plots charting collision energy (eV*) required to dissociate (A) and unfold (B) 50% of the tetrameric protein ion population for avidin (red), TTR (blue), ConA (green), and ADH (purple) are shown for a range of anion additives. Control data sets, without added ammonium salts, are marked on the plot (AcO^-).

Our CIU and CID datasets reveal a number of general points regarding the protein complexes chosen for these studies. In general, the protein complexes studied here are observed to undergo CIU at lower energy relative to CID, as observed previously^{44,59}. For each protein complex, however, the two processes are energetically separated to different degrees, with 0.28 eV separating the two transitions in ADH to 0.03 eV for TTR. Such a wide variations in the collision energies between CIU and CID processes across the protein tetramers studied here highlights the importance of assessing the stability of protein complexes in terms of both unfolding and dissociation, especially for IM-MS experiments where proteins and complexes are activated in order to obtain higher mass measurement accuracy and resolving power⁶².

A comparison of the CID and CIU data also highlights the differential effects of altering the anion composition of gas-phase protein complexes. The protein complexes exhibit a wide range of energy for both I_{tet} and I_f datasets, indicating that anions modulate the energy differences between the unfolding and dissociative transition. For example, although measurable differences in the energy required to deplete 50% of the tetramer population and 50% of the folded population is observed for most TTR CIU and CID datasets (~ 0.5 eV), unfolding and dissociation are isoenergetic processes when TTR is bound to highly stabilizing anion populations (tartrate, chloride, or nitrate). Figure 2-3 also highlights the differences between unfolding and dissociation observed among the protein complexes across all bound anion populations. In contrast to all other tetramers, ADH seems to undergo CID and CIU at drastically lower energy relative to all other protein complexes interrogated here, and bound anions seem to influence this process in a significantly different manner when compared to the other three complexes studied.

2.4.3 Classifying and ranking the effect of anions on protein stability

In order to develop a classification system that allows us to generally rank anions in terms of the stability afforded to gas-phase protein complexes through their addition in solution, subsequent binding and adduction to gas-phase protein ions, we first normalized our stability measurements to our control experiments and then combined our CIU and CID datasets to derive a consensus measure of gas-phase protein complex stability. This data is shown in Figure 2-4, and reveals the presence of at least three general levels of protein ion stabilization in our CID and CIU datasets. Remarkably, despite the differences apparent in Figure 2-3, both CIU and CID datasets generally

correlate well. As noted previously, many anions provide little or no stability to protein complex ions upon addition in solution, resulting in dissociation and unfolding threshold values similar to

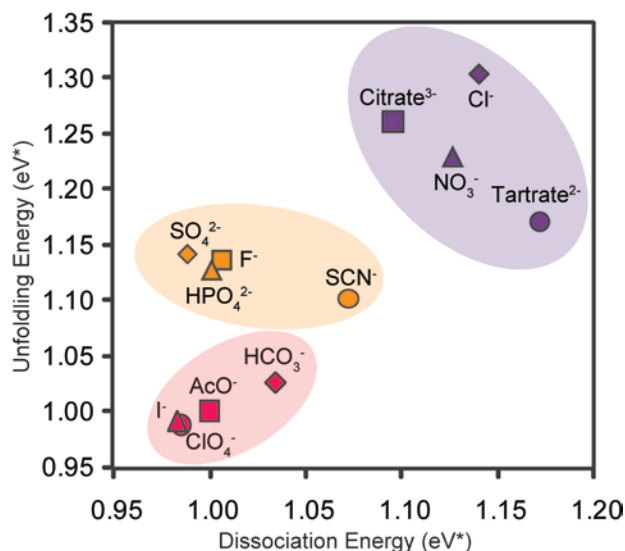


Figure 2-4. A plot of collision energy (eV*) averaged over the four protein complexes indicates differential stabilizing effect of the anions. The ability of anion additives to affect unfolding and dissociation of protein complexes is expressed by a collision energy axis normalized to the control data set. The plot reveals the anions can be categorized into three distinct groups, according to their ability to stabilize protein complexes relative to the control data set.

control experiments in pure ammonium acetate buffer systems. These anions cluster together within the same region of Figure 2-4 (light pink). The two other clusters of anions shown (orange and purple) exhibit enhanced stability relative to control (light pink) in both datasets. For example, tartrate, chloride, citrate, and nitrate are among the most efficient stabilizers of protein unfolding, as well as increasing the energy required for protein dissociation. Thus, these anions populate a ‘highly-stabilizing’ cluster shown in purple within Figure 2-4. All of the remaining anions exhibit mid-range values for CID and CIU stabilization when bound to protein complexes in the gas-phase and form a final ‘medium-stabilizing’ cluster of counter-ions (orange, Figure 2-4). Overall, these results suggest that anions influence the unfolding and dissociation processes of protein complexes in concert, rather than independently. It is worth noting that there are several exceptions to this general statement within our dataset, where unfolding or dissociation is stabilized preferentially relative to the other. For example, tartrate and sulfate anions show significantly different rank orders when unfolding and dissociation are considered separately, indicating that these salts may influence the tertiary and quaternary structure of protein complex

differentially. These highlighted differences will be the subject of further investigation in our laboratory.

2.4.4 Towards a mechanistic understanding of gas-phase protein stabilization through bound anions

Insight into the mechanism by which protein complexes are stabilized through the addition of salt in buffer solutions prior to nESI-IM-MS analysis can be obtained by observing the intact mass of protein complex ions generated as a function of buffer composition. It is reasonable to assume that the excess mass, relative to the ammonium acetate control, arises from binding of additional experimental anions and this can be converted to an average number of additional anions bound. This data is shown in Figure 2-5A, where we measured the mass of the protein complexes incubated with several salt additives under identical instrument conditions (Trap CE = 40V). Such an analysis is limited to those cases where the protein ions produced from solutions containing salt additives generate MS data having resolved MS features under identical conditions. While this limits the panel of anions that can be tested significantly from our original pool of 12, the trend observed in this data is clear. As the mass in excess of protein sequence increases, the structural stability afforded the assembly also increases. This suggests that the amount of bound counter-ions carried with the complex from solution or the nESI process is the determining factor in the stability enhancements observed in our CID and CIU datasets. The inset shown in Figure 2-5A indicates a clear positive correlation between the amount of excess mass observed bound to protein complex ions in our gas-phase measurements and the structural stability of those ions relative to both dissociation and unfolding, further indicating a role for bound anions in the stability enhancements observed here.

In order to test the hypothesis that bound buffer material is the main cause of the stability enhancement observed for gas-phase protein complexes in our data, we broadened our initial dataset to include smaller protein systems, including both CYC monomer and BLA dimer datasets (Figure I-2). Example data from the 7⁺ charge state of CYC monomer (12 kDa) is shown in Figure 2-5B, where the ions are generated from solutions with additives which are identical to those used to generate the protein complex datasets shown in this report. The data clearly demonstrate that the increase in mass observed in Figure 2-5A is due to anion binding and not other solution components. Resolved adduct populations corresponding to [H-‘anion’] type adducts where the ‘anion’ is chloride, nitrate, tartrate, perchlorate, or thiocyanate, are all observed in our monomer dataset. The maximum number of adducts bound to the CYC monomer (5-10 for high-affinity counter-ions) scales well with respect to our tetramer data shown in Figure 2-5A, where the excess mass recorded for protein tetramers corresponds to 5-10 adducts per monomer in the cases of those anion additives with high apparent protein affinity. Critically, despite the significant structural differences between the protein complexes measured in Figure 2-5A and the monomeric CYC, the observed relative protein binding affinity of the anions remains similar.

These results also agree well with previous data^{63,64} where counter-ion adduction, principally to basic sites on the surface of the protein, is observed by ESI-MS from solutions containing added

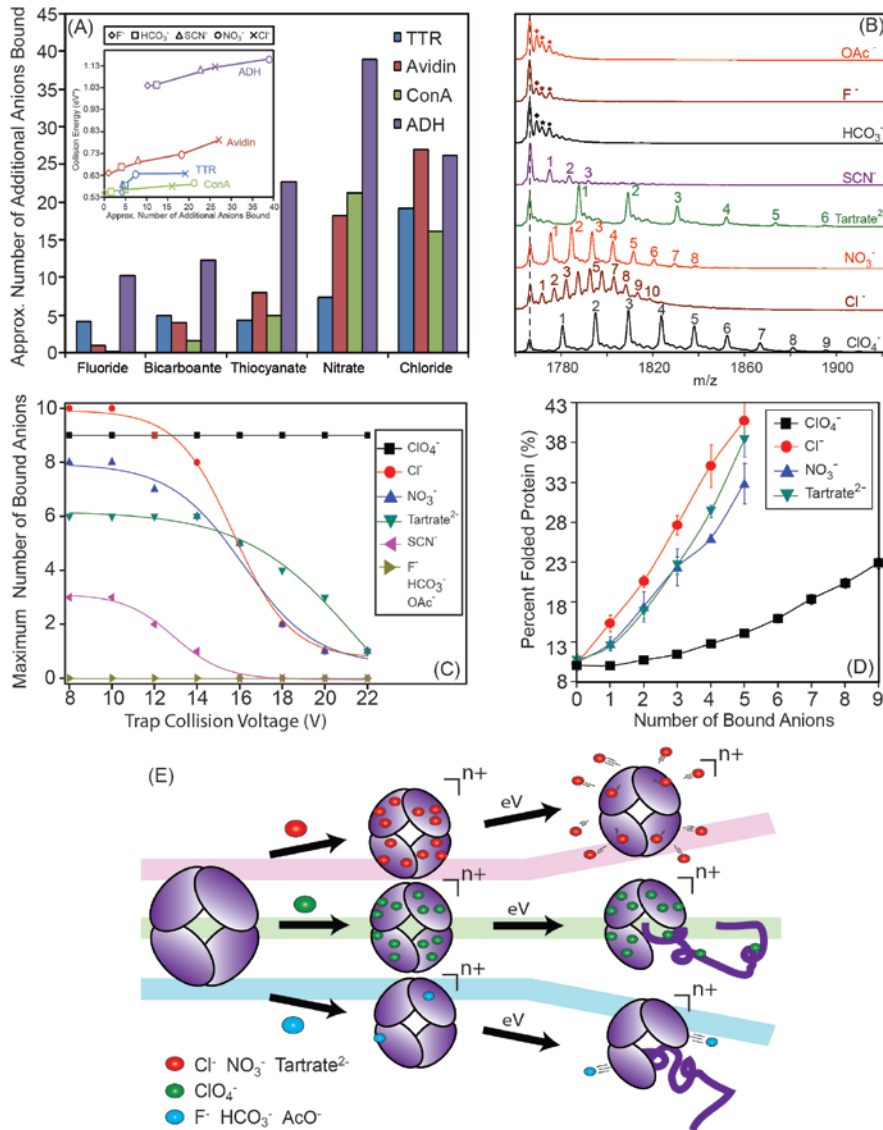


Figure 2-5. IM-MS reveals a mechanism of protein complex stabilization through anion attachment. (A) A plot of the number of residual anions that remain bound to the protein complex at a trap collision voltage of 40 V, for TTR (blue), avidin (red), ConA (green), and ADH (purple). The inset shown plots the normalized collision energy required to dissociate 50% of complex ions against the calculated number of additional anions bound to the assembly. A positive correlation is observed for all complexes. (B) Mass spectra of 7^+ CYC monomers generated from solutions containing anion additives reveal a distribution of adducts resolved by MS at trap collision voltage of 8 V. Peaks corresponding to adducts arising from sodium, potassium, and sodium+potassium-binding are marked with diamonds, stars, and circles, respectively, for the control (acetate), fluoride, and bicarbonate anions. (C) Plots of the largest number of additive counterions bound to CYC observed as a function of trap collision voltage for a range of additive anions. (D) A plot of compact protein ion signal intensity (I_f) against the number of anion adducts bound reveals a positive correlation for four high-affinity anions, with perchlorate adducts generating a significantly more-shallow slope than other additives shown here. (E) A mechanistic diagram of protein structure stabilization through bound counterions that

summarizes our current data set. Three tracks are shown: a track where anions bind the protein in high affinity and are released upon dissociation leading to high protein structural stability in the gas-phase (red); a high-affinity binding track where anions do not dissociate from the protein, leading to relatively low protein structural stability (green); and a low-affinity binding track that does not produce measurable increases in protein stability in the absence of bulk solvent (blue).

salts while changes to the ionic strength were not observed to alter the charge state distribution of the protein ions significantly⁶⁵. These previous results also cite a strong correlation between the number of protein-bound counter-ions and the relative gas-phase acidity of the anions studied^{63,64}. Our data corroborates these general findings for a wider panel of anions and proteins than reported previously (Figure I-3, Table I-1). We note that all additives that do not lead to appreciable adduct formation correlate well with those anions identified in Figure 2-3 and Figure 2-4 as having little influence on protein stability; a list that includes: acetate, bicarbonate, and fluoride salts. Conversely, many of the anions observed to bind in large numbers to CYC correlate well with those that confer significant stability to protein complex structure in the absence of bulk solvent (e.g. tartrate, chloride, and nitrate).

Although the data in Figure 2-5B clearly shows a correlation between protein-anion binding, either in solution or during the nESI process, and the stability enhancements observed in our CIU and CID datasets for protein complexes, a limited number of salt additives appear to follow a different trend. For example, perchlorate anions bind in large numbers to CYC (Figure 2-5B), but the resultant gain in stability for the gas-phase protein ion is minimal. To elucidate the difference between the action of anions like perchlorate and other anions that lead to large numbers of adducts and an appreciable increase in protein stability, we recorded MS data for CYC-anion complexes as a function of activation in the ion trap region of the instrument (prior to IM separation). Most anions that bind with high affinity, including chloride, nitrate, and

tartrate, readily dissociate from the protein as the activation voltage is increased (Figure 2-5C). In contrast, perchlorate-based adducts do not readily dissociate from the protein over the range of voltages shown in Figure 2-5C (black squares). This data, then, suggests a second condition for the effective stabilization of gas-phase protein ions through counter-ion attachment. Anions must bind with high-affinity, but must also dissociate readily from the protein in order to be an effective stabilizer. This balance between protein-anion binding in solution and gas-phase dissociation is reflected in the relative acidities, both in solution and in the gas-phase, for those anions that effectively stabilize protein structure in the absence of bulk solvent. For singly-charged anions, where protein-binding is simplified, there is a strong correlation between those anions that stabilize protein structure and a narrow range of acceptable acidity values (Figure I-3).

The correlation between the ability of adducts to dissociate from the complex and gas-phase structural stability enhancements are further corroborated by adduct-resolved CIU experiments performed for CYC-anion complexes (Figure 2-5D). The data shown for stabilizing counter-ions (chloride, nitrate, and tartrate) display positive correlations between the relative amounts of compact protein observed and the number of counter-ions bound, while a significantly shallower trend is observed for perchlorate-bound CYC. These data indicate that while perchlorate binds in larger numbers to proteins and their complexes when compared to other anion additives, the bound adducts do not preserve the protein in a compact configuration, as indicated by the low percentage of folded protein recorded as a function of the number of perchlorate adducts bound. In contrast, tartrate, chloride and nitrate-bound protein ions all retain a significantly greater folded percentage per-unit adducted anion. The trend-lines observed for all three stabilizing

counter-ions are relatively similar, having similar slopes and intercept values, further indicating a common mechanism of protein stabilization.

We have summarized the observations discussed above into a schematic diagram (Figure 2-5E) that illustrates our current understanding of the molecular mechanism of protein complex ion structural stabilization through counter-ion attachment and binding. Our mechanism delineates and classifies anions into three categories based on both their protein binding affinity and their ability to dissociate from proteins and their complexes following activation in the gas-phase. Counter-ions that exhibit a strong stabilizing influence on protein structure (red track, Figure 2-5E) both bind with high affinity and readily dissociate from the protein surface. The observed dissociation of anion-based adducts as neutrals appears to be the key metric that allows protein-adduct ion populations to retain compact, native like gas-phase conformations under conditions where protein ions produced from solutions containing more-volatile additives unfold and dissociate. It is reasonable to assume that the dissociation of adducts acts to carry away excess rotational and vibrational energy from gas-phase protein ions, thus abating any dramatic internal energy increases for the protein and allowing it to retain a compact, native-like structure. Another class of anion binds to the protein, but is not easily dissociated from the complex in the gas-phase upon activation (green track, Figure 2-5E). Typically comprised of anions that exhibit greater proton affinities than those highly-stabilizing anions described in the red track, this class of anions demonstrates a poor ability to stabilize the gas-phase structure of protein complex ions. Similarly, those anions that do not bind with high-affinity to proteins in solution, or during the nESI process, also do not stabilize gas-phase protein structure (blue track, Figure 2-5E). It is important to point out that these three anion classes, while related, are not the same as those

presented in Figure 2-4. Anions that populate the blue and green tracks in Figure 2-5E are likely to represent the weak stabilizers observed in Figure 2-4 (light pink), whereas the mild and strong stabilizers observed in that data (orange and purple) can all be placed on the red track in Figure 2-5E. As noted above, there is a strong correlation between anion acidity, both in the gas-phase and in solution, and the three classes of stabilizing anions described in Figure 2-5E. This correlation is readily apparent when singly-charged anions are considered (Figure I-3, Table I-1), where anions with low acidity fall into the blue track, those with intermediate acidity in the red track, and those with the highest acidity in the green track. Multiply-charged anions are more difficult to place within such a trend due to likely multi-dentate interactions with basic sites on the protein. Anion additives that stabilize protein structure in the absence of solvent should, therefore, possess sufficient affinity for basic sites on the protein to drive initial binding, but also have a low enough binding strength to allow for adduct dissociation and effective ‘evaporative cooling’ of the protein complex in the gas-phase.

2.5 Conclusions

In general, there are four main conclusions from our work. First, our dataset has greatly expanded the known buffer conditions and additives that are amenable to nESI of protein complexes without complete suppression of usable ion signal. All data shown here included salts at 5-10 μM , however higher concentrations are possible for many of the salts discussed, in many cases extended to mM concentrations. While lower salt concentrations are preferred for maximum mass accuracy and resolution, our data indicates that higher salt concentrations and tailored salt identity provide maximally-stabilized protein complexes for IM measurements of protein structure.

Secondly, we have ranked and classified twelve anions, for the first time, according to their effectiveness in stabilizing gas-phase protein structure, and rank orders from both CIU and CID experiments are surprisingly similar. This similarity indicates that the interactions between anion and complex are linked to both local protein structure and protein-protein interactions. We were surprised to find that some salts previously reported to be gas-phase protein denaturants, are highly-stabilizing to protein ion structure in our dataset. For example, tartrate-based salts have been used extensively in ‘top-down’ protein fragmentation experiments to increase fragment ion yield⁶⁶. While our data suggests that tartrate be classified as a stabilizing salt in most cases, the overall mechanism of gas-phase protein stabilization may involve partially unfolded forms (Figure I-4). Clearly, our data indicates that the influence of tartrate and other salts on the ‘top-down’ fragmentation efficiency via electron and collision-based activation methods requires further study.

Thirdly, we have elucidated a complete mechanistic picture of protein structure stabilization in the gas-phase achieved through nESI buffer additives. The data shown in Figure 5 clearly indicates that protein stabilization in the gas-phase is correlated with the binding affinity between the anions and proteins and complexes studied here. In order to stabilize gas-phase protein structure, anions must bind to the protein, be carried into the gas-phase as protein-anion complexes, and dissociate from the protein upon activation. The final dissociation step acts to siphon excess energy from the protein system and preserve compact gas-phase structures. Anion additives that do not bind, nor dissociate from gas-phase protein ions do not provide significant structural stabilization in CID and CIU datasets. In addition to the tetramer and protein monomer data shown here, further data collected for the (bovine) β -lactoglobulin (BLA) dimer also

correlates well with our overall mechanism (Figure I-2). Small differences in enhanced structural stability can be observed among those counter-ions that provide the greatest stability, and evidence from CIU fingerprinting, where changes in IM drift time are plotted for selected ions against activation voltage, suggest that some anions remain bound to the complex and stabilize partially unfolded structures of the complex even for strong gas-phase protein stabilizers like chloride, tartrate, and nitrate (Figure I-4). Overall, the results presented herein enable the direct manipulation of gas-phase protein complex stability by controlling the composition of the nESI sample solution. Therefore, this dataset will likely enable IM-MS by making a greater number of structurally unstable systems amenable for study in the absence of bulk solvent.

The data shown in this report prompts a comparison between the well-known Hofmeister series of anions, describing the influence the same anions upon protein stability in solution: $\text{SO}_4^{2-} > \text{HPO}_4^- > \text{F}^- > \text{Acetate}^- > \text{Citrate}^{3-} > \text{HCO}_3^- > \text{Cl}^- > \text{NO}_3^- > \text{I}^- > \text{ClO}_4^- > \text{SCN}^-$. While still and active area of research, much is currently known about the molecular mechanism surrounding Hofmeister-type stabilization of solution-phase protein structures. In general, the Hofmeister series depends upon anion hydration entropy, the ability of anions to alter water surface tension, and direct anion-protein binding⁶⁷. On first inspection, drastic differences are apparent between protein stabilizing anions in solution and in the gas-phase. For example, nitrate, thiocyanate and chloride are all strong protein stabilizers in the gas-phase, but are relative denaturants in bulk solvent. Our data present a direct measurement of anion-protein binding and can be viewed as a stabilization dynamic built entirely upon protein-anion interactions. Differences between the two rank orders can be ascribed to the lack of solvation effects in the dataset presented in this report, and highlight the importance of such affects for Hofmeister stabilization of proteins in solution.

2.6 References

- (1) Burley, S. K.; Almo, S. C.; Bonanno, J. B.; Capel, M.; Chance, M. R.; Gaasterland, T.; Lin, D. W.; Sali, A.; Studier, F. W.; Swaminathan, S. *Nature Genet.* **1999**, *23*, 151.
- (2) Chandonia, J. M.; Brenner, S. E. *Science* **2006**, *311*, 347.
- (3) Robinson, C. V.; Sali, A.; Baumeister, W. *Nature* **2007**, *450*, 973.
- (4) Alber, F.; Dokudovskaya, S.; Veenhoff, L. M.; Zhang, W. Z.; Kipper, J.; Devos, D.; Suprpto, A.; Karni-Schmidt, O.; Williams, R.; Chait, B. T.; Rout, M. P.; Sali, A. *Nature* **2007**, *450*, 683.
- (5) Alber, F.; Dokudovskaya, S.; Veenhoff, L. M.; Zhang, W. H.; Kipper, J.; Devos, D.; Suprpto, A.; Karni-Schmidt, O.; Williams, R.; Chait, B. T.; Sali, A.; Rout, M. P. *Nature* **2007**, *450*, 695.
- (6) Taverner, T.; Hernandez, H.; Sharon, M.; Ruotolo, B. T.; Matak-Vinkovic, D.; Devos, D.; Russell, R. B.; Robinson, C. V. *Accounts Chem Res* **2008**, *41*, 617.
- (7) Heck, A. J. R. *Nat. Methods* **2008**, *5*, 927.
- (8) Alber, F.; Forster, F.; Korkein, D.; Topf, M.; Sali, A. *Annu. Rev. Biochem.* **2008**, *77*, 443.
- (9) Foerster, F.; Lasker, K.; Nickell, S.; Sali, A.; Baumeister, W. *Mol. Cell. Proteomics* **2010**, *9*, 1666.
- (10) Lasker, K.; Phillips, J. L.; Russel, D.; Velazquez-Muriel, J.; Schneidman-Duhovny, D.; Tjioe, E.; Webb, B.; Schlessinger, A.; Sali, A. *Mol. Cell. Proteomics* **2010**, *9*, 1689.
- (11) Lasker, K.; Sali, A.; Wolfson, H. J. *Proteins* **2010**, *78*, 3205.
- (12) Benesch, J. L. P.; Ruotolo, B. T.; Simmons, D. A.; Robinson, C. V. *Chem. Rev.* **2007**, *107*, 3544.
- (13) Sharon, M.; Robinson, C. V. *Annu. Rev. Biochem.* **2007**, *76*, 167.
- (14) Hernandez, H.; Dziembowski, A.; Taverner, T.; Seraphin, B.; Robinson, C. V. *EMBO Rep.* **2006**, *7*, 605.
- (15) Synowsky, S. A.; van den Heuvel, R. H. H.; Mohammed, S.; Pijnappel, W.; Heck, A. J. R. *Mol. Cell. Proteomics* **2006**, *5*, 1581.
- (16) Zhou, M.; Sandercock, A. M.; Fraser, C. S.; Ridlova, G.; Stephens, E.; Schenauer, M. R.; Yokoi-Fong, T.; Barsky, D.; Leary, J. A.; Hershey, J. W.; Doudna, J. A.; Robinson, C. V. *Proc. Natl. Acad. Sci. U. S. A.* **2008**, *105*, 18139.
- (17) Sharon, M.; Mao, H. B.; Erba, E. B.; Stephens, E.; Zheng, N.; Robinson, C. V. *Structure* **2009**, *17*, 31.
- (18) Koschubs, T.; Lorenzen, K.; Baumli, S.; Sandstrom, S.; Heck, A. J. R.; Cramer, P. *Nucleic Acids Res.* **2010**, *38*, 3186.
- (19) Stengel, F.; Baldwin, A. J.; Painter, A. J.; Jaya, N.; Basha, E.; Kay, L. E.; Vierling, E.; Robinson, C. V.; Benesch, J. L. P. *Proc. Natl. Acad. Sci. U. S. A.* **2010**, *107*, 2007.
- (20) Shoemaker, G. K.; van Duijn, E.; Crawford, S. E.; Uetrecht, C.; Baclayon, M.; Roos, W. H.; Wuite, G. J. L.; Estes, M. K.; Prasad, B. V. V.; Heck, A. J. R. *Mol. Cell. Proteomics* **2010**, *9*, 1742.
- (21) Barrera, N. P.; Di Bartolo, N.; Booth, P. J.; Robinson, C. V. *Science* **2008**, *321*, 243.

- (22) Barrera, N. P.; Isaacson, S. C.; Zhou, M.; Bavro, V. N.; Welch, A.; Schaedler, T. A.; Seeger, M. A.; Miguel, R. N.; Korkhov, V. M.; van Veen, H. W.; Venter, H.; Walmsley, A. R.; Tate, C. G.; Robinson, C. V. *Nat. Methods* **2009**, *6*, 585.
- (23) Loo, J. A.; Berhane, B.; Kaddis, C. S.; Wooding, K. M.; Xie, Y. M.; Kaufman, S. L.; Chernushevich, I. V. *J. Am. Soc. Mass Spectrom.* **2005**, *16*, 998.
- (24) Bernstein, S. L.; Wyttenbach, T.; Baumketner, A.; Shea, J. E.; Bitan, G.; Teplow, D. B.; Bowers, M. T. *J. Am. Chem. Soc.* **2005**, *127*, 2075.
- (25) Ruotolo, B. T.; Giles, K.; Campuzano, I.; Sandercock, A. M.; Bateman, R. H.; Robinson, C. V. *Science* **2005**, *310*, 1658.
- (26) Ruotolo, B. T.; Robinson, C. V. *Curr Opin Chem Biol* **2006**, *10*, 402.
- (27) Kemper, P. R.; Bowers, M. T. *J. Phys. Chem.* **1991**, *95*, 5134.
- (28) Bowers, M. T.; Kemper, P. R.; Vonhelden, G.; Vankoppen, P. A. M. *Science* **1993**, *260*, 1446.
- (29) Jarrold, M. F. *J. Phys. Chem.* **1995**, *99*, 11.
- (30) Eiceman, G. A. *Crit. Rev. Anal. Chem.* **1991**, *22*, 17.
- (31) Baumbach, J. I.; Eiceman, G. A. *Appl. Spectrosc.* **1999**, *53*, 338A.
- (32) Vonhelden, G.; Wyttenbach, T.; Bowers, M. T. *Science* **1995**, *267*, 1483.
- (33) Clemmer, D. E.; Jarrold, M. F. *J. Mass Spectrom.* **1997**, *32*, 577.
- (34) Valentine, S. J.; Liu, X. Y.; Plasencia, M. D.; Hilderbrand, A. E.; Kurulugama, R. T.; Koeniger, S. L.; Clemmer, D. E. *Expert Rev. Proteomics* **2005**, *2*, 553.
- (35) McLean, J. A.; Ruotolo, B. T.; Gillig, K. J.; Russell, D. H. *Int J Mass Spectrom* **2005**, *240*, 301.
- (36) Bohrer, B. C.; Mererbloom, S. I.; Koeniger, S. L.; Hilderbrand, A. E.; Clemmer, D. E. *Annu. Rev. Anal. Chem.* **2008**, *1*, 293.
- (37) Kanu, A. B.; Dwivedi, P.; Tam, M.; Matz, L.; Hill, H. H. *J. Mass Spectrom.* **2008**, *43*, 1.
- (38) Tao, L.; Dahl, D. B.; Perez, L. M.; Russell, D. H. *J. Am. Soc. Mass Spectrom.* **2009**, *20*, 1593.
- (39) Pukala, T. L.; Ruotolo, B. T.; Zhou, M.; Politis, A.; Stefanescu, R.; Leary, J. A.; Robinson, C. V. *Structure* **2009**, *17*, 1235.
- (40) Politis, A.; Park, A. Y.; Hyung, S. J.; Barsky, D.; Ruotolo, B. T.; Robinson, C. V. *Plos One* **2010**, *5*.
- (41) Lorenzen, K.; Olia, A. S.; Uetrecht, C.; Cingolani, G.; Heck, A. J. R. *J. Mol. Biol.* **2008**, *379*, 385.
- (42) van Duijn, E.; Barendregt, A.; Synowsky, S.; Versluis, C.; Heck, A. J. R. *J. Am. Chem. Soc.* **2009**, *131*, 1452.
- (43) Hyung, S. J.; Robinson, C. V.; Ruotolo, B. T. *Chem. Biol.* **2009**, *16*, 382.
- (44) Ruotolo, B. T.; Hyung, S. J.; Robinson, P. M.; Giles, K.; Bateman, R. H.; Robinson, C. V. *Angew. Chem.-Int. Edit.* **2007**, *46*, 8001.
- (45) Benesch, J. L. P. *J. Am. Soc. Mass Spectrom.* **2009**, *20*, 341.
- (46) Felitsyn, N.; Kitova, E. N.; Klassen, J. S. *Anal. Chem.* **2001**, *73*, 4647.
- (47) Jurchen, J. C.; Williams, E. R. *J. Am. Chem. Soc.* **2003**, *125*, 2817.
- (48) Jurneczko, E.; Barran, P. E. *Analyst* **2011**, *136*, 20.
- (49) Ruotolo, B. T.; Benesch, J. L. P.; Sandercock, A. M.; Hyung, S. J.; Robinson, C. V. *Nat Protoc* **2008**, *3*, 1139.

- (50) Oomens, J.; Sartakov, B. G.; Meijer, G.; Von Helden, G. *Int J Mass Spectrom* **2006**, *254*, 1.
- (51) Green, M. K.; Lebrilla, C. B. *Mass Spectrom. Rev.* **1997**, *16*, 53.
- (52) Hofmeister, F. *Archiv Fur Experimentelle Pathologie Und Pharmakologie* **1908**, 273.
- (53) Baldwin, R. L. *Biophys. J.* **1996**, *71*, 2056.
- (54) Zhang, Y. J.; Cremer, P. S. *Curr Opin Chem Biol* **2006**, *10*, 658.
- (55) Zhang, Y.; Cremer, P. S. *Annu Rev Phys Chem*, *61*, 63.
- (56) Freeke, J.; Robinson, C. V.; Ruotolo, B. T. *Int J Mass Spectrom* **2010**, *298*, 91.
- (57) Pagel, K.; Hyung, S. J.; Ruotolo, B. T.; Robinson, C. V. *Anal Chem* **2010**, *82*, 5363.
- (58) Ruotolo, B. T.; Hyung, S. J.; Robinson, P. M.; Giles, K.; Bateman, R. H.; Robinson, C. V. *Angew Chem Int Ed Engl* **2007**, *46*, 8001.
- (59) Hyung, S. J.; Robinson, C. V.; Ruotolo, B. T. *Chem Biol* **2009**, *16*, 382.
- (60) Sobott, F.; McCammon, M. G.; Robinson, C. V. *Int J Mass Spectrom* **2003**, *230*, 193.
- (61) Jurchen, J. C.; Williams, E. R. *J Am Chem Soc* **2003**, *125*, 2817.
- (62) McKay, A. R.; Ruotolo, B. T.; Ilag, L. L.; Robinson, C. V. *J. Am. Chem. Soc.* **2006**, *128*, 11433.
- (63) Verkerk, U. H.; Kebarle, P. *J. Am. Soc. Mass Spectrom.* **2005**, *16*, 1325.
- (64) Flick, T. G.; Merenbloom, S. I.; Williams, E. R. *Anal. Chem.* **2011**, *83*, 2210.
- (65) Wang, G. D.; Cole, R. B. *Anal. Chem.* **1994**, *66*, 3702.
- (66) Han, X. M.; Jin, M.; Breuker, K.; McLafferty, F. W. *Science* **2006**, *314*, 109.
- (67) Bostrom, M.; Tavares, F. W.; Finet, S.; Skouri-Panet, F.; Tardieu, A.; Ninham, B. *W. Biophys. Chem.* **2005**, *117*, 217.

Chapter 3. Bound Cations Significantly Stabilize the Structure of Multiprotein Complexes in the Gas-phase

Han L, Hyung SJ, Ruotolo BT, Bound Cations Significantly Stabilize the Structure of Multiprotein Complexes in the Gas Phase, *Angewandte Chemie International Edition*, 2012, 51, 5692-5695.

3.1 Abstract

The characterization of multi-component protein complexes intact using MS is fast becoming a standard methodology in structural biology. Further, IM separation, capable of rapidly measuring protein size in the absence of bulk solvent, in conjunction with such intact mass measurements of complexes, promise to open new doors in structural proteomics. Such advances are fundamentally linked to a detailed understanding of the factors effecting gas-phase protein structure and the potential influence of solution conditions upon the resulting gas-phase multiprotein ions produced for analysis. Our previous work screened 12 ammonium-based anions against 5 different multiprotein systems and found that, when such anions remain bound to assemblies in the gas phase, that they can differentially stabilize or destabilize protein structures in the absence of bulk solvent. Further, the anions studied in Chapter 2 exhibited primarily an ‘evaporative cooling’ type mechanism, where dissociation of the bound anions upon protein complex activation provided the main structure stabilization mode. In this chapter we have investigated the stabilization mechanism of cations bound to positively-charged

multiprotein complex ions and found dramatic differences when compared to equivalent data for anion-bound complexes. The charge-per-unit-area of cations seems to play the largest role in selecting structurally stabilizing cations, and data from IM-MS clearly indicate that many cations stabilizing by remaining bound to the complex, in stark contrast to their anionic counterparts. We rationalize these observations through a mechanism where cations of high charge density, that bind in large numbers to protein complexes, will retain their relative binding position within the protein sequence and be less-mobile than smaller, less charge dense cations. This reduction in charge mobility also reduces Coulombic unfolding, which depends upon the mobility of charges within the protein structure to operate effectively. Multi-dentate binding of cations to multiple sites on the protein could also be a causative factor in the high stability observed for some protein-cation complexes. Finally, we summarize and compare our counterion dataset to date, and discuss the implications of our results for IM-MS measurements of gas-phase protein complexes in the context of structural proteomics.

3.2 Introduction

MS has revealed the composition, stoichiometry, connectivity, and dynamics of many multiprotein complexes that remain challenging for other structural biology tools^{1,2}. More recently, IM, a gas-phase separation technology that operates to resolve protein ions according to their size and charge^{3,4}, coupled with MS (IM-MS) has been used to generate 3D structure information from such samples⁵⁻⁷. Taken together with other gas-phase probes of biomolecules structure⁸⁻¹⁰, one can define a rapidly progressing field where long-standing protein structure challenges are being elucidated using gas-phase methodologies. Even though such gas-phase methods for protein structure analysis are proving to be very useful, their development is not

devoid of experimental challenges. Chief among these is establishing a general correlation between gas-phase measurements and protein structures in solution. Several reports have observed significant rearrangements of protein structure upon desolvation and ionization^{11,12}, although recent data suggest that these examples may be in the minority¹³. Despite this, general protocols aimed at protecting protein structure upon the removal of bulk solvent will undoubtedly biomolecular structure characterization through gas-phase structural biology approaches, like IM-MS.

Recent approaches toward the development of such a protocol use additives, both in solution prior to ionization¹⁴⁻¹⁶ and in the gas-phase prior to MS analysis¹⁷, as a means of stabilizing protein complex ions. Our group, and others, have focused on Hofmeister-type salt additives, and have recently classified a large number of anions for their ability to stabilize multiprotein structure¹⁸ using measurements of both CIU, where ions are heated with collisions with neutral gas and induced to unfold, and CID, where increased collisional heating leads to dissociation of protein complexes into a highly unfolded monomers and stripped complexes¹⁹. Our previous data revealed that anions bind to protein complexes during or prior to the nESI process and can stabilize protein ions through dissociation as neutrals, which act to carry away excess rotational and vibrational energy from the gas-phase protein ions, thus abating any dramatic internal energy increases and allowing their structures to remain compact in configurations easily correlated to X-ray and NMR datasets¹⁸. In this chapter, we study the influence of cation-based stabilizers, compare these additives to our previous anion dataset, and find dramatic mechanistic differences between the two.

3.3 Experimental

3.3.1 Materials

The proteins avidin (egg white), TTR (human), ConA (jack bean), ADH (yeast), BLA (bovine), and salts (acetate anion with ammonium, TMA, sodium, potassium, rubidium, lithium, Tris, calcium, barium, and magnesium counterions) were purchased from Sigma (St. Louis, MO, USA). All protein samples were buffer exchanged into 100 mM ammonium acetate at pH 7 using Micro Bio-Spin 6 columns (Bio-Rad, Hercules, CA) and prepared to a final concentration of 5 μ M (avidin, TTR, ConA, ADH) or 10 μ M (BLA). In order to study the influence of different salts on protein stability without significantly altering buffer capacity or solution pH, the salts were prepared as stock solutions in 100 mM ammonium acetate at a concentration of 20 mM, each of which was then added to the protein solution. Final solutions contained added salt concentrations of 2 mM for avidin, TTR, ConA, ADH and 0.5 mM for BLA samples. The total salt and protein concentrations listed above were chosen primarily to avoid ion suppression effects.

3.3.2 IM-MS and CIU/CID analysis

Typically, an aliquot of the solution (\sim 5 μ L) was analyzed using a quadrupole-IM-ToF MS instrument (Synapt G2 HDMS, Waters, Milford MA, USA)^{20,21}. Protein ions were generated using a nESI source, under conditions described previously and optimized to allow transmission of non-covalent protein complexes^{22,23}. The T-wave IM separator was operated at a pressure of \sim 3.5 mbar, and a 40 V wave height traveling at 800-1000 m/s to generate IM separation. Collisional activation in the ion trap prior to the IM separator was used to perform CIU and CID

experiments. Ions were selected in the quadrupole mass filter at an m/z corresponding to 16^+ charge state of Avidin, 19^+ of ConA, 14^+ of TTR, 24^+ of ADH tetramers and 11^+ BLA dimers. Charge states were chosen based on their intensity across each solution state studied, and control IM arrival time data were screened for evidence of overlapping non-tetrameric ions at the same m/z value. Each of these mass-selected ions was activated by increasing the trap collision voltage. For all protein-salt systems investigated here trap collision voltage was incremented by 5 V in step-wise. Data analysis and normalization were carried out in a manner identical to our previous report¹⁸. Some figures contain axes labeled in collision energy (units of eV*). The axis is a normalized version of ion kinetic energy, which takes into account both the charge on the ion and reduced mass of the ion-neutral collision complex, for making comparisons across large mass ranges¹⁸.

3.3.3 Data analysis

All mass spectra were calibrated externally using a solution of cesium iodide (100 mg/mL) and were processed with Masslynx 4.1 software (Waters, Milford, MA, USA). Spectra are shown with minimal smoothing and without background subtraction. The relative abundance of mass-selected tetrameric ions (I_{tet}) was calculated as a percentage of the total intensity of all the signals observed in the mass spectra corresponding to either intact protein complex or its corresponding fragment ions (*i.e.*, monomer or trimer). The relative abundance of the compact form observed for tetrameric ions separated by IM (I_f) was calculated as a percentage of the total intensity of the peaks in the arrival time distribution observed at a selected m/z value corresponding to intact tetramer (or dimer for BLA):

$$I_{tet} (\%) = \frac{I_{tet}}{I_{tet} + I_{mon}} \times 100$$

$$I_f (\%) = \frac{I_{\text{folded}}}{\sum I_{\text{conformers}}} \times 100$$

The average relative standard deviation for the determination of either I_{tet} (%) or I_f (%) is 2-4%. The data shown in Figure 3-1 and Figure 3-2 include axes labeled in collision energy (units of eV*). The axis is a normalized version of ion kinetic energy, which takes into account both the charge on the ion and reduced mass of the ion-neutral collision complex, for making comparisons across large mass ranges. Although the conversion used here is identical to center-of-mass energy conversion, we do not use this term in this chapter, as the definition of this quantity has clear implications for ion internal energy and these claims may not extend to the large ions studied here due to the large number of degrees of freedom possessed by protein complex ions. We use the conversion only as a means of normalizing kinetic energies for CIU and CID comparisons across broad mass ranges.

3.4 Results and Discussion

3.4.1 Measuring the stability of cation-bound protein complexes via collision induced unfolding and dissociation

Figure 3-1A and Figure 3-1B show data for tetrameric TTR (55 kDa), as an example of the data used in this chapter to study cation-stabilized multiprotein complexes. In order to demonstrate the effect of different cations on TTR, a series of tandem mass spectra (showing CID, Figure 3-1A) and arrival time distributions (showing CIU, Figure 3-1B) of the 14^+ charge state of TTR acquired at a trap collision voltage of 60 V and 55 V respectively are shown. For each, all instrument parameters are kept constant and only the composition of the nESI buffer is altered to

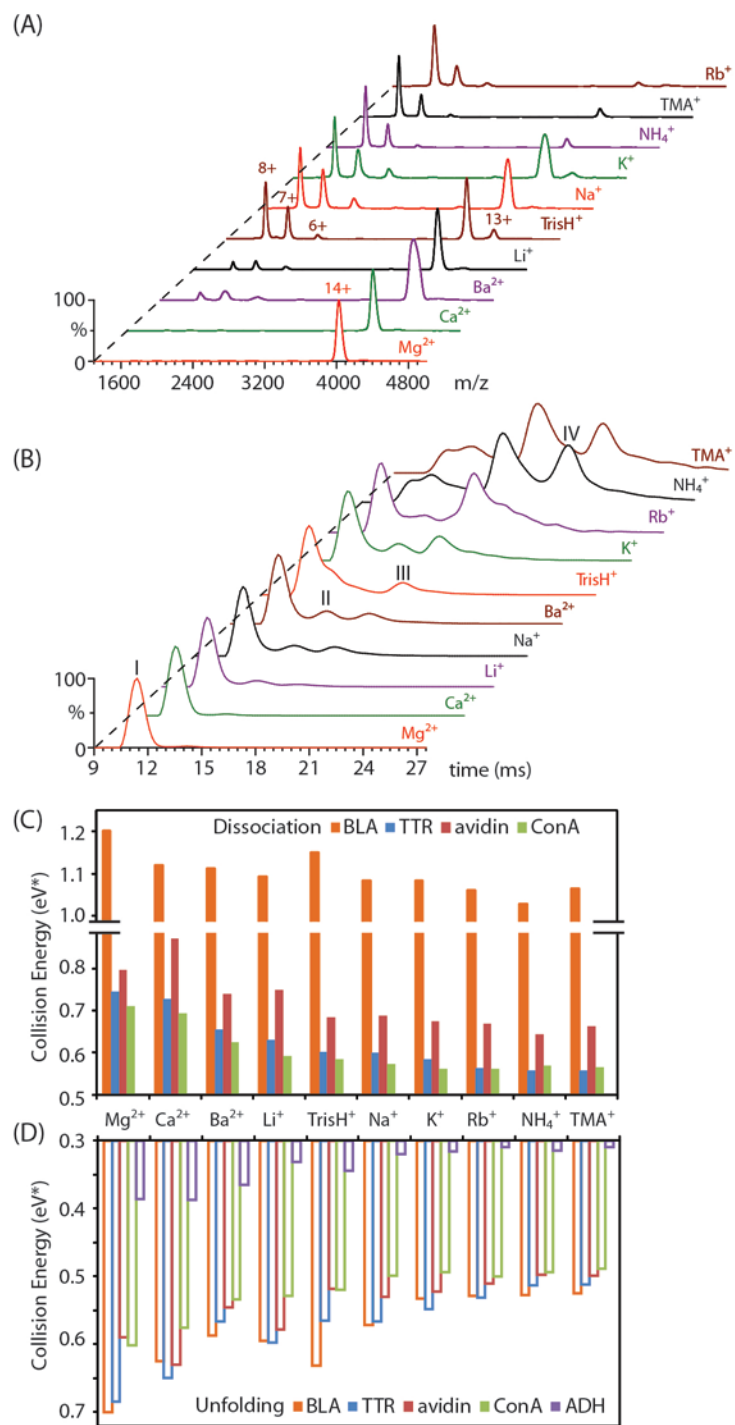


Figure 3-1. Elucidating the extent of unfolding and dissociation of the five protein complexes in the presence of different cations from IM-MS. (A) The mass spectra of TTR incubated with 10 acetate-based cations reveal different extent of dissociation. The 14⁺ charge state of TTR ions selected by the quadrupole mass filter, is activated at a trap collision voltage of 60 V. The mass spectra contain peaks corresponding to the 14⁺ charge state tetramer and the 6–8⁺ charge state monomers. (B) The arrival time distributions of 14⁺ tetrameric TTR incubated with 10 acetate-based cations acquired at a trap collision voltage of 55 V yield unfolding to different extent. The four drift time features showing a transition from compact to extended species are labeled from I to IV. Histogram plots charting collision energy (eV*) required to dissociate (C) and unfold (D) 50% of the dimeric protein ion population for BLA (orange) and tetrameric protein ion populations for TTR (blue), avidin (red), ConA (green) and ADH (purple) are shown for a range of cation additives. Control data sets, without added acetate-based salt, are marked on the plot (NH₄⁺).

contain different cationic additives. The peak corresponding to 14⁺ charge state of TTR isolated for CIU/CID broadens when incubated with added cations, as it contains unresolved peaks corresponding to a range of previously-described adducted forms (Figure II-1)²⁴. In a similar

fashion to anions, when cations dissociate from the protein complexes studied here, they do so as neutrals (bound to acetate or hydroxide counter-ions). In Figure 3-1A, signals for 14^+ TTR and 6^+ to 8^+ TTR monomer are visible at substantially different abundances as a function of cation additive, while Figure 3-1B reveals strikingly different arrival time distributions for 14^+ cation-bound TTR, with different relative abundances for compact (I) and unfolded conformer families (II-IV). These data clearly demonstrate the differential influence of cation additives on protein dissociation and unfolding

For a more quantitative measurement of such stability differences, we monitored CID and CIU data as a function of trap collision voltage (Figure II-2). From these data we constructed the histograms shown in Figure 3-1C and Figure 3-1D, which plot the ion energy (eV*) values at which the intensity observed for intact (I_{tet}) and compact (I_f) tetramer ions decrease by 50% respectively. Data include three tetrameric protein complexes other than TTR, including avidin, ConA and ADH, and dimeric BLA, screened according to their stability in the presence of the same 10 acetate-based cations. A number of general trends regarding gas-phase protein complex stability are observed. Firstly, the protein complexes studied here undergo CIU at lower energy relative to CID, as reported previously^{25,26}. We note that following incubation with stabilizing cations, ADH does not appreciably undergo CID even at the highest activation energy attainable (Figure II-3), resulting in the lack of its dissociation data set in Figure 3-1C. Secondly, cations can clearly be distinguished by their ability to stabilize protein complexes in the absence of bulk solvent. In general, Mg^{2+} and Ca^{2+} have a universally stabilizing influence on I_{tet} and I_f for all protein complexes studied here. Conversely, cations such as K^+ , Rb^+ and TMA^+ have a negligible stabilizing effect relative to control (ammonium acetate). Interestingly, $TrisH^+$, widely

used as a component of buffer solutions, exhibits a greater ability to stabilize the gas-phase protein complexes than other singly-charged cations studied here¹⁴. For example, TrisH^+ is the second-most stabilizing cation screened in our BLA dataset (behind Mg^{2+}). In addition, the relative stability of five protein complexes studied here are not influenced by cation additives, with BLA requiring the most energy to dissociate and TTR requiring the most energy to unfold¹⁸.

3.4.2 Classifying and ranking the influence of cations on protein stability

Despite these similarities, we find several significant differences in the stabilization provided by cation additives when compared with our previous anion data. Firstly, cation adducts seem to stabilize protein complexes against CID to a greater extent, on average, than equivalent anions. The ion energy at which 50% CID occurs is raised by 31% by the average cation, while this threshold is increased by only 19% by the addition of the average anion. This observation can be extended to include the general stability afforded to complexes bound by the most-stabilizing cations, the stabilities for which are in general much greater than any anion-bound complexes studied to date (Figure II-5). Conversely, anionic adducts are, in general, better stabilizers of gas-phase protein unfolding than cations. Data recorded for cation-adducted protein complexes indicate an average CIU threshold increase of only 26% where anions achieved a 36% increase in protein ion stability under similar conditions. It is therefore anticipated that the mechanism of protein structure stabilization for cation-adducted protein ions is dramatically different from their anion counterparts. Figure 3-2A shows plots of ion mass as a function of activation voltage for TTR. Previous data for anions showed a preference for complete dissociation of protein-anion adducts at relatively low activation voltages in order to siphon excess energy from the protein

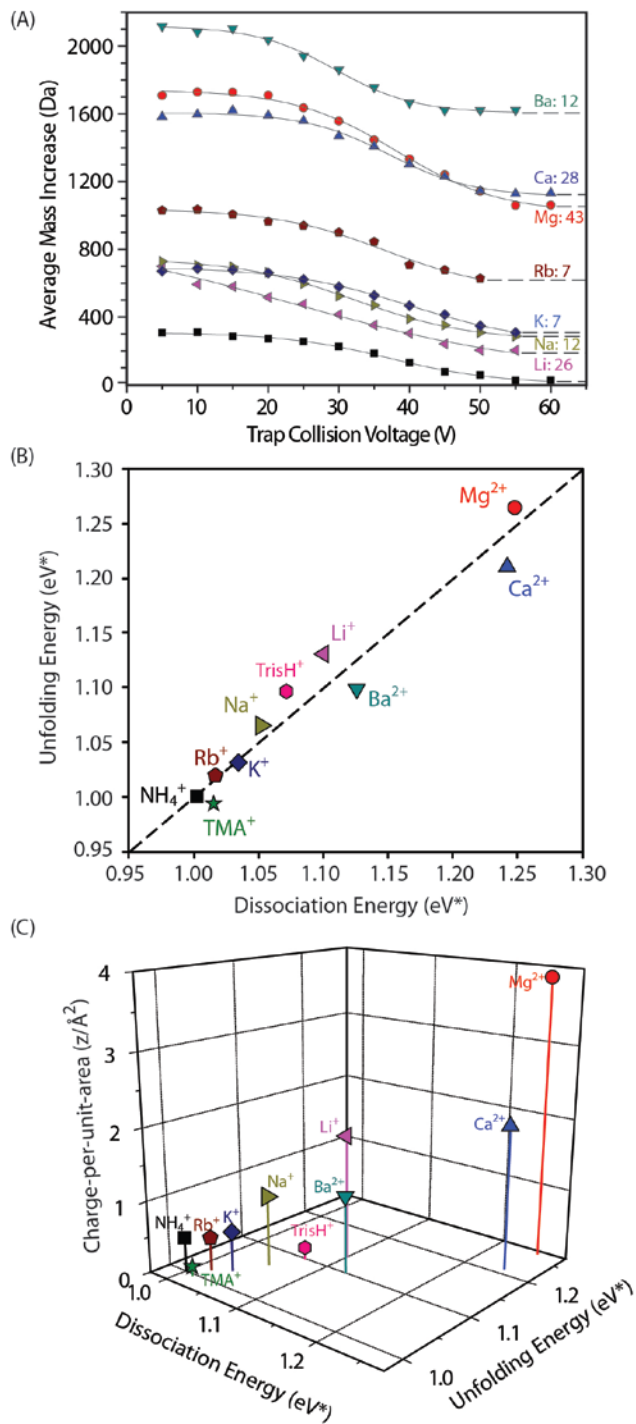


Figure 3-2. Ion mobility-mass spectrometry reveals protein complex stabilization achieved through cation attachment. (A) Plots of the measured average mass increase relative to the sequence mass of transthyretin (TTR) observed as a function of trap collision voltage for a range of cation additives. The approximate numbers of cations that stay strongly bound to the protein assembly even at large trap collision voltage are shown on the right. (B) A plot of the average CID versus CIU collision energy (eV*) averaged over the 5 protein complexes studied herein for each cation additive. The protein-cation complexes have highly-correlated unfolding and dissociation energies (dashed line). (C) Data from Figure 3-2B plotted against the charge-per-unit-area of the cations added (vertical axis) illustrate a well-correlated relationship between protein-cation complex stability and the charge-per-unit-area of added cations.

system and confer additional structural stability¹⁸. The cation adducts studied here that impart the most protein stabilization, however, tend to remain bound to the protein complex even at large activation voltage values. In further contrast to our studies of protein-anion adducts, CIU and CID stability measurements are highly correlated for cation-adducted complexes. The linear

relationship between CID and CIU stability thresholds exhibits a R^2 of 0.94 (Figure 3-2B) compared to anion-based observations reported previously ($R^2=0.55$). This data further indicates disparity between the stabilization mechanisms operative for anionic and cationic additives¹⁸.

3.4.3 Towards a mechanistic understanding of gas-phase protein stabilization through bound cations

The above differences between anionic and cationic stabilizers inform our mechanistic description of their action, which has been normalized for the relative binding affinities of the cations studied here. Whereas anions perform optimally as stabilizers when they bind to the protein and then dissociate from the complex after relatively minimal activation, the best cationic stabilizers are those that remain bound to the protein assembly in large numbers, even following extensive activation in the gas phase. These highly-stabilizing cations strongly correlate with those that have larger charge-per-unit-area values (Figure 3-2 and Figure II-5A). The larger charge-per-unit-area of these cations, much in excess of any anions that we have tested to date (Figure II-5B and Table II-1), presumably gives these adducts access to modes of stabilization that rely either upon multidentate interactions within proteins, enabling them to more effectively tether regions of its structure, or by replacing highly-mobile proton charge carriers with less mobile cationic charge carriers that restrict charge mobility and frustrate the Coulombic unfolding of subunits within the complex, which is a critical step in the asymmetric dissociation of non-covalent protein complexes²⁷⁻³¹. Although those cations that strongly-stabilize gas-phase protein structure conform to the mechanistic discussion above, evidence of the dissociative-cooling of protein structure is not absent from our cation dataset (Figure 3-2A and Figure 3-3). In summary, these data present the first mechanistic description of additive cation stabilizers that covers a broad range of both cationic additives and multiprotein complexes. We observe that, in

general, cations of high charge-per-unit-area stabilize proteins in a complimentary and significantly different way relative to most anions¹⁸, and we plan to exploit this in the future by using salt additives that are tailored to take advantage of both cationic and anionic protein adducts to improve protein structural stability. We believe that such additives are critical for IM-MS to fully-realize its potential as a high-throughput method for discovering multiprotein topology and structure, and as a means of elucidating the critical role of surfactant molecules in stabilizing gas-phase membrane protein complexes³².

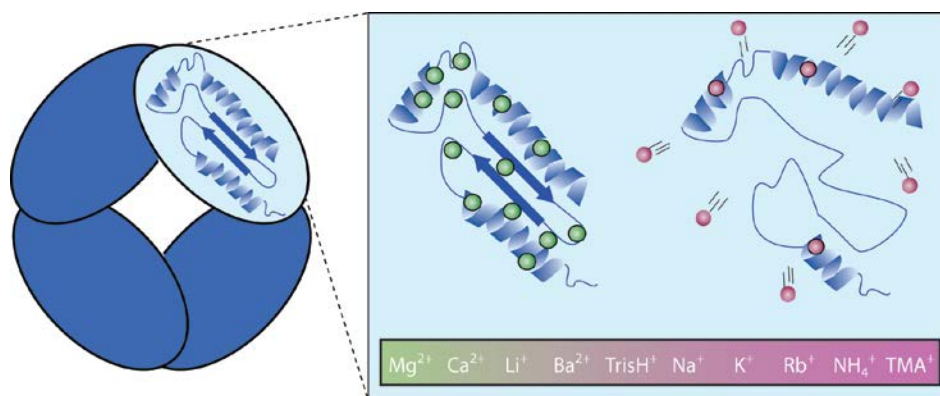


Figure 3-3. A mechanistic diagram of protein structure stabilization through bound cations that summarizes our current data set. Two models are shown: The cations of high charge density (green) that bind in large numbers to protein complexes will retain their binding position within the protein sequence and become less mobile as charge carriers. This reduction in charge mobility and possibly lower conformational flexibility through multidentate binding of cations to sites on the protein hinders Coulombic unfolding of protein subunits. Conversely, the cations of low charge density (red) that dissociate readily through collisional activation will bind in smaller numbers to proteins, which weaken the stability enhancement. Therefore the cations are ordered with regard to their ability to stabilize gas phase protein complexes, which is in good agreement with their charge density. The one exception is TrisH^+ , which is the only cation studied here capable of forming hydrogen bonds with the protein.

3.5 Conclusions

In this chapter, we study the influence of cation-based stabilizers, added prior to nESI, and compare their effect to our previous anion dataset. We find substantial differences in the extent

and mechanism of stabilization provided by cation additives when compared with our previous anion data. First, the cation additives studied here provide a substantially greater average increase in protein stability than observed previously, in both CID and CIU data. Secondly, the correlation between stability trends observed between CID and CIU datasets is much greater than observed for anion stabilizers, suggesting a link between local and global protein stabilization in the case of cation additives that was absent for anions observed previously. Finally, the charge-per-unit-area of the cations added exhibits an excellent correlation to the stabilization observed for the proteins studied here. All of these observations are combined and we construct a mechanistic picture that describes how the cations studied here stabilize proteins and protein complexes in the absence of solvent. Our data is most-consistent with a mechanism where the cations that stabilize protein complexes to the greatest degree are those that bind most-tightly to basic sites on the protein. These tightly bound cations limit charge migration, and may also tether regions of the protein together, to stabilize protein structure in the absence of bulk solvent. This mechanism stands in contrast to the mechanism we constructed to describe our anion dataset, which relies entirely on evaporative cooling.

3.6 References

- (1) Heck, A. J. R. *Nat. Methods* **2008**, *5*, 927.
- (2) Sharon, M.; Robinson, C. V. In *Annu. Rev. Biochem.*; Annual Reviews: Palo Alto, 2007; Vol. 76, p 167.
- (3) Pukala, T. L.; Ruotolo, B. T.; Zhou, M.; Politis, A.; Stefanescu, R.; Leary, J. A.; Robinson, C. V. *Structure* **2009**, *17*, 1235.
- (4) Politis, A.; Park, A. Y.; Hyung, S. J.; Barsky, D.; Ruotolo, B. T.; Robinson, C. V. *PLoS One* **2010**, *5*, e12080.
- (5) Ruotolo, B. T.; Robinson, C. V. *Curr Opin Chem Biol* **2006**, *10*, 402.
- (6) Wytenbach, T.; Bowers, M. T. In *Annu. Rev. Phys. Chem.*; Annual Reviews: Palo Alto, 2007; Vol. 58, p 511.
- (7) Zhong, Y.; Hyung, S. J.; Ruotolo, B. T. *Expert Review of Proteomics* **To Be Published**.

- (8) Breuker, K.; McLafferty, F. W. *Proc. Natl. Acad. Sci. U. S. A.* **2008**, *105*, 18145.
- (9) Green, M. K.; Lebrilla, C. B. *Mass Spectrom. Rev.* **1997**, *16*, 53.
- (10) Benesch, J. L. P.; Ruotolo, B. T.; Simmons, D. A.; Robinson, C. V. *Chem. Rev.* **2007**, *107*, 3544.
- (11) Barran, P. E.; Jurneczko, E. *Analyst* **2011**, *136*, 20.
- (12) Hogan, C. J., Jr.; Ruotolo, B. T.; Robinson, C. V.; Fernandez de la Mora, J. *J Phys Chem B* **2011**, *115*, 3614.
- (13) Benesch, J. L. P.; Ruotolo, B. T. *Curr. Opin. Struct. Biol.* **2011**, *21*, 641.
- (14) Freeke, J.; Robinson, C. V.; Ruotolo, B. T. *Int. J. Mass Spectrom.* **2010**, *298*, 91.
- (15) Flick, T. G.; Merenbloom, S. I.; Williams, E. R. *Analytical Chemistry* **2011**, *83*, 2210.
- (16) Merenbloom, S.; Flick, T.; Daly, M.; Williams, E. *Journal of the American Society for Mass Spectrometry* **2011**, *22*, 1978.
- (17) Bagal, D.; Kitova, E. N.; Liu, L.; El-Hawiet, A.; Schnier, P. D.; Klassen, J. S. *Analytical Chemistry* **2009**, *81*, 7801.
- (18) Han, L. J.; Hyung, S. J.; Mayers, J. J. S.; Ruotolo, B. T. *J. Am. Chem. Soc.* **2011**, *133*, 11358.
- (19) Benesch, J. L. P. *Journal of the American Society for Mass Spectrometry* **2009**, *20*, 341.
- (20) Zhong, Y.; Hyung, S. J.; Ruotolo, B. T. *Analyst* **2011**, *136*, 3534.
- (21) Giles, K.; Williams, J. P.; Campuzano, I. *Rapid Commun. Mass Spectrom.* **2011**, *25*, 1559.
- (22) Ruotolo, B. T.; Benesch, J. L. P.; Sandercock, A. M.; Hyung, S. J.; Robinson, C. V. *Nat Protoc* **2008**, *3*, 1139.
- (23) Hernandez, H.; Robinson, C. V. *Nat Protoc* **2007**, *2*, 715.
- (24) Verkerk, U. H.; Kebarle, P. *Journal of the American Society for Mass Spectrometry* **2005**, *16*, 1325.
- (25) Ruotolo, B. T.; Hyung, S. J.; Robinson, P. M.; Giles, K.; Bateman, R. H.; Robinson, C. V. *Angew. Chem.-Int. Edit.* **2007**, *46*, 8001.
- (26) Hyung, S. J.; Robinson, C. V.; Ruotolo, B. T. *Chem. Biol.* **2009**, *16*, 382.
- (27) Jurchen, J. C.; Williams, E. R. *J. Am. Chem. Soc.* **2003**, *125*, 2817.
- (28) Felitsyn, N.; Kitova, E. N.; Klassen, J. S. *Anal. Chem.* **2001**, *73*, 4647.
- (29) Bornschein, R. E.; Hyung, S. J.; Ruotolo, B. T. *J. Am. Soc. Mass Spectrom.* **2011**, *22*, 1690.
- (30) Erba, E. B.; Ruotolo, B. T.; Barsky, D.; Robinson, C. V. *Anal. Chem.* **2010**, *82*, 9702.
- (31) Pagel, K.; Hyung, S. J.; Ruotolo, B. T.; Robinson, C. V. *Anal. Chem.* **2010**, *82*, 5363.
- (32) Zhou, M.; Morgner, N.; Barrera, N. P.; Politis, A.; Isaacson, S. C.; Matak-Vinkovic, D.; Murata, T.; Bernal, R. A.; Stock, D.; Robinson, C. V. *Science* **2011**, *334*, 380.

Chapter 4. Dramatically Stabilizing Multiprotein Complex Structure in the Absence of Bulk Water using Tuned Hofmeister Salt Pairs

Han L, Ruotolo BT, Traveling-wave Ion Mobility-Mass Spectrometry Reveals Additional Mechanistic Details in the Stabilization of Protein Complex Ions through Tuned Salt Additives, *International Journal for Ion Mobility Spectrometry*, 2013, 16, 41-50.

Han L, Hyung SJ, Ruotolo BT, Dramatically Stabilizing Multiprotein Complex Structure in the Absence of Bulk Water using Tuned Hofmeister Salts, *Faraday Discussion*, 2013,160, 371-388.

4.1 Abstract

IM-MS is often applied to the structural elucidation of multiprotein assemblies in cases where XRD or NMR experiments have proved challenging. Such applications are growing steadily as we continue to probe regions of the proteome that are less-accessible to such high-resolution structural biology tools. Since IM measures protein structure in the absence of bulk solvent, strategies designed to more-broadly stabilize native-like protein structures in the gas-phase would greatly enable the application of such measurements to challenging structural targets. Recently, we have begun investigating the ability of salt-based solution additives that remain bound to protein ions in the gas-phase to stabilize native-like protein structures. These experiments, which utilize CIU and CID in a tandem MS mode to measure protein stability, seek to develop a rank-order similar to the Hofmeister series that categorizes the general ability of

different anions and cations to stabilize gas-phase protein structure. Here, we study calcium nitrate and magnesium chloride as potential stabilizing additives for protein structures *in vacuo*, and find that the addition of these salts to solutions prior to nESI dramatically enhances multiprotein complex structural stability in the gas-phase. Based on these experiments, we also refine the physical mechanism of cation-based protein complex ion stabilization by tracking the unfolding transitions experienced by cation-bound complexes. Upon comparison with unbound proteins, we find strong evidence that stabilizing cations act to tether protein complex structure. In addition, our evidence suggests that the relative solution-phase binding affinity of the anions and cations studied here is preserved in our gas-phase measurements, allowing us to study the influence of such interactions in detail.

4.2 Introduction

Proteins are amongst the most versatile macromolecules in living systems, and serve crucial functions in essentially all biological processes in a manner dependent upon their structures, dynamics and stabilities. Because protein assemblies are often large, heterogeneous and dynamic entities, there are numerous challenges in developing models of their high-resolution structure. Techniques such as XRD and NMR spectroscopy have been widely and successfully used to gain atomic-level structural information on a large number of protein complexes and networks¹, but despite this success, similar analyses are difficult to perform on assemblies that exhibit high degrees of flexibility, heterogeneity and polydispersity^{1,2}. Such properties are thought to be pervasive within the proteome, and are found in abundance within membrane-associated protein complexes³, a class of protein assemblies that are among the most sought-after therapeutic targets⁴. Furthermore, since neither XRD nor NMR techniques typically separate components

during analysis, both require highly purified samples. These and other challenges highlight the need to develop new approaches aimed at multiprotein structure determination^{1,2,5}.

MS and, more recently, IM-MS of intact complexes is emerging as one of many alternative approaches in the field of structural proteomics^{1,2,6-15}. It is now well established that MS can yield insights into the composition, stoichiometry and connectivity of heterogeneous multiprotein assemblies at relatively low concentrations¹⁶⁻²¹. When combined with IM, it becomes possible to separate species not only according to their mass-to-charge ratio (m/z) but also according to their ability to traverse an ion guide containing inert gas under the influence of a weak electric field, thus yielding ion size and shape information^{8,22-30}. T-wave IM separations specifically, that utilize a series of low-voltage 'waves' to propel ions for such size-dependant separations, have enabled most of the modern applications of IM-MS to structural biology^{10,31-33}. IM-MS experiments, thus, provide measurements of gas-phase protein size, which when combined with detailed molecular modeling can generate 3D topology models^{34,35}.

Although promising, the application of IM-MS for building architectural models of multiprotein complexes calls for a general correlation between gas-phase measurements and protein structures in solution. There have been several reports of significant rearrangements of protein structure upon transfer to the gas phase^{12,36}. Specifically, the processes of ESI, desolvation, transport and analysis can occur over a range of time scales and energies. As a consequence, biological molecules and assemblies can rearrange at the local residue level, unfold to more elongated conformations, and even refold to compact, yet non-native conformations³⁷⁻³⁹. Such rearrangements prompt the development of general strategies aimed at the protection of protein

structure, at every level, in the absence of bulk solvent, and would have far reaching implications in characterizing the structures of gas-phase biomolecules.

While the use of gas phase additives has been reported as a means of stabilizing protein-complex ions^{40,41}, our group focuses on pre-ionization, additive-based approaches using Hofmeister-type salts⁴²⁻⁴⁴, and have recently classified a large number of anions and cations in terms of their ability to stabilize multiprotein structure^{45,46}. For these experiments, we use both CIU, in which collisionally-heated ions are induced to create a series of unfolded conformations recorded by IM, and CID, where the same collisional heating eventually leads to protein complex dissociation into highly-unfolded monomeric and stripped complex product ions captured by MS³⁹. More importantly, our IM-MS data clearly show that anions and cations can differentially stabilize protein complexes through separate mechanisms, and that while the relative binding affinities of these buffer elements are likely retained in our measurements⁴⁷, the stabilization modes we observe are unique to the gas-phase. Whereas anions perform optimally as stabilizers when they bind to the protein and then dissociate from the complex to stabilize the system through ‘dissociative-cooling’⁴⁵, the best cationic stabilizers are those that remain bound to the protein assembly in large numbers, even following extensive activation in the gas phase⁴⁶. We have hypothesized that two modes of action are potentially critical in this later class of stabilizers. Cations either form multidentate interactions within proteins, enabling the tethering of disparate protein structural regions together, or they act to replace highly mobile protons with less mobile cations with relatively restricted mobility, thus inhibiting the Coulombic unfolding of protein subunits, which is a critical step in the asymmetric dissociation of noncovalent protein complexes⁴⁶.

In this chapter, we investigate the use of calcium nitrate and magnesium chloride as salt additives for stabilizing gas-phase protein structures, as these salts are composed of cation/anion pairs that previous results suggest should be strongly stabilizing for desolvated protein ions⁴⁵⁻⁴⁷. Our data demonstrate that both anions and cations derived from the addition of this salt in nESI solutions prior to ionization, can be used in concert to stabilize protein structures in the absence of bulk solvent to an extent not previously accessible using either constituent alone. In addition, we refine the mechanism by which cationic additives exert a stabilizing influence on gas-phase protein structure by observing the detailed structural transitions experienced by multiprotein complexes using CIU. Upon comparison with unbound proteins and control samples, we find strong evidence that stabilizing cations act to tether protein complex structure, rather than stabilize primarily through limiting charge mobility, as previously postulated.

4.3 Experimental

4.3.1 Materials

The protein tetramers TTR (human), avidin (egg white), and ConA (jack bean), the protein monomer CYC along with salts (ammonium acetate, ammonium nitrate/chloride and calcium/magnesium acetate) were purchased from Sigma (St. Louis, MO). All protein samples were buffer exchanged into 100 mM ammonium acetate at pH 7 using Micro Bio-Spin 6 columns (Bio-Rad, Hercules, CA) and prepared to a final concentration of 5 μ M (TTR, avidin, ConA) and 10 μ M (CYC). To study the influence of different salts on protein stability without significantly altering buffer capacity or solution pH, the salts were prepared as stock solutions in 100 mM ammonium acetate at a concentration of 20 mM, each of which was then added to protein solutions. Final solutions contained added salt concentrations of 4 mM for ammonium

nitrate/chloride (400 μ M for CYC), 2 mM for calcium/magnesium acetate (200 μ M for CYC) and 2 mM for calcium nitrate/magnesium chloride (200 μ M for CYC). The total salt and protein concentrations listed above were chosen primarily to avoid nESI-based ion suppression effects⁴⁸.

4.3.2 IM-MS

Sample aliquots (5 μ L) were analyzed using a quadrupole-IM-ToF MS instrument (Synapt G2 HDMS, Waters, Milford, MA). Protein ions were generated using a nESI source. The capillary of the nESI source was typically held at voltages 1.4 kV for CYC, 1.5 kV for TTR, 1.4 kV for avidin and 1.65 kV for ConA, with the source operating in positive mode. The sampling cone was operated at 50 V. The instrument settings were optimized to allow transmission of intact protein complexes and to preserve noncovalent interactions⁴⁹⁻⁵¹. The trap T-wave ion guide was pressurized to contain 3.3×10^{-2} mbar of argon gas. The ion trap was run in an accumulation mode and ion lifetimes in the trap prior to IM analysis range from 0 to 50 ms in our experiments. The T-wave IM separator was operated at a pressure of 3.5 mbar (N_2), and employed a series of DC voltage waves (40 V wave height traveling at 800-1000 m/s) to generate IM separation. The ToF-MS was operated over the m/z range of 800-15000 and at a pressure of 1.6×10^{-6} mbar.

4.3.3 CIU and CID

Collisional activation in the ion trap T-wave ion guide prior to the IM separator was used for CIU and CID of protein complexes in order to investigate the gas-phase stability of protein ions in the presence of different salts. This work was all performed in tandem-MS (quad selection) mode. Ions were selected in the quadrupole mass filter at a m/z corresponding to the 7⁺ charge state of CYC monomer, 14⁺ of TTR tetramer, 16⁺ of avidin tetramer and 20⁺ of ConA tetramer.

Charge states were chosen based on their intensity across each solution state interrogated, and control IM arrival time data were screened for evidence of overlapping non-tetrameric ions at the same m/z value. Each of these mass-selected ions were activated by increasing the trap collision voltage (Trap CE, as indicated in the instrument control software) which acts as a bias voltage between the quadrupole and the ion trap T-wave ion guide to accelerate ions to increased kinetic energies for CIU and CID experiments. For all protein-salt systems investigated here, energy-dependent arrival-time distribution profiles (CIU ‘fingerprints’) were constructed using 5 V stepwise increments of the trap CE. Upper voltage limits were identified as those where no further dissociation was observed.

4.3.4 Data Analysis

All mass spectra were calibrated externally using a solution of cesium iodide (100 mg/mL) and were processed with Masslynx 4.1 software (Waters, Milford, MA, USA). Spectra are shown with minimal smoothing and without background subtraction. The relative abundance of mass-selected tetrameric ions (I_{tet}) was calculated as a percentage of the total intensity of all the signals observed in the mass spectra corresponding to either intact protein complex ions or their corresponding fragment ions (i.e., monomer or trimer) using Equation 1. The relative abundance of the compact form observed for tetrameric ions separated by IM (I_f), which is the only feature observed under non-activating conditions, was calculated as a percentage of the total intensity of the peaks in the arrival time distribution observed at a selected m/z value corresponding to intact tetramer using Equation 2. These two values are used to chart the dissociation and unfolding of tetramers as a function of collision energy, respectively. The average relative standard deviation for the determination of either I_{tet} (%) or I_f (%) is 2-4%⁴⁵.

$$I_{\text{tet}} (\%) = \frac{I_{\text{tet}}}{I_{\text{tet}} + I_{\text{mon}}} \times 100 \quad (1)$$

$$I_{\text{f}} (\%) = \frac{I_{\text{folded}}}{\sum I_{\text{conformers}}} \times 100 \quad (2)$$

4.4 Results and Discussin

4.4.1 Gas-phase proteins and their complexes are stabilized by cationic and anionic additives through different mechanisms and to different extents

Using the protocol illustrated in Chapter 2 and 3, we have developed a classification system that allows us to generally rank cations and anions in terms of the stability they afford to gas-phase protein ions (Figure 4-1A). Our data suggests that cations (red) influence the unfolding and dissociation processes of protein complexes to similar degrees. Bound cations increase the threshold dissociation/unfolding energy in the order: $\text{NH}_4^+ \approx \text{TMA}^+ < \text{Rb}^+ < \text{K}^+ < \text{Na}^+ < \text{TrisH}^+ < \text{Ba}^{2+} \approx \text{Li}^+ < \text{Ca}^{2+} < \text{Mg}^{2+}$, progressively stabilizing gas-phase proteins to greater degrees. In contrast to cations, bound anions (blue) tend to stabilize protein complex CID and CIU to different extents. Therefore rather than a clearly-defined rank order, our IM-MS data reveals that anions can be categorized into three distinct groups. Tartrate²⁻, Cl⁻, citrate²⁻ and NO₃⁻ are among the most efficient stabilizers of protein unfolding and dissociation, populating a ‘highly-stabilizing’ cluster. In contrast, HCO₃⁻, I⁻ and ClO₄⁻ provide little or no additional stability to protein complex ions, and are thus regarded as ‘weakly-stabilizing’ salts in the gas-phase. The remaining anions including SO₄²⁻, HPO₄²⁻, SCN⁻, and F⁻ form a final ‘medium-stabilizing’ cluster. For a more quantitative comparison of the correlation between gas-phase unfolding and dissociation found in our IM-MS data, linear regression analysis was used to derive residual plots and correlation coefficients for linear fits to the anion and cation data shown in Figure 4-1A.

Figure 4-1B and Figure 4-1C show these data, and support our earlier assertion regarding the superior linearity of cation-based IM-MS stability data when compared to anion data, resulting in average residual sum of squares (RSS) values of 0.004 and 0.057 respectively. Furthermore, this analysis is also consistent with the correlation coefficients calculated for the same data (Figure 4-1B, caption), therefore suggesting a link between local and global protein stabilization in the case of cation additives that is absent for bound anions. In addition, cationic additives seem to stabilize protein complex ions against CID to a greater extent, on average, than equivalent anions while anionic adducts are, in general, better stabilizers of gas-phase protein unfolding.

The above differences between anionic and cationic stabilizers allow us to construct separate mechanistic descriptions of their action (Figure 4-1D). For anion-based stabilization, we can classify adducts into three categories based on both their protein binding affinity and ability to dissociate from proteins complexes following activation in the gas-phase. It is important to point out that these three anion classes, while related, are not the same as those presented in Figure 4-1A. The class that includes Cl^- , tartrate²⁻ and NO_3^- exhibits a strong stabilizing influence on protein structure (green track, Figure 4-1D). They can bind in large numbers and readily dissociate from the protein surface after relatively minimal activation. The observed dissociation of anion-based adducts corresponding to [H-“anion”] type neutrals acts to carry away excess rotational and vibrational energy from gas-phase protein ions, thus abating any dramatic internal energy increases for the protein and allowing it to retain a compact, native-like structure⁴⁵. In contrast, anions that do not bind (HCO_3^- and F^-), nor dissociate from gas-phase protein ions (I^- and ClO_4^-) do not provide significant structural stabilization (blue and yellow tracks respectively, Figure 4-1D). As shown in Figure 4-1D and Figure 4-1F, the gas-phase acidity of the conjugate

acid form of the anion (equivalent to anion proton affinity) correlates well with these three classes of stabilizing anions, and in turn with their relative binding affinities. This correlation is apparent when singly-charged anions are considered, where anions with low gas-phase acidity fall into the yellow track, those with intermediate affinity in the green track, and those with the highest values are in the blue track. Multiply-charged anions are more-difficult to place *a priori* due to likely multi-dentate protein interactions.

Whereas anions studied to date perform optimally as stabilizers when relying entirely on the dissociative-cooling process described above, optimal cationic stabilizers are those that remain bound to the protein assembly, even following extensive activation in the gas phase (red track, Figure 4-1D). These highly-stabilizing cations correlate with those that have larger charge-per-unit-area values, such as Mg^{2+} and Ca^{2+} shown in Figure 4-1E. The higher surface charge density of these cations, much in excess of any anions tested, gives these adducts access to modes of stabilization that rely either upon multidentate interactions within the protein, enabling them to tether regions of its structure, or by replacing highly-mobile proton charge carriers with less-mobile cationic charge carriers that restrict charge mobility and frustrate the Coulombic unfolding of subunits within the complex⁴⁶. Note that anions with low gas-phase acidity (e.g., I^- and ClO_4^-), though having higher protein binding strengths when compared to the other singly-charged anions studied here, do not reach the charge-per-unit-area values of stabilizing cations (Mg^{2+} and Ca^{2+}). Armed with this mechanistic knowledge, we have endeavored to use tailored anion/cation pairs for protein stabilization in order to make use of both stabilization mechanisms simultaneously.

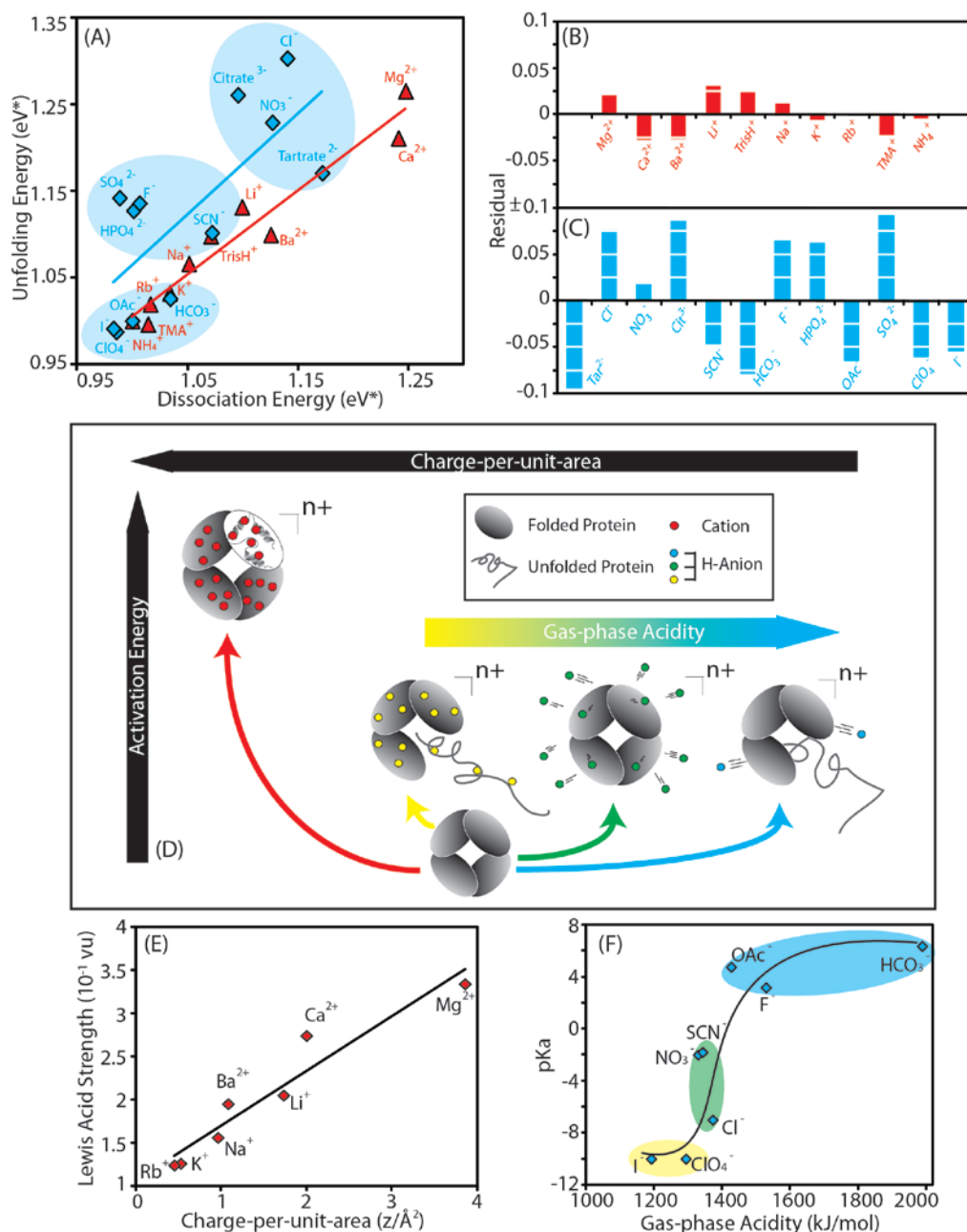


Figure 4-1. Comparison of anion and cation-mediated stabilization afforded to gas-phase protein ions. (A) A plot of the average CID versus average CIU energies (eV*) for the 5 protein complexes studied herein for cation (red) and anion (blue) additives. The plot reveals that the anions can be categorized into three distinct groups (blue background color), according to their ability to stabilize protein complexes relative to the control data set (OAc⁻). Both (B) and (C) show residual plots for stability data from best-fit linear relationships between CIU and CID energies, for cation and anion datasets respectively. The correlation between unfolding and dissociation stabilization is much higher for our cation data ($R^2 = 0.97$) relative to equivalent data recorded for anion additives ($R^2 = 0.55$). (D) A diagram depicting our current mechanistic understanding of gas-phase protein structure stabilization through bound cations and anions. Anions with mid-range acidities bind the protein in high affinity and are released upon

dissociation leading to high protein structural stability in the gas phase through dissociative cooling (green track). Anion additives that do not bind, nor dissociate from gas-phase protein ions do not provide significant structural stabilization (blue and yellow track). In contrast, high charge-per-unit-area cations, having much greater surface charge densities than any of the anions tested to date, bind in large numbers to protein complexes and remain bound to become less-mobile as charge carriers, thus affording increased stability enhancement to gas-phase protein structure (red track). (E) A plot of the charge-per-unit-area of cations against Lewis acid strength reveals a high level of correlation to the best fit line (shown). (F) A plot of the gas-phase acidity of anions against pKa reveals a positive correlation between the two parameters. The data are color-coded to indicate the membership of each anion in the three relevant mechanistic tracks depicted in Figure 4-1D, and a trend line is added to guide the eye.

4.4.2 Drastic differences of protein stabilization by cationic/anionic Hofmeister series in solution and in the gas phase

On first inspection, drastic differences are apparent between the rank order determined by our data in the gas-phase (Figure 4-1A) and the well-known Hofmeister series of cations and anions describing their influence upon protein stability in solution: $\text{TMA}^+ > \text{NH}_4^+ > \text{Rb}^+ > \text{K}^+ > \text{Na}^+ > \text{Li}^+ > \text{Ca}^{2+} > \text{Mg}^{2+} > \text{Ba}^{2+}$ and $\text{SO}_4^{2-} > \text{HPO}_4^- > \text{F}^- > \text{OAc}^- > \text{Citrate}^{3-} > \text{HCO}_3^- > \text{Cl}^- > \text{NO}_3^- > \text{I}^- > \text{ClO}_4^- > \text{SCN}^-$. For example, NO_3^- , SCN^- and Cl^- are all protein stabilizers in the gas-phase, but act as structure destabilizers in bulk solvent. Similarly, cations stabilize gas-phase proteins following a nearly reversed order relative to most measurements of protein stability carried out in solution. Multiple reports have shown that Hofmeister-type protein stabilization in solution depends upon ion hydration and the ability of ions to alter water surface tension, along with direct ion-protein binding⁵²⁻⁵⁴. In our stability measurements of desolvated proteins, the influence of both bulk solvent and local hydration layers are absent, and our data are instead dominated by overall protein-counterion binding affinity, adduct dissociation, and Coulombic effects incumbent upon protein unfolding in the gas-phase (Figure 4-1D). Thus, it is likely that the lack of protein solvation contributes substantially to the differences we observe between the stabilizing influence of Hofmeister salts in the gas-phase and in solution.

In spite of the clear differences between protein stabilization in the gas-phase and in solution noted above, it is potentially instructive to mine our current dataset for any information that may suggest critical links between our data and those collected in the condensed phase. To attempt this, we first note the strong correlation between gas-phase acidity and pKa measurements acquired in solution for the anions studied here (Figure 4-1F). As stated above, anion proton affinity seems likely to govern the relative amount of anions bound to gas-phase proteins in our data (Figure 4-1D). We also note that the surface charge density of the cations studied here have a high correlation to their Lewis acid strengths in solution. Mirroring the above anion-based correlation, we found cation charge-per-unit-area to be an able predictor of protein-cation complex stability (Figure 4-1E). Both correlations, while not representing demonstrable proof, provide some evidence that the relative binding affinities observed for protein-counterion complexes in our gas-phase measurements may mirror those in solution.

To further probe the potential correlations between our gas-phase data and protein-salt interactions in solution, we used MS to quantify the anions bound to proteins for a broad range of interacting pairs, as previous data had found a strong correlation between perchlorate binding observed by MS and the number of surface accessible basic sites on a given protein⁵⁵. It is important to note that all the data and analysis shown in Figure 4-1 is derived by normalizing the stabilization effects observed to the number of adducts bound to protein ions in the first instance. Figure 4-2A shows MS data for 7⁺ CYC monomers generated from solutions containing a range of anion additives. Unlike MS data for more-massive multiprotein complexes, where only average numbers of [H-“anion”] type adducts can be extracted from the average mass shifts observed relative to control (Figure 4-2B), the mass resolving power achieved in our CYC

experiments is sufficient to resolve individual bound populations for the anion-protein complexes observed. The total number of anions bound to each protein is indicated in the blue histograms in Figure 4-2C-F, under which the black column represents the number of basic sites already occupied by charge carriers based on the ion charges state observed. Our data show that for anions known to have strong protein interactions (including nitrate, chloride, iodide and perchlorate anions), the quantity of binding observed by MS, when added to those sites occupied by unpaired charge carriers, correlates reasonably well with the maximum expected number of binders based on the known surface assessable binding sites in solution. We attribute those cases where we observe excess binding (values exceeding the black dashed line) to anion condensation during the nESI process. Taken together with protein-ligand binding studies carried out where intensity values in MS measurements can be directly correlated to binding strengths between proteins and small molecules⁵⁶⁻⁵⁹, it is highly likely that our data represent a direct measure of protein-anion binding affinities highly correlated to those in solution. As such, it is likely that our observations, and the rank orders of stabilizing/destabilizing salts extracted from our data, serve primarily to highlight the critical importance of protein solvation in the Hofmeister stabilization of proteins in solution.

The rank order describing the stabilizing influence of protein salt interactions in the absence of solvent also exhibits reasonable agreement with a number of studies that have observed so-called 'reversed' Hofmeister series, primarily for positively charged proteins at low salt concentrations⁶⁰⁻⁶². Spectroscopic data indicates that these inversed datasets result from the differing strengths of anion associations with positively charged protein surfaces, are well-correlated with the sizes of hydrated anions, and are related directly to the hydration free energy

of stabilizing anions⁶³. While our gas-phase data correlate more-strongly to these 'reversed' Hofmeister series, a direct mechanistic correlation between the two rank orders is unlikely given what we currently understand of our gas-phase data. It is likely that continuing studies that highlight differences between gas-phase and 'reversed' Hofmeister series may further-pinpoint the role of anion hydration in solution-phase protein stabilization.

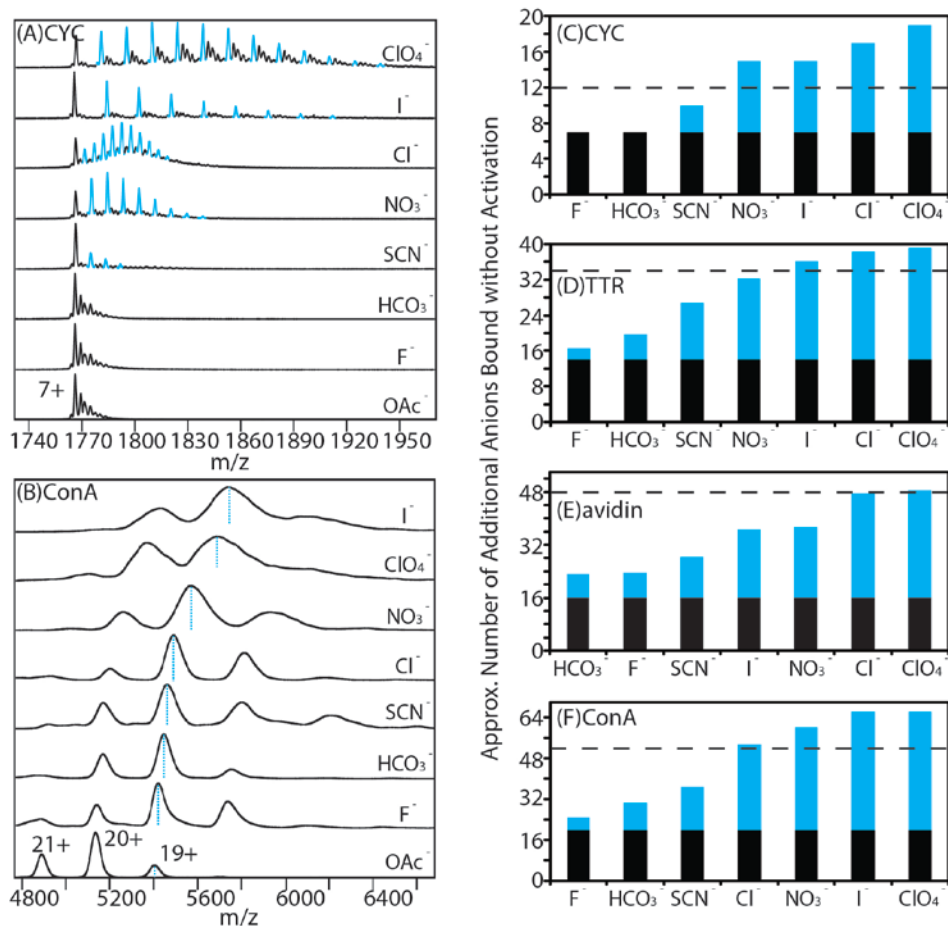


Figure 4-2. Correlations between our gas-phase data and protein-salt interactions in solution. (A) nESI-MS data of the 7⁺ charge state of CYC (10 μ M) generated from solutions containing 100 mM ammonium acetate (control) and a series of solutions containing both 100 mM ammonium acetate and 1 mM salts (ammonium-based salts with different anions) reveal a distribution of adducts (indicated as blue peaks) resolved by MS without collisional activation. Peaks corresponding to adducted ions arising from sodium, potassium, and sodium + potassium-binding are shown in black, and observed to dominate in our control (acetate), fluoride, and bicarbonate datasets. (B) nESI-MS data for tetrameric ConA (10 μ M) obtained from a solution containing 100 mM ammonium acetate (control) and a series of solutions containing both 100 mM ammonium acetate and 5 mM salts (ammonium-based salts with different anions). Each

spectrum was obtained using identical instrumental conditions without collisional activation. The centroid m/z values corresponding to the 19^+ charge state of protein-anion complexes are indicated by blue dashed lines. (C)-(F) Histogram plots showing the approximate number of residual anions bound to protein complex ions (shown as blue columns) stacked on the number of sites occupied by unpaired positive charges (shown as black columns), for CYC, TTR, avidin, and ConA, respectively. The black dashed line represents the number of surface solvent-accessible basic sites, as determined by the DEPTH program⁶⁴.

4.4.3 Tailored anion/cation combinations to enhance the stability of gas-phase proteins and multiprotein complexes

In our previous experiments, we found that the stabilization mechanism accessed by cations and anions are not mutually exclusive, and can therefore be accessed simultaneously to enhance the gas-phase stability of protein structure through tailored salts. Data demonstrate that Ca^{2+} , Mg^{2+} , tartrate²⁻, Cl^- , citrate²⁻, and NO_3^- are strongly stabilizing for protein structure in the gas-phase, and their combination leads to 8 potential salts that may be useful for IM-MS measurements of native-like protein structure. However, if we consider the binding of both free anions and cations in solution a prerequisite for the enhanced stabilization of proteins in the gas phase, then salts containing tartrate and citrate must be excluded from our list, as they can act as strong chelators for suppressing protein-metal interactions during nESI⁶⁵. Consequently, our preliminary list of highly-stabilizing salt additives is reduced to four potential choices: $\text{Ca}(\text{NO}_3)_2$, CaCl_2 , $\text{Mg}(\text{NO}_3)_2$ and MgCl_2 . In this chapter, we use $\text{Ca}(\text{NO}_3)_2$ and MgCl_2 to demonstrate such combined stabilizing effects for gas-phase protein structure.

To ensure that both cations and anions can simultaneously bind to protein complexes and are subsequently carried into the gas-phase, we performed preliminary experiments on CYC monomers doped with $\text{Ca}(\text{NO}_3)_2$, where we are able to use MS to resolve individual protein-bound populations. Data for 7^+ CYC is shown in Figure 4-3A, where monomer ions are

generated from four different buffer compositions (control/100% 100 mM NH₄OAc, 100 mM NH₄OAc with added NH₄NO₃, 100 mM NH₄OAc with added Ca(OAc)₂, 100 mM NH₄OAc with added Ca(NO₃)₂). The resolved adduct populations corresponding to [H-‘NO₃⁻’] type adducts (blue) together with Ca²⁺ adducts (red) can be observed in our CYC monomer dataset following incubation with Ca(NO₃)₂.

Following these proof-of-principle experiments, we extended our data to include 3 tetrameric protein complexes (TTR, avidin and ConA) incubated with Ca(NO₃)₂, and 2 tetrameric protein complexes (avidin and ConA) incubated with MgCl₂. MS data are shown in Figure 4-3B, Figure 4-3C and Figure 4-3D, where tetramer ions are generated from four different buffer compositions. (control/100% 100 mM NH₄OAc, 100 mM NH₄OAc with added NH₄NO₃/NH₄Cl, 100 mM NH₄OAc with added Ca(OAc)₂/Mg(OAc)₂, 100 mM NH₄OAc with added Ca(NO₃)₂/MgCl₂) In the absence of added salts, we observe intact TTR, avidin and ConA tetramers, with base peaks corresponding to the 14⁺, 16⁺ and 20⁺ tetramer charge states respectively (black). The charge states observed for these complexes change slightly upon addition of anions (NO₃⁻ or Cl⁻) and cations (Ca²⁺ or Mg²⁺) producing charge reduction and amplification when compared to control data respectively. We ascribe the observed changes in average charge state to the relative bound populations of H⁺, cations and anions found in each case, all of which can be bound as either charged or neutral species, coupled with the invariant surface areas of the proteins studied. Additionally, the peak widths observed for mass spectra acquired from anions or cations-containing solutions display significant broadening when compared with spectra obtained from complexes prepared in pure ammonium acetate, despite the use of similar instrument conditions in their acquisition. This peak broadening is attributed to a larger average number of anions or

cations bound to the surface of the gas-phase protein complex ions than ammonia or acetate adducts available in control solutions, owing to their differential volatility^{42,66}. In the presence of $\text{Ca}(\text{NO}_3)_2$ or MgCl_2 (purple), however, we notice a charge state distribution similar to control data, which can be primarily ascribed to the simultaneous binding of both cations and anions to the protein and an averaging of their differential influence on the overall charge state observed. Further evidence of simultaneous cation and anion binding is observed in the increased breadth of the MS peaks recorded from $\text{Ca}(\text{NO}_3)_2/\text{MgCl}_2$ doped solutions, which also exhibit a larger shift in centroid molecular mass when compared with samples containing either anions or cations additives. This agrees well with our observation of resolved populations corresponding to Ca^{2+} and NO_3^- both bound to CYC monomer incubated with $\text{Ca}(\text{NO}_3)_2$ (Figure 4-3A).

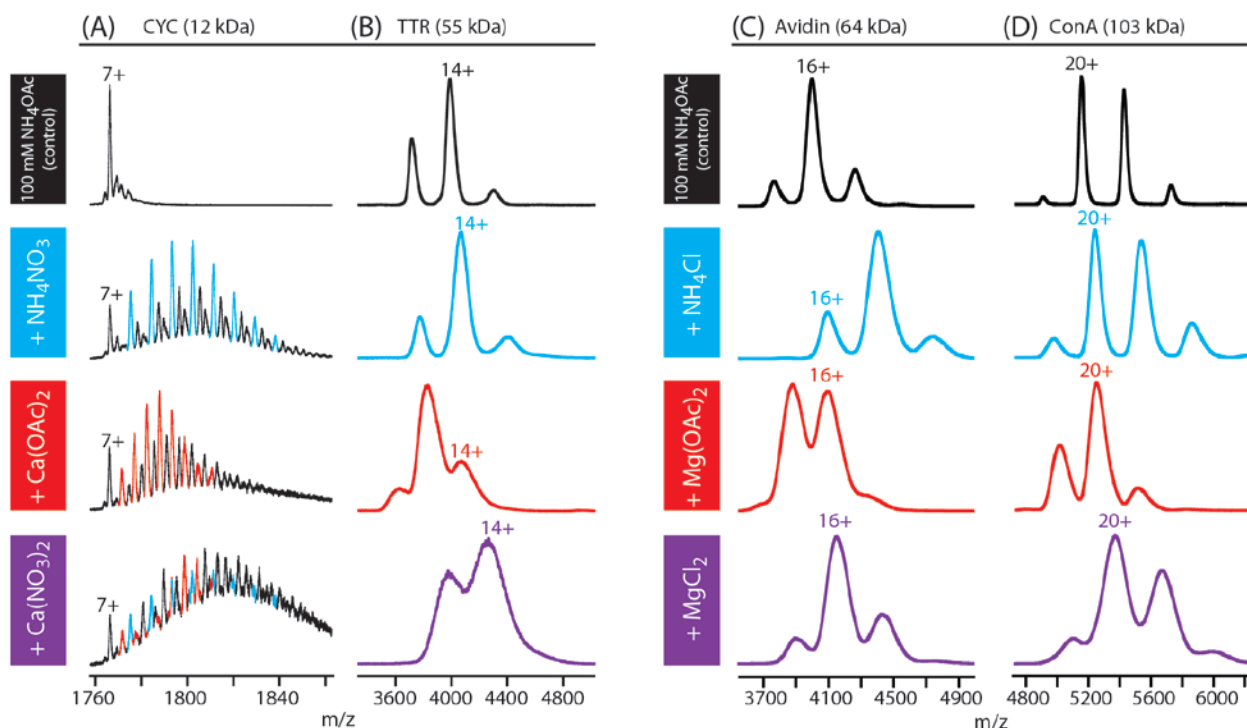


Figure 4-3. nESI mass spectra of the four protein complexes obtained from different solution conditions. (A) nESI-MS data of the 7^+ charge state for CYC obtained from ammonium acetate-based solutions containing $10 \mu\text{M}$ CYC and no added salt (control), $400 \mu\text{M}$ ammonium nitrate, $200 \mu\text{M}$ calcium acetate, or $200 \mu\text{M}$ calcium nitrate. The resolved populations of cation and anion additives are denoted by red and blue colors, respectively. The other peaks (black) except

for the apo-CYC correspond to adducts arising from sodium or potassium-binding. (B) nESI-MS data for TTR (5 μ M) generated from ammonium acetate-based solutions with no added salt (control, black), 4 mM ammonium nitrate (blue), 2 mM calcium acetate (red), or 2 mM calcium nitrate (purple). (C) and (D) nESI MS data for the avidin and ConA tetramer ions, (both 5 μ M) generated from ammonium acetate-based solutions with no added salt (control, black), 4 mM ammonium chloride (blue), 2 mM magnesium acetate (red), or 2 mM magnesium chloride (purple). Spectra for each protein complex were obtained using similar IM-MS instrumental conditions.

In order to investigate the stabilizing effects of the complexes created above, we performed CIU and CID stability measurements on monomer (CYC) and tetramer ions (TTR, avidin and ConA) created from solutions containing added $\text{Ca}(\text{NO}_3)_2$ or MgCl_2 . Figure 4-4 show histogram plots of the normalized collision energy (eV^*) at which I_{tet} and I_f for these ions decrease to 50% of their original values as a function of buffer composition. Generally, we observe that cations are stronger stabilizers than anions of gas-phase protein structure, especially when CID data are considered. This agrees well with our previous observations, which indicated that cations preferentially act to stabilize gas-phase proteins by remaining bound to the assembly at relatively high internal temperatures⁴⁶, whereas stabilizing anions mainly bind and then dissociate from protein ions to access a ‘dissociative cooling’ mechanism⁴⁵ which can, on its own, produce significant increases in protein ion stability. Most importantly, it is clear from our data that the simultaneous presence of both stabilizing cations and anions causes a significant increase in protein complex stability relative to the addition of either component in isolation, resulting in 7-8% and 10-13% average increases in gas-phase protein quaternary and tertiary structure stabilities respectively.

As a further set of control experiments, we also measured solutions where MgCl_2 additives were replaced with tetramethylammonium bicarbonate (TMAHCO_3) in equal concentrations and measured under identical instrument conditions. While our previous data identify the

components of MgCl_2 as strongly stabilizing, the same dataset indicated that the components of TMAHCO_3 provided gas-phase protein ions with no measurable increase in their structural stability when added separately to solutions prior to nESI⁴⁵⁻⁴⁷. Shown in Figure 4-4 C and Figure 4-4 D protein ions created from TMAHCO_3 doped solutions exhibit no significant increases in stability, resulting in dissociation and unfolding threshold values similar to control data acquired from ions generated from pure ammonium acetate. Though anticipated, this result is significant, as it indicates the differential stability we observe is predicated by the chemical character of the salts added rather than the increased degrees of freedom gained through potential TMAHCO_3 adduction.

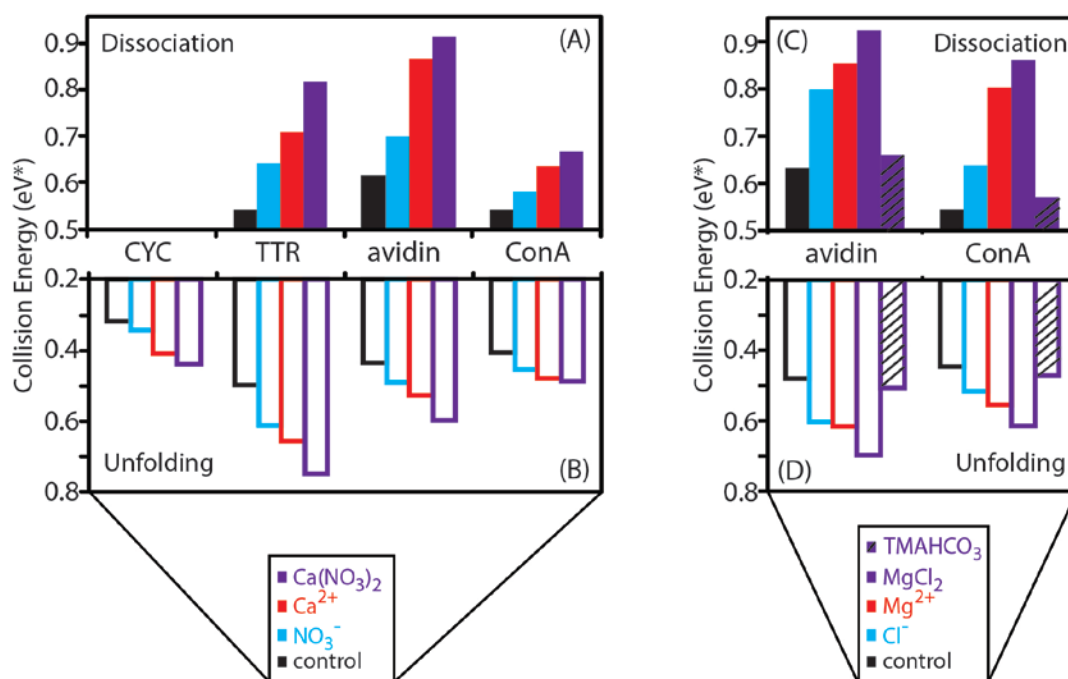


Figure 4-4. Elucidating the extent of unfolding and dissociation of the four protein complexes as a function of buffer composition from IM-MS. (A) and (B) show histogram plots of collision energy (eV*) required to dissociate or unfold 50% of the population of monomeric CYC, tetrameric avidin, ConA, and TTR generated from ammonium acetate-based solutions containing proteins and no added salt (control, black), ammonium nitrate (blue), calcium acetate (red) and calcium nitrate (purple). (C) and (D) show histogram plots of the collision energy (eV*) required for the 50% dissociation and unfolding of intact avidin and ConA generated from ammonium acetate-based solutions containing proteins and no added salt (control, black), ammonium chloride (blue), magnesium acetate (red), magnesium chloride (purple), and tetramethylammonium (TMA) bicarbonate (purple shaded). Collision Energy (eV*) is a

normalized version of ion kinetic energy, that takes into account both the charge on the ion and reduced mass of the ion-neutral collision complex.

4.4.4 The influence of tuned salt additives on protein tetramer dissociation in the gas phase

To obtain a more complete mechanistic picture of MgCl_2 protein ion stabilization in the gas phase, we also measured CID data for ConA tetramer ions generated from the four buffer compositions mentioned above. Figure 4-5B shows tandem mass spectra for 20^+ ConA tetramer ions at high collision energies (170 V acceleration). ConA tetramer ions generated from pure ammonium acetate buffer (black, control) follow the conventional asymmetric charge partitioning dissociation pathway, generating fragment ions that correspond to highly charged monomers (open square, 25.62 kDa) and lower-charge state trimers (not shown)⁶⁷. Additionally, three peptide fragments are also observed in the product ion spectrum for the ConA tetramer which have similar appearance energies to monomer ejection. These ions have intact masses of 12.94 kDa (open triangle), 12.68 kDa (low signal intensity, not marked), and 8.90 kDa (open circle), and likely correspond to the c-terminal half (residues 164-281), n-terminal half (residues 30-148), and a secondary n-terminal fragment (tentatively identified as the b_{82} ion in reference to the sequence order of the fragment, rather than the intact ConA monomer) resulting from decay of the 12.68 kDa fragment ion respectively (PDB ID: 2CNA).

ConA CID datasets also reveal a number of illuminating differences between cation and anion stabilized protein ions. For example, we observe that Mg^{2+} ions remain bound to the ConA tetramer in large numbers following extensive activation in the gas phase. This observation is reflected in the mass difference recorded between the ConA tetramer generated from Mg^{2+} doped solutions (red) and those created from control solutions (black, Figure 4-5C). We also observe a

series of resolved Mg^{2+} adducts bound to the 7^+ ions of the 12.94 kDa, C-terminal peptide fragment produced from Mg^{2+} -bound ConA tetramer (Figure 4-5A, red). Conversely, MS data for Cl^- exposed tetramer indicate that chloride adducts are completely dissociated from the protein complex prior to product ion formation (Figure 4-5A/Figure 4-5C, blue). In these experiments, as observed previously, Cl^- acts to stabilize the protein complex through a “dissociative cooling” mechanism, where chloride adducts dissociate from the tetramer upon collisional activation as neutrals to carry energy away from the activated protein ions⁴⁵.

In addition to altering the structural stability of intact protein complexes, our IM-MS measurements indicate that cation addition can alter the CID pathway accessed during protein complex dissociation. For instance, the absolute number of charges transferred to the leaving monomeric protein subunits decreases slightly when ConA is incubated with added Mg^{2+} when compared to Cl^- adducted or control samples (Figure 4-5B, red). Specifically, the charge state of the most abundant monomer (open square) ions observed from Mg^{2+} bound proteins is decreased from 12^+ to 11^+ when compared to control, in combination with significantly increased signal intensity for the 7^+ - 9^+ monomer charge states. This charge state shift is also observed in the CID of the Mg -bound avidin tetramer (data not shown). Additionally, we observe a decrease in signal intensity of 50% for the peptide fragments that typically result from low-energy ConA CID (open triangle and circle) compared with control datasets.

The observations above correlate well with our previous assertions regarding cation-mediated gas-phase protein ion stabilization. Our previous results have narrowed the available mechanisms of this process to two possibilities⁴⁶. The first requires bound cations to form strong multidentate

interactions within gas-phase proteins, thus enabling the tethering of different regions of the protein structure together and increasing structural stability. The second relies upon the decreased mobility of added cations within multiply-charged protein ions when compared with protons, which may work to restrict charge mobility and inhibit the Coulombic unfolding of subunits within the complex, thus limiting the asymmetric dissociation of noncovalent protein complexes. In contrast to the cation-bound protein ions measured here, the dissociation profiles measured for anion-bound protein complex ions are unchanged relative to control (Figure 4-5B, blue), indicative of the complete dissociation of anion-based adducts in the early stages of collisional activation. As such, it is not surprising that our CID data for proteins incubated with MgCl_2 mimics the dissociation behavior of those same samples having added Mg^{2+} rather than those doped with excess Cl^- , as the former will remain bound to influence CID while the latter will not.

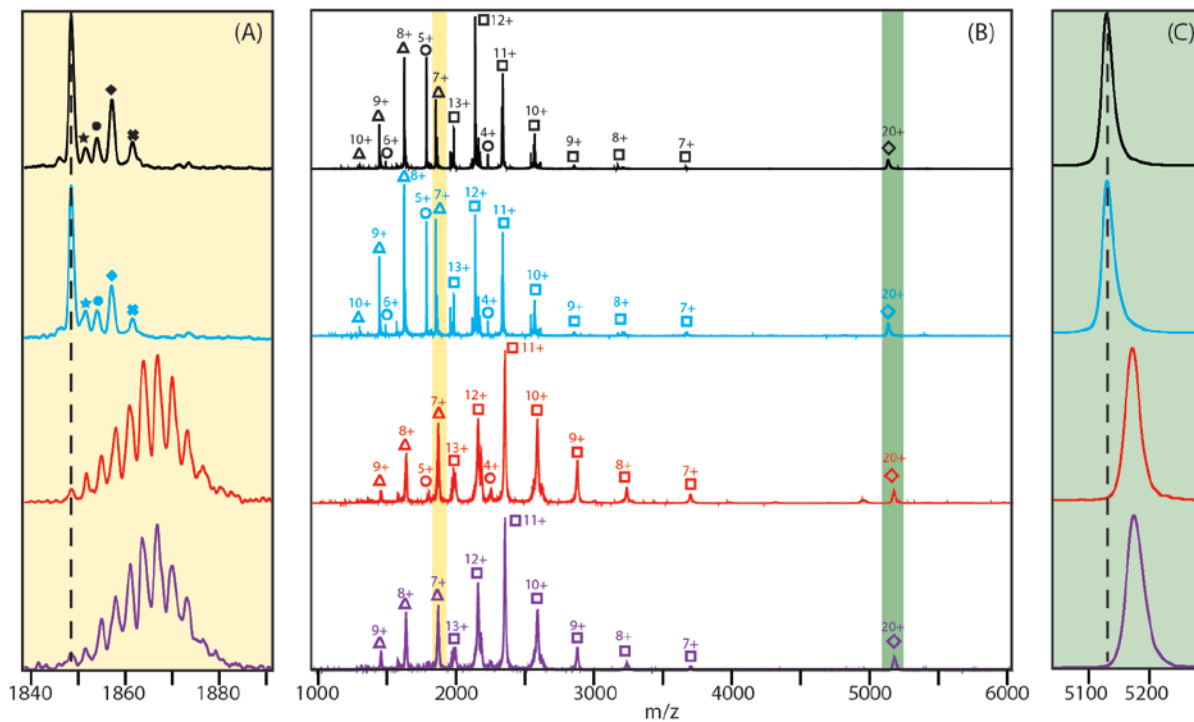


Figure 4-5. Elucidating the influence of tuned salt additives on protein tetramer dissociation in the gas phase. CID of ConA tetramer obtained from ammonium acetate-based solutions containing 10 μM ConA and no added salt (control, black), 4 mM ammonium chloride (blue), 2

mM magnesium acetate (red), 2 mM magnesium chloride (purple). Tandem mass spectra of the 20^+ charge state of ConA tetramer created from the above four buffer solutions acquired at the highest trap collision voltages where ion transmission is observed (B), where tetramer precursor ions, dissociated monomer product ions, two peptide fragment ions (12.94 kDa and 8.90 kDa) are denoted by open diamond, square, triangle, and circle, respectively. The yellow box highlights the region of the mass spectrum containing the 7^+ charge state of the 12.94 kDa peptide fragment product, and this region is shown in detail in (A). Detailed analysis reveals a distribution of Mg^{2+} adducts resolved by MS when $Mg(OAc)_2$ or $MgCl_2$ are added to the sample solutions while there are no Cl^- adducts observed adhered to the product ions when NH_4Cl is added (A). Peaks corresponding to adducts arising from sodium, potassium, sodium + potassium and sodium + potassium + potassium- binding are marked with filled stars, circles, diamonds, and crosses, respectively. The green box indicates the remaining ion signal for the 20^+ tetramer precursor ion population (C). A mass difference of ≈ 840 Da is recorded relative to control (intact mass = 102.6 kDa, in good agreement with sequence mass), indicating the tight binding of cations at high trap CE (170 V) when the ConA tetramer is incubated with Mg^{2+} . A black dashed line marks the m/z of highest abundance ($m/z = 5130$).

4.4.5 CIU unfolding ‘fingerprints’ reveal mechanistic insights in cation-bound protein stabilization

To further validate the joint stabilization provided by combined cations and anions, and provide insight into the stabilization mechanism at work, we constructed CIU unfolding 'fingerprints' for protein complex ions derived from solutions containing added $Ca(NO_3)_2/MgCl_2$ as well as control samples containing its constituent anion and cation components. Changes in the protein ion tertiary/secondary structures are induced during the CIU process, leading to several structural ensembles that are stable on the millisecond timescale and can be resolved in both IM drift time and collision energy. For clarity, CIU fingerprint data is projected as a contour plot (Figure 4-6) where intensities for the features observed are denoted by a color-based axis. Careful analysis of CIU fingerprint data allows the nature of protein stabilization to be identified by noting the conformational features that are stabilized (elongated on the collision energy axis) relative to control data^{44,45,68,69}.

Figure 4-6A shows CIU unfolding ‘fingerprints’ for TTR 14^+ ions derived from $\text{Ca}(\text{NO}_3)_2$ containing solutions, as well as control samples containing the constituent anion and cation components. Control fingerprints for the TTR tetramer (black Y-axis) reveal three major conformational families (I, II, III) observed under the conditions used for our experiments here. These features are easily resolved in drift time and have distinct patterns as a function of collision voltage. Fingerprint data acquired for TTR with added NO_3^- (blue Y-axis) shows that the most compact conformer (I) is observed at substantially higher collision voltages when compared to those ions generated from pure ammonium acetate solutions, indicating that the stabilization observed in our experiments is due primarily to the enhanced stability of this compact conformer. In contrast, TTR incubated with added Ca^{2+} (red Y-axis) displays a substantially different CIU fingerprint, with both the most compact and partially unfolded forms of the complex being stabilized. As discussed above, the differences in the fingerprints recorded for Ca^{2+} -bound and NO_3^- -bound TTR are indicative of the separate stabilization mechanisms operative for these two adduct populations. Specifically, Ca^{2+} stabilizes the complex through tight binding, such that intermediately unfolded conformers of the protein are partially stabilized. In contrast, NO_3^- stabilizes the complex through dissociative cooling, and therefore cannot, by definition, stabilize partially unfolded protein conformers. Additionally, a new intermediate unfolded species (II’) emerges in the Ca^{2+} fingerprint. This observation is also consistent with our mechanism, in which strongly-bound cations modulate the collisional unfolding process through tethering flexible regions within proteins or by limiting charge migration by replacing highly mobile proton charge carriers. Critically, fingerprint data collected from ions incubated with $\text{Ca}(\text{NO}_3)_2$ (purple Y-axis) displays elements from both the fingerprints of its constituent components, exhibiting a highly stabilized compact (I) state, a stabilized II state, and the

appearance of a II' state. Thus, our CIU fingerprint data supports the joint stabilization of protein complexes through simultaneous binding of both Ca^{2+} and NO_3^- adducts, resulting in enhanced protein stability when compared to their individual effects.

Furthermore, CIU unfolding fingerprints reveal mechanistic insights in cation-bound protein stabilization. A control fingerprint for the avidin tetramer (black Y-axis) is shown Figure 4-6B. At low trap collision voltages, the 16^+ charge state of the avidin tetramer has a drift time of ~ 10 ms, which persists to a Trap CE of 52 V and is the most compact conformer for this protein observed in our experiments. At higher collision voltage (>55 V) more elongated conformations are observed that have drift times >12 ms. Three distinct conformations in addition to the most compact protein configuration are identified under our conditions. The unfolding landscape observed in our fingerprints varies substantially as a function of the buffer compositions used to prepare samples for nESI. For example, fingerprint data acquired for avidin with added Cl^- (blue Y-axis) shows that the most compact conformer (I) is observed at substantially larger collision voltages (>65 V) when compared to those ions generated from pure ammonium acetate solutions, indicating that the increased stability observed in our experiments for the protein ions afforded by anions is due primarily to the enhanced stability of this compact conformer. In contrast, avidin incubated with added Mg^{2+} (red Y-axis) displays a different CIU fingerprint. Despite the similar degree to which the most compact conformer (I) is stabilized, we observe a partially unfolded conformer (II) that has a shorter drift time (~ 11.5 ms) and persists at higher energies (Figure 4-6B, red Y-axis). This surprising observation is attributed to the development of a new partially unfolded structure that is unique to avidin samples incubated with Mg^{2+} , and thus provides evidence supporting our cation-mediated stabilization model involving the tethering of

flexible regions within protein ions through strong multi-dentate interactions. This observation holds for ConA as well, where Mg-bound protein ions exhibit a more-gradual transition between conformer II→III without developing any discrete, resolved conformational populations (Figure 4-6C, red Y-axis). Finally, we observe conformation IV over a significantly broadened energy range when Mg(OAC)₂ is added to solutions prior to nESI. This result, as observed throughout our IM-MS dataset, stands in contrast to ions incubated in the presence of excess Cl⁻ or pure ammonium acetate buffers, where discrete and well-resolved conformational families are observed by IM. In fact, the presence of excess Cl⁻ in nESI samples has no observable effect on the drift time axis of the CIU fingerprints recorded, only the breadth of energies over which each structure is observed is affected. It is likely that such complex transitions, as observed between conformer families II and III, and the broadened energy distributions observed for highly-unfolded conformational families, as detected in conformer family IV, constitute further evidence of cation-based tethering interactions within protein monomers. Critically, fingerprint data collected from avidin and ConA tetramer ions incubated with MgCl₂ displays elements from both the fingerprints of its constituent components (Figure 4-6B/Figure 4-6C, purple Y-axis). Specifically, MgCl₂-containing samples display a highly stabilized compact state (I) resulting primarily from the dissociation of Cl⁻ adducts at lower collision voltage, as well as the multi-state transitions and broadened energy profile of highly unfolded species detected for Mg²⁺ bound protein ions. Thus, our CIU fingerprint data supports the observation that proteins and complexes incubated with MgCl₂ derive their increased stability through the simultaneous binding of both Mg²⁺ and Cl⁻ adducts, and that both dissociative cooling and tethering-type stabilization mechanisms are accessed by the resultant assemblies.

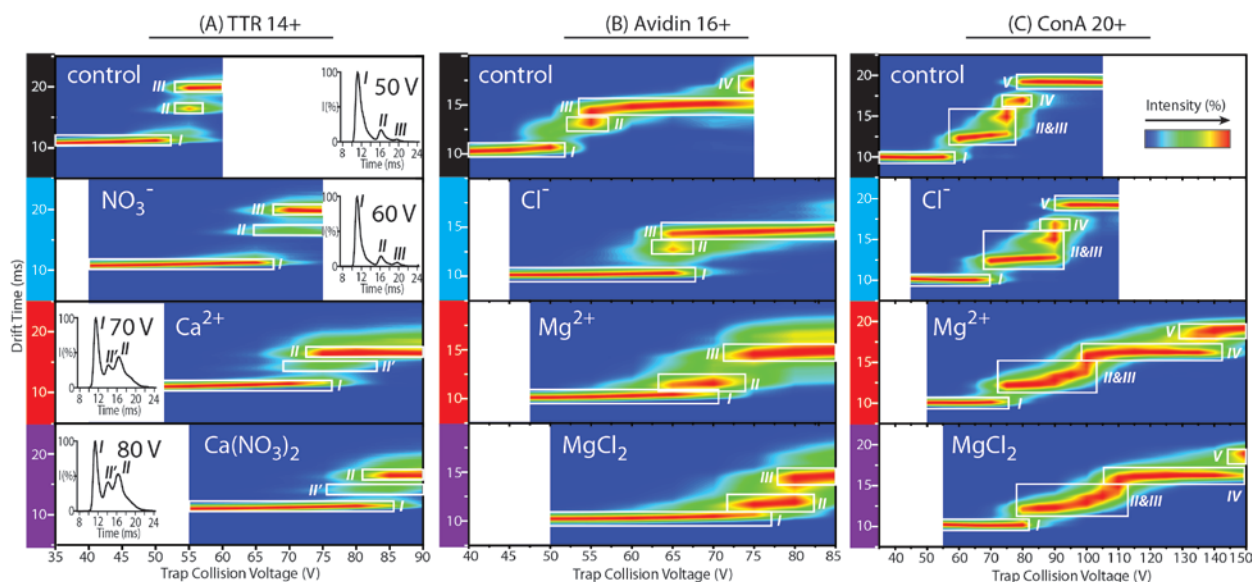


Figure 4-6. CIU fingerprint contour plots reveal combined salt effect and additional mechanistic details in cation-mediated stabilization. They are shown for 14^+ charge state of TTR tetramer (A), 16^+ of avidin tetramer (B) and 20^+ of ConA tetramer (C) generated from ammonium acetate-based solutions with no added salt (control, black Y-axis), 4 mM ammonium nitrate/chloride (blue Y-axis), 2 mM calcium/magnesium acetate (red Y-axis), or 2 mM calcium nitrate/magnesium chloride (purple Y-axis), where ion trap collision voltage is charted against IM drift time, and the ion intensities are denoted by a color-coded axis. The conformational forms for the tetramer are highlighted (white box) and labeled (I, II, II' III, IV, V)

4.5 Conclusions

The correlation between solution and gas-phase protein structure has, in part, driven the development and application of IM-MS in structural biology. For example, MS measurements have been used to study bioactive peptide aggregation⁷⁰, membrane protein structure^{71,72}, and protein stability changes upon ligand binding^{68,73}. The application of IM and MS to protein quaternary structure has rapidly developed in recent years, enabling the determination of multiprotein stoichiometry, dynamics, and 3D topology^{13,74}. However, several reports have highlighted the uncontrolled distortion of protein structure in the absence of solvent, including both the general compaction of protein size and structural rearrangements that may occur upon desolvation and transfer to the gas phase. In order to facilitate the use of gas-phase measurements

in the construction of native-state protein models, we herein investigated the stabilizing effect of $\text{Ca}(\text{NO}_3)_2$ and MgCl_2 , as these salts bear anion and cation components previously identified in isolation for their stabilizing effects. Our CIU and CID data clearly indicate that the simultaneous presence of both stabilizing cations and anions causes a significant increase in gas-phase protein quaternary and tertiary structural stability relative to their individual effects. On average, $\text{Ca}(\text{NO}_3)_2/\text{MgCl}_2$ doped samples produce gas-phase protein ions that are ~50% more stable than those produced from pure ammonium acetate buffered solutions, and ~10% more stable than those samples with cations added alone. Furthermore, our data reveal additional details in the mechanism associated with stabilizing gas-phase protein ions through cation adduction. Specifically, through our ‘CIU fingerprint’ data we are able to detect evidence of frustrated protein unfolding transitions and highly-stabilized unfolded structures for Mg-bound protein ions, and both effects are likely due to multi-dentate cation-protein interactions. Samples containing added MgCl_2 are able to access the above mode of stabilization, along with the dissociative cooling-type stabilization associated with chloride anion adduction simultaneously, to create protein complex ions having superior structural stability. In future experiments, we plan to use the mechanistic insights presented in this report to further refine stabilizing additives for the nESI-IM-MS analysis of proteins and protein complex, thus enabling the evaluation of labile protein structures not readily amenable to gas-phase studies.

Furthermore, it is likely that the number of bound anions and cations observed by MS in our data bear a strong correlation to the bound populations present in solution. As such, the dramatically different rank orders observed in gas-phase experiments when compared with solution can be taken as evidence for the critical importance of solvation effects in the mechanism of Hofmeister stabilization in solution. Finally, in addition to providing enhanced stabilizing additives for the

gas-phase measurement of native-like protein structures, it is clear that continuing measurements of protein-counterion complexes will provide a useful tool for quantifying bound cation and anion populations in support of solution-phase measurements.

4.6 References

- (1) Sali, A.; Glaeser, R.; Earnest, T.; Baumeister, W. *Nature* **2003**, *422*, 216.
- (2) Robinson, C. V.; Sali, A.; Baumeister, W. *Nature* **2007**, *450*, 973.
- (3) von Heijne, G. *Nature Reviews Molecular Cell Biology* **2006**, *7*, 909.
- (4) Pierce, K. L.; Premont, R. T.; Lefkowitz, R. J. *Nature Reviews Molecular Cell Biology* **2002**, *3*, 639.
- (5) Steven, A. C.; Baumeister, W. *Journal of Structural Biology* **2008**, *163*, 186.
- (6) Ruotolo, B. T.; Giles, K.; Campuzano, I.; Sandercock, A. M.; Bateman, R. H.; Robinson, C. V. *Science* **2005**, *310*, 1658.
- (7) Ruotolo, B. T.; Robinson, C. V. *Curr Opin Chem Biol* **2006**, *10*, 402.
- (8) Wyttenbach, T.; Bowers, M. T. In *Annual Review of Physical Chemistry* 2007; Vol. 58, p 511.
- (9) Benesch, J. L. P.; Ruotolo, B. T.; Simmons, D. A.; Robinson, C. V. *Chem. Rev.* **2007**, *107*, 3544.
- (10) Scarff, C. A.; Thalassinos, K.; Hilton, G. R.; Scrivens, J. H. *Rapid Communications in Mass Spectrometry* **2008**, *22*, 3297.
- (11) Heck, A. J. R. *Nat. Methods* **2008**, *5*, 927.
- (12) Jurneczko, E.; Barran, P. E. *Analyst* **2011**, *136*, 20.
- (13) Benesch, J. L. P.; Ruotolo, B. T. *Curr. Opin. Struct. Biol.* **2011**, *21*, 641.
- (14) Hyung, S. J.; Ruotolo, B. T. *Proteomics* **2012**, *In press*.
- (15) Zhong, Y.; Hyung, S.-J.; Ruotolo, B. T. *Expert Rev. Proteomics* **2012**, *9*, 47.
- (16) Aquilina, J. A.; Benesch, J. L. P.; Bateman, O. A.; Slingsby, C.; Robinson, C. V. *Proceedings of the National Academy of Sciences of the United States of America* **2003**, *100*, 10611.
- (17) Heck, A. J. R.; van den Heuvel, R. H. H. *Mass Spectrometry Reviews* **2004**, *23*, 368.
- (18) Hernandez, H.; Dziembowski, A.; Taverner, T.; Seraphin, B.; Robinson, C. V. *Embo Reports* **2006**, *7*, 605.
- (19) Sharon, M.; Robinson, C. V. In *Annual Review of Biochemistry* 2007; Vol. 76, p 167.
- (20) Zhou, M.; Sandercock, A. M.; Fraser, C. S.; Ridlova, G.; Stephens, E.; Schenauer, M. R.; Yokoi-Fong, T.; Barsky, D.; Leary, J. A.; Hershey, J. W.; Doudna, J. A.; Robinson, C. V. *Proceedings of the National Academy of Sciences of the United States of America* **2008**, *105*, 18139.
- (21) Hernandez, H.; Makarova, O. V.; Makarov, E. M.; Morgner, N.; Muto, Y.; Krummel, D. P.; Robinson, C. V. *Plos One* **2009**, *4*.
- (22) Clemmer, D. E.; Jarrold, M. F. *J. Mass Spectrom.* **1997**, *32*, 577.

- (23) Kaddis, C. S.; Lomeli, S. H.; Yin, S.; Berhane, B.; Apostol, M. I.; Kickhoefer, V. A.; Rome, L. H.; Loo, J. A. *Journal of the American Society for Mass Spectrometry* **2007**, *18*, 1206.
- (24) Bohrer, B. C.; Merenbloom, S. I.; Koeniger, S. L.; Hilderbrand, A. E.; Clemmer, D. E. *Annu. Rev. Anal. Chem.* **2008**, *1*, 293.
- (25) Scarff, C. A.; Patel, V. J.; Thalassinou, K.; Scrivens, J. H. *Journal of the American Society for Mass Spectrometry* **2009**, *20*, 625.
- (26) Ekeowa, U. I.; Freeke, J.; Miranda, E.; Gooptu, B.; Bush, M. F.; Perez, J.; Teckman, J.; Robinson, C. V.; Lomas, D. A. *Proceedings of the National Academy of Sciences of the United States of America* **2010**, *107*, 17146.
- (27) Uetrecht, C.; Rose, R. J.; van Duijn, E.; Lorenzen, K.; Heck, A. J. R. *Chemical Society Reviews* **2010**, *39*, 1633.
- (28) Knapman, T. W.; Morton, V. L.; Stonehouse, N. J.; Stockley, P. G.; Ashcroft, A. E. *Rapid Communications in Mass Spectrometry* **2010**, *24*, 3033.
- (29) Smith, D. P.; Radford, S. E.; Ashcroft, A. E. *Proceedings of the National Academy of Sciences of the United States of America* **2010**, *107*, 6794.
- (30) Cole, H. L.; Kalapothakis, J. M. D.; Bennett, G.; Barran, P. E.; MacPhee, C. E. *Angewandte Chemie-International Edition* **2010**, *49*, 9448.
- (31) Giles, K.; Pringle, S. D.; Worthington, K. R.; Little, D.; Wildgoose, J. L.; Bateman, R. H. *Rapid Communications in Mass Spectrometry* **2004**, *18*, 2401.
- (32) Zhong, Y. Y.; Hyung, S. J.; Ruotolo, B. T. *Analyst* **2011**, *136*, 3534.
- (33) Giles, K.; Williams, J. P.; Campuzano, I. *Rapid Communications in Mass Spectrometry* **2011**, *25*, 1559.
- (34) Pukala, T. L.; Ruotolo, B. T.; Zhou, M.; Politis, A.; Stefanescu, R.; Leary, J. A.; Robinson, C. V. *Structure* **2009**, *17*, 1235.
- (35) Politis, A.; Park, A. Y.; Hyung, S. J.; Barsky, D.; Ruotolo, B. T.; Robinson, C. V. *Plos One* **2010**, *5*.
- (36) Hogan, C. J.; Ruotolo, B. T.; Robinson, C. V.; de la Mora, J. F. *J. Phys. Chem. B* **2011**, *115*, 3614.
- (37) Badman, E. R.; Myung, S.; Clemmer, D. E. *Journal of the American Society for Mass Spectrometry* **2005**, *16*, 1493.
- (38) Breuker, K.; McLafferty, F. W. *Proceedings of the National Academy of Sciences of the United States of America* **2008**, *105*, 18145.
- (39) Benesch, J. L. P. *Journal of the American Society for Mass Spectrometry* **2009**, *20*, 341.
- (40) Sun, J. X.; Kitova, E. N.; Klassen, J. S. *Analytical Chemistry* **2007**, *79*, 416.
- (41) Bagal, D.; Kitova, E. N.; Liu, L.; El-Hawiet, A.; Schnier, P. D.; Klassen, J. S. *Analytical Chemistry* **2009**, *81*, 7801.
- (42) Freeke, J.; Robinson, C. V.; Ruotolo, B. T. *Int. J. Mass Spectrom.* **2010**, *298*, 91.
- (43) Merenbloom, S. I.; Flick, T. G.; Daly, M. P.; Williams, E. R. *Journal of the American Society for Mass Spectrometry* **2011**, *1*.
- (44) Freeke, J.; Bush, M. F.; Robinson, C. V.; Ruotolo, B. T. *Chemical Physics Letters* **2012**, *524*, 1.
- (45) Han, L. J.; Hyung, S. J.; Mayers, J. J. S.; Ruotolo, B. T. *Journal of the American Chemical Society* **2011**, *133*, 11358.
- (46) Han, L.; Hyung, S. J.; Ruotolo, B. T. *Angew Chem Int Ed Engl* **2012**.

- (47) Han, L.; Hyung, S. J.; Ruotolo, B. T. *Faraday Discussions* **2013**.
- (48) Annesley, T. M. *Clinical Chemistry* **2003**, *49*, 1041.
- (49) Hernandez, H.; Robinson, C. V. *Nat Protoc* **2007**, *2*, 715.
- (50) Ruotolo, B. T.; Benesch, J. L. P.; Sandercock, A. M.; Hyung, S. J.; Robinson, C. V. *Nat Protoc* **2008**, *3*, 1139.
- (51) Bush, M. F.; Hall, Z.; Giles, K.; Hoyes, J.; Robinson, C. V.; Ruotolo, B. T. *Anal. Chem.* **2010**, *82*, 9557.
- (52) Zhang, Y. J.; Cremer, P. S. In *Annual Review of Physical Chemistry, Vol 61*; Leone, S. R., Cremer, P. S., Groves, J. T., Johnson, M. A., Richmond, G., Eds.; Annual Reviews: Palo Alto, 2010; Vol. 61, p 63.
- (53) Zhang, Y.; Furyk, S.; Sagle, L. B.; Cho, Y.; Bergbreiter, D. E.; Cremer, P. S. *Journal of Physical Chemistry C* **2007**, *111*, 8916.
- (54) Zhang, Y. J.; Furyk, S.; Bergbreiter, D. E.; Cremer, P. S. *Journal of the American Chemical Society* **2005**, *127*, 14505.
- (55) Flick, T. G.; Merenbloom, S. I.; Williams, E. R. *Analytical Chemistry* **2011**, *83*, 2210.
- (56) Loo, J. A. *Int. J. Mass Spectrom.* **2000**, *200*, 175.
- (57) Liu, L.; Bagal, D.; Kitova, E. N.; Schnier, P. D.; Klassen, J. S. *Journal of the American Chemical Society* **2009**, *131*, 15980.
- (58) Deng, L.; Sun, N.; Kitova, E. N.; Klassen, J. S. *Analytical Chemistry* **2010**, *82*, 2170.
- (59) Kitova, E. N.; Soya, N.; Klassen, J. S. *Analytical Chemistry* **2011**, *83*, 5160.
- (60) Zhang, Y. J.; Cremer, P. S. *Proceedings of the National Academy of Sciences of the United States of America* **2009**, *106*, 15249.
- (61) Bostroem, M.; Parsons, D. F.; Salis, A.; Ninham, B. W.; Monduzzi, M. *Langmuir* **2011**, *27*, 9504.
- (62) Bostrom, M.; Tavares, F. W.; Finet, S.; Skouri-Panet, F.; Tardieu, A.; Ninham, B. W. *Biophysical Chemistry* **2005**, *117*, 217.
- (63) Marcus, Y. *Ion properties*; Wiley Online Library, 1997.
- (64) Tan, K. P.; Varadarajan, R.; Madhusudhan, M. S. *Nucleic Acids Research* **2011**, *39*, W242.
- (65) Pan, J. X.; Xu, K.; Yang, X. D.; Choy, W. Y.; Konermann, L. *Analytical Chemistry* **2009**, *81*, 5008.
- (66) McKay, A. R.; Ruotolo, B. T.; Ilag, L. L.; Robinson, C. V. *Journal of the American Chemical Society* **2006**, *128*, 11433.
- (67) Jurchen, J. C.; Williams, E. R. *Journal of the American Chemical Society* **2003**, *125*, 2817.
- (68) Hyung, S. J.; Robinson, C. V.; Ruotolo, B. T. *Chemistry & Biology* **2009**, *16*, 382.
- (69) Pagel, K.; Hyung, S. J.; Ruotolo, B. T.; Robinson, C. V. *Analytical Chemistry* **2010**, *82*, 5363.
- (70) Carulla, N.; Zhou, M.; Giralt, E.; Robinson, C. V.; Dobson, C. M. *Accounts of Chemical Research* **2010**, *43*, 1072.
- (71) Barrera, N. P.; Isaacson, S. C.; Zhou, M.; Bavro, V. N.; Welch, A.; Schaedler, T. A.; Seeger, M. A.; Miguel, R. N.; Korkhov, V. M.; van Veen, H. W.; Venter, H.; Walmsley, A. R.; Tate, C. G.; Robinson, C. V. *Nature Methods* **2009**, *6*, 585.

- (72) Zhou, M.; Morgner, N.; Barrera, N. P.; Politis, A.; Isaacson, S. C.; Matak-Vinković, D.; Murata, T.; Bernal, R. A.; Stock, D.; Robinson, C. V. *Science* **2011**, *334*, 380.
- (73) Hopper, J. T. S.; Oldham, N. J. *Journal of the American Society for Mass Spectrometry* **2009**, *20*, 1851.
- (74) Zhong, Y. Y.; Hyung, S. J.; Ruotolo, B. T. *Expert Rev. Proteomics* **2012**, *9*, 47.

Chapter 5. Charge Mobility as a Driving Force in the Collision Induced Collapse of Multiprotein Complex Ions

Han L, Arthur E, Brooks CL, Ruotolo BT, Charge Mobility as a Driving Force in the Collision Induced Collapse of Multiprotein Complex Ions, manuscript in preparation.

5.1 Abstract

MS experiments aimed at analyzing the connectivity and structure of intact multiprotein complex ions rely upon the collision induced dissociation of such ions and the analysis of their subsequent production ion populations. Furthermore, IM-MS experiments that attempt to capture solution-phase relevant size measurements from gas-phase protein complex ions depends upon a working knowledge of any remodeling or unfolding that might take place following collisional heating. Detailed mechanistic knowledge of the collisional activation process will likely enable more complete control over product ion populations and higher confidence collision cross-section values from large protein assemblies in the gas phase. One of the most surprising, and least understood, elements of the current dataset surrounding the collisional activation of multiprotein complex ions is the observation that some assemblies undergo compaction upon collisional heating, especially for assemblies bearing large cavities and in a charge-state dependent manner. Here we present new IM-MS measurements for collapse-prone protein complexes doped with

stabilizing cations. Our data indicate that charge mobility on the surface of the protein is a key factor driving the mechanism for gas-phase collapse in protein complexes, and that less mobile charge carriers can induce collapse in protein complexes having higher charge states than those possessed of primarily mobile protons.

5.2 Introduction

MS has emerged as a powerful tool for assessing nearly all levels of protein architecture^{1,2}. In order to detect the intact large protein complexes with minimal disruption, nESI is typically employed in combination with modified MS instrumentation, where the ion transmission and desolvation of larger ions following their generation is optimized³. Partnered with IM separation, MS has advanced its capacity to determine protein conformational dynamics⁴⁻⁶, folding and unfolding intermediates⁷⁻¹⁰, ligand-induced conformational changes¹¹⁻¹³, aggregation intermediates¹⁴⁻¹⁸ and 3D topology¹⁹⁻²¹. In IM-MS experiments aimed at the characterization of protein quaternary structure, detailed MS data of protein connectivity are combined with equally detailed IM measurements of gas-phase protein CCS^{22,23}. Such size information can be used, along with computational procedures, to deduce the 3D structures of large protein complexes¹⁹, and these experiments rely upon the observation that large gas-phase protein ions, in general, retain a strong memory of their solution-phase structures^{24,25}.

Despite the above noted general correlations between solution and gas-phase protein structure, the gas-phase environment has been noted to cause clear aberrations in the structure of protein ions when compared to their expected structures in a solvated environment. The most facile of these is the minor rearrangement of charged side chains on the protein exterior, which fold back

on to the protein surface, forming strong electrostatic interactions due to the lack of solvation forces in the gas phase^{26,27}. More significant reorganizations occur to some assemblies, either undergoing spontaneous compaction during the transfer into the gas phase or collapse in response to collisional activation, both of which are thought to be closely associated with their solution-phase topologies. The former spontaneous compaction has been reported for those proteins with disordered regions or linkers within complexes such as the tumor suppressor protein p53²⁸, histone multimers²⁹ and monoclonal antibodies³⁰, as well as for proteins with high flexibility within subunit-subunit interactions, including the HBV nucleocapsid (hexamer)³¹ and the *E. Coli* DNA sliding clamp loader (trimer)³². Activation-induced collapse, on the other hand, can be observed in SAP (pentamer)³³, CRP (pentamer)³⁴ and TRAP (undecamer)²⁴, all of which adopt ring-like structures with large central cavities. The degree of such compaction during collisional activation has been found to be primarily related with cavity size^{24,33}. However, the CCS reduction observed for gas-phase chaperonin GroEL^{35,36}, a barrel-like complex also with an internal cavity used for mediating protein folding, has been uniquely ascribed to electrospray-related surface tension forces³⁶.

It is also important to note that the compaction observed for SAP, CRP and TRAP is highly charge state dependent^{24,33,34}, where the lowest charge states experience the greatest degree of compaction. Previous observations utilizing charge manipulation have demonstrated the pronounced impact of charge state on the CIU and CID processes of multiprotein complex ions¹. In general, lower-charged ions are more resistant to unfolding and dissociation³⁷. Further, it has been reported that tetrameric TTR ions that possess charge states lower than those normally observed by nESI-MS when using samples prepared under 'native-like' solution conditions can

produce compact and presumably folded product ions when subjected to CID³⁷. In rare cases, charge amplification has also been observed to enhance the folded character of product ions produced by multiprotein CID, as exemplified by SAP³³. Either extensive charge reduction or amplification, followed by high energy CID, can result in the dissociation of covalent bonds within the complex to produce sequence-informative peptide ions from individual subunit termini³⁸. All of these CID pathways stand in stark contrast to the ‘asymmetric charge partitioning’ mechanism most often attributed to the CID of protein complex precursor ions having charge states close to the average values expected for protein complexes produced from native-like buffers, characterized by the migration of protons to single unfolded subunit which is then released as a highly-charged product ion along with a charge-reduced stripped-oligomer appearing at high m/z ratios³⁹. While a detailed relationship between precursor charge state and the CIU/CID process is still emerging, the influence of charge state on the gas-phase compaction previously observed for SAP and TRAP complex ions has led to a basic mechanism, which predicts that Coulombic repulsion of surface charge on a protein complex ion develops potential barriers to the compaction processes observed in high charge ions, and thus favors direct monomer unfolding³³. By reducing the charge, the energy barrier to unfolding is increased and compaction becomes increasingly accessible upon collisional activation.

In this study, we endeavor to investigate the influence of Hofmeister-type cations upon the unfolding/compaction processes in SAP and CRP ions over a range of charge states. Hofmeister-type salts, originally used to study their effects on the stabilities of biomolecules in aqueous solutions⁴⁰, have been extensively examined in the context of protein MS^{10,41-46} for their ability to increase the structural stability of multiprotein complexes in the absence of bulk solvent upon

their addition in solution in small amounts prior to nESI. IM-MS data indicate that anions perform optimally as stabilizers when they bind to the protein and then dissociate from the complex to stabilize the system through ‘dissociative-cooling’⁴², while the best cationic stabilizers are those that remain bound to the protein assembly in large numbers, even following extensive activation in the gas phase. We have previously hypothesized that two modes of action are potentially critical in cationic stabilizers. Cations either form multi-dentate interactions within proteins, enabling the tethering of disparate protein structural regions together, or they act to replace highly mobile protons with less mobile cations with relatively restricted mobility, thus inhibiting the Coulombic unfolding of protein subunits⁴¹. Recent work is in favor of the former tethering effect as a dominant force for cation-based stabilization⁴³⁴⁶. While our data show that cation binding cannot, under our conditions, rescue low charge state ions from compaction, replacing protons with less-mobile cations does enable compaction in higher charge state complexes where unfolding dominated previously. This result clearly illustrates that total charge and mobility both play a key role in partitioning activated protein ions into either compaction or unfolding-dominated pathways.

5.3 Experimental

5.3.1 Materials

SAP, purified from human serum (pentamer, 125 kDa), and recombinant human CRP, purified from *Escherichia coli* (decamer, 117 kDa) were purchased from Calbiochem (San Diego, CA). Standards used to construct CCS calibration curves, including CYC (equine heart), avidin (egg white), ConA (jack bean), ADH (*Saccharomyces cerevisiae*) and GDH (bovine liver)⁴⁷, salts (acetate anion with ammonium, guanidinium, sodium, potassium, lithium, Tris, barium, and

magnesium counterions), and the charge reducing agent, TEA, were all purchased from Sigma (St. Louis, MO). The protein samples were buffer exchanged into 100 mM ammonium acetate at pH 8 (SAP and CRP) and pH 7 (protein calibrants) using Micro Bio-Spin 6 columns (Bio-Rad, Hercules, CA) and prepared to a final concentration of 5 μ M. In order to study the influence of different salts on protein stability without significantly altering buffer capacity or solution pH, the salts were prepared as stock solutions in 100 mM ammonium acetate at a concentration of 20 mM, each of which was then added to the protein solution. Final solutions contained added salt concentrations of 2 mM. The total salt and protein concentrations listed above were chosen primarily to avoid nESI-based ion suppression effects. Charge reduction was achieved by the addition of TEA to the complex in 100 mM ammonium acetate with the final concentration of 10 mM³³.

5.3.2 IM-MS

Typically, an aliquot of the solution (~ 5 μ L) was analyzed using a quadrupole-IM-ToF MS instrument (Synapt G2 HDMS, Waters, Milford MA, USA)²³. Protein ions were generated using a nESI source in the positive mode, with the capillary typically held at 1.8 kV. The sample cone was operated at 20 V to avoid any in-source activation. Instrument settings were optimized to allow transmission of intact protein complexes and to preserve non-covalent interactions⁴⁸. The trap T-wave ion guide was pressurized to 3.5×10^{-2} mbar of argon gas. The T-wave IM separator was operated at a pressure of ~ 2.7 mbar, and a 15 V wave height traveling at 150 m/s to generate IM separation with optimal resolution⁴⁹. The ToF-MS was operated over the m/z range of 800-8000 and at a pressure of 1.8×10^{-6} mbar. In order to achieve tandem MS experiments, ions were selected in the quadrupole mass filter at an m/z and collisional activation for isolated

ions was performed in the ion trap prior to the IM separator. For all protein-salt systems investigated here trap collision voltage was incremented by 5 V in step-wise. All mass spectra were calibrated externally using a solution of cesium iodide (100 mg/mL) and were processed with Masslynx 4.1 software (Waters, Milford, MA, USA). Spectra are shown with minimal smoothing and without background subtraction.

5.3.3 Computational Cation Docking

Magnesium and guanidinium ions (Mg^{2+} and Gdm^+ respectively) were distributed on the surface of pentameric human SAP using molecular mechanics simulations with the GRONingen MAchine for Chemical Simulations (GROMACS)⁵⁰. The protein structure 1SAC was downloaded from the PDB (<http://www.rcsb.org/pdb/>), and given hydrogen atoms using the pdb2gmx utility in GROMACS. The AMBER99SB-all-atom force field⁵¹ was used to simulate the electrostatics of 1SAC and Mg^{2+} , and the antechamber program from the Antechamber package (version 1.25, <http://ambermd.org/antechamber/>)⁵² was coupled with Gaussian '03⁵³ to assign partial charges and to create an Amber-like force field for Gdm^+ . Six simulations were performed to give both ions three separate replicas each with a different randomized initial starting ion position. The proteins were simulated in a vacuum with a box size of 120 by 120 by 110 Å, and 900 ions were randomly placed throughout the box using the genion utility from GROMACS. Each simulation was run for 50 ps, and the final structure was used for CCS analysis. Programs written in Python 3.0 were used to remove all ions further than 3.5 Å from protein atoms, and to randomly remove surface-associated ions as needed. The result was a series of six protein structures each with more than 120 Mg^{2+} or Gdm^+ on their surfaces, and with each ion in an electrostatically-favorable position.

5.3.4 Determination of CCS

Experimental CCSs were determined following the method described previously⁴⁷ using CYC monomer, avidin tetramer, ConA tetramer, ADH tetramer, and GDH hexamers as calibrants. Theoretical CCSs were calculated from crystal structures in PDB and computationally docked structures derived from 5.3.3, using the IMoS Mobility Calculation Software Package developed in the Hogan group^{54,55}, which includes three algorithms: PA, EHSS, and TM. The PA CCS typically underestimates experimental CCS by 15%. For this reason, a scaled PA (eq. 1)^{2,33}, based on an empirically determined scaling factor which accounts for scattering phenomena, any missing atoms and truncations carried out to the full-length protein for a high-resolution crystal structure of the complex, is used here to correlate experimental CCS with model structures. Early IMoS calculations were benchmarked against MOBCAL^{56,57} values in our in-house validation process. The major parameter settings in the IMoS program for PA calculation include the Gas and Molecule Parameters (Gas Radius: 1.1 Å², m_gas: 4 Da, Polarization: 0.2073) and Calculation Parameters (N_rotation: 200).

$$CCS_{calc} = 1.14 \times CCS_{PA} \left(\frac{M_{exp}}{M_{pdb}} \right)^{\frac{2}{3}} \quad (1)$$

5.4 Results and Discussion

5.4.1 Assessing the effect of bound Hofmeister-type cations on lower-charged SAP/CRP ions

Previous work has suggested that SAP (125 kDa) and CRP (117 kDa), two ring-like pentameric proteins with internal cavities, undergo gas-phase compaction process upon collisional activation, prior to subunit unfolding in a charge state manner as described above. In order to examine the

non-specifically surface bound cations on the compaction of gas-phase protein complexes, we first selected low-charge state SAP/CRP ions models of compaction-prone protein assemblies.

As shown in Figure 5-1B and D, the 25^+ and 23^+ ions dominate the MS spectra for the SAP and CRP pentamers respectively when spraying from 100 mM ammonium acetate (green). With the addition of the charge reduction agent TEA, the dominant charge state was reduced to 19^+ and 17^+ , respectively (purple). Such charge reduction is due to the fact that TEA has higher gas-phase basicity (951 kJ mol^{-1}) than ammonia (819 kJ mol^{-1}), as described previously⁵⁸, and it has been proposed that the final charge state observed under such conditions is determined by the emission of potential charge carriers from ESI droplets prior to complete solvent evaporation⁵⁹. In addition to the pentameric assemblies, we observe signals corresponding to SAP and CRP decamers, as has been reported previously⁶⁰. Their charge state can also be shifted to a lower value when TEA is added, thus providing a decameric model system with a barrel-like topology. However, since the SAP decamer presents a bimodal drift time population (Figure 5-1A), as discussed in detail in Chapter 7 (Figure 7-3), only the compaction of monomodal CRP decamer ions were studied here.

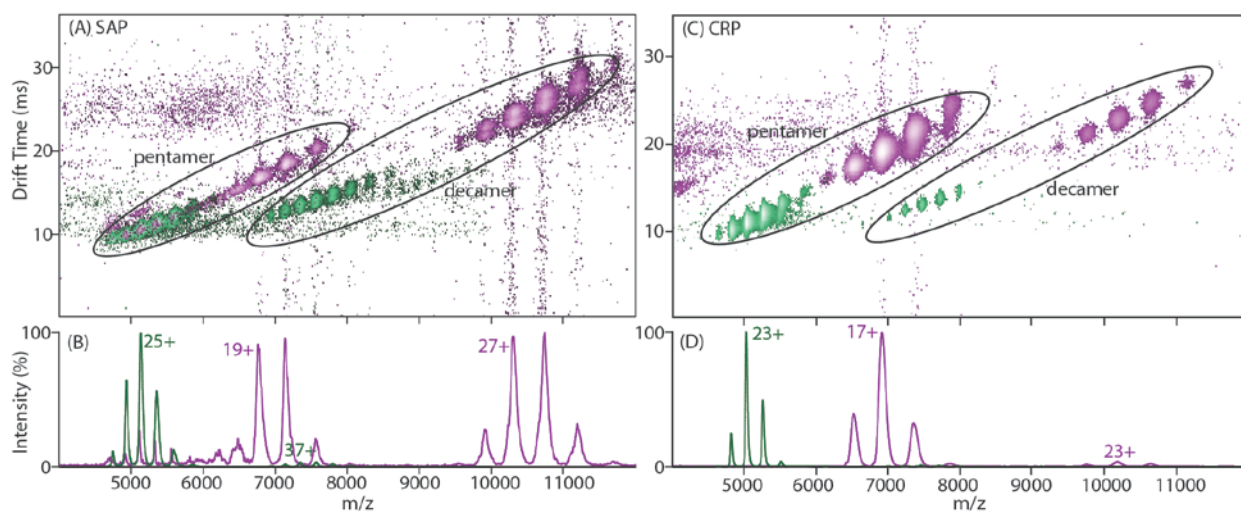


Figure 5-1. Charge reduction of SAP and CRP ions by TEA. (A) and (C) Contour plots of m/z versus drift time are shown for SAP and CRP, respectively, sprayed from 100 mM ammonium acetate with (green) and without (purple) the addition of TEA. Pentameric and decameric ions are both observed. (B) and (D) Mass spectra of SAP and CRP, respectively, are shown at 'normal' (green) and reduced (purple) charge state distributions.

Figure 5-2A, C and E shows MS data for SAP pentamer, CRP pentamer and decamer ions, respectively. The data in black (Figure 5-2A, C and E) show control spectra acquired for ions generated from 100 mM ammonium acetate. The MS signals observed shift substantially to larger centroid m/z with broadened peak widths in the presence of different acetate-based salts, reflective of different degrees of non-specific cation adduction to the surface of protein ions detected. As in previous reports, the width of the observed MS peaks can be directly correlated to the number of non-specifically bound cations adhering to the surface of a given protein ion⁶¹, as all the cations screened here have no known affinity for SAP⁶² or CRP⁶³. While it is challenging to determine the number of cations attached to proteins with high precision from our MS data, we can reasonably assume that the excess mass relative to the ammonium acetate control arises from binding of additional cations and this can be converted to an average number of cations bound to gas-phase protein ions observed⁴². By contrast, we did not observe any measurable anion adduction in our SAP and CRP experiments (Figure III-2), and it is likely that the presence of excess TEA molecules would suppress any such protein-anions interactions⁵⁸.

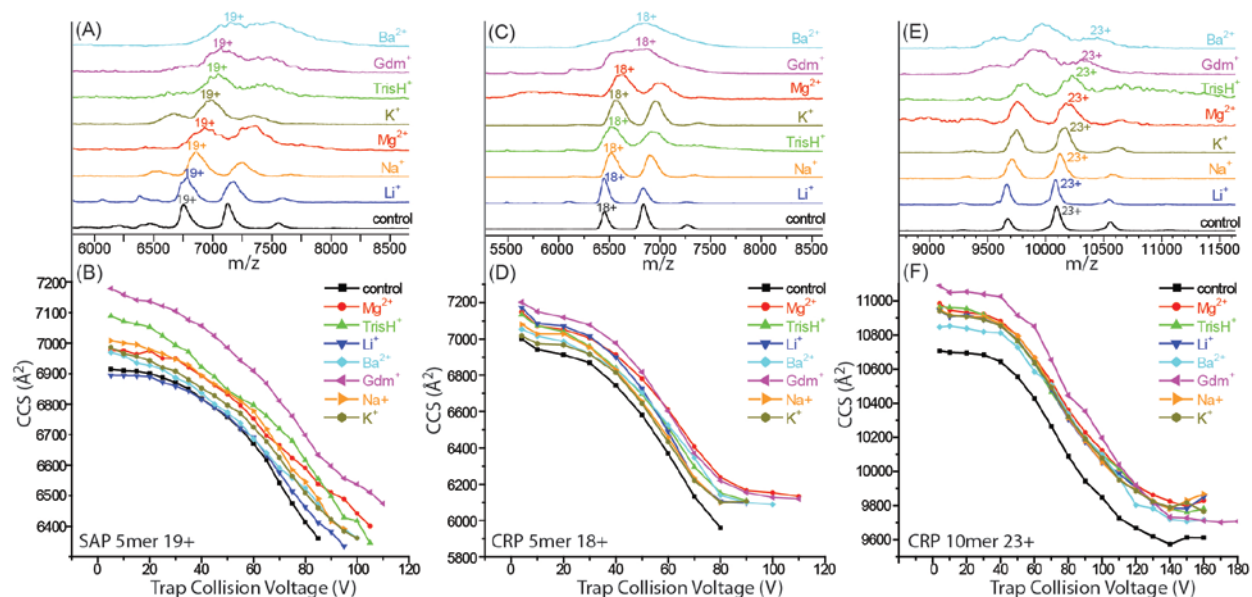


Figure 5-2. Assessing the effect of bound Hofmeister-type cations on lower-charged SAP/CRP ions. (A), (C) and (E) Mass spectra of pentameric SAP, pentameric CRP and decameric CRP, respectively, obtained from solution containing 100 mM ammonium acetate and 10 mM TEA (control, black) and a series of solutions containing both 100 mM ammonium acetate, 10 mM TEA and 2 mM salts (acetate anion with a range of Hofmeister-type cations). (B), (D) and (F) Plots of trap collision voltage against CCS for 19^+ SAP pentameric ions, 18^+ CRP pentameric ions, and 23^+ CRP decameric ions bound with different types of Hofmeister-type cations, respectively. All the data show the complete compaction after which unfolding indicated by CCS increase was observed.

Next, we examined the influence of nonspecific cation adduction on the conformation of gaseous SAP and CRP ions. For the measurements shown in Figures 5-2B, D and F, 19^+ SAP pentamer, 18^+ CRP pentamer and 23^+ CRP decamer ions bound to various cation populations were isolated in the gas-phase and subjected to collisional activation. In control data, SAP pentamer, CRP pentamer and CRP decamer ions experience 8%, 14% and 10% decrease in CCS. Upon activation, the CCS decrease (8%) we observe for 19^+ SAP ions (Figure III-1) agrees with prior MD simulations and experimental results (7%)³³, implying that the compaction observed is related to the size of the central cavity in SAP under our experimental conditions. We note that the overall charge state of the CRP decamer is too large to expect it to undergo the same degree of compaction as the lower-charged CRP pentamer. Our IM-MS data show evidence of

equivalent compaction for all SAP and CRP ions independent of the non-specifically bound cation population attached, the majority of which remained bound during over the entire activation voltage range probed, as observed in our previous data⁴¹. Quantitative compaction values in the presence of cations were nearly identical to those in control data, except for Gdm⁺, where CCSs were reduced to a greater degree for SAP pentamer (10%), CRP pentamer (20%) and CRP decamer (13%). Taken together, these data suggest that bound Hofmeister cations populations on the surface of protein complexes do not tend to alter the magnitude of size compaction observed for low charge state ion populations that are already prone to collisional remodeling in this fashion in the gas phase.

5.4.2 Probing the origin of CCS increase upon cation binding

Despite the negligible influence of Hofmeister-type cation adducts on the collapse of internal cavities within low charge state protein complex ions, cation binding does appear to measurably increase size of protein complex ions when compared with control data (Figure 5-2B, D, F). Such increases in ion CCS are observed for internal cavity-bearing oligomers such as SAP and CRP, as well as relatively compact multiprotein complexes, such as avidin tetramer (Figure 5-3). Previous IM-MS data has shown that metal-bound forms of intermediately-charged monomeric protein ions undergo relative compaction⁶⁴. However, it is highly likely that such transitions are unique to monomeric proteins that occupy charge states where multiple isoenergetic conformer families are populated simultaneously in the gas-phase, and thus such results do not apply to the compact, relatively low charge state protein complex ions studied here.

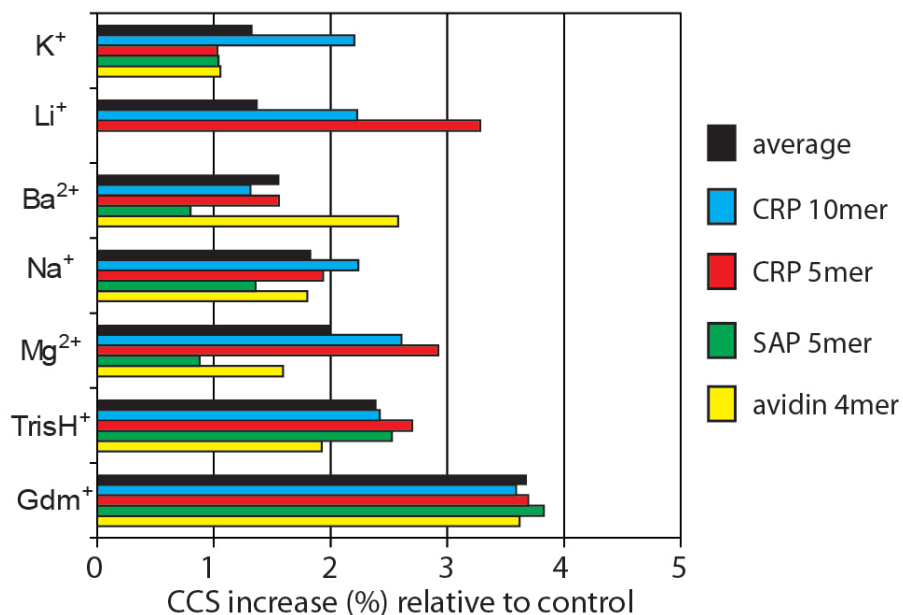


Figure 5-3. CCS increase of SAP and CRP upon cation binding. Percentage of CCS increase of avidin (yellow), SAP pentamer (green), CRP pentamer (red) and CRP decamer (blue) ions bound with 7 different types of cations relative to their unbound forms. The average CCS increase percentage among the four 4 protein complexes (black) is also shown for each cation, as ordered by its values.

A significant fraction of the CCS increases observed in Figure 5-3 must arise from the added volume of bound cations on the surface of the ions detected. To quantify these effects, we constructed molecular models where an experimentally-determined number of cations are bound to the surface of the protein, thus enabling the comparison of computationally-derived CCS values where the only variable is the identity and number of the cation adducts. For example, the measured CCS increase we record for the SAP pentamer bound with Gdm⁺ relative to apo SAP control is 3.8% (Figure 5-3), a value that persists even at high activation voltages. When compared with the CCS difference calculated for SAP model structures both with and without 50 Gdm⁺ ions (1.34%, Figure 5-4), it is clear that the size changes observed cannot be completely attributed to the extra mass and volume added to the protein complex ions through cation

binding alone. Thus, the additional size increase observed must arise from a structural rearrangement in the protein complex structure upon cation adduction.

There are two classes of structural rearrangement that are likely to be the root cause of the size increases shown in Figure 5-3. The first involves the orientation of amino acid side chains on the surface of the protein ion. Previous studies have indicated that most hydrophilic amino acid side chains will collapse onto the surface of the protein structure in the gas phase as described above²⁶, and the small magnitude of the change observed experimentally between cation-adducted and those ions free of additional cation adducts lends support to side chain rearrangement as the primary causal factor in the size changes observed in our data. A recent report has indicated that the non-covalent attachment of crown ether molecules to charged amino acid side chains on the surface of the protein ion can result in a stabilized elongated structure by solvating the positively charged ionic groups in a similar way to solvent⁶⁵. It is possible that Hofmeister-type cations, which tightly bind to the protein, surviving even extensive activation in the gas phase, can form either salt-bridge or charge-solvation interactions with the acidic sites exposed on the protein surface⁶⁶, and therefore, serve to solvate these specific groups on the protein surface. A second possible explanation for the observed CCS increase in Figure 5-3 revolves around the Hofmeister effect, in that the extent in average CCS increase observed for different protein complexes in our experiments (black columns, Figure 5-3) follows a near-reversed rank order relative to the canonical Hofmeister Series. It is possible that cation-backbone interactions drive the remodeling of protein secondary/tertiary structure in a differential manner related to similar processes observed for these cations in solution^{40,67}.

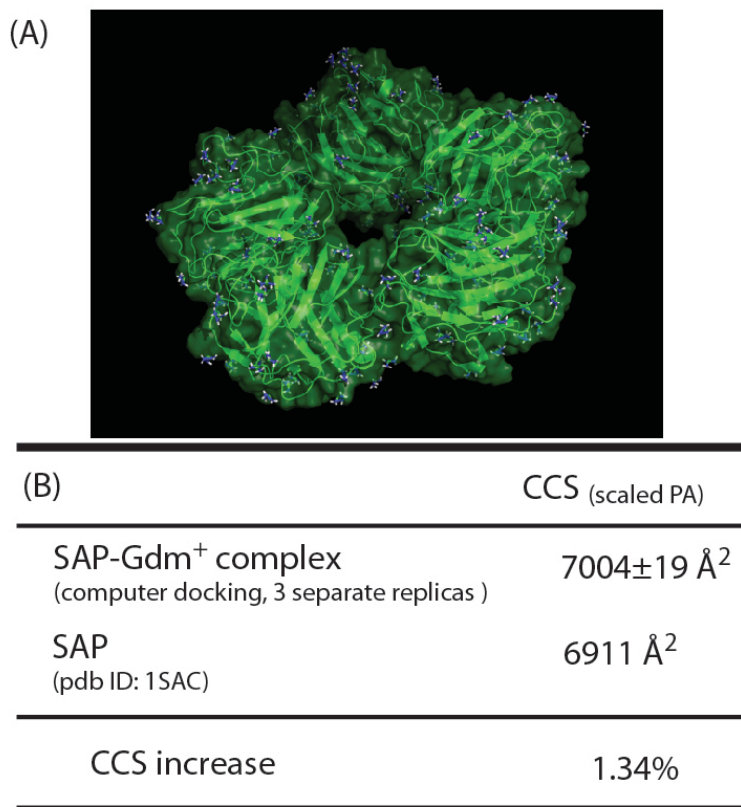


Figure 5-4. CCS difference calculated for SAP model structures with and without Gdm⁺ ions. (A) SAP crystal structure (green, PDB 1SAC) docked with 50 Gdm⁺ ions (blue and white), the number of which was calculated based on the experimental data, using GROMACS (see 5.3.3). (B) CCS increase between Gdm⁺-docked and undocked SAP.

5.4.3 Assessing the effect of bound Hofmeister-type cations on higher-charged SAP ions

As discussed above, tightly-bound cationic adducts are presumed to replace some portion of the mobile proton charge carriers present under control conditions, which would in turn limit overall charge mobility on the surface of the protein ion, and thus increase the energy barrier for Coulombic unfolding. To confirm this hypothesis, higher charge SAP ions, including 25⁺ and 26⁺, were analyzed in terms of their collision induced unfolding and compaction. Previous reports, and our control data, indicate that these ions do not undergo gas-phase compaction, due likely to dearth of highly mobile charge carrier and resultantly low barrier to subunit unfolding.

The MS data for SAP pentamer ions in the presence of 2 mM Mg^{2+} show a shift in average charge upon metal ion adduction from an average charge state of 24^+ (black, Figure 5-5A) in control data to 26^+ (red, Figure 5-5A). This effect has been reported previously, most recently in the context of trivalent metal ions (La^{3+})⁶⁸. Additionally, the peak widths observed for mass spectra acquired from Mg^{2+} -containing solutions display significant broadening when compared with MS spectra obtained from complexes prepared in pure ammonium acetate, despite acquiring the data under identical instrument conditions. Such peak broadening is indicative of non-specific adduction of buffer material to the surface of SAP ions⁶¹.

In order to examine the influence of Mg^{2+} additives on SAP collisional remodeling and compaction, the 25^+ and 26^+ charge states of the cations-adducted SAP pentamer ions were isolated separately in the quadrupole mass filter and collisionally-activated. Figure 5-5B and D plot the collision voltages used for ion activation against the CCS values recorded for the ions. We also tracked the number of cations that remain bound during activation (Figure 5-5C and E). More Mg^{2+} are observed adducted to lower charge state SAP ions (Figure 5-5C), as has been previously reported⁶⁹. Furthermore, a fraction of Mg^{2+} ions were observed to shed off as neutrals complexed with hydroxide ions during collisional activation; however, a larger portion of the original estimate remains bound through the activation process^{41,43}. While neither ion decreased in size under control conditions, according to Figure 5-5B and D, the CCS values measured for 25^+ and 26^+ SAP complex ions bound to Mg^{2+} decreased by 2.8% and 1.9% respectively (filled square) over the activation voltage range used.

This observed reduction in size can be rationalized by two competing mechanisms. The first, and most obvious, is that the shedding of adducted Mg^{2+} during activation gives rise to the size decreases observed. To evaluate this possibility, we theoretically calculated the CCS of SAP pentamer based on the crystal structure (PDB: 1SAC), docked to an varying amount of experimentally-determined Mg^{2+} ions (see Figure 5-5C) and optimized the resulting model using a simple MD relaxation protocol. When these theoretical data are compared with experimental CCS values, it is clear that the majority of the compaction observed for SAP 25^+ ions adducted to Mg^{2+} can be attributed to Mg stripping, although some small amount of compaction cannot be completely ruled out as a causative factor. SAP 26^+ ions, on the other hand, display a significant fraction of CCS decrease in excess of that which can be easily accounted for by Mg stripping (ca. 1.5%), thus clearly pointing toward the importance of mobile charges in partitioning between protein compaction and unfolding pathways following collisional activation.

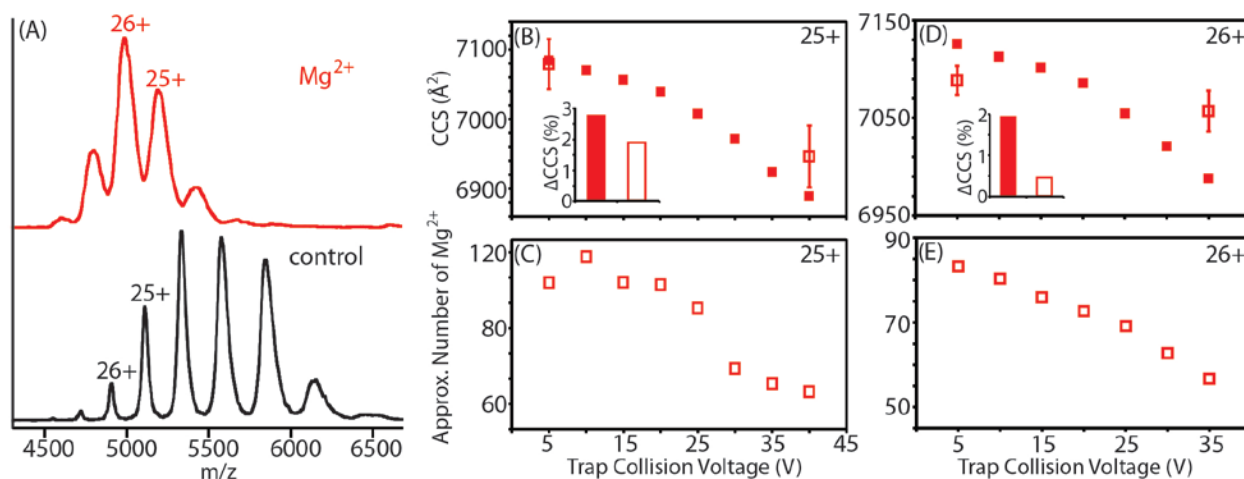


Figure 5-5. Assessing the effect of bound Hofmeister-type cations on higher-charged SAP ions. (A) Mass spectra of pentameric SAP generated from solution containing 100 mM ammonium acetate without (control, black) and with (red) 2 mM magnesium acetate show the ‘normal’ range of charge state distributions. The CCSs of SAP-Mg²⁺ complex ions at 25⁺ (B) and 26⁺ (D) charge state are plotted as a function of trap collision voltages. The CCS values measured using IM-MS data and calculated from computationally docked structures are indicated by filled and

open square, respectively. The inset figures show the CCS difference ($\Delta\text{CCS}\%$) collected at the start and end trap collisional voltage, based on experimental (filled column) and simulated (open column) data, respectively. The approximate number of magnesium cations bound to 25^+ (C) and 26^+ (E) SAP ions are also plotted *versus* trap collision voltages.

5.5 Conclusions

In this study, a series of Hofmeister-type cations were added in nESI buffer prior to ionization/desolvation to explore their effect on the gas-phase structural transitions of SAP and CRP ion at different charge states using IM-MS. The ions retained their native-like structures in the gas phase at lower energies, including their internal cavities, and were subject to collapse into more compact conformations following activation through energetic collisions with neutral gas (Ar). The degree of such compaction was found to be highly charge-state dependent, as observed previously. Our data indicate that while adducted cations could not rescue low charge state ions from pathways involving collapse following collisional activation, they both increased the size and caused higher charge states to more strongly favor compaction modes of gas-phase collisional remodeling.

The results shown here further point toward previously unknown modes in which bound cations can alter and, potentially, retain protein structures that are native-like in the absence of bulk solvent. First, the CCS increases observed in the absence of activation appear both differential and related to reversed Hofmeister series previously observed. The small magnitude of the CCS shift detected here indicates that a reorganization on a local level, and given the available options, amino acid side chains seem the most likely source. Cations are known to interact with acidic side chains on the surface of proteins to form salt-bridged structures, and this mechanism may provide a type of charge solvation effect multiple side chains are involved, similar to crown ether

experiments previously described. A potentially more-exciting observation, however, is that of importance of charge mobility in the compaction process of SAP ions. Previous mechanisms had linked protein compaction to protein charge alone, but charge mobility, which is already invoked in protein subunit unfolding, seems to be anti-correlated to the optimized conditions for protein compaction. While Mg^{2+} ions are clearly less mobile than protons, it is difficult to say to what magnitude they are less mobile. Indeed, further experiments with truly fixed charges are clearly warranted in order to clearly delineate the influence of mobile charge. Since CIU and related compactions are linked to CID product ions, it is clear that a deeper understanding and control over the mechanisms at play will provide clear analytical benefits for protein complex topology mapping and top down sequencing efforts from isolated complex ions currently underway.

5.6 References

- (1) Hyung, S. J.; Ruotolo, B. T. *Proteomics* **2012**, *12*, 1547.
- (2) Benesch, J. L. P.; Ruotolo, B. T. *Current Opinion in Structural Biology* **2011**, *21*, 641.
- (3) van den Heuvel, R. H. H.; van Duijn, E.; Mazon, H.; Synowsky, S. A.; Lorenzen, K.; Versluis, C.; Brouns, S. J. J.; Langridge, D.; van der Oost, J.; Hoyes, J.; Heck, A. J. R. *Analytical Chemistry* **2006**, *78*, 7473.
- (4) Lanucara, F.; Holman, S. W.; Gray, C. J.; Eyers, C. E. *Nat Chem* **2014**, *6*, 281.
- (5) Zhou, M.; Politis, A.; Davies, R. B.; Liko, I.; Wu, K.-J.; Stewart, A. G.; Stock, D.; Robinson, C. V. *Nat Chem* **2014**, *6*, 208.
- (6) Wytttenbach, T.; Pierson, N. A.; Clemmer, D. E.; Bowers, M. T. *Annual Review of Physical Chemistry* **2014**, *65*, 175.
- (7) Pierson, N. A.; Chen, L. X.; Valentine, S. J.; Russell, D. H.; Clemmer, D. E. *Journal of the American Chemical Society* **2011**, *133*, 13810.
- (8) Bleiholder, C.; Dupuis, N. F.; Wytttenbach, T.; Bowers, M. T. *Abstracts of Papers of the American Chemical Society* **2011**, 242.
- (9) Jenner, M.; Ellis, J.; Huang, W. C.; Raven, E. L.; Roberts, G. C. K.; Oldham, N. J. *Angewandte Chemie-International Edition* **2011**, *50*, 8291.
- (10) Han, L. J.; Ruotolo, B. T. *Angewandte Chemie-International Edition* **2013**, *52*, 8329.
- (11) Rabuck, J. N.; Hyung, S. J.; Ko, K. S.; Fox, C. C.; Soellner, M. B.; Ruotolo, B. T. *Analytical Chemistry* **2013**, *85*, 6995.

- (12) Hyung, S. J.; DeToma, A. S.; Brender, J. R.; Lee, S.; Vivekanandan, S.; Kochi, A.; Choi, J. S.; Ramamoorthy, A.; Ruotolo, B. T.; Lim, M. H. *Proceedings of the National Academy of Sciences of the United States of America* **2013**, *110*, 3743.
- (13) Hopper, J. T. S.; Oldham, N. J. *Journal of the American Society for Mass Spectrometry* **2009**, *20*, 1851.
- (14) Young, L. M.; Cao, P.; Raleigh, D. P.; Ashcroft, A. E.; Radford, S. E. *Journal of the American Chemical Society* **2014**, *136*, 660.
- (15) Bernstein, S. L.; Dupuis, N. F.; Lazo, N. D.; Wyttenbach, T.; Condron, M. M.; Bitan, G.; Teplow, D. B.; Shea, J. E.; Ruotolo, B. T.; Robinson, C. V.; Bowers, M. T. *Nature Chemistry* **2009**, *1*, 326.
- (16) Dupuis, N. F.; Wu, C.; Shea, J. E.; Bowers, M. T. *Journal of the American Chemical Society* **2011**, *133*, 7240.
- (17) Smith, D. P.; Radford, S. E.; Ashcroft, A. E. *Proceedings of the National Academy of Sciences of the United States of America* **2010**, *107*, 6794.
- (18) Bernstein, S. L.; Wyttenbach, T.; Baumketner, A.; Shea, J. E.; Bitan, G.; Teplow, D. B.; Bowers, M. T. *Journal of the American Chemical Society* **2005**, *127*, 2075.
- (19) Politis, A.; Park, A. Y.; Hyung, S. J.; Barsky, D.; Ruotolo, B. T.; Robinson, C. V. *Plos One* **2010**, *5*.
- (20) Zhou, M.; Sandercock, A. M.; Fraser, C. S.; Ridlova, G.; Stephens, E.; Schenauer, M. R.; Yokoi-Fong, T.; Barsky, D.; Leary, J. A.; Hershey, J. W.; Doudna, J. A.; Robinson, C. V. *Proceedings of the National Academy of Sciences of the United States of America* **2008**, *105*, 18139.
- (21) Lane, L. A.; Fernandez-Tornero, C.; Zhou, M.; Morgner, N.; Ptchelkine, D.; Steuerwald, U.; Politis, A.; Lindner, D.; Gvozdenovic, J.; Gavin, A. C.; Muller, C. W.; Robinson, C. V. *Structure* **2011**, *19*, 90.
- (22) Uetrecht, C.; Rose, R. J.; van Duijn, E.; Lorenzen, K.; Heck, A. J. R. *Chemical Society Reviews* **2010**, *39*, 1633.
- (23) Ruotolo, B. T.; Benesch, J. L. P.; Sandercock, A. M.; Hyung, S. J.; Robinson, C. V. *Nature Protocols* **2008**, *3*, 1139.
- (24) Ruotolo, B. T.; Giles, K.; Campuzano, I.; Sandercock, A. M.; Bateman, R. H.; Robinson, C. V. *Science* **2005**, *310*, 1658.
- (25) Ruotolo, B. T.; Robinson, C. V. *Current Opinion in Chemical Biology* **2006**, *10*, 402.
- (26) Breuker, K.; McLafferty, F. W. *Proceedings of the National Academy of Sciences of the United States of America* **2008**, *105*, 18145.
- (27) Steinberg, M. Z.; Elber, R.; McLafferty, F. W.; Gerber, R. B.; Breuker, K. *Chembiochem* **2008**, *9*, 2417.
- (28) Pagel, K.; Natan, E.; Hall, Z.; Fersht, A. R.; Robinson, C. V. *Angewandte Chemie-International Edition* **2013**, *52*, 361.
- (29) Saikusa, K.; Fuchigami, S.; Takahashi, K.; Asano, Y.; Nagadoi, A.; Tachiwana, H.; Kurumizaka, H.; Ikeguchi, M.; Nishimura, Y.; Akashi, S. *Analytical Chemistry* **2013**, *85*, 4165.
- (30) Bagal, D.; Valliere-Douglass, J. F.; Balland, A.; Schnier, P. D. *Analytical Chemistry* **2010**, *82*, 6751.
- (31) Uetrecht, C.; Barbu, I. M.; Shoemaker, G. K.; van Duijn, E.; Heck, A. J. R. *Nature Chemistry* **2011**, *3*, 126.

- (32) Park, A. Y.; Jergic, S.; Politis, A.; Ruotolo, B. T.; Hirshberg, D.; Jessop, L. L.; Beck, J. L.; Barsky, D.; O'Donnell, M.; Dixon, N. E.; Robinson, C. V. *Structure* **2010**, *18*, 285.
- (33) Hall, Z.; Politis, A.; Bush, M. F.; Smith, L. J.; Robinson, C. V. *Journal of the American Chemical Society* **2012**, *134*, 3429.
- (34) Zhou, M. W.; Dagan, S.; Wysocki, V. H. *Analyst* **2013**, *138*, 1353.
- (35) Freeke, J.; Robinson, C. V.; Ruotolo, B. T. *International Journal of Mass Spectrometry* **2010**, *298*, 91.
- (36) Hogan, C. J.; Ruotolo, B. T.; Robinson, C. V.; de la Mora, J. F. *Journal of Physical Chemistry B* **2011**, *115*, 3614.
- (37) Pagel, K.; Hyung, S. J.; Ruotolo, B. T.; Robinson, C. V. *Analytical Chemistry* **2010**, *82*, 5363.
- (38) Benesch, J. L. P.; Ruotolo, B. T.; Sobott, F.; Wildgoose, J.; Gilbert, A.; Bateman, R.; Robinson, C. V. *Analytical Chemistry* **2009**, *81*, 1270.
- (39) Jurchen, J. C.; Williams, E. R. *Journal of the American Chemical Society* **2003**, *125*, 2817.
- (40) Lo Nostro, P.; Ninham, B. W. *Chemical Reviews* **2012**, *112*, 2286.
- (41) Han, L. J.; Hyung, S. J.; Ruotolo, B. T. *Angewandte Chemie-International Edition* **2012**, *51*, 5692.
- (42) Han, L. J.; Hyung, S. J.; Mayers, J. J. S.; Ruotolo, B. T. *Journal of the American Chemical Society* **2011**, *133*, 11358.
- (43) Han, L.; Ruotolo, B. *International Journal for Ion Mobility Spectrometry* **2013**, *16*, 41.
- (44) Han, L. J.; Hyung, S. J.; Ruotolo, B. T. *Faraday Discussions* **2013**, *160*, 371.
- (45) Merenbloom, S. I.; Flick, T. G.; Daly, M. P.; Williams, E. R. *Journal of the American Society for Mass Spectrometry* **2011**, *22*, 1978.
- (46) Liu, J.; Konermann, L. *Journal of the American Society for Mass Spectrometry* **2014**, *25*, 595.
- (47) Bush, M. F.; Hall, Z.; Giles, K.; Hoyes, J.; Robinson, C. V.; Ruotolo, B. T. *Analytical Chemistry* **2010**, *82*, 9557.
- (48) Hernandez, H.; Robinson, C. V. *Nature Protocols* **2007**, *2*, 715.
- (49) Zhong, Y. Y.; Hyung, S. J.; Ruotolo, B. T. *Analyst* **2011**, *136*, 3534.
- (50) Van Der Spoel, D.; Lindahl, E.; Hess, B.; Groenhof, G.; Mark, A. E.; Berendsen, H. J. C. *Journal of Computational Chemistry* **2005**, *26*, 1701.
- (51) Hornak, V.; Abel, R.; Okur, A.; Strockbine, B.; Roitberg, A.; Simmerling, C. *Proteins: Structure, Function, and Bioinformatics* **2006**, *65*, 712.
- (52) Wang, J. M.; Wang, W.; Kollman, P. A. *Abstracts of Papers of the American Chemical Society* **2001**, *222*, U403.
- (53) Frisch, M. J. *Chemicke Listy* **2006**, *100*, A9.
- (54) Larriba, C.; Hogan, C. J. *The Journal of Physical Chemistry A* **2013**, *117*, 3887.
- (55) Larriba, C.; Hogan Jr, C. J. *Journal of Computational Physics* **2013**, *251*, 344.
- (56) Mesleh, M. F.; Hunter, J. M.; Shvartsburg, A. A.; Schatz, G. C.; Jarrold, M. F. *The Journal of Physical Chemistry* **1996**, *100*, 16082.
- (57) Shvartsburg, A. A.; Jarrold, M. F. *Chemical Physics Letters* **1996**, *261*, 86.
- (58) Catalina, M. I.; van den Heuvel, R. H. H.; van Duijn, E.; Heck, A. J. R. *Chemistry-a European Journal* **2005**, *11*, 960.

- (59) Hogan, C. J.; Carroll, J. A.; Rohrs, H. W.; Biswas, P.; Gross, M. L. *Journal of the American Chemical Society* **2008**, *130*, 6926.
- (60) Aquilina, J. A.; Robinson, C. V. *Biochemical Journal* **2003**, *375*, 323.
- (61) McKay, A. R.; Ruotolo, B. T.; Ilag, L. L.; Robinson, C. V. *Journal of the American Chemical Society* **2006**, *128*, 11433.
- (62) Emsley, J.; White, H. E.; Ohara, B. P.; Oliva, G.; Srinivasan, N.; Tickle, I. J.; Blundell, T. L.; Pepys, M. B.; Wood, S. P. *Nature* **1994**, *367*, 338.
- (63) Shrive, A. K.; Gheetham, G. M. T.; Holden, D.; Myles, D. A. A.; Turnell, W. G.; Volanakis, J. E.; Pepys, M. B.; Bloomer, A. C.; Greenhough, T. J. *Nat Struct Mol Biol* **1996**, *3*, 346.
- (64) Flick, T. G.; Merenbloom, S. I.; Williams, E. R. *Journal of the American Society for Mass Spectrometry* **2013**, *24*, 1654.
- (65) Warnke, S.; von Helden, G.; Pagel, K. *Journal of the American Chemical Society* **2013**, *135*, 1177.
- (66) Kapota, C.; Lemaire, J.; Maître, P.; Ohanessian, G. *Journal of the American Chemical Society* **2004**, *126*, 1836.
- (67) Zhang, Y. J.; Cremer, P. S. In *Annual Review of Physical Chemistry, Vol 61*; Leone, S. R., Cremer, P. S., Groves, J. T., Johnson, M. A., Richmond, G., Eds. 2010; Vol. 61, p 63.
- (68) Flick, T. G.; Williams, E. R. *Journal of the American Society for Mass Spectrometry* **2012**, *23*, 1885.
- (69) Iavarone, A. T.; Udekwu, O. A.; Williams, E. R. *Analytical Chemistry* **2004**, *76*, 3944.

Chapter 6. Hofmeister Salts Recover a Misfolded Multiprotein Complex for Subsequent Structural Measurements in the Gas Phase

Han L, Ruotolo BT, Hofmeister Salts Recover a Misfolded Multiprotein Complex for Subsequent Structural Measurements in the Gas Phase, *Angewandte Chemie International Edition*, 2013, 52, 8329-8332.

6.1 Abstract

Gas-phase measurements of protein structure are emerging as an important tool in structural biology. Such measurements, however, impose a foreign environment on proteins and risk the disruption of useful structural information relevant to biology and medicine. As a further complication, many proteins exist in a range of conformational states in solution that dynamically interact and subtly depend upon the local environment. Here, we report on the ability of a lectin tetramer to misfold into a conformational population that is created through alterations in its dimer-dimer interface. We then demonstrate that this misfolded tetramer can be recovered to a more native-like state by adding specific salts in solution prior to electrospray ionization. While anions added in this way appear to stabilize this misfolded protein in a manner consistent with the known Hofmeister series in solution, cations instead conform to a rank order associated with processes unique to the gas phase. We discuss the importance of these findings

from the point of view of lectin protein structure, protein misfolding, and gas-phase structural biology efforts in general.

6.2 Introduction

Proteins are the workhorses of the cell, the functions of which are largely predicated on their structures and dynamics. Detailed knowledge of these attributes has enabled countless breakthroughs in human health and disease^{1,2}. Many aspects, however, of protein structure remain poorly understood, including their high-order interactions^{3,4}. This knowledge gap drives the development of new tools capable of protein structure characterization, some of which operate by measuring desolvated protein structure^{5,6}. While desolvation enables the application of powerful analytical techniques that cannot be used in a solvated environment, and recent results indicate that many features of native protein structure survive in the gas-phase⁷, desolvation may also act to obfuscate critical details of protein conformation⁸. Recently, multiple strategies have emerged for observing labile protein structures in the absence of bulk water and have proven useful in stabilizing protein-small molecule interactions, globular proteins, and their complexes⁸⁻¹². Here, we report the first evidence that a misfolded protein complex, which exists both in solution and in the gas-phase, can be recovered back to a 'native-like' structure through the addition of salts prior to desorption/ionization. These data represent the first time that such a solution-phase multiprotein folding equilibrium is captured by gas-phase measurements.

Our experiments involve the direct addition of salt additives to proteins in solution, mimicking the well-known Hofmeister series^{13,14},^{13,14} followed by transfer into the gas phase using nESI. We then utilize IM-MS to measure the influence of such additives on both the composition and

structure of the resulting gas-phase ions. IM separates proteins and complexes based on their CCS. Such information can be used, along with computational procedures, to deduce the 3D structures of biomolecules¹⁵⁻¹⁷. MS can then be used to analyze the composition of ions that elute from the IM separator^{18,19}. While previous measurements have allowed us to rank the ability of bound anions and cations to stabilize proteins in the gas phase, these experiments started from thermodynamically stable proteins that were natively-folded prior to nESI and did not reflect protein stabilities in solution⁹⁻¹¹. The protein system we have chosen to study here is the lectin ConA, a ~103 kDa homo-tetramer having a dimer-of-dimers arrangement²⁰. The ConA tetramer can reversibly self-assemble to form dimers and tetramers in a manner that depends upon solution pH, temperature, and ionic strength²¹⁻²³. In addition to these properties, IM-MS reveals that the ConA tetramer can generate an alternate quaternary structure, which can be recovered back to a native-like conformation in a salt-dependant manner.

6.3 Experimental

6.3.1 Materials

ConA tetramer (jack bean), and all salts studied including cations (acetate anion with TMA, sodium, potassium, rubidium, lithium, Tris, calcium, barium, and magnesium counterions) or anions (ammonium cation with fluoride, chloride, nitrate, tartrate, hydrogen phosphate, sulfate and perchlorate counter-ions) were purchased from Sigma (St. Louis, MO, USA). All other chemicals used in this study were analytical quality, and all aqueous solutions were prepared on the Synergy water purification system (Millipore Corporation).

6.3.2 IM-MS

Typically, a sample aliquot (~5 μ L) was analyzed using a quadrupole-IM-ToF MS instrument (Synapt G2 HDMS, Waters, Milford MA, USA)¹⁹. ConA was first buffer exchanged into 100 mM ammonium acetate at pH 7 using Micro Bio-Spin 6 columns (Bio-Rad, Hercules, CA) and prepared to a final concentration of 5 μ M. ConA' was refolded by adding small amounts of salt in solution prior to nESI, where the identity of cations (acetate anion with TMA, sodium, potassium, rubidium, lithium, Tris, calcium, barium, and magnesium counterions) or anions (ammonium cation with fluoride, chloride, nitrate, tartrate, hydrogen phosphate, sulfate and perchlorate counter-ions) were altered specifically so that their effect could be evaluated individually. All salts were prepared as stock solutions in 100 mM ammonium acetate at a concentration of 20mM, before addition to the protein solution, where the final salt concentration was 2 mM. The total salt and protein concentrations listed above were chosen primarily to avoid nESI-based ion suppression effects.²⁴ Protein ions were generated using a nESI source in the positive mode, with the capillary typically held at 1.5 kV. The sample cone was operated at 50 V. Instrument settings were optimized to allow transmission of intact protein complexes and to preserve non-covalent interactions^{25,26}. The trap T-wave ion guide was pressurized to 3.3×10^{-2} mbar of argon gas. The ion trap was operated in an accumulation mode and ion lifetimes in the trap prior to IM analysis range from 0-50 ms in our experiments. The T-wave IM separator was operated at a pressure of ~ 3.5 mbar, and employed a series of DC voltage waves (40 V wave height traveling at 600-1000 m/s) to generate IM separation. The ToF-MS was operated over the m/z range of 400–8000 and at a pressure of 1.6×10^{-6} mbar.

Mass spectra were calibrated externally using a solution of cesium iodide (100 mg ml^{-1}) and processed with Masslynx 4.1 software (Waters, Milford MA, USA). CCS measurements were made using known CCS values of TTR, avidin, ADH and GDH tetramers (Sigma-Aldrich), as calibrants using the method described previously^{27,28}.

6.3.3 CIU and CID

CIU ‘fingerprints’ for ConA and ConA’ were generated through collisional activation in the ion trap T-wave ion guide prior to the IM separator in tandem-MS (Quad selection) mode. Selected ions had a m/z corresponding to the 21^+ of ConA and ConA’ and were activated by increasing the trap collision voltage (Trap CE, as indicated in the instrument control software) which acts as a bias voltage between the quadrupole and ion trap T-wave ion guide to accelerate ions to increased kinetic energies for CIU experiments. The energy-dependent arrival-time distribution profiles (CIU ‘fingerprints’) were constructed using 5 V step-wise increments in trap CE. In addition, post IM separation CID of 20^+ protein complex ions for ConA and ConA’ was performed in the ‘transfer’ T-wave ion guide in order to analyze and compare the charge state distributions of monomeric product ions.

6.3.4 CD

The CD spectra were measured with an Aviv model 202 CD spectrometer (Aviv Instruments, Lakewood, USA). A 1-mm-path-length quartz cuvette was used for scanning between 205 and 250 nm. The concentration of ConA tetramer was $5 \mu\text{M}$.

6.3.5 DSC

The DSC experiments were performed on Nano DSC (TA Instruments, New Castle, USA). The concentration of ConA tetramer was 6.0 mg/mL, equivalent to ~ 60 μ M. The measurements were performed at temperatures from 45 to 95 °C at a scan rate of 2 °C/min. The reference solution in all the calorimetric experiments was 100 mM ammonium acetate and all samples were degassed before measurement. The DSC data were fit with two-state scaled model by using the software NanoAnalyze (TA Instrument, USA) to obtain the temperature (T_m) at which maximum heat exchange occurs.

6.4 Results and Discussion

6.4.1 Capturing misfolded form of ConA by IM-MS

ConA has been long studied for its mitogenic, cell surface, and highly-selective metal-binding (Mn^{2+} and Ca^{2+}) properties²⁰. While many reports indicate that the protein interfaces within the complex can be disrupted to produce alternative structural forms^{21,22}, the native holo-protein complex exists primarily within a narrow conformational space, as observed across all charge states observed in our IM-MS measurements (Figure 6-1A, black dashed box/line). When the protein is exposed to freeze-thaw cycles or a small amount of denaturant in solution, however, we observe a new set of peaks having longer drift times (Figure 6-1B, red dashed box/line). Since all the ions shown in Figure 6-1 are measured under identical instrument conditions, we can rule out the possibility that these new signals result from different levels of collisional activation. Furthermore, tandem MS experiments (see below), and the fact that the results shown in Figure 6-1A and Figure 6-1B were acquired from solutions having identical protein

concentrations, confirm that the features observed at longer drift times are a tetrameric form of ConA. Therefore, we assign these new features to an additional conformer of the ConA tetramer which coexists with its native form in solution and is apparently stable on the timescale of our experiments (minutes to hours), having slightly higher average charge (Figure IV-1). In Figure 6-1C and Figure 6-1D, this alternate form of ConA (ConA') is ~12% larger (CCS = 6040 Å²) than the compact form typically observed (CCS = 5400 Å²)²⁷.

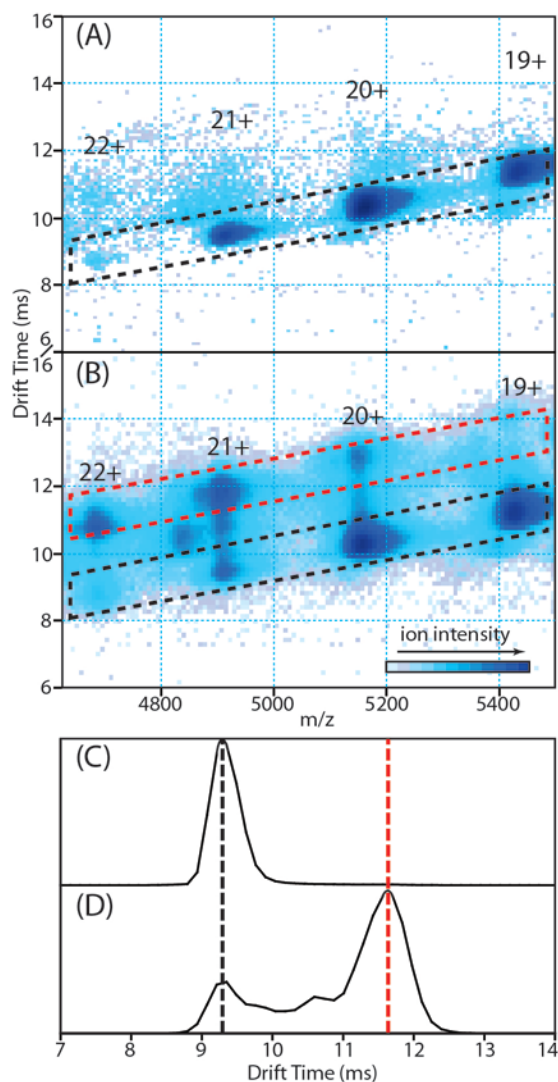


Figure 6-1. Capturing misfolded form of ConA by IM-MS. An alternative form of the ConA tetramer is observed by comparing IM-MS data acquired from control (100 mM ammonium acetate) conditions (A) and following multiple freeze-thaw cycles (B). The conversion between ConA (black dashed box) and ConA' (red dashed box) can be equally affected by adding small amounts of MeOH or HAC in solution prior to nESI. Drift time distributions for 21⁺ charge state tetramer ions are shown in (C) and (D) for ConA and ConA' respectively (same m/z). The centroid CCS of peaks corresponding to ConA and ConA' are highlighted with black and red dashed lines respectively (black: 5400, red: 6040 Å²).

To probe the origin of ConA', and further verify our assignment above, we undertook a series of experiments where we aimed to structurally characterize the conformations of sub-assemblies and subunits produced under conditions favoring either ConA or ConA' (Figure IV-2). As noted above, we found that both small amounts of HAc (adjusted to a minimum pH of 5.2) and MeOH (up to 30% by volume) convert ConA to ConA'. In addition, for those conditions that give rise to significant amounts of ConA' tetramer, we observe a mirrored set of conformational changes in the protein monomers produced upon complex disruption. For example, in a weakly-acidic solution, ConA tetramer is disrupted to produce monomers in a relatively narrow band of structural states; however, increasing the solution MeOH content to 10% generates both ConA' and low charge state monomers, the latter existing within at least three conformational families simultaneously. Furthermore, we note that the dimers produced under any set of solution conditions exhibit a single, relatively narrow CCS distribution. From this data, we conclude that the structural transformations observed within the ConA tetramer are caused by deformations in the monomeric subunits of ConA that do not influence the overall size of ConA dimers. Furthermore, while polar protic solvents (i.e., MeOH, Figure IV-3) can efficiently produce ConA', polar aprotic solvents (i.e., DMSO, Figure IV-4) cannot. CIU and CID confirm the stoichiometry of ConA' as well as its construction from likely unfolded protein subunits, as the misfolded tetramer produces unfolding patterns having ΔCCS values identical to ConA yet ejects monomers that cover a broader range of charge states upon dissociation in the gas phase (Figure IV-5).

6.4.2 Gas-phase structures reflecting those in solution

In order to ascertain if the changes in gas-phase protein complex structure observed in our IM-MS data are mirrored in solution, we conducted CD and DSC experiments on ConA/ConA' containing solutions designed to mimic those used for our gas-phase measurements (Figure 6-2). Figure 6-2A shows the far-UV CD spectra between 250-205 nm for ConA in the presence of different amounts (% v/v) of MeOH at pH 7. Native ConA exhibits a band at 223 nm (black curve, 100 mM ammonium acetate control), which is characteristic of proteins dominated by β -sheet character^{29,30}. When ConA is prepared in 100 mM ammonium acetate solutions containing varying amounts of (vol/vol) MeOH, we observe a red shift of ~4 nm in combination with a decrease in ellipticity, indicative of ConA structure disruption (green curve). We observe that solutions containing greater than 40% added MeOH dramatically reduces CD absorptivity. This result strongly correlates with our IM-MS data that shows evidence of ConA' formation at similar MeOH concentrations (Figure IV-3). We also observe similar CD signals at lower MeOH amounts (10-30%) upon acidification of ConA containing solutions (Figure 6-2B), which also agrees with IM-MS results (Figure IV-2). Due to the large far-UV absorptivity of DMSO, and related chemical noise, CD data from such solutions was not collected.

In addition to CD, we also measured the thermal stability of ConA tetramer by means of DSC (Figure 6-2C). Due to the boiling point of MeOH (65 °C), MeOH-containing samples were buffer exchanged following incubation times sufficient to alter ConA structure, prior to DSC measurements. Data for ConA tetramer prepared in 100 mM ammonium acetate alone reveals two thermal unfolding transitions (control). The high temperature transition peak has a T_m of ~85 °C, which agrees with that of native ConA previously reported³¹. The lower temperature

transition peak (T_m : ~ 78 °C) likely corresponds to a small amount of ConA dimer in solution, which co-exists with the tetramer under such solution conditions. After incubation in 10% MeOH in a weakly acidic solution, ConA undergoes a significant shift in thermal stability (T_m : ~ 67 °C). Increasing MeOH content to 20% further destabilizes ConA (~ 55 °C). In sharp contrast to these results, the addition of 10%-20% DMSO to ConA solution has no influence on protein stability, in good agreement with IM-MS data (Figure IV-4).

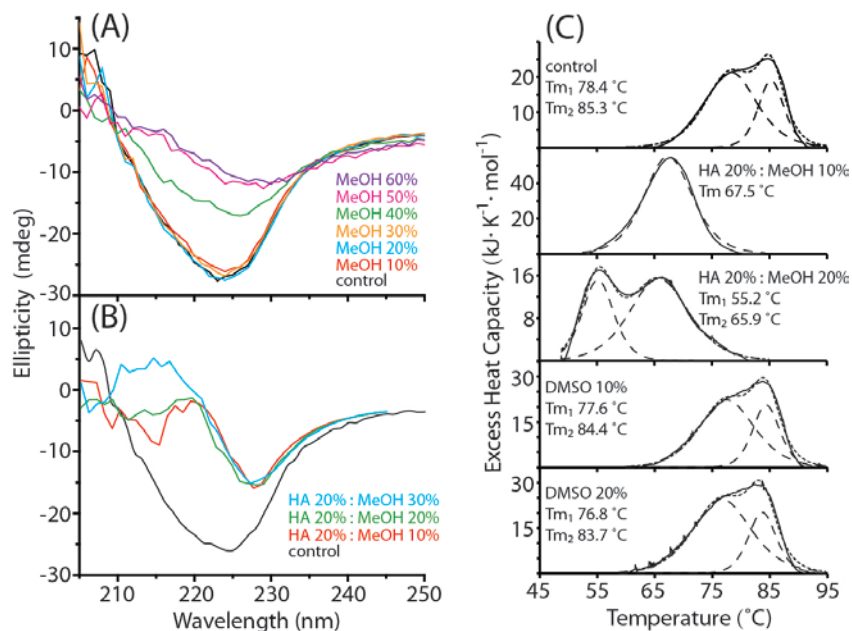


Figure 6-2. Effect of disrupting agents on ConA structure and stability in bulk solution. (A) Far-UV CD spectra of 5 μ M ConA as a function of MeOH concentration (0-60%, vol/vol) in 100 mM ammonium acetate buffer, pH 7. (B) Far-UV CD spectra of 5 μ M ConA as a function of MeOH concentration (0-30%, vol/vol) in 100 mM ammonium acetate buffer, pH 5.2. (C) DSC scans of ~ 60 μ M ConA (top, 100 mM ammonium acetate) and 4 additional aqueous solvent compositions prepared using varying amounts of MeOH or DMSO (as marked). The experimental data and fits are indicated by solid and dashed lines, respectively

In summary, to probe the solution structure of ConA under conditions that mimic those used for our nESI-IM-MS samples, we performed CD and DSC measurements. Control samples prepared in ammonium acetate buffer display a bimodal DSC profile, with melting temperatures (T_m) corresponding well with known values for the intact tetramer and dimer (85.3 and 78.4 °C

respectively)³¹, and a CD spectrum with a strong band at 220 nm, characteristic of beta sheet protein structure. Preparation of ConA in solutions containing MeOH and acid reveals shifts in the CD spectra toward higher wavelengths and reduced intensities in a manner dependent upon organic/acid solution content, as well as dramatic decreases in the T_m values recorded from DSC, all in a manner highly-correlated with IM-MS results. Critically, the addition of DMSO caused no measurable change in ConA stability in solution, mirroring exactly our gas-phase results.

6.4.3 Hofmeister anions/cations recovering misfolded ConA

Given the verification of our assignment of the IM peaks observed in Figure 6-1, as well as their origins in solution, we then attempted to recover the misfolded ConA' structure by adding small amounts of anions and cations in solution prior to nESI. Our results indicate a differential stabilization and refolding effect for cations and anions on ConA/ConA' tetramers (Figure 6-3). Our data show that multiply charged cations and anions have a greater ability to convert ConA' to CCS values that agree well with ConA data when compared to singly-charged cations in our experiments, which involve adding 2 mM of either acetate-based cations or ammonium-based anions to 5 μ M solutions of ConA' in 100 mM ammonium acetate. As expected, we observe that MS peaks broaden considerably when involatile salts are added prior to nESI, due to the non-specific adduction of many anions or cations to the surface of the protein. Conversion between ConA' and ConA is often incomplete in our dataset, producing significant populations of a new intermediate at $\sim 5770 \text{ \AA}^2$ and slightly swelled ($\sim 1\%$) final sizes. Both anions and cations convert ConA' to ConA in a concentration dependent manner (Figure IV-6) and recovered ConA ions produce CIU fingerprints that are nearly identical to control data (Figure IV-7).

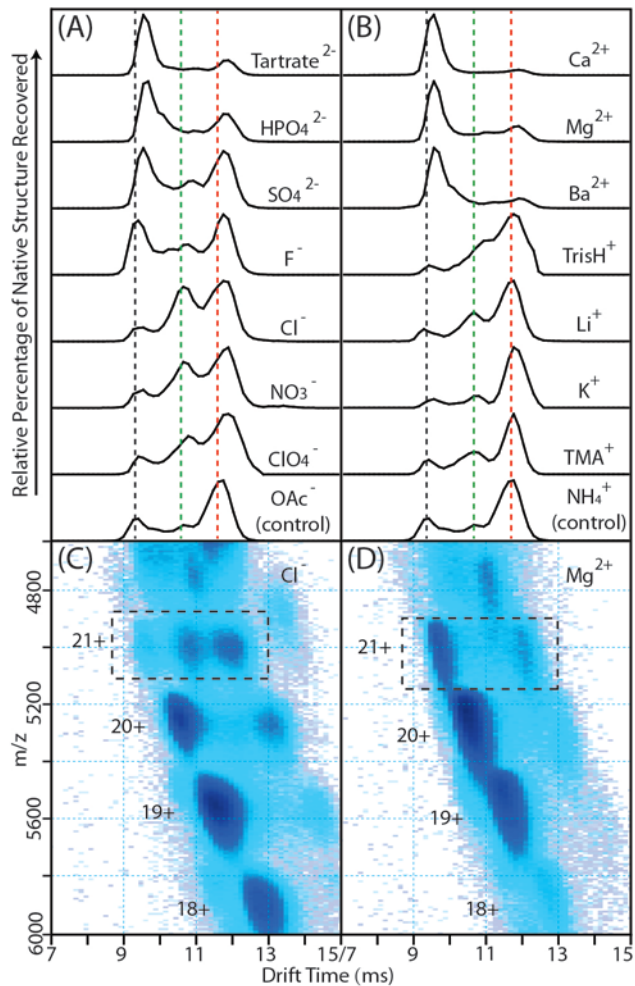


Figure 6-3. Hofmeister anions/cations recovering misfolded ConA. Drift time distributions measured for 21^+ charge state of ConA' tetramer in 100 mM ammonium acetate solutions (control, following freeze-thaw) are treated by increasing the concentration of Hofmeister anions (A) and cations (B) to 2mM prior to nESI, and are ordered according to the relative amount of ConA recovered. Dashed lines mark the peaks corresponding to ConA (black) and ConA' (red) together with a partially misfolded intermediate (green). The drift time versus m/z contour plots obtained for ConA' after the addition of Cl^- and Mg^{2+} are shown in (C) and (D), respectively, with the 21^+ charge state of the tetrameric species highlighted (black dashed box).

6.4.4 Monitoring the recovery of ConA' to ConA by salts in solution through CD and DSC

We undertook further DSC and CD measurements on ConA' samples treated with selected anions and cations to verify their action on protein structure in solution (Figure 6-4). For solution experiments designed to monitor anions-based recovery of ConA', we selected three anions (SO_4^{2-} , Cl^- and ClO_4^-) which are regarded as strongly, medium and weakly stabilizing agents respectively in the canonical Hofmeister series. In contrast to our nESI-IM-MS measurements,

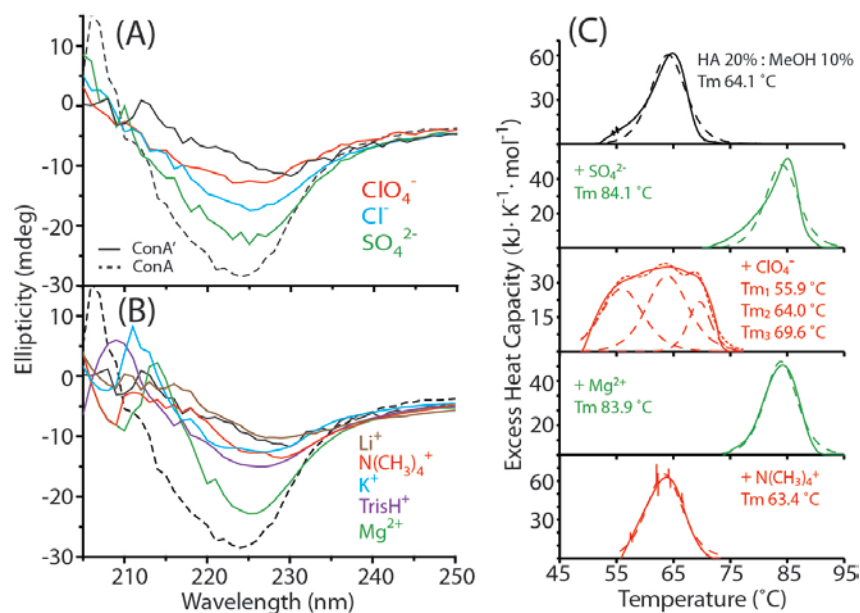


Figure 6-4. Recovery of the ConA' structure upon addition of specific salts in bulk solution. (A) and (B) are Far-UV CD spectra of 5 μM ConA' generated from 45% (vol/vol) MeOH (black solid) in the presence of 1 M ammonium-based anions (sulfate, chloride and perchlorate) and 1 M acetate-based cations (TMA, magnesium, potassium, lithium and tris), respectively. The CD spectrum corresponding to native ConA (black dotted) is also included for comparison. (C) DSC scans for 60 μM ConA' generated from 20%:10% (vol/vol) HAC: MeOH (top) with 1 M added ammonium sulfate, ammonium perchlorate, magnesium acetate and TMA acetate (bottom). The experimental data and fit data are indicated by solid and dashed line, respectively.

CD and DSC measurements in solution used salt concentrations high enough to elicit Hofmeister effects in bulk solution (1 M)³². As shown in Figure 6-4A, the absorption band at ~ 220 nm exhibits greater intensity upon addition of SO_4^{2-} (green) when compared to Cl^- (blue), indicating a more efficient recovery of β -sheet conformation, whereas ClO_4^- has little effect on the rescue of native ConA structure (red). As such, our CD data agree both with the Hofmeister series and our IM-MS data. Further agreement between solution and gas-phase results is discovered when DSC data acquired for ConA' prepared in 10% MeOH under weakly-acidic conditions is considered. In the presence of 1 M ammonium sulfate, native ConA stability is recovered, and perchlorate has no influence on protein stability (Figure 6-4C), also in agreement with IM-MS data. We note that solution pH changes by <0.2 when SO_4^{2-} and ClO_4^- are present in our experiments. Thus, it

is likely that the addition of SO_4^{2-} converts ConA' to ConA using the Hofmeister effect, rather than shifts in pH and buffer capacity. The recorded thermal unfolding transition for SO_4^{2-} containing ConA solutions results in a T_m shift from ~ 64 °C to ~ 84 °C, the latter a characteristic value for native ConA. Conversely, the DSC trace for ClO_4^- -incubated ConA' exhibits three main features all with depressed stabilities (T_m : 56, 64, 70 °C), indicative of a disrupted ConA structure. Taken together, anion data mirror our IM-MS measurements, and the expected Hofmeister series, precisely (Figure 6-3A).

Surprisingly, our CD and DSC data for added cations in solution follows an inverse Hofmeister series. For example, Mg^{2+} is a protein destabilizer in the canonical Hofmeister series, but acts to dramatically recover ConA structure (Figure 6-4B) and thermal stability (T_m : ~ 84 °C, Figure 6-4C), whereas $\text{N}(\text{CH}_3)_4^+$, an expected stabilizer, does not act to alter ConA conformation or stability in a measurable way. We attribute this result to the relatively negatively charged ConA surface under our conditions ($\text{pI}=5.4$) and the relatively low concentration for cations added (1 M), as has been previously observed for positively charged protein and anions in low abundance (<300 mM)^{32,33}. The discrepancy between the threshold concentrations needed to illicit reversed Hofmeister effects observed for anions and cations is likely due to the enhanced ability of anions to alter water structure, in general, which typically leads to their enhanced Hofmeister effect when compared to equivalent cations for experiments carried out in solution³². While this general result maps well onto our IM-MS dataset, the general agreement achieved between our IM-MS data and a previous survey of gas-phase only protein stability measurements provides, arguably, a better fit for the cation mediated stability shifts observed in this report¹¹. For example, Li^+ exhibits the poorest ability to stabilize ConA in solution, and predictions made from a reversed

Hofmeister point of view would typically place this cation as an intermediate destabilizer. It is therefore reasonable to conclude that a combined effect exists where cations are able to recover ConA' in solution and also prevent this rescued form from converting to an elongated quaternary structure upon desolvation by tethering the flexible regions of the protein complex during the transmission into the gas phase. In addition, in our reports, as in our data here, stronger shifts in protein stability were observed when multiply-charged salt additives were used versus those having a single charge, which we interpreted as related to the ability of such salts to form direct, multi-dentate interactions with the protein.

In summary, these data confirm that anions stabilize ConA in solution according to the Hofmeister series for biopolymers (Figure 6-4)^{13,14}. Conversely, CD and DSC measurements show that cations can act to stabilize ConA according to a 'reversed' Hofmeister series, likely due to its relatively low pI (5.4)³². Overall, our IM-MS data agrees well with our CD and DSC findings. We also note a strong correlation between the cation-related results shown in Figure 6-3, and our previous data aimed exclusively at gas-phase protein complex stability¹¹. Binding stoichiometries estimated from MS data (Figure IV-8) and the known selectivity of the ConA metal binding sites rule out the influence of specific cation-protein interactions in our dataset³⁴.

6.4.5 Possible mechanisms driving the CCS change in ConA tetramer, dimer and monomer

Based on our IM-MS (Figure 6-1, Figure IV-2, Figure IV-3, Figure IV-4) and CD/DSC (Figure 6-2) data, we have evaluated several potential mechanisms that explain the appearance of ConA' under some solution conditions. A pictorial summary of these are shown in Figure 6-5. In one

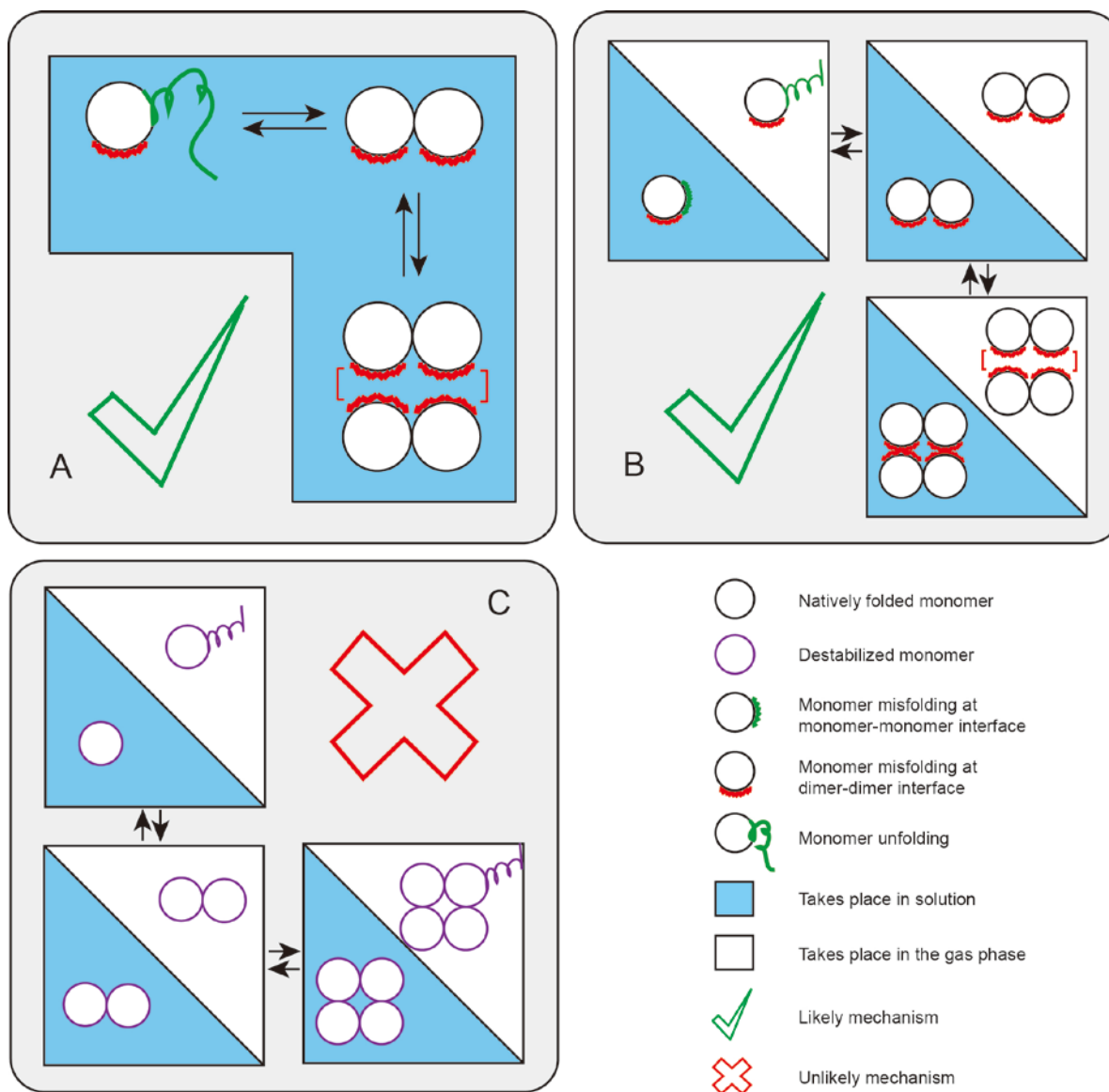


Figure 6-5. A schematic diagram showing three possible mechanisms that describe the formation of ConA' from ConA. See the legend included and the text for a detailed description.

scenario, the disruption of key H-bonds within the ConA dimer interface loosens it to produce ConA' in solution (Figure 6-5A). While this engenders misfolding at the interface, the rearranged tertiary structure is compact at the dimer scale and serves only to prevent the dimer-dimer interdigitation observed in native ConA. Monomers, once released from the dimer undergo unfolding at their now exposed monomer-monomer interfaces, producing a range of unfolded

structures. We treat each of these as equilibrium based (reversible) processes. In a related mechanism (Figure 6-5B) the ConA dimer-dimer interface is still loosened to create ConA', but dramatic changes in protein size occur only upon desolvation. This holds for monomers as well, where destabilized monomer units undergo dramatic unfolding only in the absence of solvent. In a final scenario considered (Figure 6-5C), monomer building blocks of ConA are destabilized in solution, leading to asymmetric unfolding of the tetramer in the gas phase to produce ConA'. Again, similar forces influence the monomers in the gas-phase, but not the dimers, potentially due to differential amounts or densities of charge deposited on each ion surface during nESI.

The first scenario (Figure 6-5A) has the strongest agreement with all of our data, in that our CD/DSC data show that large structure and stability changes occur in bulk solution. In the other two mechanisms shown in Figure 6-5, protein structure changes occur primarily in the gas-phase. Currently, however, we cannot map the magnitude of the structure changes observed in our solution-phase datasets to those obtained by IM-MS, therefore it is still possible that some portion of the structural change observed by IM-MS occurs as a direct result of desolvation. The third model shown (Figure 6-5C) invokes asymmetric unfolding of a single subunit to form ConA'. The gas-phase is the only environment where such asymmetric unfolding is thought to take place, and since our CD/DSC suggests that substantial unfolding/misfolding takes place in solution, that makes this mechanism less likely than the other two shown. If cation/anion recovery (Figure 6-3 and Figure 6-4) and CIU fingerprinting (Figure 6-5A and Figure 6-5B) data are included in our analysis, the model shown in Figure 6-5C becomes even less likely. These data invoke clear methods of recovery that take place in bulk solution, and critically show that the ConA' monomers that comprise the tetramer undergo similar unfolding to those in ConA,

suggesting that asymmetric unfolding has yet to take place in ConA' prior to collisional activation. Cation-based stabilization, while generally agreeing with results found for ConA in bulk solution shown in Figure 6-4, also agree with previous gas-phase stability measurements of protein-cation complexes, thus potentially lending more credence to the importance of the model shown in Figure 6-5B¹¹. Therefore, some combination of the models shown in Figure 6-5A and Figure 6-5B explain (and are consistent with) all of the data we present in this report.

6.4.6 Comparison of ConA salt stabilization to Literature Hofmeister effects

There are a number of different sets of results that describe the differential effects of salts on the stability and solubility of solutes in solution. For example, Randall and Failey studied the ability of different salts to solublize a range of different solutes, including gases (H₂, N₂, O₂, CO₂, NH₃, He, etc.) and other non electrolytes (I₂, nitrobenzaldehyde, etc.), developing a rank order for their influence with significant differences to Hofmeister's original order (where primarily protein solutes were studied)³⁵. For Anions, Randall and Failey's rank order is: SO₄²⁻ > ClO₄⁻ > Cl⁻ > CH₃COO⁻ > Br⁻, I⁻ > NO₃⁻ and Hofmeister's original rank order is: SO₄²⁻ > H₂PO₄⁻ > F⁻ > Cl⁻ > Br⁻, NO₃⁻ > ClO₄⁻³⁵. While we, at no point, attempted a strict quantification of the stabilities enhancements afforded by anions to ConA, our data shown in Figure 6-3 clearly is more highly-correlated with Hofmeister's original rank order than with the Randall and Failey order. For example, the Randall and Failey order classifies ClO₄⁻ as a relative stabilizer, whereas both our data and the Hofmeister order make the opposite assessment. Minor disagreements between our anion data and the canonical Hofmeister series can be seen in the relative positions of SO₄²⁻ and H₂PO₄⁻, which are reversed in our data, but still both classified as strongly stabilizing. This small discrepancy is unlikely to be significant, and we conclude that our data and the Hofmeister series

are strongly correlated. This result is not surprising, given the origins of the Randall and Failey rank order in the study of simple solutes, many of which can be treated as non-electrolytes. Recent data have strongly indicated that the charge and chemical nature of the solute is a key determining factor in the salt-based stabilization effects observed³².

Cation effects are less-studied in the Hofmeister community, as they are usually diminished in strength relative to their anionic analogs³². The typical rank order associated with the Hofmeister effect for protein solutes is: $\text{NH}_4^+ > \text{K}^+ > \text{Na}^+ > \text{Li}^+ > \text{Mg}^{2+} > \text{Ca}^{2+}$, while the Randall and Failey rank order is: $\text{Na}^+ > \text{K}^+ > \text{Li}^+ > \text{Ca}^{2+} > \text{Mg}^{2+} > \text{NH}_4^+$ ³⁵. Neither our IM-MS nor our DSC/CD data agrees with either of these rank orders, despite their differences. Strongest agreement is found to a reversed form of the Hofmeister rank order, or with our previous rank order that measures the stability of protein-cation complexes in the absence of solvent. While a reversed Hofmeister series agrees well with our IM-MS data, discrepancies exist when compared with our DSC/CD data. The key difference between the two datasets is Li^+ , which is intermediately stabilizing in our IM-MS data, but destabilizing in our DSC/CD data. However, overall, we observe good agreement between our solution and gas-phase datasets. Reversed Hofmeister effects have been observed in some instances in the context of anions in cases where the solute bears charges of opposite polarity¹⁴. The pI of ConA is 5.4, which gives the protein an overall negative charge at pH 7, potentially serving to drive to the reversal of the canonical Hofmeister series both in solution and reflected in our IM-MS data for ConA.

6.5 Conclusions

The implications of the data presented in this chapter are broad, and encompass many long-standing issues in gas-phase protein structure. The observation of ConA', which had eluded detailed structural characterization until this report, speaks to the power of the IM-MS approach for detecting such small, environment-dependent shifts in protein quaternary structure. Our model for the origin of ConA' invokes a loosened dimer-dimer interface for the tetramer²¹⁻²³, misfolded-yet-compact dimers, and monomers that unravel upon their release from higher order complexes. In addition, it is possible that desolvation may exaggerate the structural differences between ConA and ConA', leading to CCS values that, while predicated on clear structure changes in solution, result from conformers that are unique to the gas phase. Also, through the addition of specific anions and cations in solution we demonstrate that the differential recovery of ConA' to ConA can be followed in the gas phase by IM-MS. Our anion data agrees well with Hofmeister's original rank order, as well as recent biopolymer stability measurements in solution³⁵. Conversely, while agreeing well with our DSC and CD data, the relative abilities of cations to stabilize the ConA'/ConA transition agrees well with a reversed Hofmeister series, potentially owing to the negative charge of the protein at pH 7³². Furthermore, our data represent some of the strongest evidence to date suggesting a clear memory effect linking gas-phase protein structures to their analogs in solution³⁶⁻⁴¹. Recent evidence supporting a detailed solution memory for gas-phase biomolecules has focused on peptides⁴⁰, small proteins^{37,41}, and local interactions within larger biomolecules³⁹. The results shown here expand the scope of such evidence dramatically to include the global architecture of large multiprotein complexes, their misfolded analogs, and Hofmeister stabilization.

6.6 References

- (1) Robinson, C. V.; Sali, A.; Baumeister, W. *Nature* **2007**, *450*, 973.
- (2) Stefani, M.; Dobson, C. M. *J. Mol. Med.* **2003**, *81*, 678.
- (3) Misura, K. M. S.; Baker, D. *Proteins* **2005**, *59*, 15.
- (4) Zhang, Y. *Curr. Opin. Struct. Biol.* **2008**, *18*, 342.
- (5) Heck, A. J. R. *Nat. Methods* **2008**, *5*, 927.
- (6) Ruotolo, B. T.; Robinson, C. V. *Curr Opin Chem Biol* **2006**, *10*, 402.
- (7) Benesch, J. L. P.; Ruotolo, B. T. *Curr. Opin. Struct. Biol.* **2011**, *21*, 641.
- (8) Bagal, D.; Kitova, E. N.; Liu, L.; El-Hawiet, A.; Schnier, P. D.; Klassen, J. S. *Anal. Chem.* **2009**, *81*, 7801.
- (9) Freeke, J.; Bush, M. F.; Robinson, C. V.; Ruotolo, B. T. *Chem. Phys. Lett.* **2012**, *524*, 1.
- (10) Han, L.; Hyung, S.-J.; Mayers, J. J. S.; Ruotolo, B. T. *Journal of the American Chemical Society* **2011**, *133*, 11358.
- (11) Han, L. J.; Hyung, S. J.; Ruotolo, B. T. *Angew. Chem.-Int. Edit.* **2012**, *51*, 5692.
- (12) Merenbloom, S. I.; Flick, T. G.; Daly, M. P.; Williams, E. R. *J. Am. Soc. Mass Spectrom.* **2011**, *22*, 1978.
- (13) Record, M. T.; Zhang, W. T.; Anderson, C. F. *Adv. Protein Chem.* **1998**, *51*, 281.
- (14) Zhang, Y. J.; Cremer, P. S. *Curr Opin Chem Biol* **2006**, *10*, 658.
- (15) Clemmer, D. E.; Jarrold, M. F. *J. Mass Spectrom.* **1997**, *32*, 577.
- (16) Wyttenbach, T.; Bowers, M. T. *Modern Mass Spectrometry* **2003**, *225*, 207.
- (17) Zhong, Y. Y.; Hyung, S. J.; Ruotolo, B. T. *Expert Rev. Proteomics* **2012**, *9*, 47.
- (18) Giles, K.; Williams, J. P.; Campuzano, I. *Rapid Communications in Mass Spectrometry* **2011**, *25*, 1559.
- (19) Zhong, Y.; Hyung, S.-J.; Ruotolo, B. T. *Analyst* **2011**, *136*, 3534.
- (20) Hardman, K. D.; Ainsworth. *Biochemistry* **1972**, *11*, 4910.
- (21) Arrondo, J. L. R.; Young, N. M.; Mantsch, H. H. *Biochimica et Biophysica Acta (BBA) - Protein Structure and Molecular Enzymology* **1988**, *952*, 261.
- (22) Auer, H. E.; Schilz, T. *International Journal of Peptide and Protein Research* **1984**, *24*, 569.
- (23) Srinivas, V. R.; Reddy, G. B.; Ahmad, N.; Swaminathan, C. P.; Mitra, N.; Surolia, A. *Biochimica et Biophysica Acta (BBA) - General Subjects* **2001**, *1527*, 102.
- (24) Annesley, T. M. *Clinical Chemistry* **2003**, *49*, 1041.
- (25) Ruotolo, B. T.; Benesch, J. L. P.; Sandercock, A. M.; Hyung, S. J.; Robinson, C. V. *Nat Protoc* **2008**, *3*, 1139.
- (26) Hernandez, H.; Robinson, C. V. *Nat Protoc* **2007**, *2*, 715.
- (27) Bush, M. F.; Hall, Z.; Giles, K.; Hoyes, J.; Robinson, C. V.; Ruotolo, B. T. *Anal. Chem.* **2010**, *82*, 9557.
- (28) Taverner, T.; Hernandez, H.; Sharon, M.; Ruotolo, B. T.; Matak-Vinkovic, D.; Devos, D.; Russell, R. B.; Robinson, C. V. *Accounts Chem. Res.* **2008**, *41*, 617.
- (29) Naeem, A.; Khan, A.; Khan, R. H. *Biochemical and Biophysical Research Communications* **2005**, *331*, 1284.
- (30) Sinha, S.; Mitra, N.; Kumar, G.; Bajaj, K.; Surolia, A. *Biophysical Journal* **2005**, *88*, 1300.

- (31) Sanders, J. N.; Chenoweth, S. A.; Schwarz, F. P. *Journal of Inorganic Biochemistry* **1998**, *70*, 71.
- (32) Zhang, Y. J.; Cremer, P. S. In *Annual Review of Physical Chemistry, Vol 61*; Leone, S. R., Cremer, P. S., Groves, J. T., Johnson, M. A., Richmond, G., Eds.; Annual Reviews: Palo Alto, 2010; Vol. 61, p 63.
- (33) Zhang, Y. J.; Cremer, P. S. *Proceedings of the National Academy of Sciences of the United States of America* **2009**, *106*, 15249.
- (34) Shoham, M.; Kalb, A. J.; Pecht, I. *Biochemistry* **1973**, *12*, 1914.
- (35) Lo Nostro, P.; Ninham, B. W. *Chem. Rev.* **2012**, *112*, 2286.
- (36) Baumketner, A.; Bernstein, S. L.; Wytttenbach, T.; Bitan, G.; Teplow, D. B.; Bowers, M. T.; Shea, J. E. *Protein Sci.* **2006**, *15*, 420.
- (37) Jenner, M.; Ellis, J.; Huang, W. C.; Raven, E. L.; Roberts, G. C. K.; Oldham, N. J. *Angew. Chem.-Int. Edit.* **2011**, *50*, 8291.
- (38) Li, J. W.; Taraszka, J. A.; Counterman, A. E.; Clemmer, D. E. *Int. J. Mass Spectrom.* **1999**, *185*, 37.
- (39) Liu, L.; Michelsen, K.; Kitova, E. N.; Schnier, P. D.; Klassen, J. S. *Journal of the American Chemical Society* **2012**, *134*, 3054.
- (40) Pierson, N. A.; Chen, L. X.; Valentine, S. J.; Russell, D. H.; Clemmer, D. E. *Journal of the American Chemical Society* **2011**, *133*, 13810.
- (41) Wytttenbach, T.; Bowers, M. T. *J. Phys. Chem. B* **2011**, *115*, 12266

Chapter 7. Ion Mobility Mass Spectrometry Differentiates Multiprotein Complex Structures formed in Solution and in Electrospray Droplets

Han L, Ruotolo BT, Ion Mobility Mass Spectrometry Differentiates Multiprotein Complex Structures formed in Solution and in Electrospray Droplets, manuscript in preparation.

7.1 Abstract

IM-MS has become an essential tool in the characterization of peptide and protein self-assembly pathways implicated in the etiology of a number of human amyloid diseases. Here, we report IM-MS data for two large protein complexes, bovGDH and SAP, which possess higher-order complexes and multiple quaternary structure populations, one of which is strongly favored at high protein concentrations. Through the application of IM-MS, CID, and small molecule binding, we assign structures to these multi-conformer ions and link these data to their concentration dependence, enabling us to differentiate complexes that pre-exist in solution from those that most-likely form during electrospray ionization.

7.2 Introduction

MS has become an established technology for deciphering function and dysfunction of complicated biological entities¹⁻³. In combination with IM^{4,5}, MS has elucidated the assembly of

viral capsid proteins and characterized the structure of assembly intermediates^{6,7}. IM separates proteins and complexes based on their CCS, and such size information can be used, along with computational procedures, to deduce the three-dimensional structures of biomolecules⁸. When applied to the interrogation of peptide and protein oligomer populations formed during the early stages of fibrillar aggregates, IM-MS enabled the determination of previously unknown topologies and stoichiometries associated with pathological conditions, ranging from neurodegenerative disorders to systemic amyloidosis⁹⁻¹¹. Most recently, chemical CXL coupled with MS has emerged as a novel, robust tool to map proteome-wide interaction networks that govern critical cellular processes^{12,13}. While these MS-based approaches reveal the architecture and dynamics of complex oligomeric proteins and large-scale protein-protein connections within polydisperse systems at low concentrations¹⁴, determining the specificity of interactions that point to biological significance can still pose a challenge. Such difficulty arises from the formation of nonspecific complexes during ESI or its low-flow variant nanoflow ESI (nESI), used in MS analysis of protein complexes¹. When high protein concentrations are used in nESI, there is a significant probability of trapping more than one protein within the offspring droplets that give rise to ion formation. This leads to the production of non-specific assemblies, which are distinct from the interactions derived from the proteins having an affinity for each other in solution. Therefore, it is critical to discriminate between nESI-induced crowding artefacts and those truly reflective of those assemblies found in bulk solution. In order to tackle this problem, multiple strategies have emerged, including the use of non-binding reference proteins¹⁵, reporter molecules^{16,17}, HDX¹⁸, and Monte Carlo simulation¹⁹. However, in addition to observation of aberrant protein binding stoichiometries, which all of the methods above seek to obviate, it is possible that alternate protein quaternary structures are preferred in the crowded environment

found within rapidly evaporating nESI droplets²⁰⁻²². Here we report the first evidence that IM-MS can be applied to distinguish such conformational nESI-artefacts from those formed in bulk solution.

7.3 Experimental

7.3.1 Materials

GDH purified from bovine liver (bovGDH) and *Proteus spp.* (bacGDH) were purchased from Sigma (St. Louis, MO, USA). SAP purified from human serum and recombinant human CRP purified from *Escherichia coli* were purchased from Calbiochem (San Diego, CA, USA). Standards used to construct CCS calibration curves (CYC (equine heart), avidin (egg white), ConA (jack bean), ADG (*Saccharomyces cerevisiae*) and GDH (bovine liver)²³, and molecules used to perform the SAP-ligand binding experiment (calcium acetate and dAMP) were purchased from Sigma. Protein samples were buffer exchanged into 100 mM ammonium acetate at pH 7 (bovGDH, bacGDH and CCS calibrants) and pH 8 (SAP and CRP) using Micro Bio-Spin 6 columns (Bio-Rad, Hercules, CA) and prepared to a final concentration of 5 μ M to 80 μ M for bovGDH and 5 μ M to 30 μ M for SAP to perform concentration dependent analysis, and 5 μ M for CCS calibrants.

7.3.2 IM-MS

Sample aliquots (\sim 7 μ L) were analyzed using a quadrupole-IM-ToF MS instrument (Synapt G2 HDMS, Waters, Milford MA, USA)²⁴. Protein ions were generated using a nESI source in the positive mode, with the capillary typically held at 1.5 kV (for bovGDH and bacGDH) and 1.8 kV

(for SAP and CRP). The sample cone was operated at 20 V to avoid in-source activation. Instrument settings were optimized to allow transmission of intact protein complexes and to preserve non-covalent interactions^{4,25}. The trap traveling-wave ion guide was pressurized to 3.6×10^{-2} mbar of argon gas. The traveling-wave ion mobility separator was operated at a pressure of ~ 3.5 mbar, and employed a series of DC voltage waves (15 V wave height traveling at 150 m/s) to generate ion mobility separation with optimal resolution. The ToF-MS was operated over the m/z range of 800-15000 (for bovGDH and bacGDH) and 800-9000 (for SAP and CRP) and at a pressure of 1.8×10^{-6} mbar.

7.3.3 CID

Tandem-MS (Quad selection) mode was performed and collisional activation was performed as described previously using a trap collision voltage of 200 V, which is the maximum accessible voltage in the ion trap, was not sufficient to profoundly dissociate 52⁺, 55⁺ and 57⁺ charge state of bovGDH dodecamer precursor ions. Therefore the transfer collision voltage (Transfer CE, as indicated in the instrument control software) was used to further activate ions in the ion transfer traveling-wave ion guide, which sits after the ion mobility separator. The energy-dependent CID profile was constructed over the trap collision voltage range.

7.3.4 Ligand binding and CRP interaction

The SAP complex with Ca²⁺ and dAMP was formed by the addition of calcium acetate to SAP followed, after thorough mixing, by dAMP to final concentrations of 4 mM salt/ligand and 5 μ M SAP. The mixture was incubated at pH 8 for 18 hours at room temperature. To study the interactions between SAP and CRP, mixtures were incubated for 2 hours at a ratio of 1:1 in the

absence of calcium acetate. Excess ligands or other impurities were removed before analysis with a single Micro Bio-Spin buffer-exchange step.

7.3.5 Data analysis

Mass spectra were calibrated externally using a solution of cesium iodide (100 mg/mL) and processed with Masslynx V4.1 software (Waters, Milford MA, USA). CCS measurements were made using known CCS values of standards using the method described previously^{23,26}. It is noteworthy that the masses and mobilities of the bovGDH and bacGDH dodecameric ions are outbracketed by the current calibrant database, potentially resulting in small CCS errors (3-4%) as previously described²³.

7.3.6 Protein-protein docking

Protein-protein docking was performed with HEX 6.3 software²⁷ (<http://hex.loria.fr/>) using 'ligand' and 'receptor' PDB crystal structures of SAP (PDB ID: 1SAC) and CRP (PDB ID: 1GNH) from PDB (<http://www.rcsb.org./pdb>). Protein docking was employed to establish models for SAP/SAP (via 'ABAB' mode) and CRP/CRP (via 'BAAB', 'BABA' and 'ABBA' modes) stacked decamer formation that could potentially arise from nonspecific interaction and, therefore, no electrostatic correlation and energy minimization aimed to simulate biologically-relevant complex structure were employed. Instead, center-to-center distance between the two pentamers was assessed, using the existing crystal structure of SAP 'ABBA' decamer (PDB ID: 1LGN) as a reference. Carbohydrate is not visible in the SAP crystal structure and so, when constructing the SAP 'BAAB' model via carbohydrate-carbohydrate interaction, the oligosaccharide structure at Asn32 was modeled using the coordinates of the oligosaccharide

chain at the Fc region in the crystal structure of human IgG1 b12 (PDB ID: 1HZH) while the pentamers were rotated 36° relative to each other. This achieves the SAP ‘BAAB’ best-fit structure according to the previous X-ray and neutron scattering analysis, which leads to the center-to-center separation of 3.4-3.5 nm between the two pentamers, larger than that without carbohydrate interaction (2.7 nm)²⁸. Visualization of the docked complex was carried out using PyMol (<http://pymol.sourceforge.net/>) molecular graphic program.

7.3.7 Theoretical CCS determination

CCSs were calculated for the docked and crystal structures using PA method implemented in DriftScope V2.1 (Waters, Milford MA, USA). The PA CCS typically underestimates experimental CCS by 15%. For this reason, a scaled PA (eq. 1), based on an empirically determined scaling factor which accounts for scattering phenomena, any missing atoms and truncations carried out to the full-length protein for a high-resolution crystal structure of the complex, is used here to correlate experimental CCS with model structures.

$$CCS_{calc} = 1.14 \times CCS_{PA} \left(\frac{M_{exp}}{M_{pdb}} \right)^{\frac{2}{3}} \quad (1)$$

7.4 Results and Discussion

7.4.1 IM-MS reveals biomodal dodecamer conformations for bovGDH

GDH is a homohexameric enzyme ubiquitous in most organisms, playing a pivotal role in nitrogen and carbon metabolism²⁹. Unlike primitive organisms, mammalian GDH exhibits strong negative cooperativity with respect to the coenzyme and is heavily regulated by a wide array of allosteric effectors³⁰⁻³². Mammalian GDH is a stacked dimer of trimers, with each subunit

composed of three domains: the Glu binding domain, the NAD binding domain, and the antenna domain, which is not found in bacterial and fungal GDHs³¹. These antennae protrude from the three subunits within the trimers and wrap around each other, facilitating intersubunit communication during negative cooperativity and allosteric regulation, which is unique to the animal kingdom³⁰.

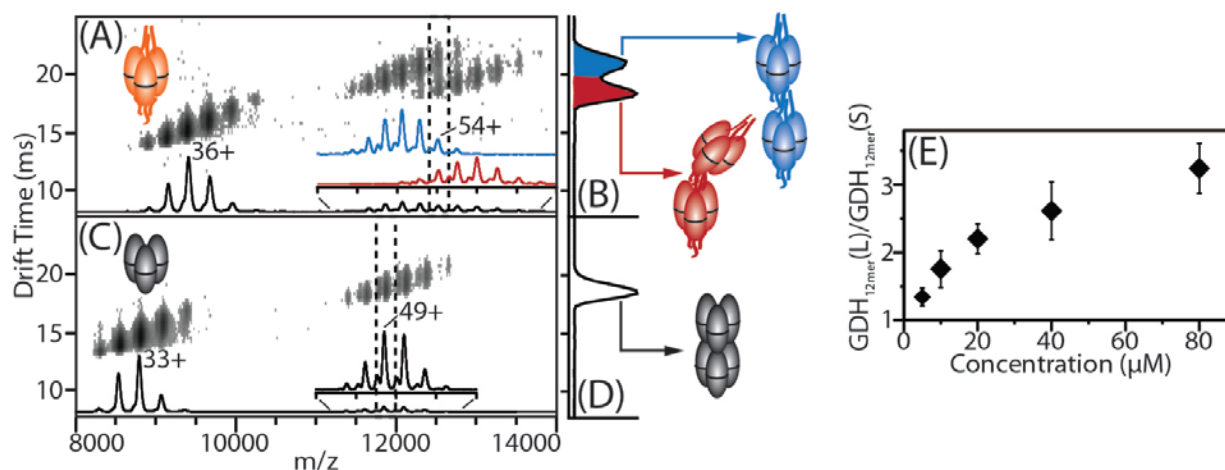


Figure 7-1. IM-MS reveals bimodal dodecamer conformations for boVGDH. IM-MS data for boVGDH. (A) and bacGDH (C) acquired from pH~7 ammonium acetate buffered solutions (20 µM) and at identical instrument conditions reveal ion signals for both hexamer and dodecamer. Bimodal and unimodal drift time distributions are observed for the 54⁺ charge state of boVGDH dodecamer (B) and the 49⁺ bacGDH dodecamer (D), respectively. Concentration-ramp analysis is performed where the abundance ratio of larger over smaller boVGDH dodecamer is plotted against concentrations (E).

Figure 7-1A shows the IM-MS data for boVGDH sprayed from 100 mM ammonium acetate buffered solution (pH=7.0), revealing the presence of intact hexamer (ca. 337 kDa) with 36⁺ as the most-intense charge state. More surprisingly, a second species is also observed at lower abundance, which is consistent with a dimerized assembly (ca. 675 kDa) displaying two different features. The observation of two dodecameric families is attributed to IM separation as indicated by two series of peaks in ATD (Figure 7-1B), with measured CCS values of 21,798 Å² ±0.7%

and $23,885 \text{ \AA}^2 \pm 1\%$. In addition, a remarkable shift in charge state distribution by ca. 6% between these large and small dodecameric species (blue and red respectively, inset Figure 7-1A) is consistent with the difference in their experimental CCS. It is noteworthy that this observation is not a result of gas-phase unfolding by using the minimal activation conditions. Instead, the abundance of the larger bovGDH dodecamer relative to the smaller one increases as the protein concentration is raised in solution (Figure 7-1E, Figure V-2), indicating that this form is generated primarily from crowding forces within nESI droplets. In addition, by comparing experimental CCS values with those calculated from the existing protein-protein packing architectures visible between X-ray unit cells using the scaled PA method, we assign the larger bovGDH dodecamer to a linearized quaternary structure ($23,371 \text{ \AA}^2$), where the small hexamer-hexamer contact area is generated by the antenna regions. The smaller dodecamer is assigned to a bent quaternary structure ($22,751 \text{ \AA}^2$) which bears substantially larger hexamer-hexamer contacts, in that the antenna of one interacts with both the top of the NAD domain and the antenna of the adjacent hexamer³³ (Figure 7-1B, Table V-1). The bent topology is strongly favored since the catalytic mouth of bovGDH opens in its apo state, under which it tends to form long filaments with a more helical arrangement that was previously observed in both XRD³³ and TEM³⁴ experiments. This polymerization process is thought to play an essential role in the crowded environment of the mitochondria through the formation of multienzyme complexes^{33,35}, though the connection between higher-order assembly and enzymatic activity remains the subject of debate^{36,37}. These data indicate that the smaller curvature bovGDH dodecamer originates from more specific protein-protein interactions that are of critical biological significance, since the bovGDH sample is not bound with any substrates or coenzymes as demonstrated by measurement of bovGDH under denaturing conditions (Figure V-1). To further verify this

assignment, we performed experiments on bacterial GDH (bacGDH, hexamer, ca. 290 kDa), which shares a 92% fold similarity with bovGDH but lacks the antenna region (Table V-3). Ions observed for this protein in dodecameric form display only a single conformation (Figure 7-1C and Figure 7-1D), thus confirming the importance of the bovGDH antenna in driving the formation of bimodal dodecamer conformations. The average CCS obtained is in close agreement with theoretical values based on the bacGDH docked model (Table V-1), which is attributed to non-specific protein-protein associations since GDH self-polymerization is rare in bacterial cells³⁸.

7.4.2 Larger dodecameric bovGDH follows an atypical CID pathway

To further characterize the two observed bovGDH dodecamers, CID was performed. Dodecameric bovGDH ions at 52⁺, which predominantly adopt the smaller conformation (Figure 7-1A), follow the asymmetric dissociation CID pathway common within protein complex CID datasets, marked by the ejection of highly charged monomers (red, Figure 7-2A). In contrast, 57⁺ dodecamer ions adopting primarily the larger conformational state (Figure 7-1A) dissociate into not only unfolded monomers, but also hexamers with charge states centered at 30⁺, which accounts for nearly half of the charge carried by the precursor, and is thus a ‘symmetric’ dissociation pattern (blue, Figure 7-2A). 55⁺ ions, that adopt both structures for the dodecamer, display a similar CID profile observed for the 57⁺ described above, however we detect hexamer products ions in lower abundance (purple, Figure 7-2A). It is important to note that this atypical dissociation behavior for larger bovGDH dodecamer is not charge state-driven, as no products of symmetric dissociation are observed for any charge state of the bacGDH dodecameric precursor (Figure 7-2B).

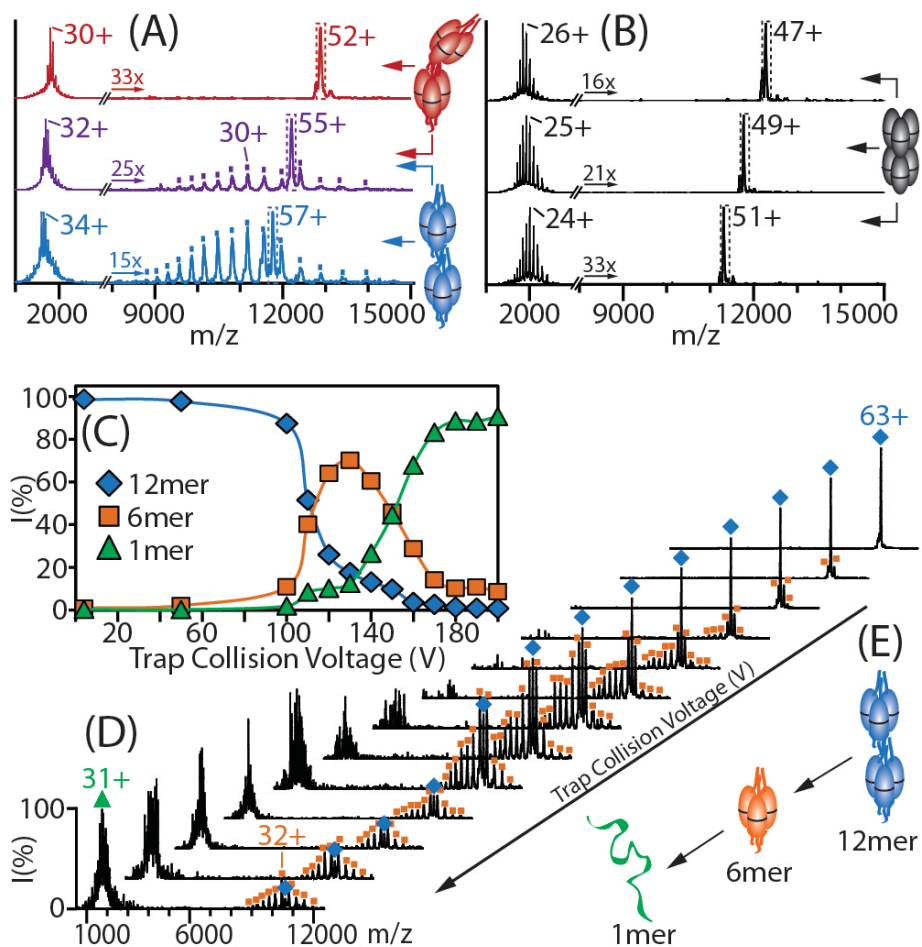


Figure 7-2. Larger dodecameric boGDH follows an atypical CID pathway. Tandem MS data of boGDH dodecamer precursors of the 52⁺, 55⁺ and 57⁺ charge state at trap collision voltage of 200 V and transfer collision voltage of 150 V (A) is compared with that of 47⁺, 49⁺ and 51⁺ bacGDH dodecamer at trap collision voltage of 180 V (B). Plot of precursor and product ion intensity for the larger boGDH dodecamer versus trap collision voltage indicates that hexamer formation is a low-energy intermediate product ion (C). Stacked CID MS spectra of the larger boGDH dodecameric ions at 63⁺ (D). Schematic representation illustrates its unique CID pathway (E).

In order to characterize its unusual gas-phase dissociation, CID datasets were generated for the larger boGDH dodecamer at elevated trap collision voltages (Figure 7-2D). Figure 7-2C shows the relative intensity of dodecamer precursor and hexamer/monomer products as a function of collisional voltages, indicating that the larger boGDH dodecamer is susceptible to dissociation into compact hexamers, which is in good agreement with our aforementioned assignment

towards a linearized quaternary structure with a weak hexamer-hexamer interface. A portion of the monomer products arise from hexamers ejected with excess kinetic energy undergoing subsequent dissociation (Figure 7-2E). Meanwhile, we cannot rule out the release of monomers directly from the dodecamer precursor during CID, revealed by the concurrence of low-signal monomeric and hexameric product ions at the early stage of the energy ramp (Figure 7-2C and Figure 7-2D).

The observation of symmetric CID product ion populations for boVGDH has far-reaching implications. Previous research has identified other multiprotein complexes which display this unusual CID behavior, including ‘charge-reduced’ TTR ions³⁹, ‘supercharged’ pentameric SAP⁴⁰ and dodecameric boiling SP-1 ions⁴¹, where their unusual form of dissociation is thought to be governed by the overall charge density of the precursor ions selected for activation. Only two protein complexes have been reported that dissociate atypically in the absence of charge manipulation agents: the hetero hexameric textilotoxin⁴² and the tetrameric 2-keto-3-deoxyarabinonate⁴³. The atypical textilotoxin dissociation is driven by the inability of subunits to unfold, due to the presence of several intramolecular disulfide bonds, while the atypical CID pattern observed in the 2-keto-3-deoxyarabinonate is attributed to one dimer-dimer interface being much smaller than the other. This suggests that the unusual CID behavior of the larger boVGDH dodecamer results from an intimate relationship between subunit architecture and gas-phase dissociation behavior. As such, the data presented here broaden significantly the potential uses of CID data for determining the structural details of multiprotein complexes.

7.4.3 IM-MS reveals biomodal decamer conformations for SAP

IM-MS analysis of intact human SAP in the absence of Ca^{2+} at pH 8.0 reveals a bimodal drift time distribution for the decamer, highlighting two distinct gas-phase structures (Figure 7-3A and Figure 7-3B). This has been reported formerly, but no detailed elucidation was provided⁴⁴. As the principal member of the pentraxin family of plasma proteins, SAP adopts a planar, disc-like configuration composed of 5 identical subunits, and is named for its universal association with amyloid deposits *in vitro*, protecting them from proteolysis⁴⁵. The two faces of the SAP pentamer, defined as A and B, are characterized by five α -helices and five double Ca^{2+} -binding sites⁴⁶, which is indicated by red and green in the model structure respectively (Figure 7-3A). Notably, each SAP monomer is glycosylated with a single N-linked biantennary oligosaccharide at Asn32 on the A-face⁴⁷ (yellow in the model structure, Figure 7-3A). SAP pentamers can be packed face-to-face, and decamers formed from the A-A⁴⁸, A-B⁴⁹, and B-B⁴⁶ interface have all been reported, dependent upon solution conditions. In Ca^{2+} -free solution at alkaline pH, SAP pentamers have been previously shown by X-ray and neutron scattering to be stacked between the A-faces via carbohydrate-carbohydrate interactions²⁸. The scattering analysis favored the ‘BAAB’ configuration in which two pentamers were out of alignment by a 36° rotation and the oligosaccharide chains were extended such that the decamer was somewhat loosely-packed. More importantly, specific carbohydrate interactions between the two pentamers rotated by 36° resemble those between the two oligosaccharide chains at the center of the Fc fragment of IgG, based on which we constructed the SAP ‘BAAB’ decamer model (Table V-2). Good agreement is found between its computationally calculated CCS ($11,244 \text{ \AA}^2$) and the experimental value that corresponds to the larger SAP decamer observed in the IM dataset ($11,302 \text{ \AA}^2 \pm 1.3\%$, Figure 7-3B). By contrast, we ascribe the smaller SAP decamer shown in bimodal conformations to

‘ABBA’ or ‘ABAB’ type which is more tightly-packed (Figure 7-3B), as evidenced by the similarity between experimental and theoretical CCS (Table V-2). In the absence of Ca^{2+} and other biologically-important small molecules, this ‘ABBA’ or ‘ABAB’ decamer is not stabilized and we identify it as likely resulting from a nESI crowding effect that is concentration-dependent (Figure 7-3E). Control data for CRP, which lacks glycosylation but shares 96% fold similarity with SAP (Table V-3), exhibits a single conformational state (Figure 7-3C and Figure 7-3D), which is assumed to incorporate ‘BAAB’, ‘ABBA’ or ‘ABAB’ decameric structures with CCS values that cannot be resolved by IMS separation (Table V-2), thus strongly supporting this assignment.

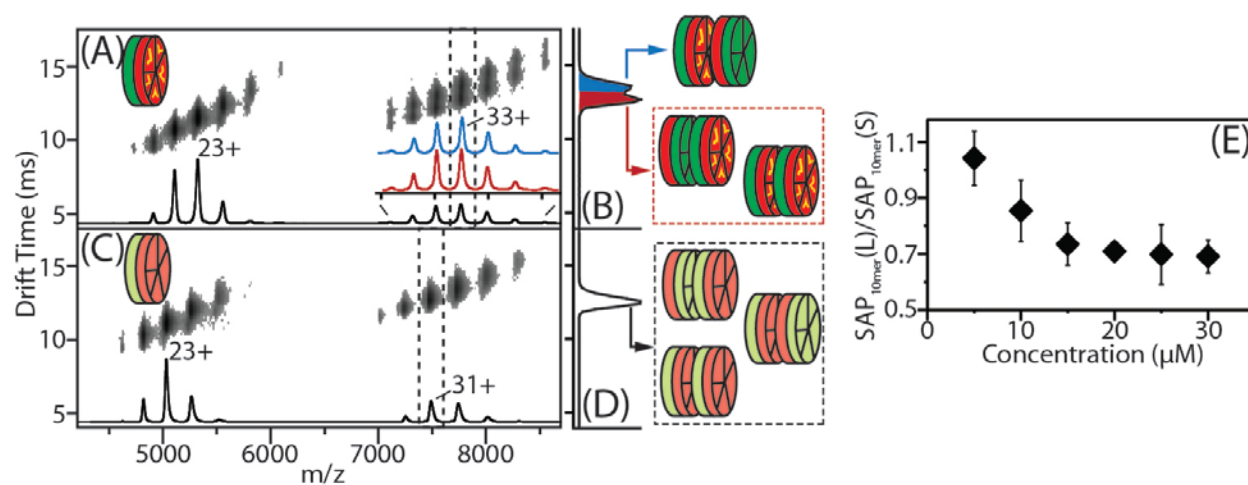


Figure 7-3. IM-MS reveals bimodal decamer conformations for SAP. IM-MS data for SAP. (A) and CRP (B) acquired from pH8 ammonium acetate (10 μM) and at identical instrument conditions reveal ion signals for both pentamer and decamer. Bimodal and unimodal drift time distributions are observed for the 33^+ charge state of the SAP decamer (B) and the 31^+ CRP decamer (D) respectively. Concentration-ramp analysis is performed where the abundance ratio of larger over smaller SAP decamer (E) is plotted against concentration.

7.4.4 Ligand binding experiments drive the formation of a specific SAP decamer

To further validate the role of glycan-glycan interaction at the A-A interface in driving the formation of loosely-packed SAP decamer, SAP was mixed 1:1 with CRP, which is non-

glycosylated. In the absence of Ca^{2+} the abundant signal has a molecular mass of $242,709 \pm 7$ Da, corresponding to a species comprised of one SAP pentamer and one CRP pentamer (purple, Figure 7-4A). This suggests that CRP binds preferentially to SAP to form a mixed decamer in Ca^{2+} -free buffer. As expected, no bimodal drift time distribution is found for this hetero-decamer (purple, Figure 7-4C), similar to CRP homo-decamer (orange, Figure 7-4C). To verify this, we incubated SAP in the presence of physiological levels of Ca^{2+} with dAMP, which is known to favor SAP 'ABBA' decamer formation by bridging the two Ca^{2+} ions of each monomer and stabilizing a B:B face decamer via ligand base stacking⁴⁶. Figure 7-4B shows a trimodal charge state distribution, representative of SAP decamers with no (red), half (green) and full (blue) occupancy of dAMP. Upon completion of dAMP load, the population of SAP decamer structures shifts significantly from the larger CCS to the smaller CCS conformer (red \rightarrow green \rightarrow blue, Figure 7-4C), in line with the enrichment of 'ABBA' type decamer by the ligand, further strengthening the structural assignment.

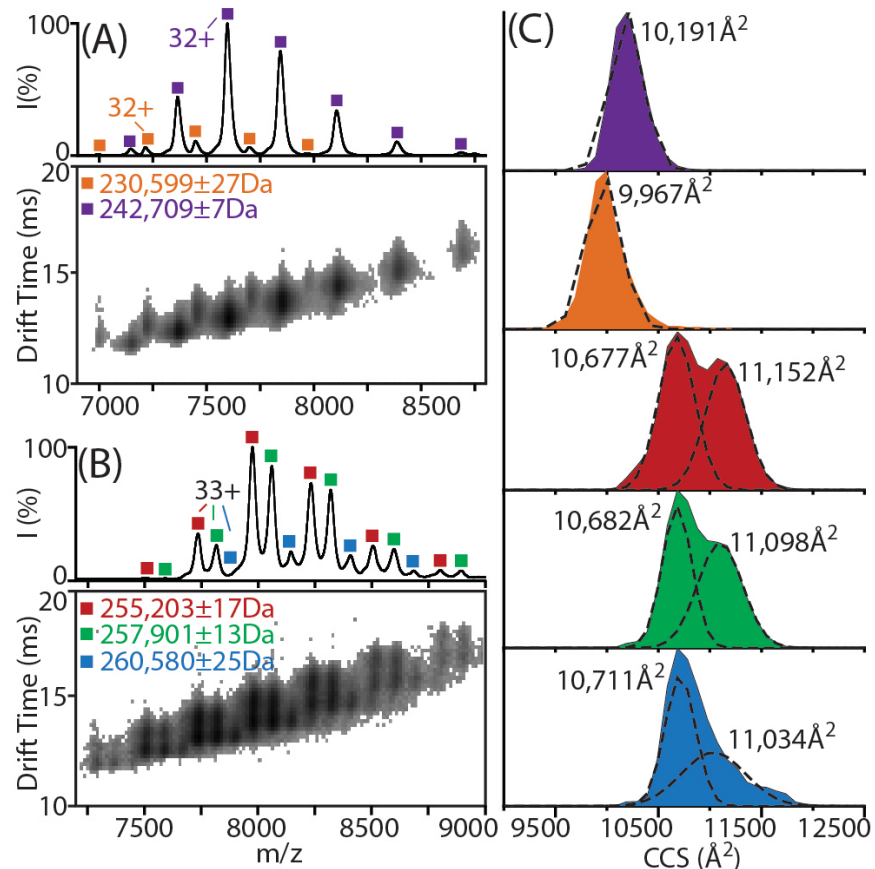


Figure 7-4. Ligand binding experiments drive the formation of a specific SAP decamer. IM-MS data of SAP and CRP (1:1) acquired in the absence of Ca^{2+} reveal the dominant presence of a new decameric species stacked between one SAP pentamer and one CRP pentamer (purple), as well as CRP decamer at very low abundance (orange) (A). IM-MS data of SAP after 18 h of incubation in the presence of calcium acetate and dAMP exhibit three different SAP decamers with no (red), half (green) and full (blue) occupancy of dAMP (B). CCS distributions are shown for 32^+ charge state of these five species with matching colors (C). The Gaussian-fitted data are indicated by dashed lines, with CCS values shown for the centroid.

7.5 Conclusions

This chapter addresses one of the pivotal challenges in IM-MS, that is to differentiate between biologically relevant and artifactual interactions within macromolecules in the gas phase. Using well studied multiprotein systems we demonstrate, for the first time, that IM-MS data can differentiate between specific and nonspecific protein-protein interactions in boVGDH and SAP. IM-MS for boVGDH presents strong signals for both hexamer and dodecamer at low ($5 \mu\text{M}$)

concentrations, the latter of which possess a bimodal IM distribution. The larger of these two bovGDH dodecamers is strongly favored as the protein concentration is raised in solution, indicating that this form is generated primarily from crowding forces within nESI droplets. By filtering experimental CCS values against the many protein-protein packing architectures visible between X-ray unit cells, we assign the larger bovGDH structure to a linearized quaternary structure, where the small hexamer-hexamer contact area is driven by interactions between the protruding 'antenna' regions. The smaller bovGDH structure is assigned a bent quaternary structure that bears substantially larger hexamer-hexamer contacts. These assignments were confirmed using bacGDH, which shares a 92% fold similarity with bovGDH but lacks the antenna region. Ions observed for this protein display a single conformation, thus confirming the importance of the bovGDH antenna in driving the formation of bimodal dodecamer conformations. Finally, and most surprisingly, the larger bovGDH dodecamer follows an atypical CID pathway, resulting in hexamer product ions. This unusual CID phenomenon is not observed in either the smaller bovGDH form or bacGDH dodecamers, and clearly supports our structural assignment. Comparable data for SAP reveals two dodecamer forms of the assembly, one of which is attributed to nESI crowding effects. In this case, bimodal conformations are ascribed to the sites of glycosylation on one face of the SAP pentamer, creating a glycan-glycan contact face conformer that is larger than other possible dodecamer forms. This assignment is confirmed both through control data for CRP, which lacks glycosylation but shares 96% fold similarity with SAP, and through ligand binding experiments that drive the formation of specific complexes.

The implications of the data presented here are broad and encompass long-standing issues in gas phase structural proteomics. An urgent challenge in this field is the need to distinguish specific

from nonspecific protein-protein interactions in nESI MS. This is analogous to a fundamental challenge in X-ray crystallography, where nonspecific interfaces are formed by the crystal contacts that are not subject to any natural selection and thus lack biological specificity⁵⁰. Whereas the geometries and chemical compositions of interfaces are generally used for comparison between specific *versus* crystal-packing contacts⁵¹, we have endeavored to take advantage of the global complex structure as a probe to differentiate protein-protein interactions of biological relevance from those derived from the crowding effect. The work presented in this chapter highlights the potential value IM-MS could bring to this field by resolving the binary quaternary structure populations for the bovGDH dodecamer and the human SAP decamer. This capability could provide important new insight into crucial structural biology fields in human medicine, including the characterization of different topologies in the oligomerization of amyloid-related proteins⁵², as well as elucidating different compositions in the aggregation of monoclonal antibody products in the biotherapeutics pipeline⁵³.

7.6 References

- (1) Benesch, J. L. P.; Ruotolo, B. T.; Simmons, D. A.; Robinson, C. V. *Chemical Reviews* 2007, 107, 3544.
- (2) Heck, A. J. R.; van den Heuvel, R. H. H. *Mass Spectrometry Reviews* 2004, 23, 368.
- (3) Wyttenbach, T.; Bowers, M. T. In *Annual Review of Physical Chemistry* 2007; Vol. 58, p 511.
- (4) Ruotolo, B. T.; Benesch, J. L. P.; Sandercock, A. M.; Hyung, S. J.; Robinson, C. V. *Nature Protocols* 2008, 3, 1139.
- (5) Uetrecht, C.; Rose, R. J.; van Duijn, E.; Lorenzen, K.; Heck, A. J. R. *Chemical Society Reviews* 2010, 39, 1633.
- (6) Knapman, T. W.; Morton, V. L.; Stonehouse, N. J.; Stockley, P. G.; Ashcroft, A. E. *Rapid Communications in Mass Spectrometry* 2010, 24, 3033.
- (7) Uetrecht, C.; Versluis, C.; Watts, N. R.; Wingfield, P. T.; Steven, A. C.; Heck, A. J. R. *Angewandte Chemie-International Edition* 2008, 47, 6247.
- (8) Politis, A.; Park, A. Y.; Hyung, S. J.; Barsky, D.; Ruotolo, B. T.; Robinson, C. V. *Plos One* 2010, 5.

- (9) Bleiholder, C.; Dupuis, N. F.; Wyttenbach, T.; Bowers, M. T. *Abstracts of Papers of the American Chemical Society* 2011, 242.
- (10) Smith, D. P.; Radford, S. E.; Ashcroft, A. E. *Proceedings of the National Academy of Sciences of the United States of America* 2010, 107, 6794.
- (11) Young, L. M.; Cao, P.; Raleigh, D. P.; Ashcroft, A. E.; Radford, S. E. *Journal of the American Chemical Society* 2014, 136, 660.
- (12) Herzog, F.; Kahraman, A.; Boehringer, D.; Mak, R.; Bracher, A.; Walzthoeni, T.; Leitner, A.; Beck, M.; Hartl, F. U.; Ban, N.; Malmstrom, L.; Aebersold, R. *Science* 2012, 337, 1348.
- (13) Stengel, F.; Aebersold, R.; Robinson, C. V. *Molecular & Cellular Proteomics* 2012, 11.
- (14) Hyung, S. J.; Ruotolo, B. T. *Proteomics* 2012, 12, 1547.
- (15) Sun, J. X.; Kitova, E. N.; Wang, W. J.; Klassen, J. S. *Analytical Chemistry* 2006, 78, 3010.
- (16) Sun, J.; Kitova, E. N.; Sun, N.; Klassen, J. S. *Analytical Chemistry* 2007, 79, 8301.
- (17) Sun, N.; Sun, J. X.; Kitova, E. N.; Klassen, J. S. *Journal of the American Society for Mass Spectrometry* 2009, 20, 1242.
- (18) Hossain, B. M.; Konermann, L. *Analytical Chemistry* 2006, 78, 1613.
- (19) Lane, L. A.; Ruotolo, B. T.; Robinson, C. V.; Favrin, G.; Benesch, J. L. P. *International Journal of Mass Spectrometry* 2009, 283, 169.
- (20) Lin, H.; Kitova, E.; Johnson, M.; Eugenio, L.; Ng, K. S.; Klassen, J. *Journal of the American Society for Mass Spectrometry* 2012, 23, 2122.
- (21) Hogan, C. J.; Ruotolo, B. T.; Robinson, C. V.; Fernandez de la Mora, J. *The Journal of Physical Chemistry B* 2011, 115, 3614.
- (22) Mora, J. *Journal of the American Society for Mass Spectrometry* 2012, 23, 2115.
- (23) Bush, M. F.; Hall, Z.; Giles, K.; Hoyes, J.; Robinson, C. V.; Ruotolo, B. T. *Analytical Chemistry* 2010, 82, 9557.
- (24) Zhong, Y.; Hyung, S.-J.; Ruotolo, B. T. *Analyst* 2011, 136, 3534.
- (25) Hernandez, H.; Robinson, C. V. *Nature Protocols* 2007, 2, 715.
- (26) Taverner, T.; Hernandez, H.; Sharon, M.; Ruotolo, B. T.; Matak-Vinkovic, D.; Devos, D.; Russell, R. B.; Robinson, C. V. *Accounts Chem. Res.* 2008, 41, 617.
- (27) Ritchie, D. W.; Venkatraman, V. *Bioinformatics* 2010, 26, 2398.
- (28) Ashton, A. W.; Boehm, M. K.; Gallimore, J. R.; Pepys, M. B.; Perkins, S. J. *Journal of Molecular Biology* 1997, 272, 408.
- (29) Smith, T. J.; Peterson, P. E.; Schmidt, T.; Fang, J.; Stanley, C. A. *Journal of Molecular Biology* 2001, 307, 707.
- (30) Smith, T. J.; Schmidt, T.; Fang, J.; Wu, J.; Siuzdak, G.; Stanley, C. A. *Journal of Molecular Biology* 2002, 318, 765.
- (31) Peterson, P. E.; Smith, T. J. *Structure with Folding & Design* 1999, 7, 769.
- (32) Li, M.; Li, C. H.; Allen, A.; Stanley, C. A.; Smith, T. J. *Neurochemistry International* 2011, 59, 445.
- (33) Banerjee, S.; Schmidt, T.; Fang, J.; Stanley, C. A.; Smith, T. J. *Biochemistry* 2003, 42, 3446.
- (34) Josephs, R.; Borisy, G. *Journal of Molecular Biology* 1972, 65, 127.
- (35) Barry, R. M.; Gitai, Z. *Current Opinion in Microbiology* 2011, 14, 704.
- (36) Cohen, R. J.; Benedek, G. B. *Journal of Molecular Biology* 1979, 129, 37.

- (37) Zeiri, L.; Reisler, E. *Journal of Molecular Biology* 1978, 124, 291.
- (38) Aghajanian, S.; Hovsepian, M.; Geoghegan, K. F.; Chirunyk, B. A.; Engel, P. C. *Journal of Biological Chemistry* 2003, 278, 1067.
- (39) Pagel, K.; Hyung, S. J.; Ruotolo, B. T.; Robinson, C. V. *Analytical Chemistry* 2010, 82, 5363.
- (40) Hall, Z.; Politis, A.; Bush, M. F.; Smith, L. J.; Robinson, C. V. *Journal of the American Chemical Society* 2012, 134, 3429.
- (41) Erba, E. B.; Ruotolo, B. T.; Barsky, D.; Robinson, C. V. *Analytical Chemistry* 2010, 82, 9702.
- (42) Aquilina, J. A. *Proteins-Structure Function and Bioinformatics* 2009, 75, 478.
- (43) van den Heuvel, R. H. H.; van Duijn, E.; Mazon, H.; Synowsky, S. A.; Lorenzen, K.; Versluis, C.; Brouns, S. J. J.; Langridge, D.; van der Oost, J.; Hoyes, J.; Heck, A. J. R. *Analytical Chemistry* 2006, 78, 7473.
- (44) Zhou, M. W.; Huang, C. S.; Wysocki, V. H. *Analytical Chemistry* 2012, 84, 6016.
- (45) Tennent, G. A.; Lovat, L. B.; Pepys, M. B. *Proceedings of the National Academy of Sciences of the United States of America* 1995, 92, 4299.
- (46) Hohenester, E.; Hutchinson, W. L.; Pepys, M. B.; Wood, S. P. *Journal of Molecular Biology* 1997, 269, 570.
- (47) Pepys, M. B.; Rademacher, T. W.; Amatayakulchantler, S.; Williams, P.; Noble, G. E.; Hutchinson, W. L.; Hawkins, P. N.; Nelson, S. R.; Gallimore, J. R.; Herbert, J.; Hutton, T.; Dwek, R. A. *Proceedings of the National Academy of Sciences of the United States of America* 1994, 91, 5602.
- (48) Emsley, J.; White, H. E.; Ohara, B. P.; Oliva, G.; Srinivasan, N.; Tickle, I. J.; Blundell, T. L.; Pepys, M. B.; Wood, S. P. *Nature* 1994, 367, 338.
- (49) Thompson, D.; Pepys, M. B.; Tickle, I.; Wood, S. *Journal of Molecular Biology* 2002, 320, 1081.
- (50) Bahadur, R. P.; Zacharias, M. *Cellular and Molecular Life Sciences* 2008, 65, 1059.
- (51) Bahadur, R. P.; Chakrabarti, P.; Rodier, F.; Janin, J. *Journal of Molecular Biology* 2004, 336, 943.
- (52) Bleiholder, C.; Do, T. D.; Wu, C.; Economou, N. J.; Bernstein, S. S.; Buratto, S. K.; Shea, J. E.; Bowers, M. T. *Journal of the American Chemical Society* 2013, 135, 16926.
- (53) Paul, R.; Graff-Meyer, A.; Stahlberg, H.; Lauer, M.; Rufer, A.; Beck, H.; Briguet, A.; Schnaible, V.; Buckel, T.; Boeckle, S. *Pharm Res* 2012, 29, 2047.

Chapter 8. Conclusions and Future Directions

8.1 Conclusions

As the critical importance of protein-protein interactions becomes more defined, the capability of MS experiments to study protein flexibility, heterogeneity and polydispersity will position this tool for dramatically increased use in the future^{1,2}. For example, our current pool of structural MS technologies include: HDX, CXL, OFP, limited proteolysis, AP, and IM separation, and each of these are actively establishing themselves as crucial tandem technologies for revealing the structure of multiprotein complexes at various levels of structural resolution³. However, the ionization of intact multiprotein complexes and their removal from bulk solvent, while likely preserving a substantial portion of protein structure and organization, imposes a foreign environment on proteins that may cause structural rearrangements to occur, not reflective of their native conformational state. Thus, it is also necessary to develop the general strategies aimed at protecting the structure of multiprotein complexes, at every level, in the absence of bulk solvent, in parallel with MS technologies capable of measuring gas-phase protein structure. Efforts have been made in this area by tuning instrumental conditions^{4,5}, manipulating analyte charge state⁶ and employing the specific ligand binding⁷⁻⁹. The approach taken in this thesis (Chapters 2-5) involves the protection of gas-phase protein complex structure through the addition of salts in solution prior to ionization/desolvation. We have screened a series of Hofmeister-type cations¹⁰ and anions¹¹ for their ability to increase the structural stability of multiprotein complexes in the

absence of bulk solvent. By assessing the CID and CIU profiles of several multiprotein systems in the gas phase upon addition of cations and anions respectively on the Synapt G2 IM-MS platform, the stability afforded to the multiprotein complexes by ions was determined quantitatively, leading to the mechanistic understanding of stabilization. Our data shows that cations and anions stabilize gas-phase protein structures through different mechanisms. For example, cations tend to tightly bind protein complexes and act to reduce Coulombic unfolding¹⁰. In stark contrast to cations, anion-protein complexes exhibit primarily a ‘dissociative cooling’ type mechanism characterized by the dissociation of protein-bound anions upon collisional activation¹¹. These differences have led us to study the combined effects of stabilizing cations and anions on gas-phase proteins, and identify those salts that bear anion/cation pairs having the strongest stabilizing influence on protein structures in vacuo^{12,13}. Furthermore, we demonstrate the ability of Hofmeister anions and cations to recover the structure of ‘misfolded’ or partially-denatured proteins prior to IM-MS analysis and measurement (Chapter 6)¹⁴.

In addition to the potential for structural rearrangement of proteins upon transfer into the gas phase, it is possible that nonspecific protein-protein/ligand complexes could be produced the ESI¹⁵. Such nonspecific interactions do not reflect the solution stoichiometry or structures, and can thus frustrate the ability of MS to interrogate polydisperse, dynamic protein assemblies as well as the solution oligomers related to protein aggregation. IM-MS experiments performed for this thesis (Chapter 7) seek to identify the origins of protein complex structures, not just stoichiometries, in a manner related to the ESI process. Our IM-MS data differentiates between specific and artefactual multiprotein conformations for two systems: bovGDH and SAP.

8.2 Further directions

8.2.1 Develop specific small molecule strategies for stabilizing the native-like structure of gas phase proteins

As an alternative to salt-based protein stabilization for gas-phase proteins, organic molecules interacting with protein ions to increase structural stability should be further developed in the future. The general strategy would likely revolve non-covalent small organic molecules that bind to a specific location on a protein surface to replace solvent contacts or around potential protein charge sites for structure stabilization. CE type molecules and sugars would both work stabilizing agents that target different regions of the protein structure. Stated more specifically, crown ethers (Figure 8-1A) preferentially form complexes with ionized basic residues exposed on the protein surface¹⁶; and sugar molecules can form interactions with the hydrophilic surface of soluble proteins (Figure 8-1B). As reported by Pagel *et al*¹⁷, CE compounds bind non-covalently to primary amines, *e.g.* lysine side chains, and serve to solvate the ionic charge present. The IM-MS data collected showed that CE binding can compensate for rearrangements local to the charge site observed for CYC. This is an excellent reason to suspect that CE binding to charge carrying residues will produce a measurable increase in structural stability by shielding the protein from Coulombic strain and, thus, protect topological information. In a similar fashion, sugar molecules can be chosen to preferentially interact with the hydrophilic surface of protein complexes, and thus stabilize the surface structure of gas-phase assemblies. In addition, chemical cross-linking could be utilized for tethering of extremely flexible protein regions into fixed positions for maximum stability in the gas phase (currently being pursued by the Ruotolo group in collaboration with Phil Andrews, UM Biological Chemistry).

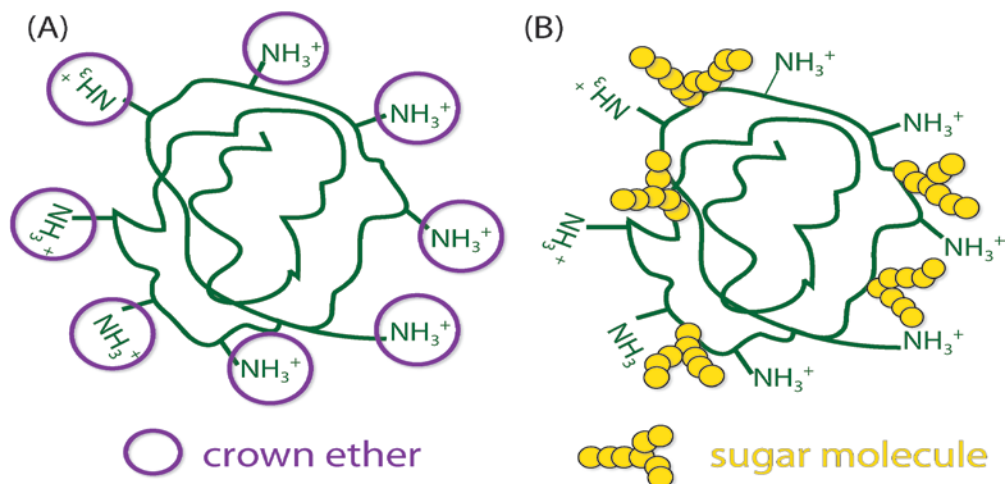


Figure 8-1. Develop specific small molecule strategies for stabilizing the native-like structure of gas phase proteins. (A) CE binds -NH_3^+ exposed on the protein surface and form n:1 (CE:protein) types of supramolecular complexes. (B) Polysaccharides bind to proteins through hydrophobic interactions

These new strategies could be rapidly applied to an ever-expanding roster of challenging, flexible protein systems that seem to undergo spontaneous remodeling in the absence of bulk solvent. An example of an excellent target system for such stabilization efforts is the trimeric protein complex composed of 3 DnaX (τ/γ) protein subunits (Figure 8-2A), which interacts with δ and δ' to form the clamp loader, the asymmetric pentameric ring¹⁸, and is critically important in DNA replication. It has been shown that the DnaX (τ/γ) trimer, which is an ATP-driven motor, is a highly-flexible protein that possesses both an open and closed state. However, such structural flexibility apparently causes the protein complex to collapse into a closed form upon transfer to the gas phase¹⁹ (Figure 8-2C). Protein structure stabilization strategies could be used to retain both its closed and open structures when in the absence of bulk solvent (Figure 8-2B).

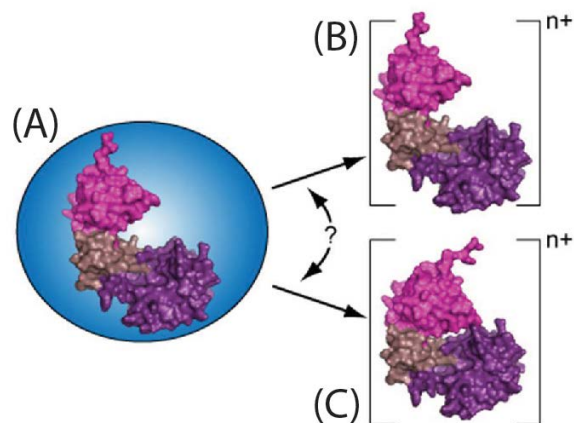


Figure 8-2. Open and closed structures of DnaX (τ/γ) trimer. The open form of DnaX (τ/γ) trimer as the functional component of clamp loader (A) collapses into a closed state (C) when transmitted to the gas phase. Strategies need to be developed to retain its open structure in the solvent-free environment (B).

8.2.2 Develop IM-MS for differentiating disulfide-mediated structural isoforms in monoclonal antibodies

This thesis has highlighted the unique capacity of IM-MS to capture small, environment-dependent shifts in the higher-order structure of a large multiprotein complex, and to differentiate specific and nonspecific protein-protein interactions, respectively. A growth area for IM-MS involves distinguishing between different disulfide patterns in monoclonal antibodies. Monoclonal antibody drugs have been fast developed during the past decades due to its high specificity and low side-effects²⁰. However, due to the large-scale manufacturing and recombinant DNA technology is employed, antibody products are subject to multiple modes of degradations²¹. One of the most common degradation products is disulfide scrambling, as exemplified by human IgG2 produced recombinantly in Chinese hamster ovary (CHO) cells, where three distinct disulfide-related structural isoforms were revealed by chromatographic and electrophoretic methods²². Compared with these relatively slow techniques, IM-MS has been

demonstrated for the rapid characterization of its disulfide variants, which makes itself a potential high-throughput QC tool for these protein biopharmaceuticals in the near future^{22,23}.

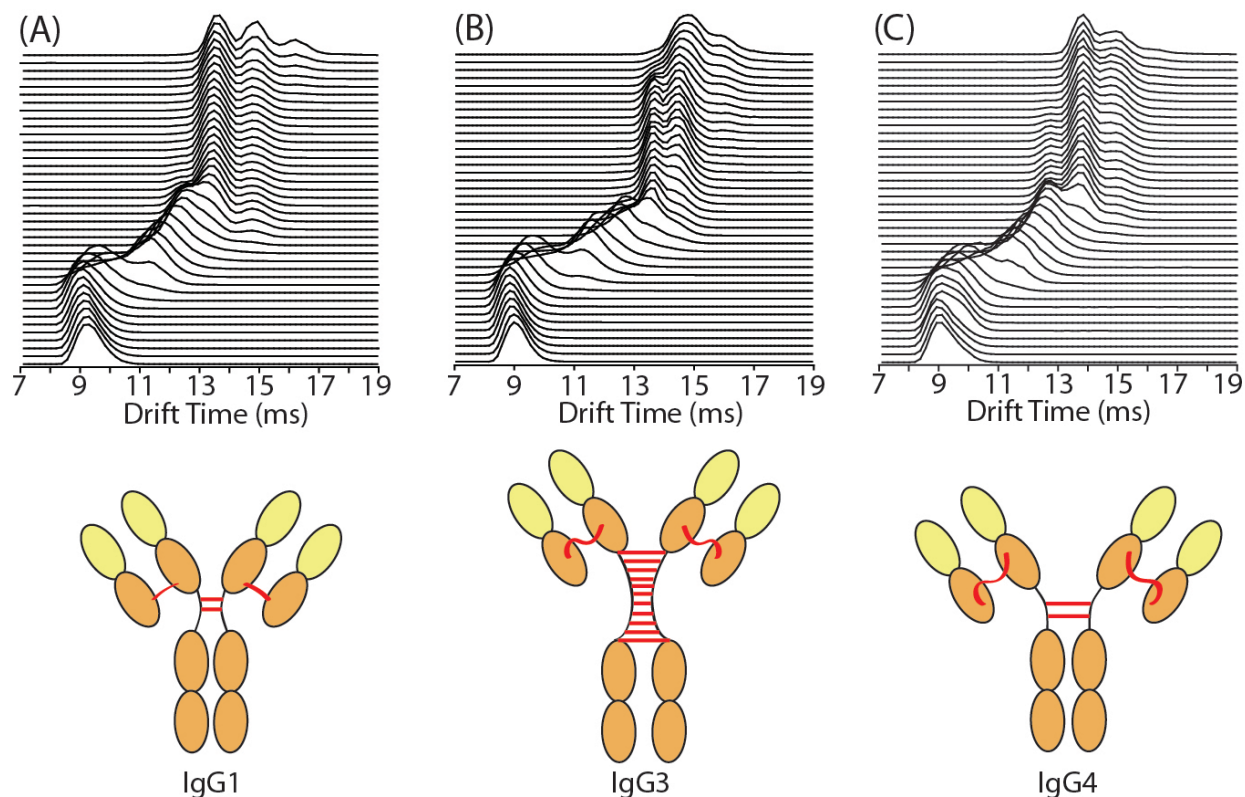


Figure 8-3. CIU ‘fingerprints’ reveal disulfide pattern differences in IgG subclasses. Stacked drift time distributions of human IgG1 (A), IgG3 (B) and IgG4 (C) at elevated trap collision voltages ranging from 5 V to 200 V, reveal the differences, responsive to various antibody disulfide patterns.

Nevertheless, the IM separation on commercially-available platforms fails to resolve all the three disulfide variants, which opens possibilities for a CIU ‘fingerprint’ protocol to better detect the antibody disulfide heterogeneity. The CIU ‘fingerprint’ is characterized by the changes in the tertiary/secondary structures of protein ions induced during the CIU process, leading to several structural ensembles that are stable on the millisecond timescale, hence it enables us to observe not only ground-state compact structure, but also a series of activated conformational families^{8,12,13}. Figure 8-3 shows the CIU fingerprints for purified IgG1, IgG3 and IgG4 from

human myeloma plasma which share the same light chain (kappa) and heavy chain (gamma). Significant differences are observed between IgG1 and IgG3 fingerprints, each having different amounts of inter-disulfide linkages (Figure 8-3A and B), and more importantly, between IgG1 and IgG4, which possess equal numbers of inter S-S bonds but different disulfide bonding patterns (Figure 8-3A and C). Future work in this area will undoubtedly aim to enlarge the pool of antibodies with known disulfide bond patterns, such that we can build an ‘antibody disulfide CIU fingerprint database’ for the identification of unknown species and the quantification of disulfide bonds and pattern isoforms quickly.

8.2.3 Develop IM-MS for distinguishing various topologies in antibody dimerization

In addition to disulfide scrambling, another aspect of antibody degradation involves the formation of antibody oligomers and higher molecular weight aggregates. Aggregation of a monoclonal antibody can result from several types of stresses encountered during production, transport, and storage such as exposure to low pH during chromatographic separation, high temperature excursions, stress during flow filtration, freeze-thaw and freeze-drying processes, exposure to silicone oil, tungsten, and other materials in syringes and, agitation during transportation²⁴. Given the complex issues surrounding antibody aggregates, there is interest in understanding this phenomenon as it pertains to therapeutic influence (i.e., efficacy), bioactivity, and stabilization²⁵.

Antibody dimers tend to make up the predominant species of antibody aggregates²⁶, and to become the intermediates towards the high molecular weight (HMW) aggregates²⁷. Various types of antibody dimers can be formed in different subclasses and under different stresses. For

example, an IgG2 dimer formed at pH 6.0 was found to have identical secondary and tertiary structure as the intact antibody molecule. It was the covalent dimer consisted of both disulfide linked antibody molecules and another species (~26%) that was formed due to nondisulfide covalent bonds between two heavy chains. However, the dimer formed at pH 4.0 have altered secondary and tertiary structure²⁷. In contrast, the dimerized form of an IgG1 monoclonal antibody (Roche) was found to majorly bear non-covalent components, and adopt different association geometries under three different stress conditions revealed by SEC-HPLC and TEM²⁸. Shown in Figure 8-4, dimers induced by process stress were associated by a single non-covalent interaction site between two Fab domains in a characteristic “bone-like” structure. Low pH stress generated more stable but also non-covalently associated dimers without chemical alterations in a typical “closed” conformation. Light-induced dimers, exhibiting various different conformations, were the most stable dimers with various chemical modifications leading to a broad range in size, charge and hydrophobicity. These dimers showed differential potency and antigen binding affinity. While pH stress dimer showed bioactivity and antigen binding affinity similar to the native monomer, light stress dimer fully lost its positive performance.

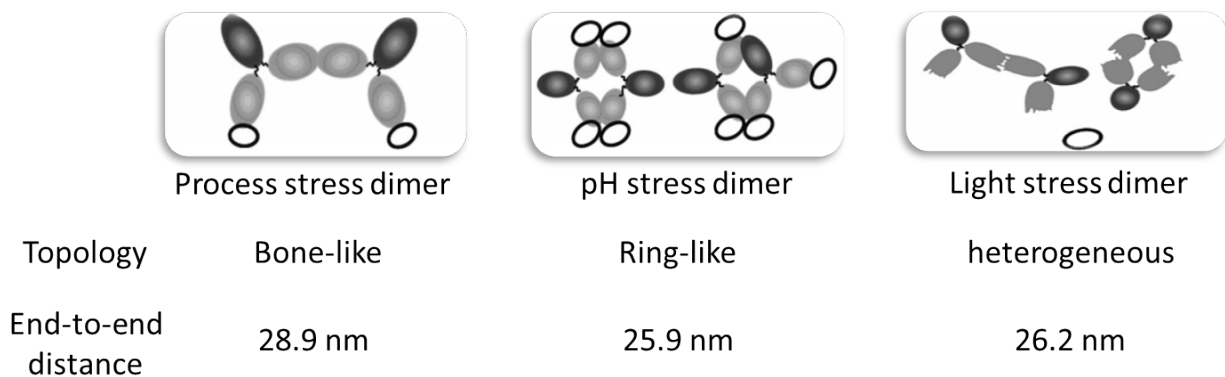


Figure 8-4. Schematic representations of the three proposed dimer conformations and their ability to bind antigen. The Fab domain of the antibody is shown in grey and the Fc domain in black. The antigen is represented by the oval-shaped open circles.

These differences in the conformation and interaction type for antibody dimers, and in turn their differential therapeutic influence (*i.e.*, efficacy), prompt the development of a powerful technology to differentiate between these ‘good’ vs ‘bad’ dimers in industrial settings. Therefore, future efforts should be made to develop IM-MS for the quick identification of different dimers based on their sizes and shapes, and further the detailed elucidation of antibody aggregation pathways under various stresses.

8.3 References

- (1) Robinson, C. V.; Sali, A.; Baumeister, W. *Nature* **2007**, *450*, 973.
- (2) Sali, A.; Glaeser, R.; Earnest, T.; Baumeister, W. *Nature* **2003**, *422*, 216.
- (3) Hyung, S. J.; Ruotolo, B. T. *Proteomics* **2012**, *12*, 1547.
- (4) Laganowsky, A.; Reading, E.; Hopper, J. T. S.; Robinson, C. V. *Nature Protocols* **2013**, *8*, 639.
- (5) Ruotolo, B. T.; Benesch, J. L. P.; Sandercock, A. M.; Hyung, S. J.; Robinson, C. V. *Nature Protocols* **2008**, *3*, 1139.
- (6) Morgner, N.; Robinson, C. V. *Current Opinion in Structural Biology* **2012**, *22*, 44.
- (7) Wyttenbach, T.; Grabenauer, M.; Thalassinos, K.; Scrivens, J. H.; Bowers, M. T. *Journal of Physical Chemistry B* **2010**, *114*, 437.
- (8) Hyung, S.-J.; Robinson, C. V.; Ruotolo, B. T. *Chemistry & Biology* **2009**, *16*, 382.
- (9) Ruotolo, B. T.; Giles, K.; Campuzano, I.; Sandercock, A. M.; Bateman, R. H.; Robinson, C. V. *Science* **2005**, *310*, 1658.
- (10) Han, L. J.; Hyung, S. J.; Ruotolo, B. T. *Angewandte Chemie-International Edition* **2012**, *51*, 5692.
- (11) Han, L. J.; Hyung, S. J.; Mayers, J. J. S.; Ruotolo, B. T. *Journal of the American Chemical Society* **2011**, *133*, 11358.
- (12) Han, L. J.; Hyung, S. J.; Ruotolo, B. T. *Faraday Discussions* **2013**, *160*, 371.
- (13) Han, L.; Ruotolo, B. *International Journal for Ion Mobility Spectrometry* **2013**, *16*, 41.
- (14) Han, L. J.; Ruotolo, B. T. *Angewandte Chemie-International Edition* **2013**, *52*, 8329.
- (15) Benesch, J. L. P.; Ruotolo, B. T.; Simmons, D. A.; Robinson, C. V. *Chemical Reviews* **2007**, *107*, 3544.
- (16) Ly, T.; Julian, R. R. *Journal of the American Society for Mass Spectrometry* **2006**, *17*, 1209.
- (17) Warnke, S.; von Helden, G.; Pagel, K. *Journal of the American Chemical Society* **2013**, *135*, 1177.
- (18) Gulbis, J. M.; Kazmirski, S. L.; Finkelstein, J.; Kelman, Z.; O'Donnell, M.; Kuriyan, J. *European Journal of Biochemistry* **2004**, *271*, 439.

- (19) Park, A. Y.; Jergic, S.; Politis, A.; Ruotolo, B. T.; Hirshberg, D.; Jessop, L. L.; Beck, J. L.; Barsky, D.; O'Donnell, M.; Dixon, N. E.; Robinson, C. V. *Structure* **2010**, *18*, 285.
- (20) Chames, P.; Van Regenmortel, M.; Weiss, E.; Baty, D. *British Journal of Pharmacology* **2009**, *157*, 220.
- (21) Yu, B. L.; Vizel, A.; Young, M.; Morando, A.; He, B. *Abstracts of Papers of the American Chemical Society* **2007**, 234.
- (22) Bagal, D.; Valliere-Douglass, J. F.; Balland, A.; Schnier, P. D. *Analytical Chemistry* **2010**, *82*, 6751.
- (23) Jones, L. M.; Zhang, H.; Cui, W. D.; Kumar, S.; Sperry, J. B.; Carroll, J. A.; Gross, M. L. *Journal of the American Society for Mass Spectrometry* **2013**, *24*, 835.
- (24) Brych, S. R.; Gokarn, Y. R.; Hultgen, H.; Stevenson, R. J.; Rajan, R.; Matsumura, M. *Journal of Pharmaceutical Sciences* **2010**, *99*, 764.
- (25) Rosenberg, A. *AAPS J* **2006**, *8*, E501.
- (26) Gronski, P.; Seiler, F. R.; Schwick, H. G. *Molecular Immunology* **1991**, *28*, 1321.
- (27) Van Buren, N.; Rehder, D.; Gadgil, H.; Matsumura, M.; Jacob, J. *Journal of Pharmaceutical Sciences* **2009**, *98*, 3013.
- (28) Paul, R.; Graff-Meyer, A.; Stahlberg, H.; Lauer, M. E.; Rufer, A. C.; Beck, H.; Briguët, A.; Schnaible, V.; Buckel, T.; Boeckle, S. *Pharmaceutical Research* **2012**, *29*, 2047.

Appendices

Appendix I. Chapter 2 Supporting Information

Stabilization of avidin tetramer by salt additives is dependent on additive concentration.

In order to test the hypothesis that binding of anion additives influences the stability of multiprotein complexes, we generated protein ions under different concentrations of anion additives (chloride and perchlorate, selected for their stabilizing and mildly destabilizing effect, respectively) and investigated their stability with respect to CIU and CID. Larger concentrations of anion additives are expected to increase the population of anion-bound protein complex ions. Indeed, the amount of residual additives that remain bound to protein ions was shown to be positively correlated to the concentration of additive anion (data for CYC, not shown). When interrogated for their stability with respect to unfolding and dissociation, the protein complex becomes increasingly stabilized with higher concentration of additives (Figure I-1). Interestingly, perchlorate, which was classified for its destabilizing character, results in protein ions more stable above a threshold concentration around ~20 mM. Thus, together with the result presented in Figure 2-5A, these results demonstrate that the quantity of anions that remain bound to protein complexes after desolvation is a key determinant for the stability of protein-anion complexes.

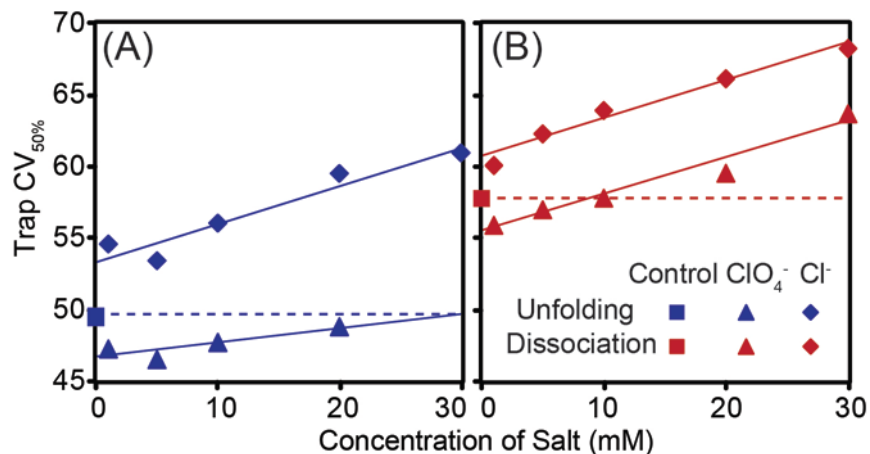


Figure I-1. Stabilization of avidin tetramer by salt additives is dependent on additive concentration. Plots charting the trap collision voltages required to dissociate (A) and unfold (B) 50% of the tetrameric protein ion population for avidin are shown for control (square), perchlorate (triangle), and chloride (diamond). A clear positive correlation between the concentration of salt and the trap collision voltage is indicated with a solid line

Anion additives stabilize BLA, a dimeric protein

The anion-based strategy for stabilizing protein complex was tested on a dimeric protein complex (BLA). The stability of BLA in the presence of a range of solution additives (20 μ M of BLA incubated in 200 μ M anion additive with ammonium acetate buffer) was assessed by interrogating 11⁺ charge state of the complex with a trap collision voltage ramp applied prior to IM-MS separation. The result shows a clear increase in the activating voltage required to unfold and dissociate the protein with addition of salts in solution (Figure I-2). Plots of the collision energy (eV*) at which 50% of the complex dissociate or unfold reveals the relative ability of the anions to influence the processes. For example, nitrate, chloride and tartrate are identified as strong stabilizers, while bicarbonate and perchlorate are weak or non-stabilizing additives. The results show an excellent agreement with the classifications derived in the main text of our paper, despite significant differences in the quaternary structure and oligomeric state.

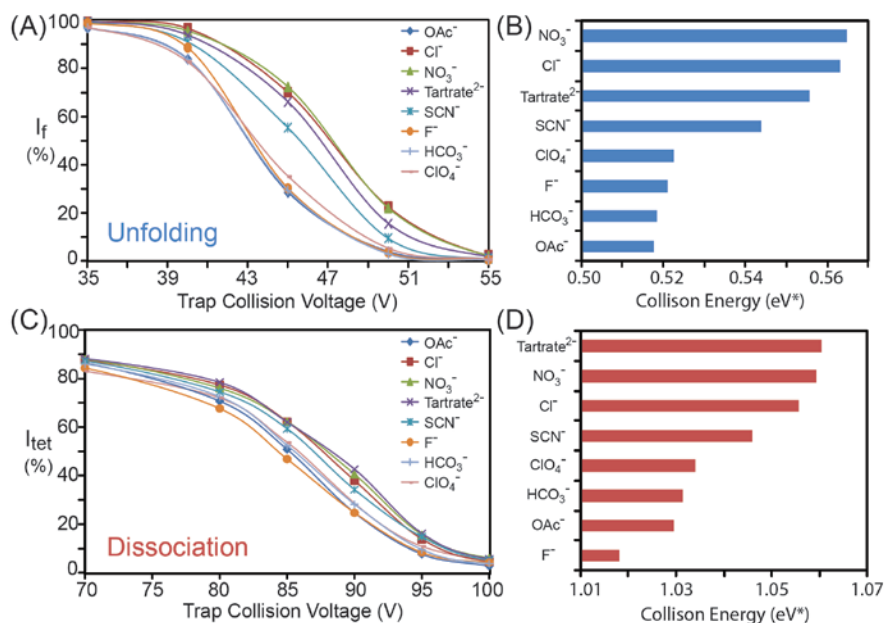


Figure I-2. Anion additives stabilize BLA, a dimeric protein. Plots of the relative intensities of compact BLA 11^+ ions (I_f , A) and the relative intensities of BLA 11^+ ions (I_{tet} , B) are shown as a function of trap collision voltage. Histogram plots charting the collision energy required to unfold (C) and dissociate (D) 50% of the protein ion are shown for a range of anion additives.

Binding affinity of anion additives is related to both solution-phase and gas-phase physical parameters

Our study into the mechanistic details of gas-phase protein structure stabilization through anion additives proposes that both the binding affinity of anions to protein complex, and the ease of dissociation of adducts from protein complex, are key processes that affect the stability of protein complexes in the gas phase. Physical constants that are thought to be associated with such processes were compiled into Table I-1. We observe that less acidic anions with high pKa, such as acetate, fluoride, and bicarbonate have weak affinity and are weak stabilizers of gas-phase protein structure (Figure I-3). By contrast, anions with intermediate pKa, including chloride and nitrate, are acidic thus bind more strongly and act as protein structure stabilizers in the absence of bulk solvent. Interestingly, those anions that are most acidic, such as iodide and perchlorate are weak protein structure stabilizers in the gas-phase. The pKa and gas-phase acidity,

however, predicts that the affinity of these anions for protein will be high. Thus, these parameters should provide a good estimation of the extent of adduct formation, and indicates that the best stabilizers have intermediate values of pKa and gas-phase acidity.

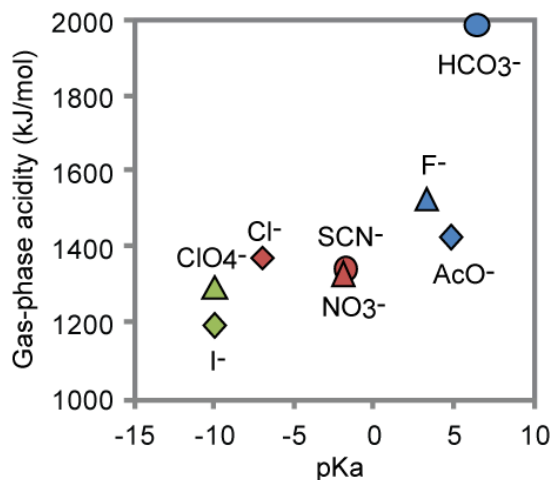


Figure I-3. A plot of the gas-phase acidity against pKa reveals a positive correlation between them. The colour indicates weak (blue), intermediate (green) and good stabilizer (red) of protein complex structure in gas-phase.

CIU data reveal subtle differences in the partially unfolded intermediates

Insights into the mechanism by which the bound anion population stabilizes the structure of multiprotein complexes can be examined by probing the CIU pathway taken by the assembly, and how the stabilities of intermediate structures populated along the unfolding pathway are altered upon changing the counter-ions bound to the complex. Protein complex unfolding can be observed by monitoring changes in the drift time of protein complexes as a function of collision voltage (Figure I-4A and C) For clarity, data is also projected as contour plots (Figure I-4B and D) where the intensity of the features observed are denoted by a color-based axis. At least five intermediate and partially unfolded structural families can be observed for the protein complexes shown here (ConA and ADH). Upon comparing the intermediate structural families observed for protein tetramer ions generated from solutions comprised of different anion populations, both the drift time and the order in which the four major conformational families are populated are

conserved among different anion-protein combinations, illustrating a common element within the CIU “fingerprint” for the ADH and ConA tetramers. Indeed, each of the protein complexes studied in this report exhibit these reproducible fingerprints, and can be unambiguously differentiated based upon CIU pathway alone.

The CIU fingerprints recorded can be used to assess whether the compact geometry observed at low collision energies is stabilized or if stability is instead conferred to unfolded intermediate structures of the complex instead. In Figure I-4D, data acquired with added sulphate shows that the most compact conformer of ADH is observed at substantially higher collision voltages (boxed region) than either control experiments or when fluoride salts are added to the tetramer in solution. Interestingly, in some cases, intermediate unfolded forms of the complex are stabilized in addition to the compact conformer. For example, the CIU fingerprint for the ConA tetramer shows that the addition of nitrate stabilizes not only the most compact conformation of ConA, but also a partially unfolded conformation, evidenced by an elongation of the boxed area relative to control (Figure I-4A and B). A subtly different result is shown for the ADH tetramer in Figure I-4D, where enhanced stability is achieved upon addition of tartrate anions, one of the most-stabilizing salts identified, through interacting with both the most compact form of the tetramer and the unfolded form of the complex observed at lowest energies. Both of these results suggests that anions can remain bound to the tetramer and interact with unfolded structures to stabilize the protein complex through tight interactions.

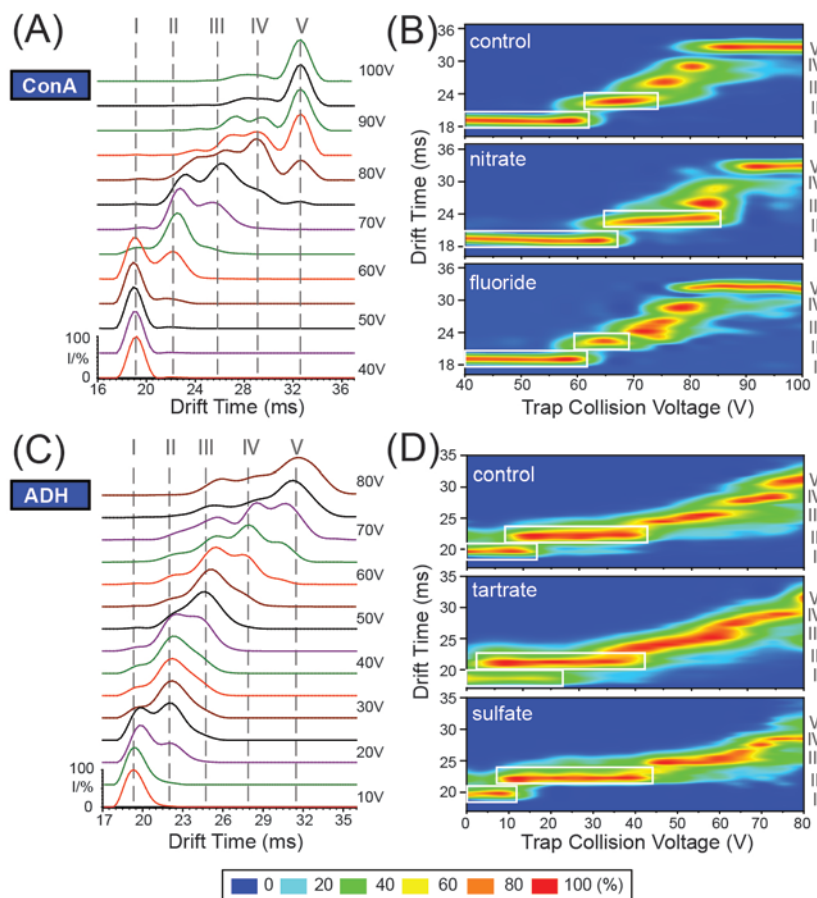


Figure I-4. CIU data reveal subtle differences in the partially unfolded intermediates. The complete arrival time distributions of selected charge states of ConA (A and B) and ADH (C and D) tetramer acquired at the corresponding trap collision voltages show a transition from compact to extended ion conformations. The peak centroids, corresponding to the intermediate structural families observed, are labeled (I-V). For each dataset, a contour plot (or ‘fingerprint’) is shown, where ion trap collision voltage is charted against ion mobility drift time, and the ion intensities are denoted by a color-coded axis (blues correlated to low ion intensity, where reds indicate high ion intensity). Compact and partially unfolded tetramer I and II are highlighted (white box) indicating the types of conformers stabilized by the addition of anions in solution.

Adducts removal upon activation

ESI-generated protein ions can carry a number of solvent and solute molecules with them into the gas-phase, leading to an increase of the mass of the protein complex. The removal of residual molecules can be promoted by applying activating voltage to the trap collision cell of the instrument. Figure I-5 shows the degree of salt retention on avidin and TTR, as a function of the trap collision voltage. The removal of salts follows a sigmoidal decay wherein the mass steadily

decreases to a point where no further desolvation occurs with increase in the activating voltage. The mass obtained at this point is in close agreement with the sequence mass of the protein complex.

Concurrent with the removal of salts, activation of protein ions leads to an increase in the internal energy of the ions and subsequent structural rearrangements. In order to identify a possible correlation between the removal of salts and activation of protein ions, we compared plots corresponding to the measured mass and unfolding, or dissociation of avidin and TTR under the equivalent conditions. We observe that the amount of residual molecules bound to protein complex decreases substantially but only up to the point when the complex begins to unfold. By contrast, avidin experiences a significant degree of unfolding as residual molecules are removed, indicating that the two events occur simultaneously. The data also show that the desolvation of protein complex ions generated from nitrate salt-containing solutions requires harsher conditions when compared to fluoride-salt containing solutions - which are similar to control. This observation is shared between all tetrameric protein complexes we investigated, indicating that nitrate has a higher binding affinity for proteins compared to fluoride in general.

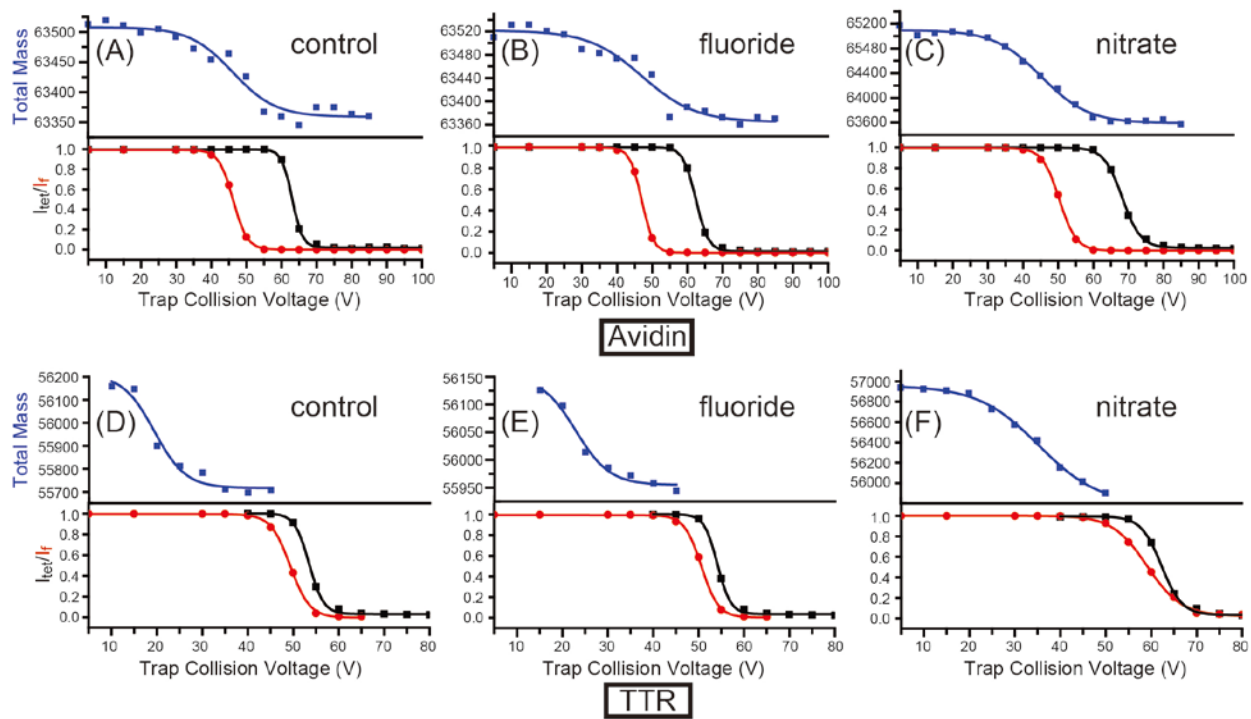


Figure I-5. Adducts removal upon activation. The mass of protein complex (blue), unfolding (red) and dissociation (black) yields varies as a function of trap collision voltage. Data is shown for avidin (A-C) and TTR (D-F). The influence of nitrate in delaying the course of unfolding and dissociation is evident.

Table I-1. Physical constants of selected Hofmeister anions including pKa, gas-phase acidity and ionic radii. The values are reported only for singly-charged anions.

Anion	pKa	Gas-phase acidity (kJ/mol)	Ionic radii (100 pm)
Perchlorate	-10	1192.0	2.40
Iodide	-10	1293.7	2.20
Nitrate	-2	1329.7	1.79
Thiocyanate	-1.8	1343.0	2.13
Chloride	-7	1372.8	1.81
Acetate	4.75	1427.0	2.32
Fluoride	3.17	1529.3	1.33
Bicarbonate	6.35	1988.7	1.56

* pKa, Gas-phase acidity and ionic radii were obtained from Ion Properties (Yizhak Marcus) and CRC Handbook of Chemistry and Physics and NIST Chemistry WebBook

Table I-2. Physical property of proteins studied herein represents a broad range of thermodynamic stabilities and sizes.

Protein	$\Delta G^{\text{diss a,b}}$ (kcal/M)	Surface Area ^b (\AA^2)	Buried Area ^b (\AA^2)	Isoelectric Point
TTR	15	19290	6290	4.7 ^c
Avidin	43.9	20250	13400	10.5 ^d
ConA	9.8	32140	8800	5 ^e
ADH	20.1	48930	14850	5.4 ^f
BLA ^h				5.2 ^g
Cyt C				10.25 ^g

a. ΔG^{diss} indicates the free energy of assembly dissociation, in kcal/M. The free energy of dissociation corresponds to the free energy difference between dissociated and associated states. Positive values of ΔG^{diss} indicate that an external driving force should be applied in order to dissociate the assembly, therefore assemblies with $\Delta G^{\text{diss}} > 0$ are thermodynamically stable.

b. Reference from Protein interfaces, surfaces and assemblies service PISA at European Bioinformatics Institute (http://www.ebi.ac.uk/pdbe/prot_int/pistart.html), authored by E. Krissinel and K. Henrick

c. Uversky, V. N., and Fink, A. L., "Part A: Protein Aggregation and Conformational Diseases Series" in Protein Misfolding, Aggregation and Conformational Disease, Springer, p. 259 (2006)

d. Andrea, Z., et al., Protein Expr. Purif. 32(2003) 167-174

e. Ueta, R.R., and Dimiz, F.B., Colloids Surf. B Biointerfaces. 61(2008) 244-249

f. Sund, H., and Theorell, H., "Alcohol Dehydrogenases" in The Enzymes, VII, 2nd ed., Academic Press, NY, p. 25 (1963)

g. Righetti, P.G., J. Chromatogr. A 1037 (2004) 491-499

h. No assembly information available.

Table I-3. Triplicate measurements of CIU and CID avidin tetramer and example standard deviation calculation.

Measurements	E_{com} (eV)	
	Dissociation	Unfolding
1	0.646	0.477
2	0.593	0.508
3	0.617	0.493
Average \pm s.d. (% s.d.)	0.619 \pm 0.027 (4.28 %)	0.493 \pm 0.016 (2.39 %)

Appendix II. Chapter 3 Supporting Information

One example showing peaks with and without cationization

In Figure II-1, the mass spectrum of TTR from solutions containing 100 mM ammonium acetate can be regarded as the peak without cationization (control). The peak becomes broad to different extents in the presence of different acetate-based salts (2 mM), showing differential degree of cationization. Such broadening is a product of a series of overlapping charge states corresponding to protein complex ions that adhere to different amounts of cations, which cannot be resolved by MS¹. Also addition of acetate anions with doubly charged cations (Mg²⁺, Ca²⁺, Ba²⁺) results in a slight increase in average charge state values while some of the singly charged alkaline metal cations added (Li⁺, Na⁺, K⁺, Rb⁺) cause the charge reduction slightly. Therefore, 14⁺ charge state, highlighted in dashed box, was chosen for isolation based on their intensity across each solution state interrogated.

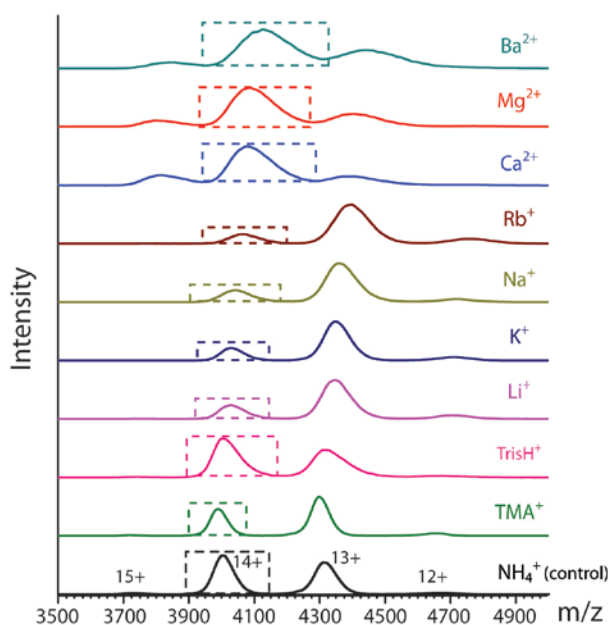


Figure II-1. One example showing peaks with and without cationization. nESI mass spectra of tetrameric TTR (55 kDa) obtained from solution containing 100 mM ammonium acetate (control, black) and a series of solutions containing both 100 mM ammonium acetate and 2 mM salts

(acetate anion with TMA, Tris, lithium, potassium, sodium, rubidium, calcium, magnesium, and barium counterions). Each spectrum was obtained using identical instrumental conditions. 14^+ charge state of all TTR-adduct complexes, shown in dashed box, was isolated for CIU/CID.

Details as to the CIU and CID data collected

For quantitative measurement of the differences in the stability conferred to tetrameric protein by bound cations, the trap collision voltage at which ions undergo CID and CIU is monitored, and plots of trap collision voltage versus the intensity observed for intact (I_{tet}) and compact (I_f) tetramer ions are shown in Figure II-2C and Figure II-2D respectively. All curves show typical sigmoidal decay. Based on these plots, a simplified descriptor of tetramer stability is constructed by plotting collision energy (units of eV^*) at which the intact/compact tetramers (I_{tet} / I_f respectively) decrease to 50% of their initial values (Figure II-2E).

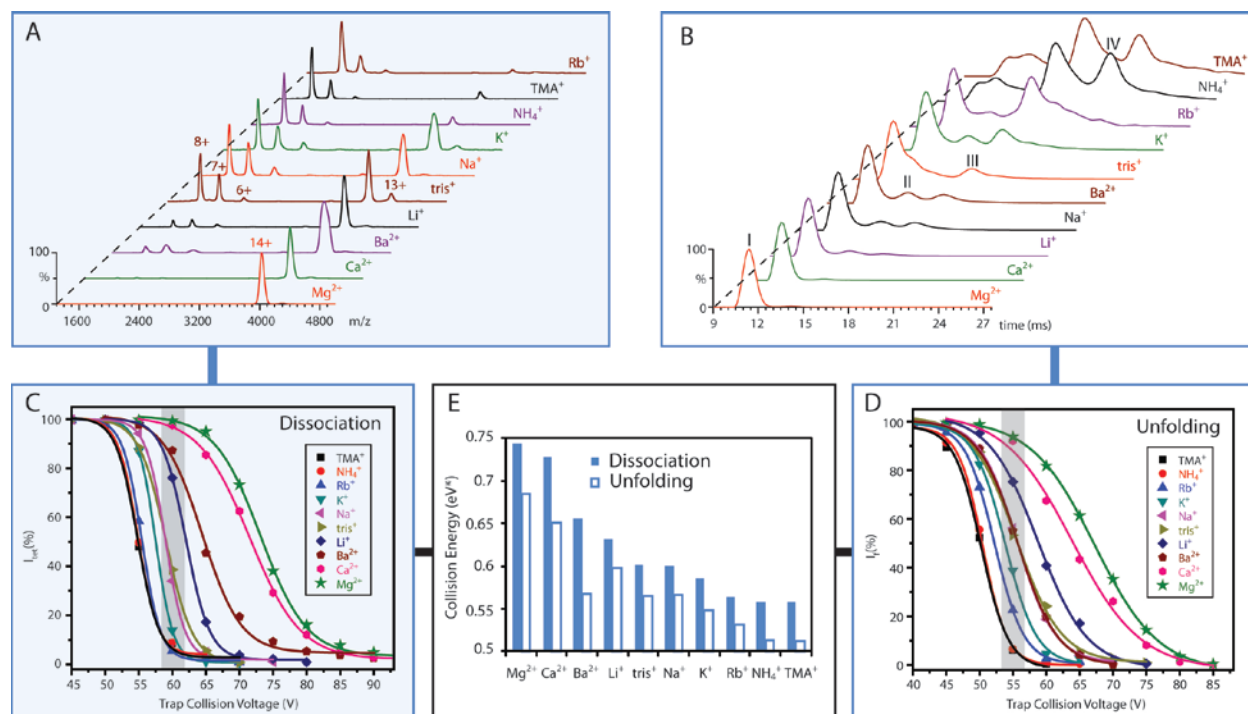


Figure II-2. Workflow chart of measuring the stability of cation-bound TTR by IM-MS. (A) The mass spectra of TTR incubated with 10 acetate-based cations reveal different extent of dissociation. The 14^+ charge state of TTR ions selected by the quadrupole mass filter, acquired at a trap collision voltage of 60 V which was applied to the ions in the trapping region between the quadrupole mass analyzer and ion-mobility region of the instrument. Peaks corresponding to 14^+ charge states of tetramer and $6-8^+$ charge states of monomer are shown. (B) The arrival time

distributions of 14^+ TTR incubated with 10 acetate-based cations acquired at a trap collision voltage of 55 V yield unfolding to different extent. The four conformations showing a transition from compact to extended species are labeled from I to IV. (C) Plots of the relative intensities of intact TTR tetramer 14^+ ions generated with solutions containing 10 different cations (I_{tet}) are shown as a function of trap collision voltage. I_{tet} acquired at a trap collision voltage of 60 V are marked in a grey box. (D) Plots of the relative intensity of compact TTR tetramer 14^+ ions (I_f) are shown as a function of trap collision voltage. I_f acquired at a trap collision voltage of 55 V are marked in a grey box. (E) A histogram showing the 50% dissociation yield (blue) and unfolding yield (white) for TTR tetramers generated from solutions with various cation additives is shown.

Detailed data regarding ADH dissociation

In Figure II-3, the relative intensity of intact ADH tetramer ions incubated with Mg^{2+} is still high at the maximum value the trap collision voltage can go (200 V), with different TRAP DC bias tuned. This indicates that ADH-Mg complex does not appreciably undergo CID even at the highest activation energy, which makes it impossible to plot the complete sigmoidal decay curve of I_{tet} as a function of trap collision voltage as shown in Figure II-2C.

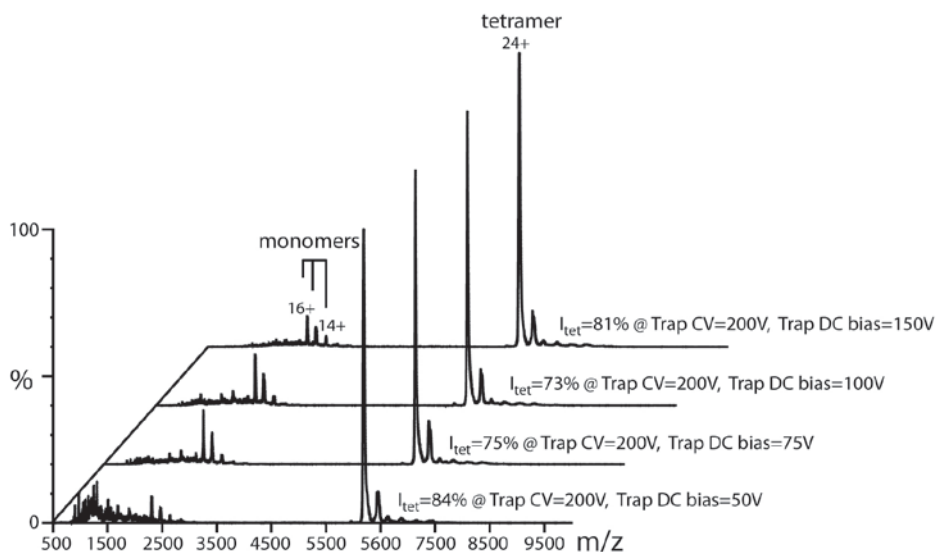


Figure II-3. Detailed data regarding ADH dissociation. Tandem mass spectra of 24^+ charge state of ADH incubated with magnesium cations at the maximum accelerating potential difference attainable by Synapt G2 instrumentation (200 V), with different Trap DC bias set, all results in high I_{tet} .

Further observations revealing the potential difference in stabilization mechanism provided by cationic and anionic additives

Learning from our previous study which implied a role for bound anions in observed stability enhancement², we probed the number of bound cation additives, carried with the complex from solution or the nESI process by measuring the mass of the protein complexes incubated with the acetate-based cations under identical instrument conditions (Trap CV=4 V). Based on the assumption that the excess mass, relative to the ammonium acetate control arises from binding of additional cations added in solution, we plotted the estimated average number of additional cations bound to the tetramers at the very low activation energy against the stability enhancement observed in our CIU data. This is shown in Figure II-4, where singly and multiply charged cations are grouped separately with different colors (2⁺: black squares; 1⁺: red circles; TrisH⁺ is excluded). The two groups indicate a strong positive correlation between the amount of excess mass and structural stability conferred to the four tetrameric protein assemblies studied here, implying that the bound buffer material is an important factor behind the added stability to the proteins. However, Mg²⁺ and Ca²⁺, which are considered to be strong stabilizers, bind in smaller numbers to the protein complexes at the initial voltage than Li⁺ that lies in the medium-stabilizing cluster. This is different from that is observed for anion stabilizer which exhibited a “dissociative cooling” type mechanism, featuring a higher structure stabilization effect provided by greater number of anions bound first and dissociated upon collisional activation¹. Therefore, this clear charge dependence reveals a potentially different stabilization mechanism that relies on the chemical nature of cations. Also worth noting is TrisH⁺ (purple triangle), which acts as an outlier relative to other cations. It affords slight structural stabilization effect to TTR and avidin equally to Na⁺ because of its little binding at the low acceleration voltage (Figure II-4A/Figure

II-4B). Conversely, some of TrisH^+ cations are observed to bind to ConA and ADH, resulting in a higher stability increase, approaching or even above Li^+ (Figure II-4C/Figure II-4D).

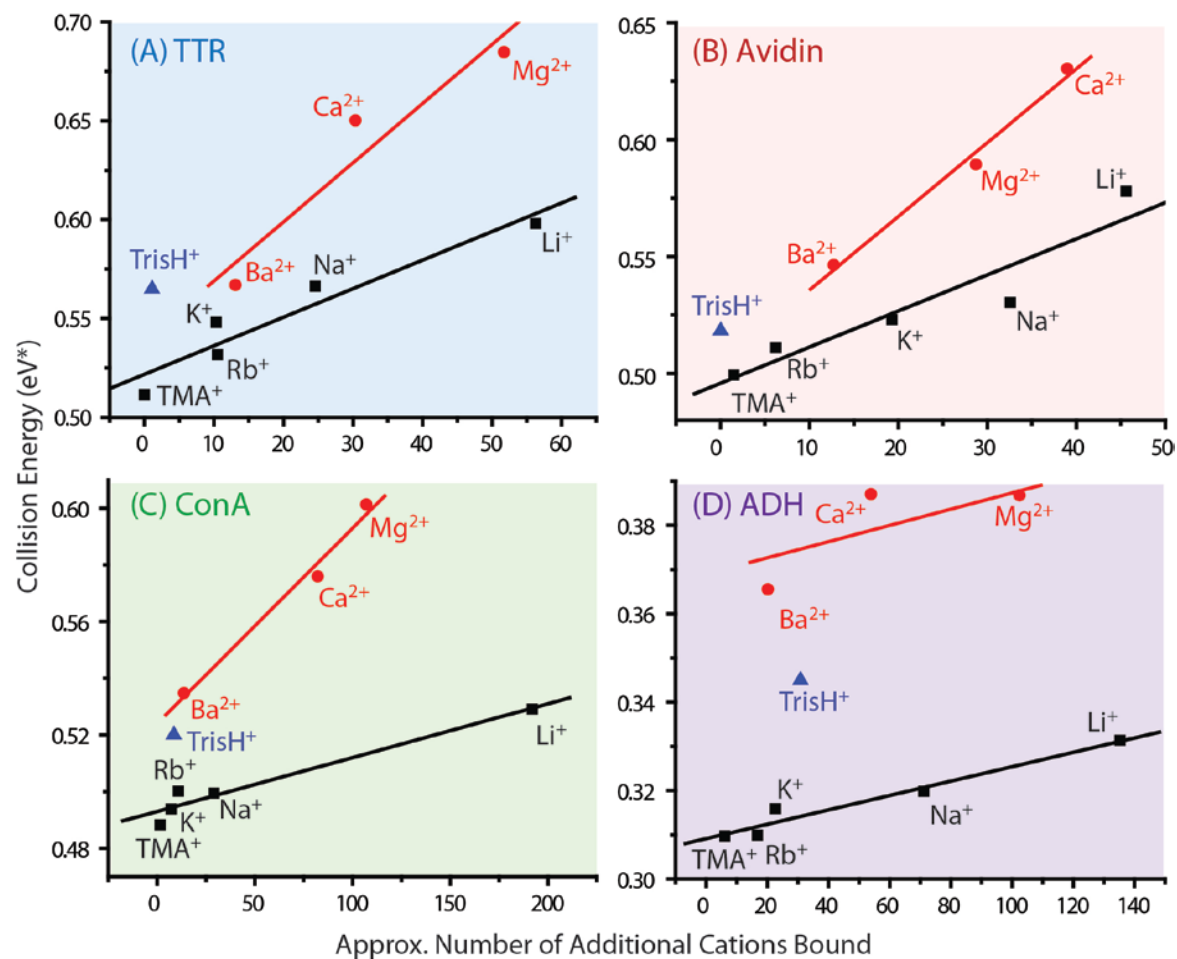


Figure II-4. Further observations revealing the potential difference in stabilization mechanism provided by cationic and anionic additives. Plots of the normalized collision energy required to unfold 50% of complex ions against the calculated number of additional cations that are bound to the protein complex at a trap collision voltage of 4 V, for TTR (A), avidin (B), ConA (C) and ADH (D). A positive correlation is observed for all complexes when doubly and singly charged cations (except TrisH^+) are treated separately. All lines are added to guide the eye, and are not intended to be theoretical fits to the data presented.

Charge-per-unit-area as an important factor for different mode of stabilization

As illustrated in Figure 3-2C in the main text, the stability conferred to the gas-phase assembly increases with the charge-per-unit-area of all cations but TrisH^+ . This is shown more clearly in Figure II-5A, which displays a perfect correlation between the charge-per-unit-area of the cations and their ability to stabilize the protein complexes from unfolding in the gas phase ($R^2=0.954$), with TrisH^+ excluded. Cations of higher charge-per-unit-area, such as Mg^{2+} and Ca^{2+} , which bind in large numbers to protein complexes, will retain their binding position within the protein sequence and become less mobile as charge carriers. This reduction in charge mobility and possibly lower conformational flexibility through multidentate binding of cations to sites on the protein hinder Coulombic unfolding of protein subunits³. On the other side, cations of low charge-per-unit-area, that scales in line with the anions studied previously (Figure II-5B), does not display an appreciable stabilizing effect mentioned above, resulting from the weakness to lock down charge carriers and tether together multiple sites within proteins (not including TrisH^+). Instead, dissociative cooling becomes the dominant effect, equivalent to their anionic counterparts. A low charge-dense cation as TrisH^+ is, it exhibits a medium-range stabilizing influence on gas-phase protein structure, thus suggesting its potential for H-bonding and more-directed interactions with the protein surface on top of the electrostatic interaction. For exact values of charge-per-unit-area, see Table II-1.

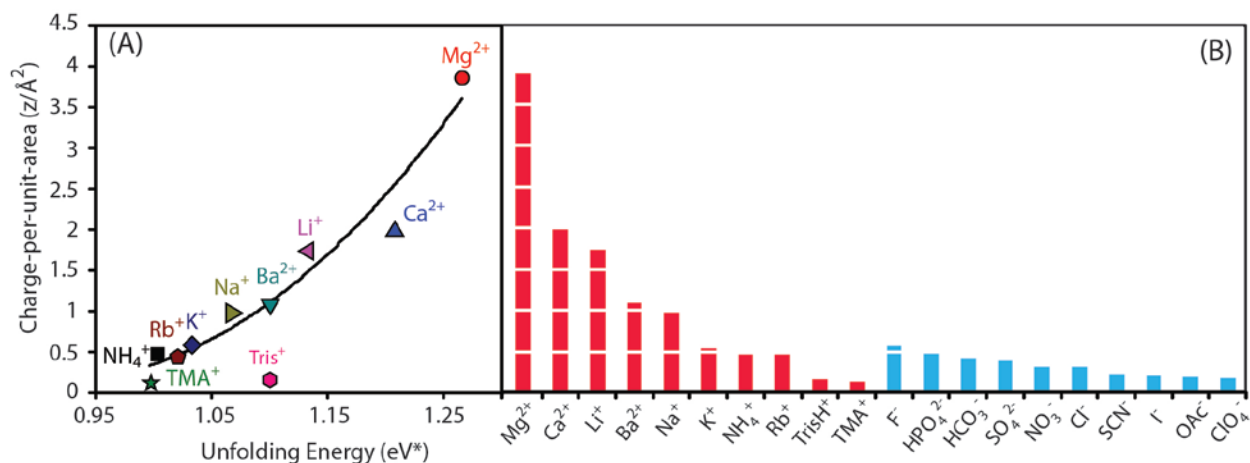


Figure II-5. Charge-per-unit-area as an important factor for different mode of stabilization. (A) The plot extracted from Figure 3-2C clearly shows an excellent correlation between the charge-per-unit-area of the cations and the stabilization observed for the proteins studied here ($R^2=0.954$) only when TrisH⁺ is excluded. (B) Charge-per-unit-area of the cations (red) and anions (blue) studied shows cations in general possess significantly higher charge per-unit area compared to anions.

Table II-1. Physical constants of selected Hofmeister cations and anions including charge, ionic radii and charge-per-unit-area

Cation	Charge	Ionic Radii (Å)	Charge Per-unit-area (z/Å ²)
Mg ²⁺	2	0.72	3.858025
Ca ²⁺	2	1	2
Li ⁺	1	0.76	1.731302
Ba ²⁺	2	1.36	1.081315
Na ⁺	1	1.02	0.961169
K ⁺	1	1.38	0.5251
NH ₄ ⁺	1	1.48	0.456538
Rb ⁺	1	1.49	0.45043
TrisH ⁺	1	2.55 ^a	0.153787
TMA ⁺	1	2.8	0.127551
Anion	Charge	Ionic Radii (Å)	Charge Per-unit-area (z/Å ²)
F ⁻	1	1.33	0.565323
HPO ₄ ²⁻	2	2	0.5
HCO ₃ ⁻	1	1.56	0.410914
SO ₄ ²⁻	2	2.3	0.378072
NO ₃ ⁻	1	1.79	0.3121
Cl ⁻	1	1.81	0.305241
SCN ⁻	1	2.13	0.220415
I ⁻	1	2.2	0.206612
OAc ⁻	1	2.32	0.185791
ClO ₄ ⁻	1	2.4	0.173611

^a. K. Nakashima, S. Tuboi, J. Biol. Chem. **1976**, 251, 4315-21.
Other ionic radius were obtained from Ion Properties (Yizhak Marcus).

References

1. A. R. McKay , B. T. Ruotolo , L. L. Ilag , C. V. Robinson , *J. Am. Chem. Soc.* **2006**, 128, 11433-11442.
2. L. Han, S. J. Hyung, J. J. S. Mayers, B. T. Ruotolo, *J. Am. Chem. Soc.* **2011**, 133, 11358-11367.
3. a) J. C. Jurchen, E. R. Williams, *J. Am. Chem. Soc.* **2003**, 125, 2817-2826; b) I. Sinelnikov, E. N. Kitova, J. S. Klassen, *Journal of The American Society for Mass Spectrometry* **2007**, 18, 617-631; c) S. V. Sciuto, J. Liu, L. Konermann, *Journal of The American Society for Mass Spectrometry* **2011**, 22, 1679-1689; d) S. N. Wanasundara, M. Thachuk, *J. Phys. Chem. A* **2009**, 113, 3814-3821.

Appendix III. Chapter 5 Supporting Information

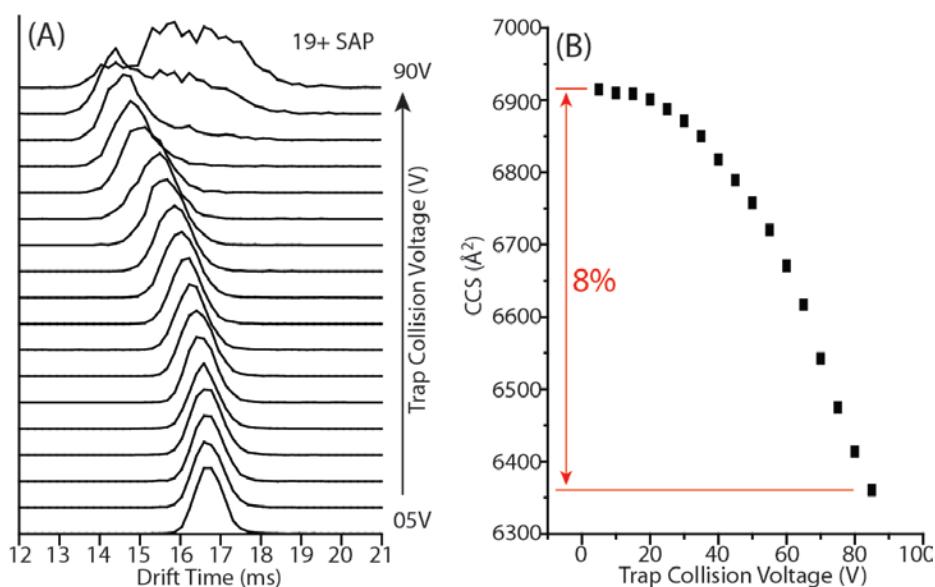


Figure III-1. SAP compaction upon collisional activation. (A) Stacked drift time distributions for 19⁺ charge state of SAP pentameric ion as a function of trap collision voltages varied from 5 V to 90 V in 5 V steps, revealing a decrease in drift time with increasing collisional activation. (B) The plot of trap collision voltage against CCS for 19⁺ SAP pentamer shows an 8% decrease, in line with the collapse into SAP internal cavity.

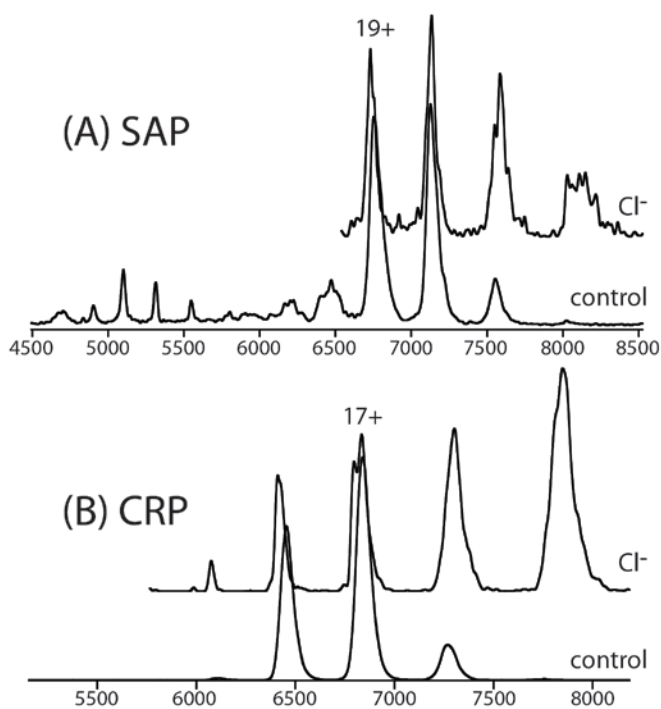


Figure III-2. Hofmeister-type anions cannot bind charge-reduced SAP ions. (A) and (B) Mass spectra of pentameric SAP and CRP, respectively, at reduced charge state distribution, generated from TEA-doped ammonium acetate buffer in the absence and presence of 4 mM ammonium chloride. Comparison between the datasets with and without Cl^- suggests negligible amount of the anions bound to the protein ions.

Appendix IV. Chapter 6 Supporting Information

Comparison of ConA and ConA' MS data

We are able to isolate the MS data corresponding to only ConA and ConA' (Figure IV-1) using careful control of solution conditions and spectral post-processing. We observe an increase in average charge state for tetrameric ConA' (red) relative to ConA (black), indicated by higher signal intensity corresponding to the 21⁺ charge state and a new 22⁺ peak. This increase in average charge correlates well with our increased CCS measurements (ConA' has a 12% larger CCS than ConA). The charging of intact protein complexes by nESI is known to be dependent upon protein surface area, and simple estimates of this attribute based on CCS allow us to predict an increase of ~1 charge for ConA' relative to ConA based on literature data¹.

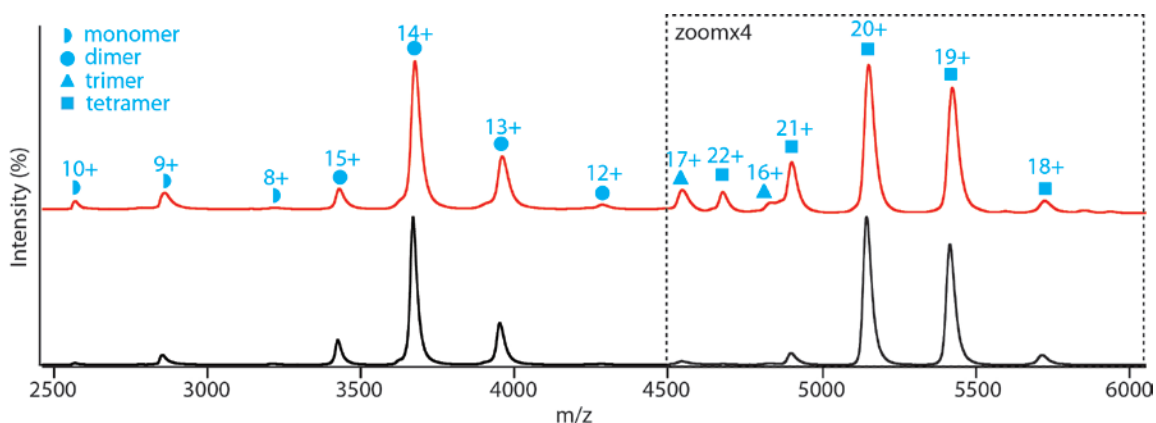


Figure IV-1. Comparison of ConA and ConA' MS data. Mass spectra of ConA obtained from nESI solutions prepared using control (100 mM ammonium acetate) conditions (black) and following multiple freeze-thaw cycles (red). The charge states are indicated for tetramers (square), trimers (triangle), dimers (circle) and monomers (half circle). The spectra are magnified 4 fold above 4500 m/z.

Verifying the assignment of ConA' as a misfolded form of ConA tetramer through solution-phase disruption

To probe the origin of ConA', we endeavored to structurally characterize its subcomplexes and subunits. It should be noted that ConA can exist as tetramer, dimer and monomer under all solution compositions tested herein. Small amounts of other forms such as trimer and hexamer are believed to arise from the nonspecific interactions formed during the ESI process. Figure IV-2 exhibits the controlled distortion of native state ConA by dissolving it into 100 mM ammonium acetate solutions containing 20% (vol/vol) glacial HAc (pH = 5.2) and 0%-30% (vol/vol) MeOH. In this weakly-acidic solution, the ConA tetramer evolves from a native-like form (black dotted line) to a structure having longer drift times (red dotted line) as the fraction of MeOH is raised (Figure IV-2A). This new conformer has a similar CCS to the ConA' formed following several freeze-thaw cycles, thus we refer to both similarly, and this feature dominates the 21⁺ of ConA tetrameric ions when the MeOH volume fraction reaches 20%. In addition, the 10⁺ ion of ConA monomer undergoes significant conformational changes with increasing MeOH concentration (Figure IV-2C) while there is no significant change for the 15⁺ ConA dimer (Figure IV-2B).

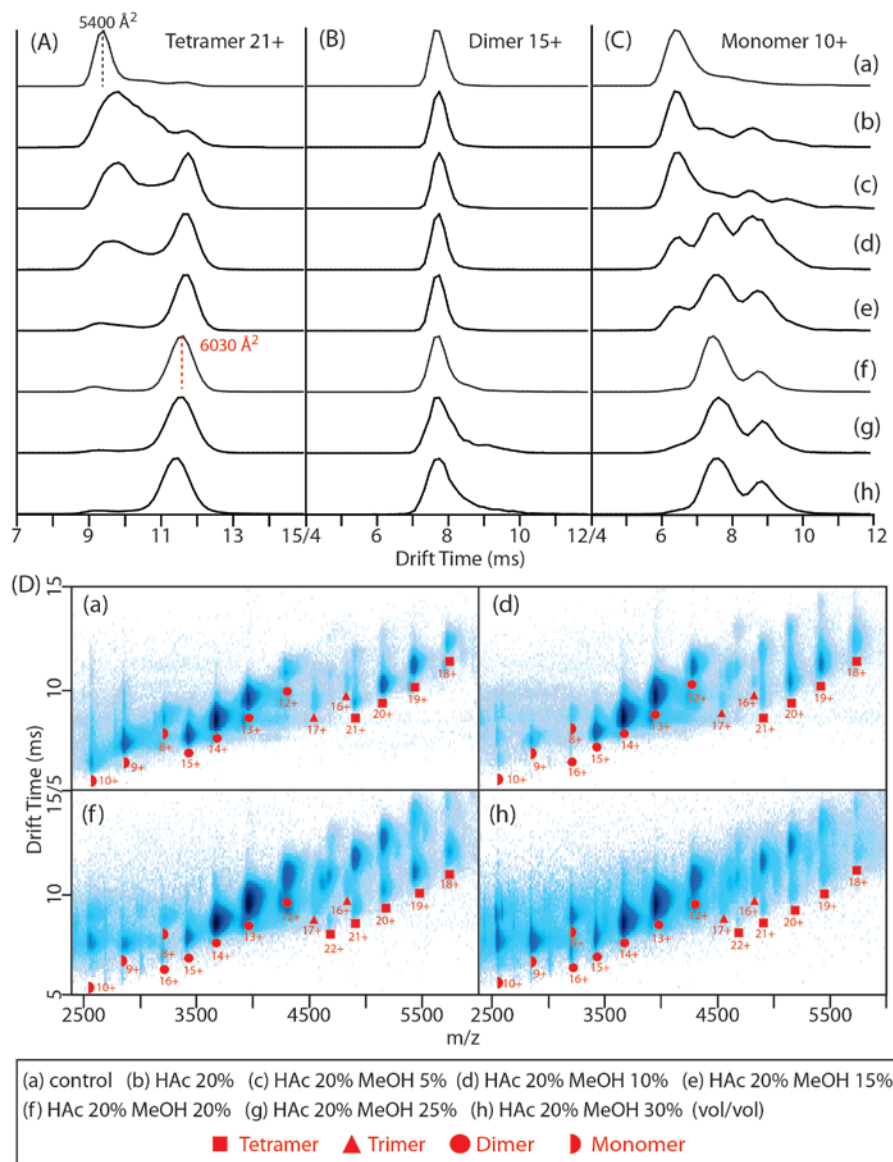


Figure IV-2. Generation of misfolded ConA by acid and MeOH. Controlled distortion of native-like ConA (control in solution (a) containing 100 mM ammonium acetate) by 7 different HAC:MeOH solutions (b to h). (A), (B) and (C) show the drift time distributions measured for the 21⁺ charge state of ConA tetramer, 15⁺ of dimer and 10⁺ of monomer in 8 different solution compositions, respectively. The 20%:20% HAC:MeOH was selected for use in Figure IV-4, Figure IV-7 and Figure 6-5. (D) Drift time versus m/z contour plots obtained for ConA/ConA' ions formed from 4 solution compositions (a, d, f and h). Trimers observed here most likely result from the nonspecific interaction of monomer and dimer during the ESI process.

To further study ConA' structure, the complex was dissolved into 100 mM ammonium acetate solutions containing 0%-50% (vol/vol) MeOH (Figure IV-3) and 0%-60% (vol/vol) DMSO

(Figure IV-4), which are polar protic and aprotic solvents respectively. A greater population of ConA' is produced as the volume fraction of MeOH is increased, whereas the CCS observed for DMSO containing solutions remains virtually unchanged from the value expected for 'native-like' ConA. We note that the tetramer size is observed to increase (by ~1%) in a manner correlated with DMSO addition, but we do not observe any production of ConA' at any DMSO solvent fraction. Larger amounts of MeOH (>50%) or DMSO (>60%) are required to completely deplete the tetramers observed (data not shown).

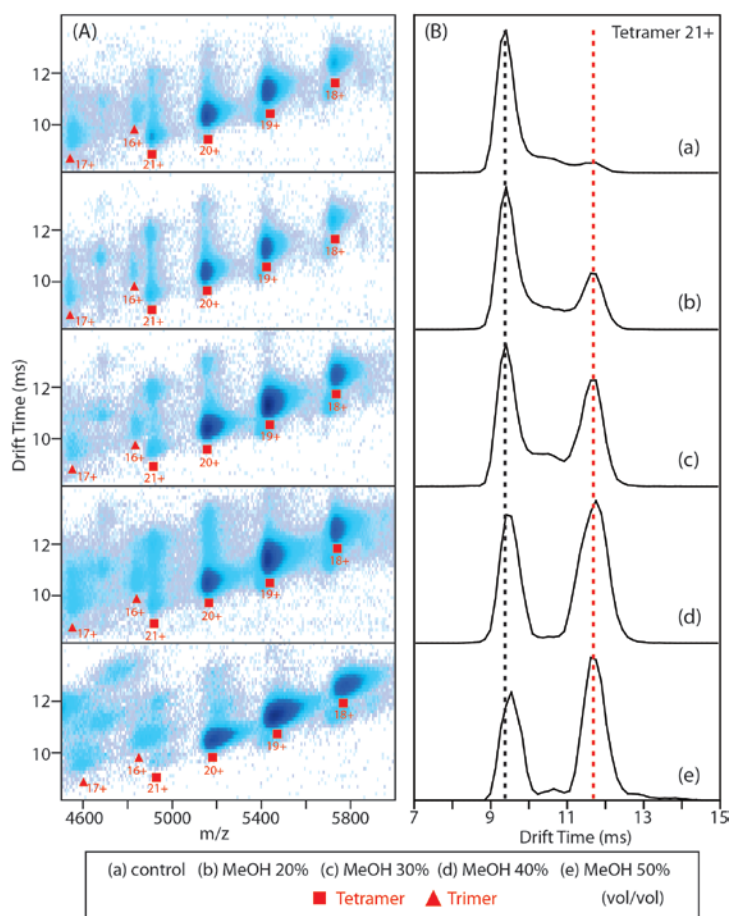


Figure IV-3. Generation of misfolded ConA by MeOH. Controlled distortion of ConA (control in solution (a) containing 100 mM ammonium acetate) by 4 different MeOH fractions in aqueous solution (b to e). (A) Drift time versus m/z contour plots obtained for ConA/ConA' tetramer ions formed from 5 solution compositions (as indicated). (B) Drift time distributions measured for 21⁺ charge state of ConA tetramer, from the 5 solution compositions shown in A. The increase in the MeOH fraction progressively produces a greater population of ConA' (red dashed line) relative to ConA (black dashed line).

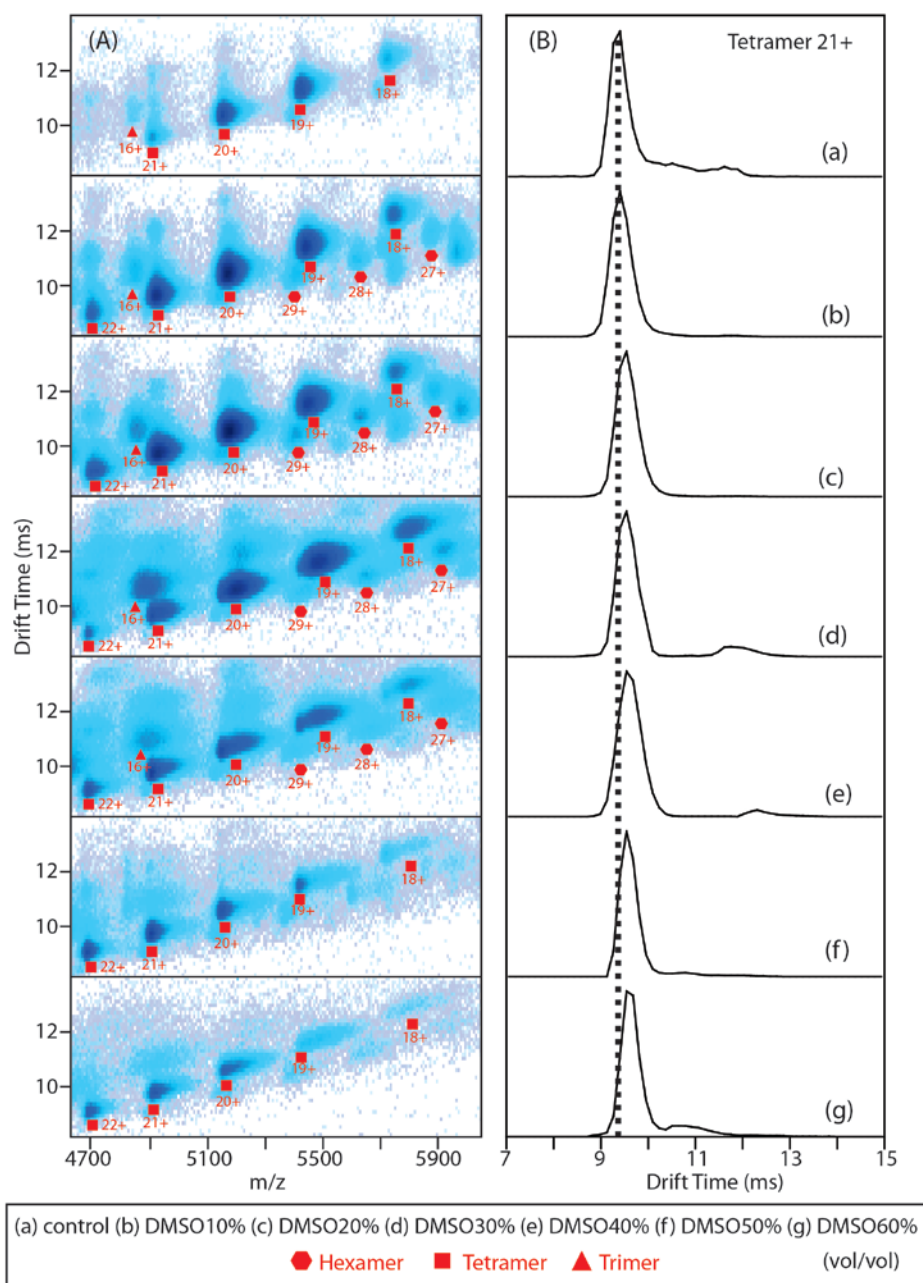


Figure IV-4. DMSO fails to produce misfolded ConA. Controlled distortion of ConA (control in solution (a) containing 100 mM ammonium acetate) using 6 different aqueous solvent compositions having varying amounts of DMSO (b to g). (A) Drift time versus m/z contour plots obtained for ConA tetramer ions formed from different DMSO solution compositions. Small signals for nESI artifact trimers and hexamers can also be observed. Additionally, DMSO results in slight supercharging of ConA tetramer where 22^+ charge state is observed, which can be attributed largely to surface tension effects². (B) Drift time distributions measured for the 21^+ charge state of the ConA tetramer measured from the solution compositions indicated. A slight increase in ConA CCS is observed (1%), in a manner correlated with the increased fraction of DMSO used as a solvent.

Confirmation of the ConA' assignment as a misfolded form of ConA through collisional activation

Additional insight into the structure of ConA' can be obtained through collisional activation. Using IM-MS, we can construct a 'CIU fingerprint' for 21^+ of ConA (Figure IV-5A) and ConA' generated by incubating ConA in a 20%:20% HA:MeOH solution (Figure IV-5B)^{3,4}. Both ConA and ConA' occupy the same number of intermediate unfolded conformations, beginning from the most compact conformer (I and I') having a ~12% difference in CCS, and reaching a similar maximally-unfolded conformation (IV and IV') having a shared CCS value of 7550 \AA^2 . Post-IM CID was also performed on ConA and ConA' in ion transfer which sits after the IM cell. In this sense, the dissociated products (monomers and fragments) bear the same drift time as their precursor tetrameric ions. These data are shown in Figure IV-5C, and we observe that monomeric product ions produced from ConA' exhibit lower charge states (6^+ and 7^+) than those produced from ConA. This result also points to a potential difference in structure between the monomers that comprise the tetramer quaternary structures observed, consistent with the data shown in Figure IV-1. The mass difference measured between ConA and ConA' (Figure IV-5D), following activation to remove residual buffer ions from the gas-phase protein complexes, is negligible, implying that there is no measurable release of the specifically-bound metal ions that provide conformational stability to ConA (Mn^{2+} and Ca^{2+}).

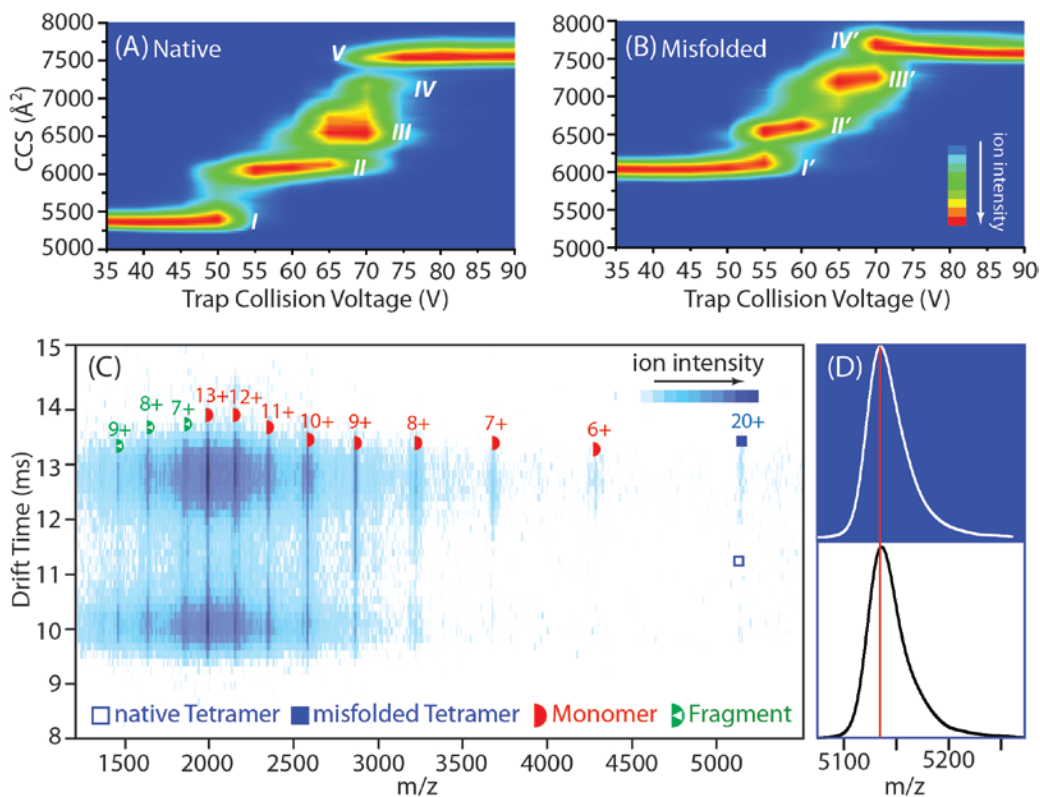


Figure IV-5. Confirmation of the ConA' assignment as a misfolded form of ConA through collisional activation. Collisional activation of native ConA and its misfolded form (ConA'). (A) and (B) are CIU fingerprint contour plots for 21^+ ConA and ConA' respectively, where trap collision voltage is charted against IM drift time, and ion intensities are denoted by a color-coded axis. The conformational forms observed for ConA (I, II, III, IV) and ConA' (I', II', III' and IV') are labeled. (C) Drift time versus m/z contour plots obtained for 20^+ ConA and ConA' following post-IM CID. Unfolded monomers and truncated fragments⁵ with wide charge state distributions are observed at a collision voltage of 180 V. (D) Comparison of MS data for the misfolded (upper) and native-like (lower) forms of 20^+ of ConA tetramer at a transfer collision voltage of 60 V where the majority of residual buffer ions have been removed. A negligible mass difference is recorded (intact mass = 102.7kDa), with red dashed line marked at the m/z of highest abundance ($m/z = 5135$).

Cation concentration-dependent recovery of ConA'

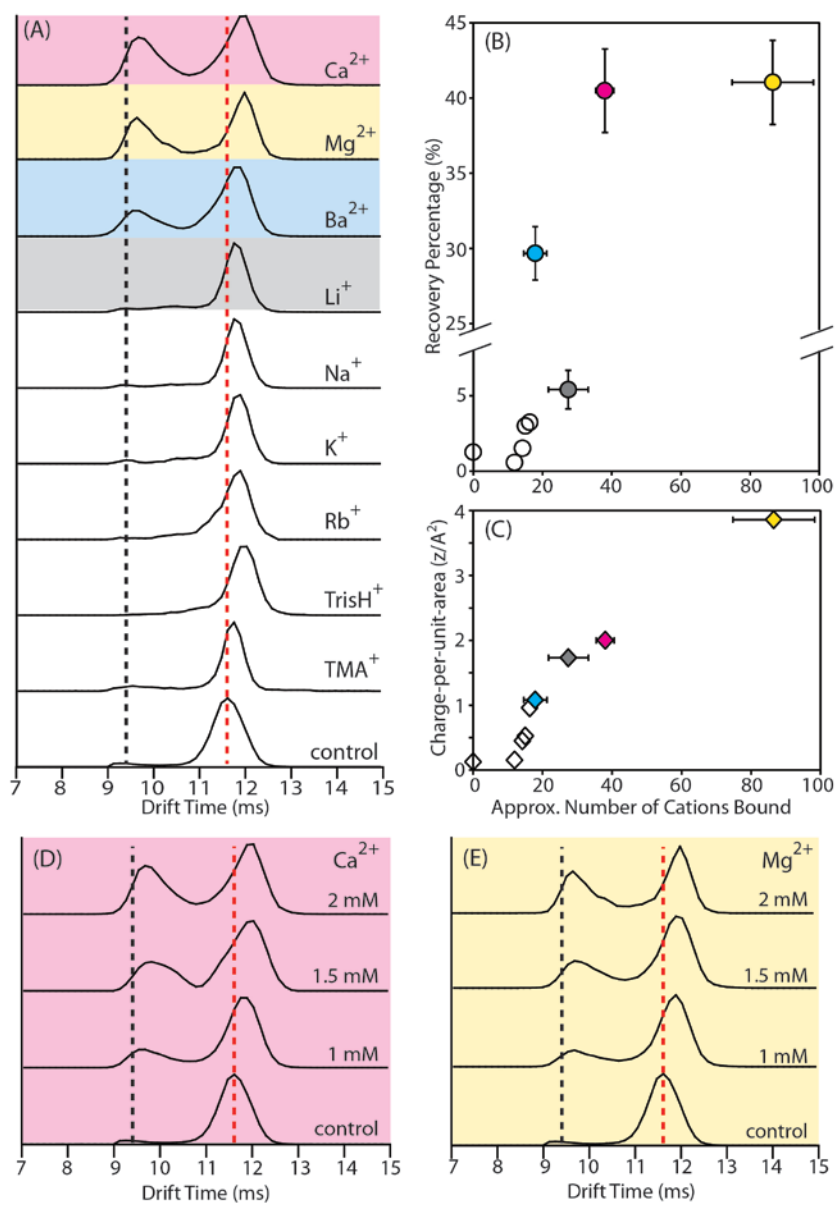


Figure IV-6. Cation concentration-dependent recovery of ConA'. The addition of cations in solution recovers ConA' to ConA in a concentration dependent manner. For all data, black and red dashed lines are inserted in order to guide the eye along drift times corresponding to ConA and ConA' respectively. (A) Drift time distributions measured for 21⁺ charge state of ConA' tetramer incubated with 9 different acetate-based cations (2 mM) in solution. (B) A plot of the average number of cations bound to gas-phase proteins versus % recovery to ConA observed. (C) The average number of cations bound to gas-phase ConA' proteins plotted against the charge-per-unit-area of the cations added. A strong correlation is observed between protein-cation binding affinity and the charged area of the added cations. In (B) and (C), four cations are highlighted (red: Ca²⁺; yellow: Mg²⁺; blue: Ba²⁺; grey: Li⁺) for discussion in the text. (D) and (E) show concentration-dependent analysis, in which drift time distributions measured for 21⁺ ConA' incubated with Ca²⁺ and Mg²⁺ are stacked according to the concentration of the added cations.

Anions recover the misfolded ConA in a fashion nearly identical to solution-phase Hofmeister series (Figure 6-3A) but cations do not (Figure 6-3B). Such a discrepancy led us to probe the effect of cations in a detailed manner, focusing on the 21^+ of misfolded ConA tetramer (ConA') created through incubating ConA in an 20%:20% HA:MeOH solution, and then adding a series of acetate-based cations at fixed concentrations (Figure IV-6A). The data agree well with the rank order we have determined previously, and we can quantitatively assess the recovery percentage achieved, calculated as a fraction of native conformer over the sum of all conformational ensembles observed, which is further plotted against the average number of cations bound (Figure IV-6B). Generally, there is a positive correlation between the % recovery achieved and the amount of cations bound to gas-phase ConA' ions (Figure IV-6C). This highlights the importance of the cations bound to the gas-phase proteins in converting ConA' to ConA. However, we detect a significant difference in the extent of recovery in the cases of Li^+ (grey) and Ba^{2+} (blue), although Li^+ binds in larger numbers to the protein (Figure IV-6B). As observed previously, multiply charged cations (Ca^{2+} , Mg^{2+} and Ba^{2+}), which can form multidentate interactions within proteins in the gas phase, can recover the protein complex more-effectively. It is worth noting that the cation-protein interactions studied here are deemed 'non-specific' because there are no specific binding sites for Mg^{2+} and Ba^{2+} in ConA⁶. Even in our Ca^{2+} data, specific binding is not likely to contribute to the recovery observed, as our Ca^{2+} data mirrors those cations known to be nonspecific ConA binders. This can be confirmed by our concentration-dependent analysis, where larger concentrations of both Ca^{2+} and Mg^{2+} are observed to increase the population of native ConA similarly (Figure IV-6D and Figure IV-6E). Previous data has shown that Mg^{2+} cannot interact with the specific metal binding sites within ConA.

Verifying recovered ConA' being identical to ConA through collisional activation

As discussed above, high charge density cations (i.e. Mg^{2+} and Ca^{2+}) are able to recover ConA' back to a native-like structure in solution for measurement in the gas phase. To investigate the local structural similarity of recovered ConA' to ConA produced from pure ammonium acetate solutions, CIU fingerprint analysis was performed for 21^+ ConA' ions recovered through the addition of Mg^{2+} (Figure IV-7). We note that prior to the addition of Mg^{2+} , IM-MS data indicates that protein in solution was not completely in a disrupted state, containing 44% ConA and 56% ConA' (Figure IV-7A, red). For a direct comparison, the CIU fingerprinting experiment was also performed for 21^+ ConA without any disruption, in the presence of an equal Mg^{2+} concentration (2 mM, Figure IV-7B,C). Cation-mediated CIU fingerprints exhibit strikingly different unfolding pathways when compared with ions produced from 100 mM ammonium acetate buffer³. The two CIU fingerprints recorded share the same unfolding pattern, and are thus indicative of a similar local structure for recovered ConA' and ConA tetramer.

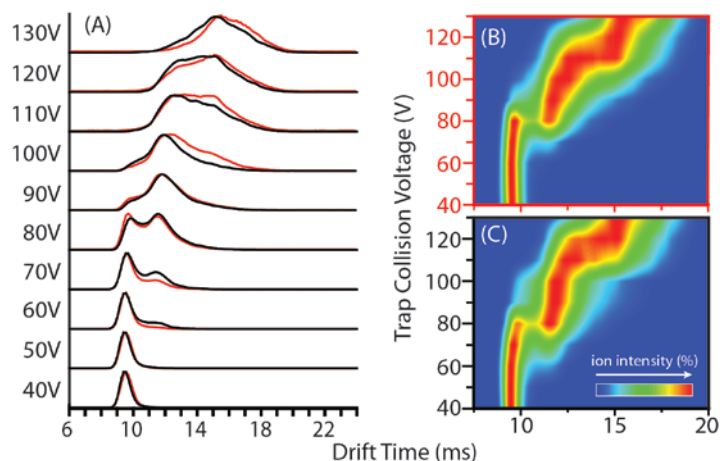


Figure IV-7. Collisional activation of ConA' and ConA incubated with added Mg^{2+} . (A) The arrival time distributions of 21^+ charge state of Mg^{2+} -recovered ConA' (red) and Mg^{2+} -incubated ConA (black) acquired at the corresponding trap collision voltages. (B) and (C) are complete

CIU fingerprint contour plots for 21⁺ ions of Mg²⁺-recovered ConA' and Mg²⁺-incubated ConA respectively, where ion intensities are denoted by a color-coded axis.

Calcium nonspecifically binding to ConA'

As discussed above, we observe no evidence for the release of specifically-bound metal ions from ConA upon conversion to ConA'. Appropriately bound Mn²⁺ and Ca²⁺ ions are required for sugar binding, and we have observed that samples containing significant amounts of disrupting agents can still bind sugars known to be tight binders to native ConA by MS (data not shown). Furthermore, the number of divalent metal ions adhered to the protein far exceeds the known binding stoichiometry of the native protein, further indicating that a non-specific Hofmeister effect is primarily operative in the stability shifts observed in our data. For example, MS data collected and compared between ConA' and ConA' incubated with 2 mM Ca²⁺ (Figure IV-8) displays a mass shift of 1.8 kDa. If it is assumed that all of the excess mass recorded is due to Ca²⁺ binding (an assumption that is supported by much control data for smaller protein systems)⁷, then a binding stoichiometry close to 1:45 results, which is far above the 4 expected binding sites on ConA.

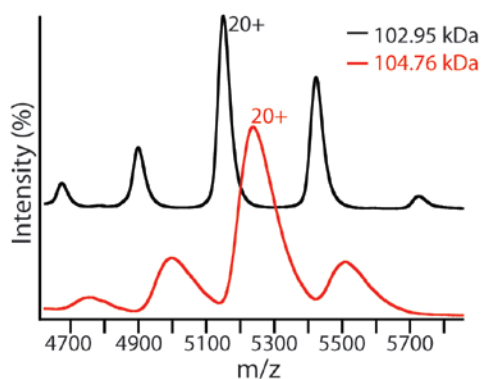


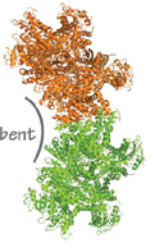
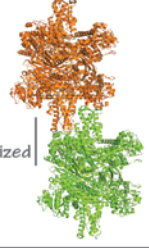
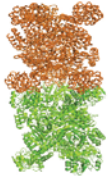
Figure IV-8. Calcium nonspecifically binding to ConA'. nESI mass spectra of ConA' (5 μ M) generated with 20%:20% HAC: MeOH and the same ConA' (5 μ M) further incubated with 2 mM Ca²⁺, colored by black and red, respectively. The 2 spectra were obtained using identical instrumental conditions. The molecular weight of ConA' and Ca²⁺-bound ConA' is indicated (kDa).

References

- (1) Benesch, J. L. P.; Ruotolo, B. T.; Simmons, D. A.; Robinson, C. V. *Chem. Rev.* **2007**, *107*, 3544.
- (2) Iavarone, A. T.; Williams, E. R. *Journal of the American Chemical Society* **2003**, *125*, 2319.
- (3) Han, L. J.; Hyung, S. J.; Ruotolo, B. T. *Faraday Discussions* **2012**, In Press.
- (4) Freeke, J.; Bush, M. F.; Robinson, C. V.; Ruotolo, B. T. *Chem. Phys. Lett.* **2012**, *524*, 1.
- (5) Han, L.; Ruotolo, B. T. In *International Journal for Ion Mobility Spectrometry* 2013; Vol. 16, p 41.
- (6) Shoham, M.; Kalb, A. J.; Pecht, I. *Biochemistry* **1973**, *12*, 1914.
- (7) Han, L. J.; Hyung, S. J.; Ruotolo, B. T. *Angew. Chem.-Int. Edit.* **2012**, *51*, 5692.

Appendix V. Chapter 7 Supporting Information

Table V-1. Experimental and theoretical CCS for bovGDH and bacGDH dodecamers

Complex	Structure ^a	pdb	6mer-6mer interaction ^b	Contact area ^c [Å ²]	MW theor. [Da]	CCS calcd. (scaled PA) [Å ²]	MW exp. [Da]	z	CCS exp. [Å ²]
bovine glutamate dehydrogenase dodecamer (bovGDH _{12mer})		1NR7	the antenna of one interacts with the top of the NAD domain and the antenna of the adjacent hexamer	1,642	668,714	22,751	675,077 ±18 Da	54	21,612
	53							21,706	
								52	21,777
								51	21,825
								50	22,072
								Avg.	21,798 ±0.7%
		3MW9	most of the contacts between the hexamers are made by the antenna region	680	668,714	23,371	675,268 ±32 Da	59	23,894
								57	23,603
								56	23,704
								55	24,036
								54	24,323
								Avg.	23,885 ±1.0%
bacteria glutamate dehydrogenase dodecamer (bacGDH _{12mer})		2YFH	Hex docking		581,162	20,003	579,768 ±29 Da	49	20,146
								48	19,953
								47	19,969
								46	20,175
								45	20,535
								Avg.	20,155 ±1.0%

a. In the dodecamer structure, two hexamers are indicated by orange and green.

b, c. Reference from Banerjee, S. *et al.* *Biochemistry* **2003**, 42, 3446-56.

Table V-2. Experimental and theoretical CCS for SAP and CRP decamers

Complex	Structure ^a	pdb ^b	MW theor. [Da]	CCS calcd. (scaled PA) [Å ²]	Protecting ligands ^c	MW exp. [Da]	z	CCS exp. [Å ²]
serum amyloid P component decamer (SAP _{10mer})		1SAC HEX docking	254,625	11,244	Ca ²⁺ : ionic interactions between calcium ions and carboxylate groups	255,896 ±43	33	11,120
							32	11,169
							31	11,278
							30	11,348
							29	11,383
		28	11,519					
		Avg.	11,302	±1.3%				
		1SAC HEX docking	254,625	10,582		255,984 ±29	33	10,613
							32	10,686
	31				10,819			
	1LGN	254,625	10,610	Ca ²⁺ , dAMP: base stacking of dAMP adenine rings	30	10,913		
					29	11,051		
					28	11,150		
	Avg.	10,872	±1.9%					
c-reactive protein decamer (CRP _{10mer})		1GNH Hex docking	230,470	9,990	Ca ²⁺ : ionic interactions between calcium ions and carboxylate groups	230,956 ±28 Da	32	9,691
							31	9,780
							30	9,832
		29	9,859					
		Avg.	9,845	±0.7%				
		1GNH Hex docking	230,470	9,998		Ca ²⁺ , dAMP: base stacking of dAMP adenine rings	32	9,691
	31				9,780			
	30				9,832			

a. For SAP and CRP pentamers, the two faces characterized by α -helix and β -sheet are defined as A (red) and B (green), respectively.

b. Some structures were derived from the protein-protein docking using HEX 6.3 software based on the crystal structures.

For details, see Materials and Methods in Supporting information.

c. Reference from i) Hohenester, E. *et al.* J Mol Biol **1997**, 269, 570-8. ii) Emsley, J. *et al.* Nature **1994**, 367, 338-45.

Table V-3. Structural similarity analysis between bovGDH and bacGDH hexamers, and between SAP and CRP pentamers using TM-align. (<http://zhanglab.ccmb.med.umich.edu/TM-align/>)

bovGDH vs. bacGDH			SAP vs. CRP		
RMSD ^a	Seq_ID ^b	TM-score ^c	RMSD	Seq_ID	TM-score
2.24	0.33	0.92	1.25	0.52	0.96

a. RMSD (root-mean-square deviation) is used to measure similarity in global structure

b. Seq_ID is used to measure similarity in sequence

c. TM-score is used to measure similarity in topology fold.

0.0 < TM-score < 0.30, random structural similarity

0.5 < TM-score < 1.00, in about the same fold

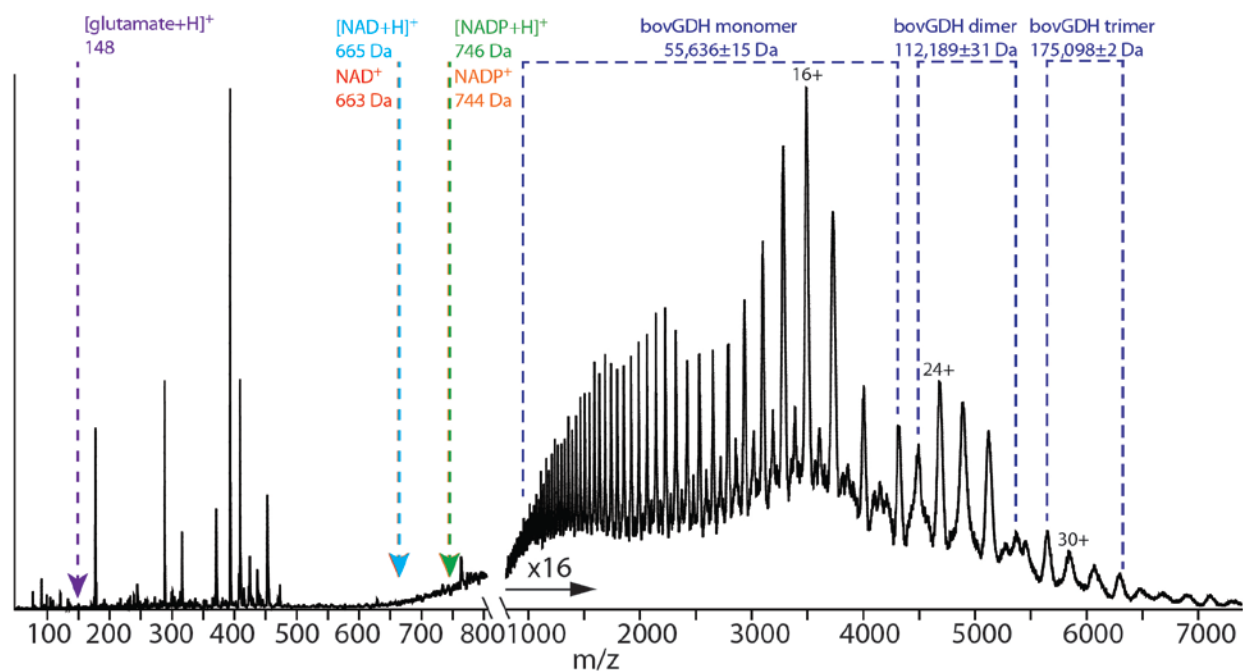


Figure V-1. Mass spectrum of denatured bovGDH hexamer. It is prepared by incubation in 49:49:2 (v:v:v) water:MeOH:HAc solution for 4 hours, reveals signals corresponding to bovGDH monomeric, dimeric and trimeric ions, but no glutamate, NAD(H) and NADP(H) ions. Peaks not annotated are thought to be due to other impurities or noise.

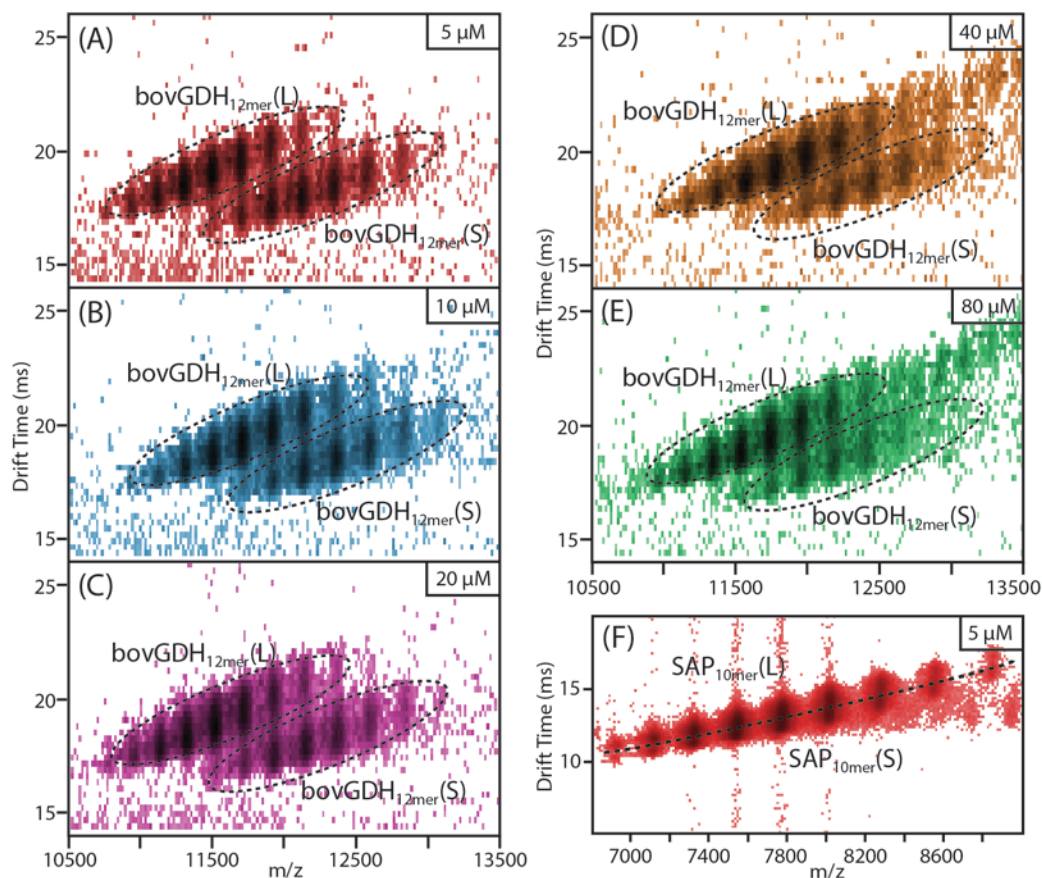


Figure V-2. bovGDH and SAP concentration-dependent analysis. It is based on IM-MS data for bovGDH at varied concentrations (A→E), which exhibit larger and smaller dodecamers, labelled by bovGDH_{12mer}(L) and bovGDH_{12mer}(S) respectively, in different abundance ratio. IM-MS data for SAP at 5 μM exhibit the decamers in two different structures, SAP_{10mer}(L) and SAP_{10mer}(S), divided by dotted lines (F). This is an example showing that such resolution could result in slightly larger standard deviation when the abundance ratio is calculated (Figure 7-3E).